Distance-dependent fluorescence emission in solid hybrid structures of colloidal CdS Quantum Dots and Gold Nanoparticles

A study upon fluorescence enhancement related to proximity effect induced by Hexylamine

Luca Ceresa n.83213

Thesis to obtain the Master of Science Degree in

Materials Engineering

Supervisor: Prof. José Paulo Sequeira Farinha
Co-supervisor: Prof. Matthew Moffitt

Examination Committee

Chairperson: Prof. Pedro Miguel Gomes Abrunhosa Amaral
Supervisor: Prof. José Paulo Sequeira Farinha
Members of the Committee: Prof. Ermelinda Maria Sengo Maçôas

11 / 2017

The experimental part of the present work has been conducted in the

laboratory "Moffitt Lab"

at the University of Victoria - Canada

under the supervision of professor Matthew Moffitt.

Table of Contents

List of figures

List of tables

List of employed colors

Samples from LC1-063 to LC1-083

■ Only PS-CdS slides or 350 nm ex.

■ PS-CdS + Hexylamine slides or 370 nm ex.

■ PS-CdS + GNPs slides or 380 nm ex.

■ PS-CdS + Hexylamine + GNPs slides or 390 nm ex.

Samples from LC1-087 to LC1-094

■ LC1-087

■ LC1-088

■ LC1-092

■ LC1-094

Samples from LC1-099 to LC1-119

■ Ratio R

■ Ratio R1

■ Ratio R2

■ Replicate i

■ Replicate ii

■ Replicate iii

■ LC1-114

■ LC1-116

■ LC1-119

I. ABSTRACT

Fluorescent quantum dots were first discovered in 1980 and have immediately been considered as astonishing structures because of their properties, intermediate between those of bulk semiconductors and discrete molecules, due to the high surface-to-volume ratios that characterizes them. Constituted by semiconductor materials, such as cadmium, selenium, sulfur and tellurium, they have been observed to be able to absorb specific wavelengths of an incoming radiation by promoting their electrons to higher energy levels, and to provide photoluminescence when the electrons returned to the ground state. Moreover, their interaction with metal nanoparticles was investigated by many researchers who discovered that an enhanced photoluminescence was provided by the proximity between the two mentioned components. This effect was referred to as metal enhanced fluorescence (MEF). Quantum dots and metal nanoparticles were utilized together to develop hybrid solutions and solid structures able to work as high performing photonic crystals and sensors. Moreover, applications as biomarkers are envisaged which could overcome the drawbacks of their intrinsic toxicity and take advantage of their outstanding optical properties.

Fluorescence emission analysis in films of hybrid materials composed of quantum dots and metal nanoparticles is difficult to be conducted because of reasons involving reproducibility and consistency in the results. First and foremost, a previously prepared solution of quantum dots and metal nanoparticles must be dropped on a surface, namely a glass slide, and subsequently solvent annealed to give rise to a smooth layer. This process is affected by many factors that can cause differences among the obtained samples, even if they come from the same solution. For instance, humidity and temperature can cause a different result when the fluorescence emission of the glass slides is tested. Moreover, the intrinsic variability of the fluorometer apparatus, namely temperature affected variations in the emitted light or in the detected signal can pose some difficulties when the results are compared. For example, measures taken at very different instants of time can be non-reliably compared. The present work considers an alternative method based on the calculation of signal ratios with the aim to reduce the effect of the intrinsically present variation caused by the utilized equipment.

Different ratios GNP/QDM (Gold Nanoparticles/Quantum Dots Micelles) (0.01 – 0.1) have been investigated in a hybrid material composed of PS surrounded CdS quantum dots and gold nanoparticles. The reducing agent Hexylamine has been used to provide an effective connection between quantum dots and metal nanoparticles. Samples belonging to series A (1A, 2A, 3A, 4A, 5A) present exclusively PS-CdS and gold. The numeric index stands for the increasing ratio GNP/QDM. The absence of Hexylamine provides the formation of a random dispersion of the two components. On the other hand, samples belonging to series B (1B, 2B, 3B, 4B, 5B) contain PS-CdS, Gold and Hexylamine and the considered GNP/QDM ratios are the same as series A. The added Hexylamine should ensure a closer proximity between the components. Finally, samples 0 and 00 respectively contain only PS-CdS and PS-CdS with Hexylamine. Each single glass slide has been produced three times and the results have been averaged.

Three different ratios have been established. R is the ratio between the emission with gold with Hexylamine over the emission with gold without hexylamine (R = B/A). This is useful to evaluate the effect of the reducing agent in the emission of samples containing the same (and increasing) amount of gold. What can be observed is that when the amount of gold is low, the emission of sample B is clearly lower than the one of A. As gold increases, the Hexylamine is effective in binding gold and QDs with the result that the ratio oversteps 1 indicating a stronger emission by sample B. From sample 3, the trend is reversed probably because the high amount of gold prioritizes the scattering effect. Furthermore, the results are affected by a high variability and error most likely due to an intense scattering caused by the high quantity of gold.

Ratio R1 reports the emission with gold without Hexylamine over the emission without gold without Hexylamine (R1=A/0). From sample 1 to sample 4 it is possible to observe a clear effect of auto absorption. In fact, the increasing amount of gold is responsible

for a decreasing ratio. Sample 5 seems to reverse the trend and it can be due to scattering. However, as previously asserted, this phenomenon, causes a large error that prevents from establishing a clear explanation for the position of the last sample.

Ratio R2 reports the emission with gold with Hexylamine over the emission without gold with Hexylamine (R2=B/00). The same decreasing trend observed in ratio R1 is still observable with the addition that the resulting curve is flattened. This means that the Hexylamine is effective in providing a close proximity among the components which, in turn, leads to a more consistent auto absorption effect. This is mostly visible in the comparison between ratio R2 and R1 for sample 1. In fact, in spite of the presence of error bars, the difference between R2 and R1 is appreciable. On the contrary, from sample 2, the errors cause the generation of undistinguishable results.

The present work was particularly useful in establishing that the addition of Hexylamine is effective in approaching nanoparticles and quantum dots by initially providing a stronger auto absorption effect which is visible in the ratio R lower than 1 and in the large gap between R1 and R2. The increase in the quantity of gold, subsequently, demonstrated that the close proximity between the two components causes an effect of photoluminescence enhancement, known as Metal Enhanced Fluorescence, observable in the ratio R which is higher than 1. Less clear is the trend with high amounts of gold, probably due to variability caused by the scattering phenomenon. Despite some weak points related to reproducibility and uncertain reliability on samples comparison, the present study offers numerous perspectives on the investigation of the interaction between quantum dots and metal nanoparticles in films deposited on rigid supports.

Keywords: CdS Quantum dots, Gold Nanoparticles, Raft copolymerization, Metal Enhanced Fluorescence, solvent annealing.

II. SCOPE OF THE THESIS

The scope of the present work is to thoroughly analyze the role and influence of the distance between fluorescent Quantum Dots and a plasmonic component (i.e. gold nanoparticles) in the fluorescence emission phenomenon. Various studies have been conducted about the performance of light emitting Quantum Dots in the presence of metal nanoparticles. However, most of the current literature, only reports results about analysis conducted in solution. On the contrary, few investigations have been carried out as far as the case of a layer of solution deposited on a support is concerned. In fact, many factors must be taken into account when the solution is spread over a surface. Among them, the evaporation of the solvent and the structure of the layer around the Quantum Dots play a fundamental role in defining the actual performance of a layer with respect to the one of a stable solution.

The utilized Quantum Dots for the present study are composed of Cadmium Sulfide and are characterized by a layer of Polystyrene around them. These so-called PS-CdS Quantum Dots have been produced through a method based on Raft Copolymer self - assembly which ensures the formation of the CdS in the core of a micelle. In particular, the Raft copolymer is dissolved in dioxane and subsequently cadmium acetate is added to generate a first step micellar structure which core contains the ion Cd^{2+} and a layer of PS plays the role of a corona. Later, by adding Sodium sulfide, a reaction with the inner ion occurs giving rise to a core of CdS surrounded by chains of PS. The work entitled "Enhanced Photoluminescence from Micellar Assemblies of Cadmium Sulfide Quantum Dots and Gold Nanoparticles" by Farinha et al. has been utilized as a guide line for the current thesis work. More specifically, their work applied to a solution of Quantum dots and Gold Nanoparticles has been adapted to study their interaction in the solid state by depositing a layer of hybrid material on a glass substrate.

The phenomena through which metal nanoparticles affect the Quantum Dots fluorescence are mainly three. One of them is likely to decrease the observable fluorescence while other two are likely to increase it. In particular, the effect called auto-absorption consists in a reduction of the resultant fluorescence because CdS QDs and Gold NPs respectively emit and absorb the same wavelength. Accordingly, part of the light emitted by quantum dots is reabsorbed by gold and this results in a decrease of the observable fluorescence. On the other hand, the intrinsic scattering emission by Gold NPs causes an increase in the apparent fluorescence. However, since scattering competes with absorption, it could also decrease the detected photoluminescence. In fact, scattering is really difficult to be unequivocally interpreted and its effect can reduce the reproducibility within samples. Moreover, the most interesting effect, is the so-called MEF or rather Metal Enhanced Fluorescence. This consists in the Plasmon resonant particles becoming surrounded by an enhanced localized electromagnetic field when excited at their local surface plasmon resonance (LSPR). The result is a local enhancement of the electric field in close proximity to the metal, which in turn leads to a more efficient excitation of QDs in the nearby micelle cores with a consequent growth in the final emission.

As previously anticipated, the main scope of the thesis work is to investigate the role of the distance between QDs and Gold Nanoparticles in a layer of solution deposited on a glass substrate. In order to produce a well-structured work, two different conditions have been studied. In the first one, a solution of PS-CdS with Gold Nanoparticles has been analyzed and the role of the distance has been hypothesized. With the aim to confirm the obtained result, a second condition has been established in which some homopolymer has been added to increase the initial distance between the two mentioned components. The last step was useful to verify the role of the close proximity between QDs and Metal NPs and, accordingly, the general influence of their reciprocal distance.

CHAPTER 1

THESIS INTRODUCTION

This first chapter presents the main role of introducing the whole thesis work in terms of background, contents, motivations, objectives, methods and thesis' structure description. In particular, the studied topic, or rather the interaction between fluorescent Quantum Dots and Metal Nanoparticles has widely been investigated since it represents a very promising subject as far as the development of bioimaging and sensors is concerned. What follows is a brief state of the art about the interaction between fluorescent components like Quantum Dots or fluorophores and plasmonic components like Metal Nanoparticles. This will be accompanied by the most significant information which is important to provide as prerequisites to thoroughly understand the conducted work. After, a more specific analysis will be dedicated to the present work with the aim to explain its fundamental meaning and importance.

1.1 BACKGROUND AND STATE OF THE ART

The heart of the current thesis work is the study of the interaction between Quantum Dots and Metal Nanoparticles. Thus, before presenting some of the reported results, it is fundamental to explain which are the commonly observed phenomena involved in the aforementioned interaction.

First of all, what is referred to as scattering is always present when Metal Nanoparticles (MNPs) are stimulated by an incoming radiation. This is a fundamental point as far as the experimental section of this thesis is concerned. In fact, as it will be better explained later, when the emission of a hybrid material composed of QDs and MNPs is measured, it is crucial to consider that MNPs are actually scattering light and it is necessary to find a way to distinguish the scattered light from the actual emission coming from QDs. Moreover, it is important to take into account that the measured emission can be both increased or decreased by the action of the scattering components (i.e. MNPs). In fact, if a direct analysis of a layer is performed (i.e. front – face analysis) the revealed signal is likely to be increased by the action of the metal. Therefore, the detector will receive a higher intensity compared to the one exclusively coming from the QDs. On the contrary, if a back – face analysis is conducted, the scattering action of MNPs is more likely to reduce the detected signal because the scattering direction is mainly opposite with respect to the detector's position.

Secondly, the so-called auto absorption effect plays a fundamental role in the field of QDs-metal NPs interaction. In fact, if the emission wavelength of QDs is similar to the absorption wavelength of MNPs, some of the radiation emitted by QDs will be stolen by MNPs and the detected signal will be lowered. Even though this is simply a general paragraph, an example is useful to understand the current point. Indeed, GNPs characterized by a diameter of 3-5 nm present a main absorption wavelength of 520 nm. In turn, similar sized QDs emit mainly at the same wavelength. Therefore, the auto absorption effect can occur and some of the emitted radiation coming from QDs will be retained by GNPs before reaching the detector.

Finally, the plasmonic effect or field effect is a very interesting phenomenon which is able to increase the signal coming from QDs. This effect gave origin to the topic of Metal Enhanced Fluorescence (i.e. MEF) where the term "enhanced" has been used to say that the presence of metal is able to strengthen the signal emitted by the fluorescent component (i.e. QDs). The MEF phenomenon has been explained by asserting that when metal nanoparticles are stimulated by a radiation, a local enhancement of the electric field around them takes place and consequently, a more efficient excitation of QDs occurs. In other words, MEF is caused by an increased excitation rate due to the enhanced local field experienced by QDs or fluorophores and the electromagnetic coupling with the metal NP situated nearby. [1] As a result, the fluorescence detected signal results to be increased.

All the previous effects are strongly related to the so-called Localized Surface Plasmon Resonance (i.e. LSPR) typical of metal NPs which is an important phenomenon occurring when an incoming radiation interacts with them. In particular, when a light beam hits a particle, it follows a mutual oscillation of electron charge in resonance with the visible light. This event is fundamental to explain the typical color of Gold nanoparticles, which depends on the absorbed and reflected wavelength, the consequent scattering phenomenon and the crucial increase of electric field around the particle, which gives rise to the aforementioned field or plasmonic effect providing what was referred to as Metal Enhanced Fluorescence.

An intense study has been conducted on the interaction between QDs and Metal Nanoparticles in solution. On the contrary, studying the same topic in the solid state, or rather analyzing the behavior of solid layers of a hybrid material composed of Quantum Dots and Metal Nanoparticles presents a higher level of complexity and consequently a lower level of knowledge and mastery. This inherent complexity is mainly due to the necessity of simultaneously taking into account the evaporation of the solvent and the structure of the layer around the Quantum Dots which play a fundamental role in defining the actual performance of a layer with respect to the one of a stable solution. Below, some examples of studies conducted in solutions and on solid hybrid layers are presented.

As far as studies in solution are concerned, their main goal is to understand the role of MNPs when these are located near to fluorescent quantum dots. More specifically a key role is played by the distance between the two components. In this regard, it is essential to refer to the problem of stability of QDs and MNPs. In fact, because of their high surface to volume ratio, due to their small size, either QDs and MNPs present a strong tendency to aggregate. Therefore, to maintain their properties, they have to be stabilized and this is done by functionalizing their surface. In addition, the mentioned surface functionalization is not only useful to keep QDs or MNPs apart. In fact, it is also fundamental to establish a binding between them without allowing them to touch. This proximity without contact is necessary to induce the MEF effect and to prevent the phenomenon of quenching which occurs when fluorescent and plasmonic components get into physical contact. If this happens, a reduction of the radiation emission is observed and the MEF effect is extinguished.

In their work, Huang et al. synthesized ZnCdSeS QDs-gold NPs hybrid in aqueous solution by using a bi-functional linker mercaptoacetic acid (MPA). [2] Here, the gold NPs are described as isolated metallic nanostructures in which the LSPR is excited because of the collective oscillations of free electrons. As a consequence, the electric field is enhanced as described above and the distance between metal and QD is reported to play an important role in varying the fluorescence enhancement. However, a drawback is described about studies conducted in solution. In fact, highly control is required on uniformity and dispersibility of nanoparticles which sometimes can be difficult to achieve. Both water and chloroform-dispersed QDs have been observed to show a peak of absorption at 520 nm. Likewise, GNPs showed their absorption peak at the same wavelength. In order to investigate the role of the amount of GNPs on the LSPR effect, different hybrids have been created with an increasing quantity of GNPs from 0 to 120 µl. The reported absorption spectra showed the same trend for GNPs, QDs and hybrid materials. However, the intensity of the absorption peak related to QDs resulted to increase as the amount of gold increased.

About the PL spectra, a clear fluorescence enhancement was observed only until the added amount of 60 µl of GNPs solution. In fact, when further gold was added, the result was a reduction of the fluorescence intensity. Therefore, Huang et al. affirmed that two mechanisms were competing. On the one hand, the PL enhancement due to the increase of absorption and radiative rate caused by LSPR and dominating only until the added amount of 60 µl of GNPs solution. On the other hand, PL quenching occurring when GNPs and QDs got into physical contact. This last phenomenon is attributed to energy and charge transfer between gold and QDs. Specifically, according to Yin et al. the main reason for this phenomenon is the reverse charge transfer occurring from semiconductor to the metal at the interface. [3] [2] To conclude, it is clear that until when GNPs are under a certain amount, their action is intended to increase the PL because of the LSPR and field effect. As soon as a limit is reached, a contact between GNPs and QDs occurs which causes the quenching to happen.

Another fundamental study, which provided the inspiration and a guide line for the current thesis work, was reported by Farinha et al. [4] By using a solution of tetrablock copolymer chains of poly (acrylic acid)-b-polystyrene-TTC-polystyrene-b-poly (acrylic acid), where TTC represents a single trithiocarbonate group, they induced micellization upon the addition of cadmium sulfide. Specifically, transient micelles were formed which were characterized by a poly (cadmium acrylate) core. Subsequently, through the addition of sodium sulfide, the formation of a single CdS quantum dot was observed inside a flower-like micelle which corona was composed of polystyrene and a TTC group per each "petal". The described structure takes the name of quantum dot micelle (QDM) and results to be very interesting because the addition of a reducing agent can effectively cut the TTC group giving rise to thiols which can, in turn, connect to the surface of GNPs. Therefore, a hybrid structure composed of GNPs and QDs in solution can be easily prepared. Moreover, the PS chains connecting QDs and GNPs provided a good obstacle against PL quenching and a precise location control of embedded NPs. Different amounts of GNPs have been added in order to study their action on photoluminescence and emission lifetime. In particular, the molar ratio of GNPs to QDMs has been defined as R_{GNP} and its investigated values have been 0.001, 0.007, 0.011, 0.015 and 0.077. A good colloidal stability has been observed and only a small increase of the hydrodynamic diameter of the conjugates following the GNPs increase has been reported.

As far as the photoluminescence analysis is concerned, Farinha et al. reported how GNPs can absorb some of the excitation radiation and also reabsorb some of the light emitted by QDs (i.e. auto absorption effect) by hiding the fluorescence enhancement given by the field effect. Therefore, in order for the latter to be visible, a correction needs to be applied on the measured emitted radiation. Moreover, an average emission amplification (i.e. EA) has been calculated by dividing the corrected emission intensity corresponding to each QDM-GNP by the intensity of the QDMs alone. The EA has been reported to increase as the R_{GNP} and the excitation wavelength increase.

Finally, Farinha et al. asserted that no significant change in the emission lifetime was observable, meaning that the interaction between QDMs and GNPs does not cause a significant change in the relaxation pathways of QDs. Moreover, they demonstrated that the observed enhancement was not determined by a simple scattering by GNPs. Instead they affirmed that GNPs act as antennae for the incoming radiation. Specifically, when excited at their LSPR, they become surrounded by an enhanced electromagnetic field able to optimize QDs excitation. [4]

About studies conducted on solid hybrid layers of fluorescent QDs and MNPs, the same mechanism to explain the MEF effect is still valid, as Lidong Li et al. [5] reported in their review. More precisely, they affirmed that the excitation rate of a fluorophore or a QD can be increased by the enhanced local field caused by the excitation of the LSPR. In addition, the nonradiative decay is accelerated resulting in an increased quantum yield and a decreased fluorescence lifetime. Another issue that was introduced for the study in solution and that is particularly crucial for hybrid films of QDs and MNPs is the control over their reciprocal distance. In fact, the fluorescence emitter (i.e. QD) has to be near enough to the plasmonic component since the field effect presents a nearly exponential decrease with distance from the metallic surface. On the other hand, an excessively short distance or even a contact, can result in an undesired PL quenching. Therefore, a spacer interlayer is necessary to separate QDs and MNPs and a linker needs to be used to bridge them. The advisable distance has been reported to be between 5 and 30 nm. [5] In order to realize such spacer/linker, different materials have been utilized, among which silica, synthetic polymers, DNA and proteins. Furthermore, different procedures can be applied to realize these hybrid nanostructures. For instance, lithographic techniques can provide nanopatterns characterized by high order and "precisely controlled sizes, shapes and interparticle separations". [5] However, this technique results to be expensive, time-consuming and not applicable to large area devices. In spite of being particularly difficult to apply, it has been used by Xiaoying et al. to create hybrid nanostructures of well-organized arrays of colloidal QDs and a self-assembled layer of GNPs. [6] Firstly, they produced lithographically generated nanoscale patterns with tailored surface chemistry in order to achieve a high selectivity and a precise confinement of QDs into well-organized arrays. After, a monolayer of close-packed GNPs was added to introduce the plasmonic component as a fluorescence enhancer.

SEM observations of the described structure confirmed the precise location of QDs only on the so-called anchor spots while no QDs have been observed in the inert regions of the silicon substrate. Moreover, a confocal microscope has been used to investigate the PL enhancement provided by the GNPs. It was observed that the size of the bright spots became larger with the increase of the pre-pattern spot size. Moreover, a clear enhancement of fluorescence intensity provided by GNPs was revealed. The same experiment has been conducted for red, yellow and green QDs and the calculated average enhancement factors for the three colors red, yellow and green were respectively, 4.6, 5.3 and 4.8. As far as green QDs are concerned, a clear auto absorption effect has been noticed. In fact, green QDs emit at 520 nm which is also the absorption wavelength associated to LSPR of about 5 nm sized GNPs. A further investigation has been conducted by Xiaoying et al. who produced Silica-covered CdSe QDs and used them for the same experiments previously described. Beside a higher induced local strain in the hybrid film compared to the case without Silica, a larger average enhancement factor of 11 has been reported. About the distance between QDs and GNPs, in the case without Silica its value has been calculated by summing the functionalization of both components and approximated to 6 nm. Differently, upon Silica encapsulation, the measured distance was 11 nm which seems to be the optimal one to achieve the highest enhancement factor.

Beside the described lithographic method, other procedures to realize hybrid films of QDs and MNPs have been developed. The common point to all these synthesis processes is the necessity to establish a good connection between the fluorescent and the plasmonic components by simultaneously controlling and tuning their reciprocal distance in order to vary the resulting fluorescence properties. In particular, the role of spacer can be taken by a dielectric layer, a Langmuir-Blodgett film, a polymeric structure or a biomolecular layer. [5] Specifically, the current thesis work is based upon the use of a polymeric layer which, in turn, results to be a very widespread and versatile method.

The application of polymeric materials as spacers has been allowed by the development of the spin-coating technique which permitted to prepare a polymeric matrix in the nanometer range. In fact, sometimes, the polymers not only serve as spacers, but also as a matrix for the QDs/fluorophores or MNPs to be embedded. [5] An interesting example is the work reported by Chen et al. [7] who deposited both CdSe QDs and GNPs on elastomeric polydimethylsiloxane (PDMS) and were able to tune the distance between the two components by simply applying an external stress on the PDMS film. Initially, the excessively close proximity between QDs and GNPs caused a fluorescence quenching. However, as the separation distance increased, under a higher external stress, the measured intensity increased accordingly, and a maximum was reached at the distance of 12 nm which is coherent with previously mentioned results. [6] The use of block copolymers (BCPs) as spacers found numerous applications in the field of interaction between QDs and MNPs. In fact, BCPs have been observed to be able to independently form ordered structures with diverse morphologies which can represent an ideal template to create large scale arrays for nano-photonic applications. Moreover, these structures can behave as plasmonic arrays because they can easily host QDs and MNPs which reciprocal position can be effectively tuned and controlled. For example, M. Haridas and J.K Basu have varied the density of GNPs and CdSe QDs independently inside a BCP matrix in order to investigate the role of these parameters on the final optical properties of the hybrid array. [8] [9] CdSe QDs capped with pyridine have been synthesized according to the method suggested by Peng et al. [10] and based upon the use of CdO as precursor instead of the normally utilized $Cd(CH_3)_2$ to produce CdSe, CdTe or CdS QDs. Moreover, thiol terminated polystyrene (PST) capped GNPs have been produced according to the method reported by Sutton et al. and based upon the reduction of gold chloride in the presence of PST. [11] In this case, the thiol group at the extremity of the PS chains allowed for a good interaction with GNPs. Furthermore, arrays of CdSe QDs and hybrid arrays of CdSe QDs and GNPs have been prepared using a BCP template composed of polystyrene and poly vinyl pyridine (PS-P4VP). Specifically, this BCP is known to form hexagonal arrays of cylinders of P4VP in the PS matrix. In addition, the selective interaction between pyridine ligands at the surface of the CdSe QDs and the P4VP in the BCP allows for the QDs to be located exclusively into the P4VP cylinders while the PST capped GNPs remain inside the PS region. This simplicity in precisely controlling location and dispersion of particles allows to independently control density and interparticle distance. The volume fraction of QDs was 0.0135 for all samples belonging to series C3L, while it was doubled to 0.027 for all samples of series C3H. In addition, the volume fraction of GNPs was varied from 0.0019

to 0.0056 in all samples. The most important conclusion which was reported involves PL emission which increased as the amount of gold increased. However, this effect was less pronounced in sample C3H than in C3L and this is because C3L samples had a lower amount of QDs and consequently more GNPs per QD were available and their effect in enhancing the PL was more visible. On the contrary, PL lifetime measurements revealed a lifetime decrease as the gold was increased, and this effect was more pronounced in C3H samples. The reason for this counter-intuitive event has been attributed by M. Haridas et al. to the lower interparticle distance of samples C3H compared to samples C3L, this resulting in a more efficient energy exchange among QDs mediated by GNPs. Moreover, the existence of two different lifetimes has been hypothesized. The first shorter one, or rather τ_1, originates from collective interaction among QDs, while the second longer one, or rather τ_2, is related to radiative electron hole recombination in isolated QDs. It has been observed that the first one becomes the dominant relaxation mode when the quantity of gold is increased, and it is much more affected than τ_2. In fact, this demonstrates the real interaction between QDs and plasmonic component. [9]

1.2 THESIS WORK PRESENTATION

Even though characterized by a further complexity, the fundamental subject of the current research work is the interaction between Quantum Dots (QDs) and Gold Nanoparticles (GNPS). Specifically, what was thoroughly investigated is the role of the close proximity between the two components in enhancing the photoluminescence which is a typical feature of Quantum Dots. In particular, Quantum Dots are constituted by a semiconductor material, such as CdS, CdSe or CdTe and belong consequently to the category of inorganic fluorescent materials. On the contrary, fluorophores are also defined as organic dyes and their behavior differs from the one of the mentioned Quantum Dots. However, they will not be specifically considered here. Both Quantum Dots and fluorophores are referred to as fluorescent components, while metal nanoparticles, usually made of Gold or Silver, are defined as plasmonic component.

The necessity to understand and explain the complex variety of phenomena arising from the interaction between QDs and MNPs, which was explained in the previous paragraph, justifies the interest towards the current field and represents the main motivation for the related research. In fact, this inherent complexity contributed to render QDs and metal NPs very interesting and astonishing. Thus, their characteristics have been studied for decades and Metal Enhanced Fluorescence has recently become a really hot topic. By providing an increased emitted fluorescence by QDs, beside a better photo stability, the presence of a plasmonic component seems to be able to improve the field of optoelectronics, such as photonic devices and sensors, and the area of biological applications, such as biomarkers and imaging devices. About the last-mentioned application, the intrinsic toxicity of QDs seems to represent an obstacle against their usage into human bodies, but an appropriate treatment like the one described in this thesis, and based upon a surrounding polymer layer, seems to be promising in guaranteeing a better compatibility.

As far as the current research work is specifically concerned, two main approaches have been conducted with two different objectives. Initially, a layer of CdS QDs surrounded by a corona of Polystyrene (PS) (i.e. PS-CdS) was dropped on a glass substrate. Later, the dipping into a reducing agent called Hexylamine was thought to able to treat the PS chains by cutting a group called TTC and dividing the PS chains into two halves, each of which terminating with a thiol group (i.e. -SH). The latter should have provided the connection with the added GNPs. Moreover, the treatment with different amount of solvent THF should have provided a different swelling of the PS by causing a different interparticle distance between QDs and GNPs. This would have provided the opportunity to study the role of the distance between the two components in establishing a certain fluorescence emission. However, technical difficulties were encountered when the reducing agent was added, and no encouraging results were obtained. Therefore, a different approach was applied which consisted in the drop casting and solvent annealing of an already prepared solution of QDs and GNPs

with and without the presence of Hexylamine. In this way, two conditions were compared, namely a first random dispersion of GNPs among QDs when no Hexylamine was present, and a more ordered situation when the close proximity between the two components was ensured by the addition of Hexylamine. To overcome complications arising from the employed apparatus, a system of ratios comparison was applied. Specifically, instead of comparing the direct emission of samples, ratios of emissions were rather compared. More precisely, three ratios were established, namely R, R1 and R2. R is the ratio between the emission of the sample with GNPs and Hexylamine and the emission of the sample with GNPs without Hexylamine. By preparing different samples with an increasing amount of GNPs, it was possible to test the action of the reducing agent in the different conditions. Moreover, R1 and R2 are respectively the ratios between the emission of the sample with GNPs and without GNPs in absence and presence of Hexylamine. They were particularly useful to establish the role of Gold in both the studied conditions. A final theory was elaborated according to which when the role of Hexylamine is tested, if the amount of gold is kept low, the consequence of the close proximity induced by the reducing agent is mainly the auto absorption effect. Oppositely, an evident field effect arises from the addition of further GNPs. Finally, uncertain results appeared with a high quantity of GNPs probably due to the intense scattering. Moreover, if the role of gold is observed, a stronger auto absorption effect is reportable if an increasing amount of metal is added. To conclude, the addition of Polystyrene Homopolymer was utilized to verify the current theory.

The objective of identifying a pattern in the relationship between QDs and GNPs was achieved by applying the explained method of ratios establishment since the previous attempts didn't properly work. This was due to issues related to the incapability of the reducing agent to correctly affect the deposited layer of PS-CdS prior to the application of GNPs. However, some minor drawbacks were still present in the applied method, which caused some points to remain unresolved. For instance, a component of results uncertainty and unreliable comparability remained because of various reasons. Firstly, considerable differences affected replicates of samples which were averaged, and which were supposed to have the same features. Instead, because of synthesis issues related to solvent annealing, they presented inequalities which rendered the results affected by a large error which made the comparison not always significant. Specifically, the long time elapsing between the production of the first and last sample was not advisable since different conditions of temperature, humidity and pressure could have seriously affected the obtained results. Moreover, a more reliable and precise drop casting method should have been applied to reduce thickness inequalities which could have caused unwanted differences among results. However, despite the presence of minor problems, a good and thorough study on the relation between QDs and GNPs was conducted together with a deep investigation on the role of their reciprocal distance. The latter opened good perspectives on the possibility of improving the field of biological imaging based on the use of PS-CdS as a biomarker which performance could be improved by GNPs as a plasmonic component providing Metal Enhanced Fluorescence.

The present thesis work is organized in four different sections. In particular, after this introductory chapter, Chapter 2 illustrates all materials and methods utilized for the current thesis work to prepare raw materials and to assemble them into the final analyzed device. Chapter 3 reports a detailed list of all the conducted experiments with the obtained results together with a qualitative explanation. Subsequently, Chapter 4 makes some conclusions by better explaining the results introduced in Chapter 3 and by providing a more precise explanation, leading to a final theory to explain the interaction between QDs and GNPs mediated by the action of Hexylamine. In addition, the unresolved problems are listed, and applications and future perspectives are suggested. Finally, an Appendix presents an analytical overview on all the touched topics and it has an explanatory role, useful to understand the meaning of the conducted research. Specifically, a short insight on polymer chemistry is reported with particular attention dedicated to RAFT copolymerization. After, it follows some theory about QDs and Metal NPs with the main occurring phenomena when they are approached. Finally, a detailed state of the art is reported about the study of their interaction in solution and in the solid state.

CHAPTER 2

MATERIALS AND METHODS

INTRODUCTION

This second chapter is intended to describe all materials and methods that have been used in the current thesis work. In particular, the followed steps to produce the Tetrablock Copolymer and a description of it will be presented first, followed by the explanation of the synthesis and characterization methods for CdS QDs and GNPs. Subsequently, two different approaches will be described which have been chronologically applied to build a layer of hybrid material composed of CdS QDs and GNPs on a glass substrate. More precisely, the qualitative results obtained with the first approach will be presented here to motivate the procedural change towards the second approach. Chapter 3 will be entirely dedicated to describing the results obtained with the two different approaches. The utilized nomenclature for samples identification will be thoroughly explained and finally the investigation procedures applied to the mentioned samples will be elucidated. Materials and methods that are about to be listed and described here have been taken directly from the work by Farinha et al. entitled "Enhanced Photoluminescence from Micellar Assemblies of Cadmium Sulfide Quantum Dots and Gold Nanoparticles" which, as previously asserted, represents the fundamental source of inspiration for the current work.

2.1 SYNTHESIS OF TETRABLOCK COPOLYMER

As far as the polymer is concerned, it is essential to underline that it is a symmetric tetrablock copolymer characterized by chains composed by two Polystyrene groups, two Poly Acrylic Acid groups and a central Trithiocarbonate group. In order to obtain the final polymeric structure, three main steps have to be performed, namely the production of the RAFT chain transfer agent (CTA), the synthesis of the PAA-TTC-PAA Macro-CTA and finally the polymerization of styrene. The first step is achieved by mixing hexane (60 ml), carbon disulfide (13.77 g), chloroform (58.81 g), acetone (26.26 g) and tetrabutylammonium hydrogen sulfate (1.21 g). Subsequently, an aqueous solution of sodium hydroxide 50 wt % (100.99 g, 1.26 mol) has to be added dropwise over a period lasting about 90 minutes. In order to dissolve the solid, 600 ml of water must be added followed by the addition of 60 ml of concentrated HCl (37%) to lower the solution's pH. The so obtained brown-colored solid is purified by repeated recrystallizations in a mixture of acetone and hexane to produce the final yellow crystalline solid. In figure 1 the formula of the final trithiocarbonate-based CTA is reported.

As it will be better illustrated later, the TTC group (highlighted in red in figure 1) plays a fundamental role because it provides the polymer chain with the capability of being cut by a reducing agent. In particular, in the present work this action is accomplished through the addition of Hexylamine which is able to brake the bonds between carbon and sulfur by giving rise to two thiol terminated chains.

Once the CTA is adequately produced, it is used to provide the polymerization of Acrylic Acid previously distilled under vacuum. Farinha et al. [4] reported a final conversion of 97 % achieved after a polymerization procedure of 90 minutes. Figure 2 illustrates the effect of the CTA on the Acrylic Acid monomer resulting in the synthesis of the macro chain transfer agent PAA-TTC-PAA.
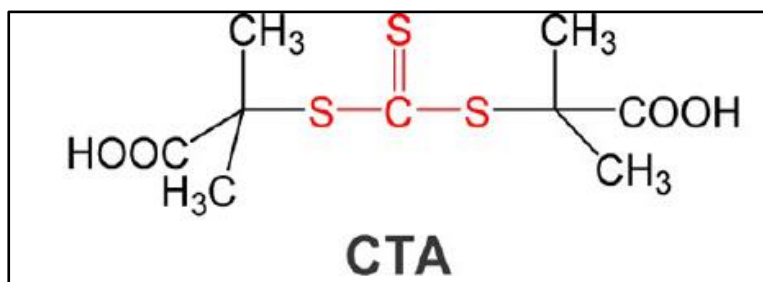
Figure 1: RAFT Chain-Transfer Agent (CTA) *[4]*
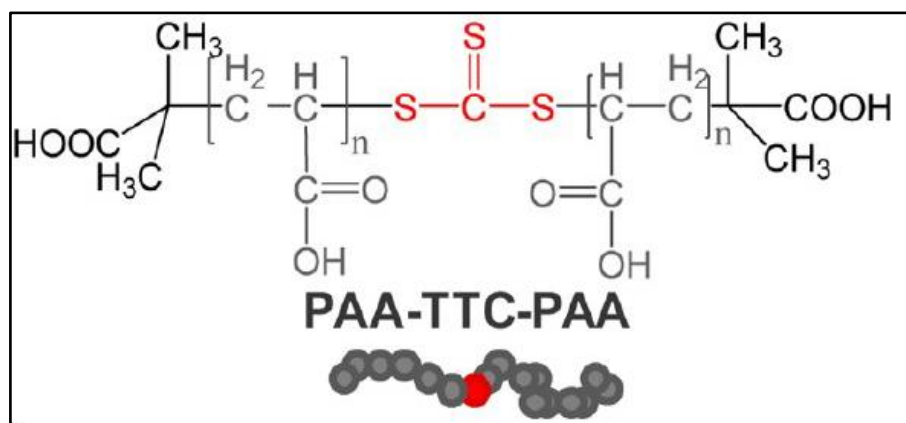
Figure 2: Synthesis of PAA-TTC-PAA *[4]*

The so produced macro chain transfer agent is used to carry out the polymerization of the Styrene monomer. In particular, 1.60 g of RAFT macro CTA, 10.1 g of DMF, and 1.40 g of Styrene are mixed in a Schlenk tube through a magnetic stirrer. A polymerization of 46 % was reported by the group. In figure 3 it is possible to observe the final symmetric tetrablock copolymer. It is important to mention the last step of precipitation in methanol and dissolution in THF followed by further reprecipitations in methanol and final drying to ensure a complete removal of DMF [4].
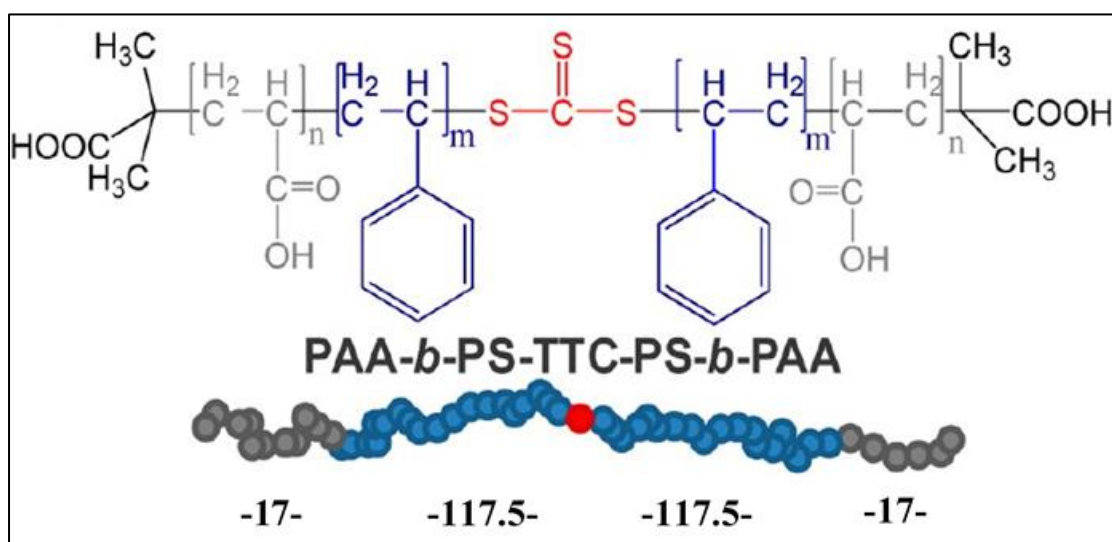
Figure 3 Final symmetric tetrablock copolymer *[4]*

The final tetrablock copolymer is thus characterized by two lateral blocks of Poly Acrylic Acid composed of 17 repeating units each, two intermediate blocks of Polystyrene composed of 117.5 repeating units each and a central molecule of trithiocarbonate that will be fundamental in the synthesis procedure of CdS QDs.

The described series of steps to produce the tetrablock copolymer hasn't been part of the current thesis work. In fact, the substance had already been produced at "Centro de Química-Física Molecular" at Instituto Superior Técnico in Lisbon – Portugal.

2.2 CADMIUM SULFIDE QUANTUM DOTS MICELLES (CdS QDMs)

The present paragraph is devoted to explaining the synthesis method to produce fluorescent CdS QDs and to characterize them with respect to their size and fluorescence emission. A brief description of the working principles at the base of the employed techniques will be provided followed by the analysis conducted on rough measurements to obtain specific results.

2.2.1 CdS QDMs Synthesis

In order to produce CdS Quantum Dot-containing Block Copolymer Micelles (QDMs), the previously described PAA-PS-TTC-PS-PAA tetrablock copolymer was dissolved in filtered 1-4 dioxane to a concentration of 0.5% w/w. To provide a perfect solubilization, the dispersion was kept at 25° C overnight under a vigorous magnetic stirring. Thereafter, the formation of micelles with poly (cadmium acrylate) cores was induced by adding a 0.25 M solution of $CdAc_2$ in methanol to a stoichiometric ratio of 1 mol of $CdAc_2$ per mol of COOH group. More specifically, in order to determine the mass of $CdAc_2$ and the volume of methanol to mix, it is useful to recall that molarity is defined as the ratio between the number of moles of solute (mol) and the volume of solvent (l). Moreover, the number of moles is equal to mass (g) divided by molecular weight (g/mol). Therefore, to find the mass of $CdAc_2$ to be used, it is important to highlight that the number of moles of $CdAc_2$ is exactly the same as the number of moles of the COOH groups. In turn, the moles of COOH are the same as the moles of PAA which can be calculated based upon the added mass of tetrablock copolymer, by remembering that each polymer chain has 34 PAA repeating units. It follows an example of a series of numeric steps to clarify this procedure.

$$Polymer\ Moles = \frac{Polymer\ Mass}{Polymer\ MW} = \frac{0.0306\ g}{27000\ g/mol} = 1.1333 \cdot 10^{-6}$$

$$PAA\ Moles = Polymer\ moles \cdot 34 = 3.8533 \cdot 10^{-5}$$

$$PAA\ Moles = CdAc_2\ moles$$

$$CdAc_2\ Mass = CdAc_2\ moles \cdot CdAc_2\ MW = 0.0102\ g$$

$$0.25\ M = \frac{CdAc_2 moles}{Vol\ MeOH} \rightarrow Vol\ MeOH = \frac{CdAc_2 moles}{0.25}$$

$$Vol\ MeOH = \frac{3.8533 \cdot 10^{-5}}{0.25} = 0.1541\ ml$$

An important consideration that needs to be made is that in order to simplify synthesis procedures and to ensure an accurate result, it is always advisable to work with easily measurable quantities. Therefore, since the obtained amounts were too low to be accurately measured, a bulk 0.25 M solution of CdAc$_2$ in methanol was previously prepared and the amount corresponding to the volume of solvent (i.e. 0.1541 ml) was added to the solution of tetrablock copolymer and dioxane. The obtained solution was kept under vigorous magnetic stirring overnight at 25° C. In figure 4, it is possible to observe the micellization occurring when cadmium acetate gets into contact with the tetrablock copolymer. In particular, as previously introduced, a core of poly (cadmium acrylate) is generated which is surrounded by a layer of PS. Furthermore, the core is characterized by the presence of ions Cd^{2+} which are generated when cadmium interacts with the solvent dioxane and which are crucial for the following step. In fact, in order to synthesize a quantum dot into the micelle core, the addition of a 1.9 M solution of Na$_2$S in a mixture of 1:1 methanol and water is necessary. Specifically, it was added to a ratio of 0.4 mol of Na$_2$S per 1 mol of COOH groups.
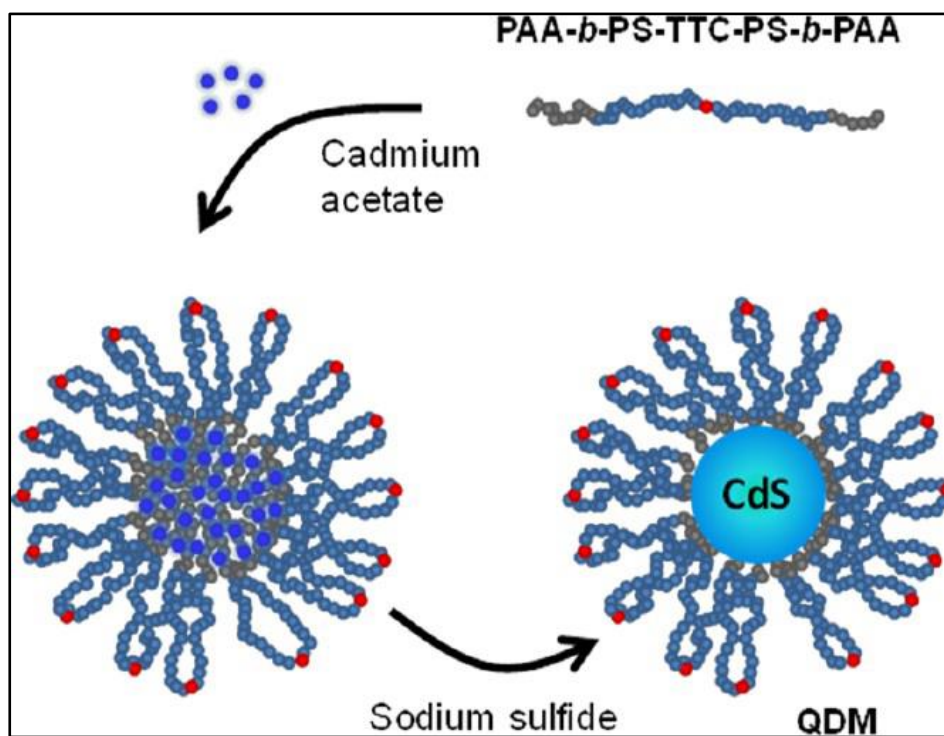
Figure 4 PS-CdS QDMs synthesis based upon mixing of tetrablock copolymer, cadmium acetate and sodium sulfide solutions *[4]*

Therefore, as previously done, once the number of moles of COOH or PAA has been calculated, it is easy to define the number of moles of NA$_2$S by imposing a ratio of 1:0.4. Next, the required Na$_2$S mass can be defined and finally, by applying the molarity definition with a value of 1.9, it is possible to calculate the right amount of solvent to be added. Specifically, this volume has to be composed by 50 % of water and 50% of methanol. It follows a numeric example.

$$PAA\ Moles = Polymer\ moles \cdot 34 = 3.8533 \cdot 10^{-5}$$

$$Na_2S\ Moles = PAA\ Moles \cdot 0.4 = 1.5413 \cdot 10^{-5}$$

$$Na_2S \; mass = \; Na_2S \; Moles \cdot Na_2S \; MW = 0.0012 \; g$$

$$1.9 \; M = \frac{Na_2S \; moles}{Vol \; Solvent} \rightarrow Vol \; Solvent = \frac{Na_2S \; moles}{1.9}$$

$$Vol \; Solvent = \frac{1.5413 \cdot 10^{-5}}{1.9} = 0.0081 \; ml = 8.1 \; \mu l$$
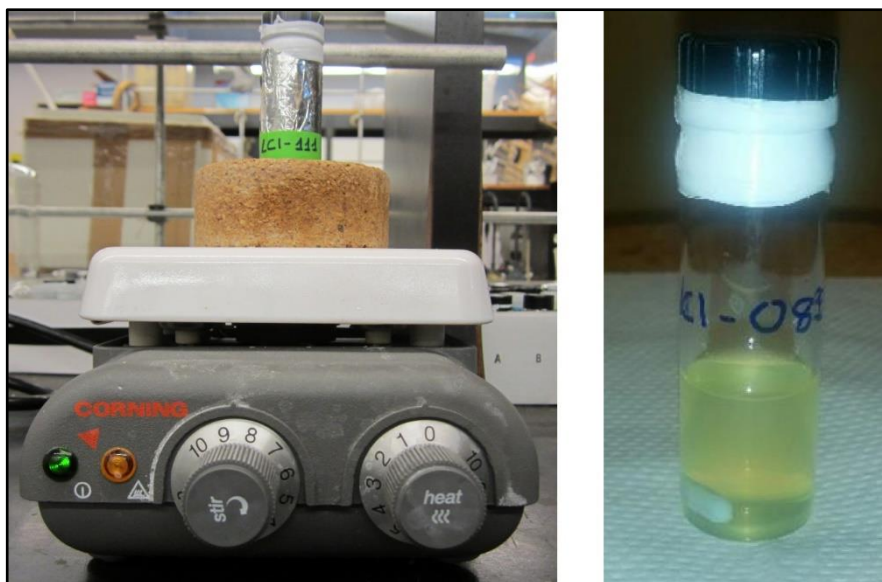
Figure 5 PS-CdS QDMs solution in vial protected by aluminum foil under magnetic stirring
and non-wrapped vial showing a homogeneous yellow PS-CdS QDMs containing solution

Since the resulting mass and volume are very low and difficult to be accurately measured, a bulk 1.9 M solution was previously prepared and 8.1 µl added to the main solution. A few seconds after the addition of Na_2S, the color of the dispersion turned into yellow as a confirmation that the synthesis of CdS QDs had occurred. Figure 5 illustrates the formation of a single QD into the micelle core which is surrounded by a PS corona. More precisely, the so-called quantum dot micelle (QDM) presents a "flower like structure" because each chain around the core looks like a petal which apex is characterized by the presence of the TTC group. The produced dispersion was kept overnight at 25° C under vigorous magnetic stirring. Moreover, protection from light was ensured by wrapping the vial in aluminum foil to prevent QDs photobleaching and the concentration was maintained unaltered by sailing the vial with Teflon tape. Figure 5 shows the utilized magnetic stirrer and the vial containing the dispersion for sample n.111. Moreover, a non-wrapped vial of sample n.083 shows the yellow color and the homogeneous appearance of the solution where the PS layer is able to impart to the QDs a good organic solvent solubility allowing them to be well dispersed and to maintain their properties.

2.2.2 CdS QDMs Characterization

In order to thoroughly characterize the produced CdS QDMs, two main fields have been considered. First and foremost, it is essential to identify their dimension mainly because the amount of gold that will be added later, to create the hybrid material, depends on it.

Therefore, the UV-vis absorption technique was applied. Secondly, a photoluminescence analysis is required to verify the optical quality of the QDs. The latter was performed by using a Xe lamp fluorometer. Finally, size and fluorescence are related as explained in the Appendix. Consequently, UV-vis absorption and fluorescence analysis must display a good coherence.

2.2.2.1 CdS QDMs dimensional characterization

To determine the quantum dots size, UV-vis absorption was applied. This technique, meaning "Ultraviolet-visible spectroscopy" or "Ultraviolet-visible spectrophotometry" is based upon the use of light in the visible and adjacent ranges. In particular, in this region of the electromagnetic spectrum, atoms and molecules undergo electronic transitions. More specifically, absorption spectroscopy measures transitions from the ground state to excited states. On the contrary, fluorescence spectroscopy deals with transitions from the excited state to the ground state. The main principle at the base of UV-vis is that molecules which possess π-electrons or non-bonding electrons (i.e. n-electrons) can absorb energy in the form of ultraviolet or visible light in order to excite these electrons to higher anti-bonding molecular orbitals. The more easily excited the electrons (i.e. the lower energy gap between the HOMO and the LUMO), the longer the wavelength of light they can absorb. There are four possible types of transitions (π-π*, n-π*, σ-σ*, and n-σ*), and they can be ordered in the following way σ-σ* > n-σ* > π-π* > n-π*. [12]

A typical UV-vis absorption spectrum is obtained by stimulating a sample within a range of wavelengths some of which are absorbed. Specifically, the peaks position depends on the present molecules and functional groups. Indeed, it is possible to conduct a qualitative analysis to identify which elements or groups are being observed. Moreover, UV-vis is routinely used to carry out quantitative determination of different analytes and the so-called Beer-Lambert law states that the measured absorbance is directly proportional to the concentration of a certain analyte. In particular, the complete relation is the following:

$$A = \log_{10} \frac{I_0}{I} = \varepsilon c L$$

In the previous equation, A is the absorbance, I_0 is he intensity of the incident light at a certain wavelength, I is the intensity of the transmitted light, L the so-called path length through the sample, ε the extinction coefficient or molar absorptivity which is typical of each species and wavelength and finally c in the concentration of the absorbing species. Moreover, the absorbance can also be related to the transmittance, the latter being defined as the ratio between the intensity of light passing through the sample and the intensity of light before it passes through it. In particular, transmittance is expressed as a percentage and the equation relating transmittance and absorbance is the following:

$$A = -\log(\%T / 100\%) \text{ [12]}$$

UV-vis spectroscopy was applied to the solution containing PS-CdS QDMs. More specifically, a cuvette containing pure solvent (i.e. 1-4 dioxane) was previously inserted into the UV-vis spectrometer to set the base line of the measurement by using the command "Blank". Next, a diluted PS-CdS QDMs solution in 1-4 dioxane (10% V/V) was prepared and the absorption analysis was performed through the command "Sample". More precisely, the same measure was performed three times following a 90° rotation of the cuvette each time in order to average the obtained values and to obtain more significant results. Because of quantum confinement effects, nanoscale semiconductors exhibit a distinct shoulder which can be used in conjunction with the band edge to calculate particle sizes and size distributions. [4]

Figure 6 shows a typical absorption spectrum corresponding to a solution of PS-CdS QDMs. On the X-axis, the excitation wavelengths are indicated, while the absorbance values are reported on the Y-axis. Two important absorption threshold wavelength

values need to be considered. First, the so-*called shoulder absorption threshold* corresponds to the wavelength at which the slope begins to increase. In other words, this is the point coinciding with the shoulder tip. Second, the *edge absorption threshold* is a wavelength value which can be identified as the intersection of the lines respectively tangent to the "edge area" of the peak and the spectrum base line.
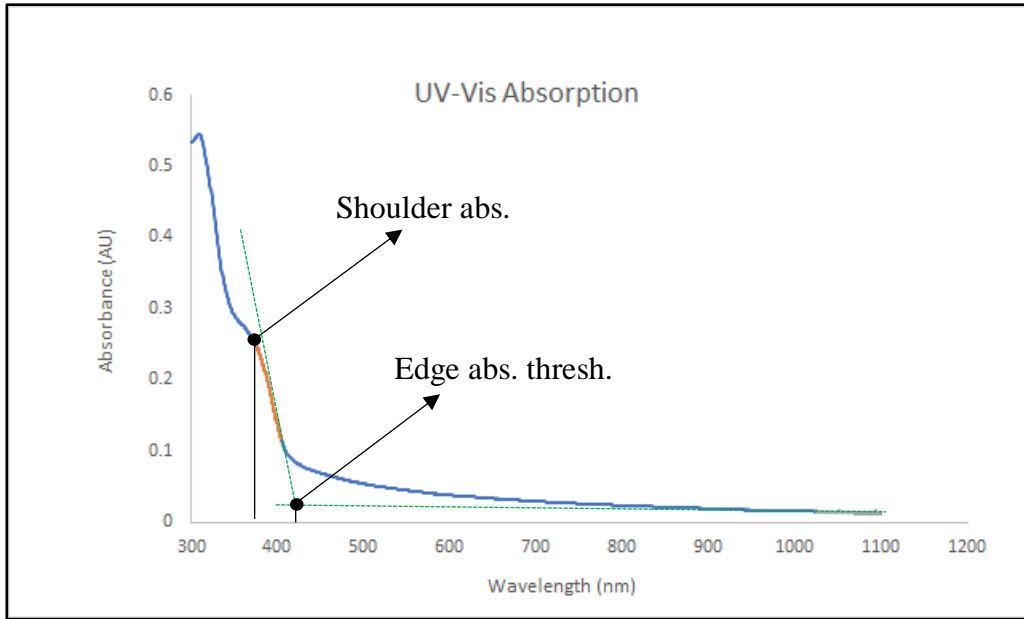
Figure 6 Typical UV-vis absorption spectrum of PS-CdS QDMs solution

In order to estimate the QDs diameter (i.e. D_{CdS}) the following expression was applied where λ_{thresh} can either be the shoulder or the edge absorption threshold.

$$D_{CdS}\ (\lambda_{thresh}) = 1/(0.1338 - 0.0002345\ \lambda_{thresh})$$

Consequently, two different values of diameter are provided, namely $D_{CdS}(\lambda_{sh})$ and $D_{CdS}(\lambda_e)$ if the shoulder or the edge absorption threshold is utilized respectively. Specifically, the two diameter values reflect the presence of different size distributions among the produced QDs. As far as the present thesis work is concerned, the shoulder absorption threshold was utilized to calculate the mean particle diameter which resulted to be in the range 2-3 nm for each produced solution.

2.2.2.2 CdS QDMs optical characterization

The second important characterization procedure that was conducted on the produced PS-CdS samples, was intended to investigate their optical properties. In particular, their photoluminescence (i.e. PL) emission was tested by using the Xe lamp fluorometer F900 Edinburgh Instruments which is shown in figure 7.

Specifically, this instrument is based upon a tunable radiation emission provided by a Xenon lamp (labelled as A in figure 7) which interacts with a sample situated in a sample holder, identified as E. When the studied sample is a solution, it is kept in a cuvette container which can easily be secured under the cover and interacts with the incoming radiation as shown in figure 8. As explained in the Appendix, the energy absorbed by QDs is useful to promote electrons towards higher energy levels. Subsequently, the jump to the ground state is identified as emitted photons which are recognized by the detector labelled as B in figure 7. In order for the

13

Xe lamp to be warm enough to properly emit the desired radiation, a time of 45 minutes is required. After that, the temperature is kept constant by a system of fans. Furthermore, the detector needs to be kept at low temperature, to accurately measure the emitted radiation and this is accomplished by using the cooling system labelled as C.
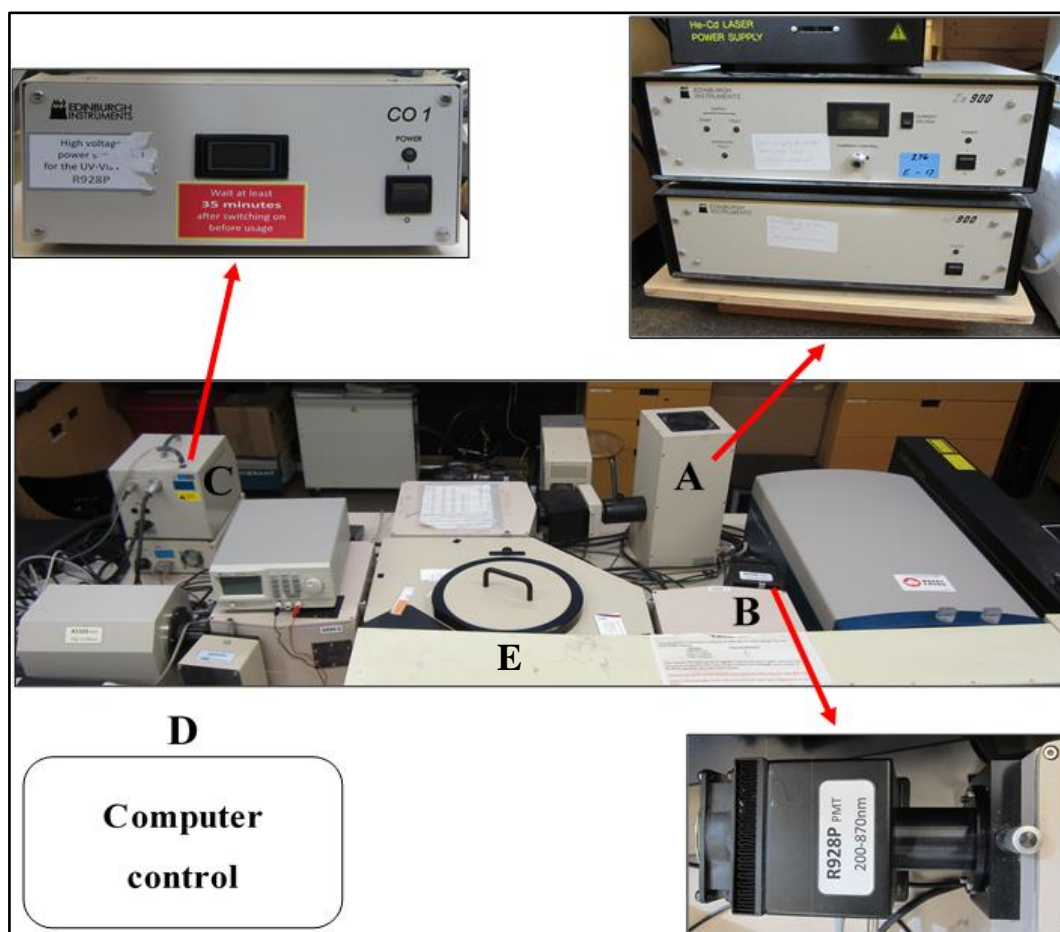
Figure 7 Xe lamp fluorometer apparatus: (A) Xe lamp, (B) Detector, (C) Detector cooling system, (D) Computer control for data storage, (E) Sample holder

This Xe lamp fluorometer is able to emit a specific wavelength, to perform the so-called *emission measurement* on the QDs solution, or to emit a certain range of wavelengths to perform an *excitation measurement* as it will be explained below. The selection of the desired mode is made by a computer which also displays the resulting spectra and allows to manipulate and storage the obtained results.

A detailed schematic of the radiation path is visible in figure 8. [13] Specifically, the Xenon lamp produces a broad spectrum of high intensity radiation in the UV-Vis-IR range. After, the arc from this lamp is imaged onto the entrance slit of the excitation monochromator, which selects a specific excitation wavelength with a specific bandwidth. Subsequently, this radiation passes through a beam splitter, where a small percentage is reflected onto a reference detector, an iris, which is able to control the intensity, and is finally focused into the sample. A lens system collects a portion of any luminescence from the sample and focuses it onto the emission monochromator. The latter selects a wavelength and a spectral bandwidth of the emission and finally passes the light into a photomultiplier tube (i.e. PMT) that is specifically what is labelled as B in figure 7.

As previously introduced, a software can be used to select *excitation* or *emission measurement*. Precisely, as far as the former is concerned, the Xe lamp emits a radiation in a certain wavelength range and the different wavelengths are selectively absorbed by the sample according to its nature and properties. This means that some of the produced wavelengths will be absorbed by the sample while others will be simply transmitted. The resulting spectrum will show high values of counts on the Y-axis corresponding to

those wavelengths which are highly absorbed. On the contrary, those wavelengths which are not absorbed result as low values of counts. Intuitively enough, the spectrum resulting from this analysis will be similar to the one obtained with the UV-vis spectroscopy measure. In fact, they both provide information on those wavelengths which are more likely to be absorbed. In figure 9, a typical excitation spectrum is shown.
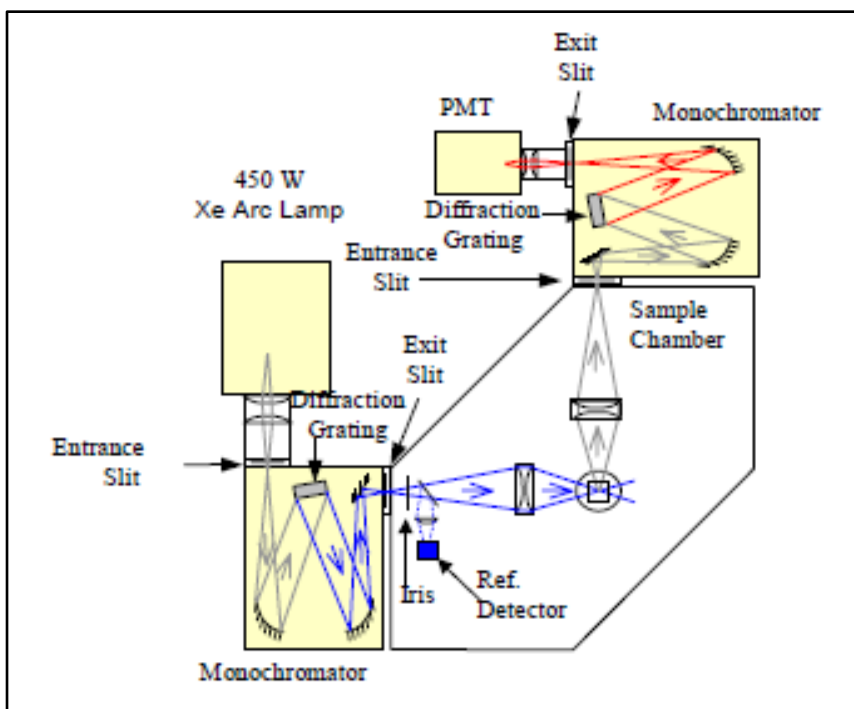
Figure 8 Schematic representation of the light path from the Xe lamp to the detector *[13]*

As it is observable, the excitation range of wavelengths coming from the Xe lamp is 300-500 nm. This chosen range reflects the previous knowledge related to the fluorescence emission of 2-3 nm sized QDs presenting a peak at about 520 nm. Since it is known that the maximum emission peak is situated at this wavelength, it is useful to excite between 300 and 500 nm which is slightly below 520 nm.
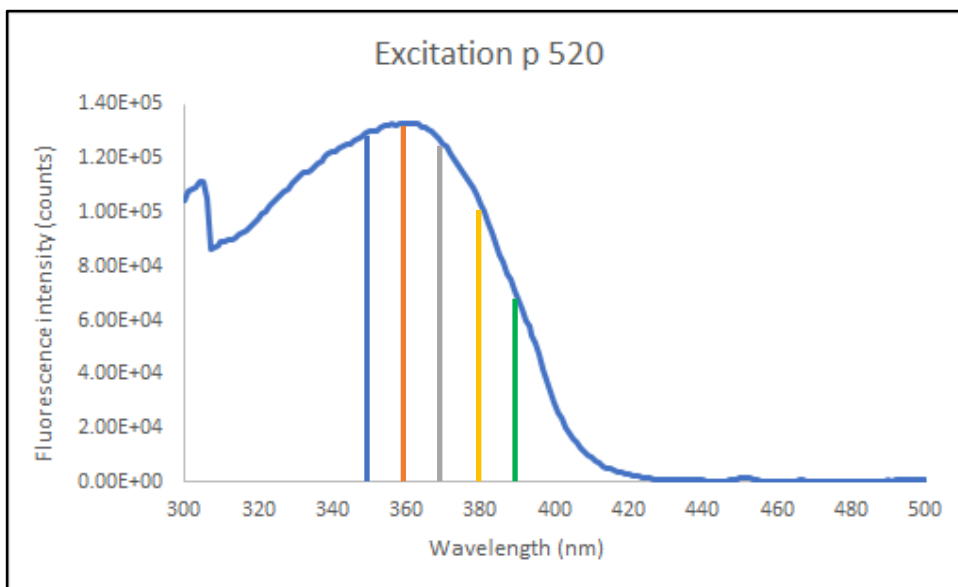
Figure 9 Typical excitation spectrum of PS-CdS QDMs solution

The counts values on the Y-axis are a clear indication of how intensely the different excitation wavelengths are absorbed by the PS-CdS QDMs solution. Specifically, it can be noticed that the most absorbed wavelength is about 360 nm which corresponds to the peak of the excitation spectrum. The wavelength 350 nm is slightly more absorbed than 370 nm which is followed by 380 and 390 nm. This means that if the sample is excited exclusively at the most absorbed wavelength (i.e. 360 nm), it will show the highest emission intensity. In fact, in order to evaluate the PL radiation emitted by the sample after it is hit by a monochromatic signal, the so-called emission measurement can be selected and performed. Figure 10 illustrates the result of this experiment. In particular, the sample was stimulated with different monochromatic radiations, namely 350, 360, 370, 380 and 390 nm. As previously anticipated, the emission spectrum presented a peak at about 520 nm and its intensity reached the maximum value when the incoming radiation was 360 nm, or rather the most absorbed one. The other wavelengths showed a corresponding decreasing intensity from 350 to 390 nm.
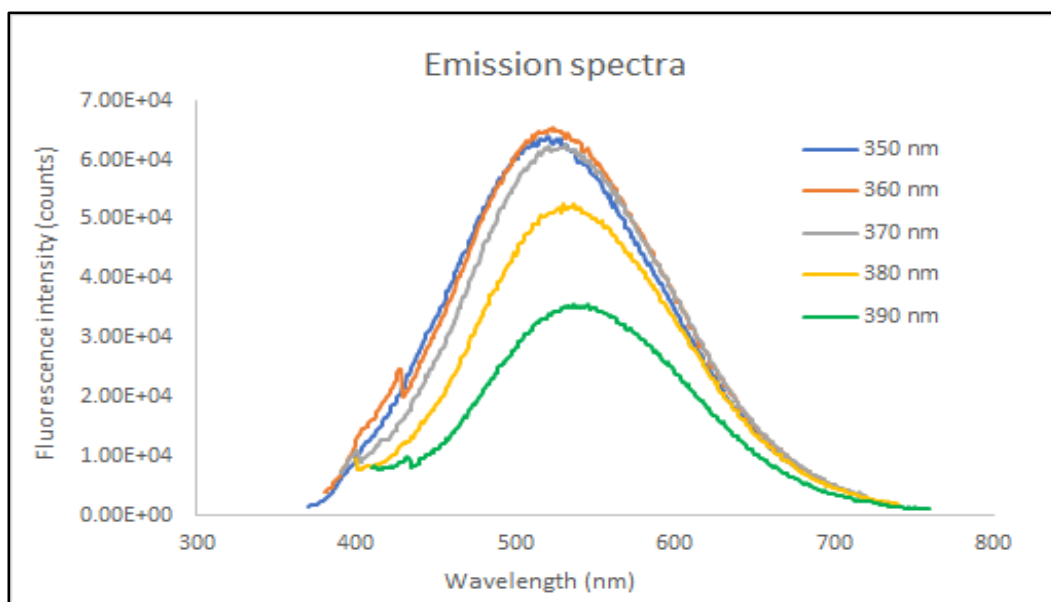
Figure 10 Typical emission spectra of PS-CdS QDMs solutions excited at increasing wavelengths (350, 360, 370, 380 and 390 nm)

Beside the decreased intensity following the increased excitation wavelength, another important phenomenon which had already been observed by Farinha et al. [4] involves the peaks position. In fact, as it can be seen, as the wavelength is increased from 350 nm to 390 nm, the emission peak slightly shifts towards longer wavelengths. This phenomenon has been attributed to the particle size distribution by asserting that larger and lower energy particles within the distribution are more likely to be excited at higher wavelengths.

Finally, it is necessary to comment on the good coherence existing between UV-vis spectroscopy measure and fluorescence analysis. As it is affirmed in the Appendix, the bigger the QDs size, the longer the emitted wavelength. In fact, the calculated QDs diameter (i.e. 2-3 nm) has been observed to emit at about 520 nm in previous works. [4] [6] Consequently, it is possible to conclude that the produced sample is properly working, and the dimension of 2-3 nm and the corresponding emission wavelength of 520 nm can be confirmed.

2.3 GOLD NANOPARTICLES (GNPs)

The present paragraph deals with production and characterization procedures for water based- and toluene based-gold nanoparticles. In fact, even if the majority of the current thesis work has been conducted with gold nanoparticles dispersed in toluene, at the beginning of the study, some gold nanoparticles dispersed in water have been produced. Therefore, the applied synthesis method will be described to produce water and toluene based-GNPs and the characterization procedure based on transmission electron microscope (TEM) will be explained.

2.3.1 Water based-GNPs synthesis

As thoroughly illustrated in the Appendix, the so-called Turkevich synthesis method has been applied for decades to produce water dispersed gold nanoparticles with tunable emission. [14] The same method was reproduced during the current thesis work because the original idea was to study the interaction between QDs and water dispersed GNPs to investigate the swelling effect of the PS chains around PS-CdS, induced by the addition of THF as it will be explained later. Even though this path was finally abandoned, it is worth describing how GNPs dispersed in water can be easily and effectively produced.

The first step consists in the preparation of a 0.01% solution of gold chloride trihydrate ($H[AuCl_4] \cdot 3H_2O$) which was produced by mixing 0.01 g of powder with 100 g of water in a three-neck round bottom flask with a capacity of 250 ml. The latter was mounted on a fume hood support so that it could be close to a glass container situated beneath. The container was filled with paraffin oil and placed on a round heating plate which could provide magnetic stirring as well and a magnetic stirrer was inserted into the flask to ensure the solution mixing. The heating plate was switched on and the temperature was set at 100°C by using a thermometer inserted into one of the necks of the round bottom flask. The thermometer sensor had to be submerged into the liquid solution to detect the reached temperature, but it had to be kept at the right depth not to be hit by the rotating magnetic stirrer. Next, the paraffin oil container was risen until when the round bottom flask was into the oil for about 1/3 of its diameter or, more generally, until when the solution level coincided with the external oil level. This step is fundamental to transmit the heat to the gold chloride solution so that the desired reaction can occur. In figure 11, a schematic representation of the described apparatus is visible.
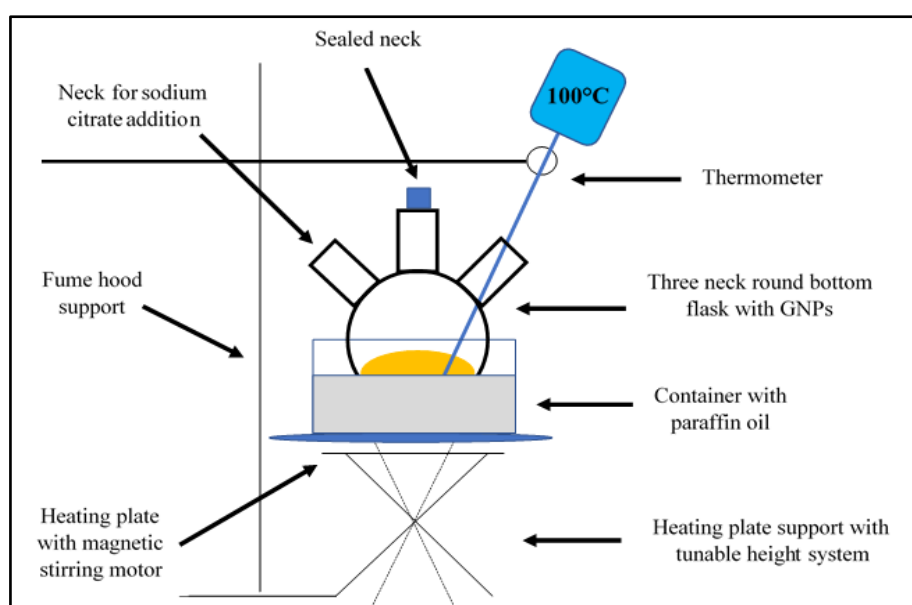
Figure 11 Schematic representation of Turkevich method apparatus

While the temperature increases, a 1% w/w solution of sodium citrate in water needs to be prepared. In particular, this component is fundamental to stabilize the GNPs and to prevent them from aggregating. Thus, as soon as the previous solution reached 100° C and began to boil, 2 ml of the sodium citrate solution were added through one of the three necks of the flask. The first step of nucleation began about 30 seconds after the addition and it was identified thanks to the color turning to blue. During the next 5 minutes, the solution was left under boiling and stirring and after about 70 seconds, the color changed from blue to red indicating the formation of monodisperse GNPs. After 5 minutes, the heating plate was switched off and lowered in order to allow a gradual cooling of the round bottom flask containing the formed GNPs solution. The latter was left under magnetic stirring until when the room temperature was reached. After that, the GNPs aqueous solution was moved into a plastic bottle to be later characterized.

2.3.2 Toluene based-GNPs synthesis

In order to investigate the interaction between GNPs and QDs and the influence of their reciprocal distance, toluene based-GNPs have been employed. The previously introduced Brust method has been applied in the following way. First and foremost, it was necessary to produce an aqueous solution of $H[AuCl_4] \cdot 3H_2O$. Specifically, in order to synthesize a 0.30 mM solution, 0.118 g of $H[AuCl_4] \cdot 3H_2O$ were mixed with 10 ml of deionized (D.I.) water. As far as this first step is concerned, it is important to underline how difficult and simultaneously fundamental it is to accurately measure the exact amount of material to achieve the desired final result. In particular, the extremely high reactivity of $H[AuCl_4] \cdot 3H_2O$ caused a visible interaction with the utilized metallic spatula and it was arduous to transfer to the vial all the material picked up on the spatula surface. Therefore, it was extremely useful and functional to utilize as a scoop the upper part of a glass pipette which was less reacting in the presence of $H[AuCl_4] \cdot 3H_2O$. The so produced solution was transferred to a 150-ml round bottom flask which was positioned on a magnetic stirring plate and kept on equilibrium with a cork round support. Moreover, a magnetic stirrer was inserted, and the solution was left under vigorous stirring for 15 minutes. Meanwhile, a solution of tetraoctylammoniumbromide (ToABr) in toluene was prepared. To achieve a molarity value of 50 mM, 0.729 g of ToABr powder were mixed with 26.7 ml of pure toluene. The present solution was independently stirred for 15 minutes and subsequently mixed with the aqueous solution of gold chloride. The obtained solution was left under vigorous stirring for 30 minutes. As it is illustrated in the Appendix, ToABr is an effective phase transfer agent and it is able to move the gold from the aqueous phase to the organic one. Indeed, after the first 30 minutes a phase separation was observed, and all the gold was situated within the organic phase. The stabilizing role that was carried out by sodium citrate in water based-GNPs, is now fulfilled by dodecanethiol which needs to be added to the previous solution under stirring. Thus, 67 µl of pure dodecanethiol were added dropwise and the solution was left under vigorous stirring until the bottom was clear. The amount of time that was necessary to accomplish this step varied according to the sample under production and was in a range of 10 – 20 minutes. Finally, a reducing agent must be added in order to transform the gold into gold nanoparticles. Therefore, a 0.4 M aqueous solution of sodium borohydride ($NaBH_4$) composed of 0.126 g of $NaBH_4$ and 8.33 ml of water was freshly prepared and added dropwise quickly to the previous solution. The role of $NaBH_4$ is to carry out reduction which is simultaneously controlled and finally arrested by the previously added dodecanethiol. The so produced solution was left under vigorous stirring and at room temperature overnight.

The following day, after having separated and discarded the water phase, a fundamental step had to be carried out which consisted in the solvent evaporation achieved through a rotovap machine. In figure 12, the appearance of the GNPs-containing organic phase is shown, while figure 13 illustrates a schematic of the utilized rotovap apparatus. [15] Precisely, the label A represents the round bottom flask containing the previously prepared GNPs solution while B is a water container which temperature can be increased and controlled.

Figure 12 GNPs-containing toluene phase before solvent evaporation

First and foremost, the round bottom flask must be clamped and put under rotation. Next, the water container needs to be risen until when the flask is submerged enough into the water, which temperature can be adjusted in order to favor the solvent evaporation. The pumping system can be connected by the outlet labelled as H and the pump action begins to be effective when the valve is opened. Specifically, the combined action of rotation, heating and pumping induces a rapid evaporation of the solvent which is extracted from A and re-condensed in another flask labelled as G. The immediate condensation is allowed by the presence of a cooling system composed of circulating cold water indicated as F in the picture. Moreover, a clamping system made of vertical and horizontal components is able to fix all parts together (E and D). The rotovap procedure is quite complex to be carried out in a proper manner. In fact, different parameters have to be controlled together. For example, temperature must be kept at the right level to ensure an appropriate evaporation rate. Likewise, rotational velocity doesn't have to be excessively high. Even more importantly, when the pump begins to suck an intense bubbling is likely to occur in the evaporating solution. This must be avoided because an exploding bubble could cause some material to reach the pumping system with a consequent damage of it. Therefore, beside an attentive way of proceeding and to act on the outlet pumping valve, a component called bump trap (C) is positioned between the round bottom flask and the pumping and condensation area. This element can capture the material eventually coming from an exploded bubble and can prevent it from reaching vital components. Finally, the apparatus which was actually used for the current thesis work was equipped with a further condensation system based upon dry ice. In particular, a second condenser was immersed in a container full of dry ice which low temperature (-78°C) ensured a complete solvent condensation before its vapors could reach the pump.

After a time varying from 5 to 15 minutes, almost all the toluene was evaporated, and the remaining material appeared as a very viscous black solution. To obtain the final result, a washing step in ethanol and acetone was performed. More specifically, the 150-ml round bottom flask containing the GNPs was filled with pure ethanol and left about 12 hours to let the nanoparticles set apart. In fact, after this time it was easy to observe a clear deposition of GNPs at the bottom of the flask. Subsequently, the ethanol was discarded, and the flask was filled with fresh pure ethanol again. The same procedure was repeated with ethanol another time and with acetone twice. The amount of time that was necessary to achieve particles deposition was shorter and shorter as the number of washing steps increased. In fact, few minutes were required to obtain particles settling down after five washings. Finally, after the last acetone discard, the obtained GNPs were dried in the vacuum oven at room temperature overnight.
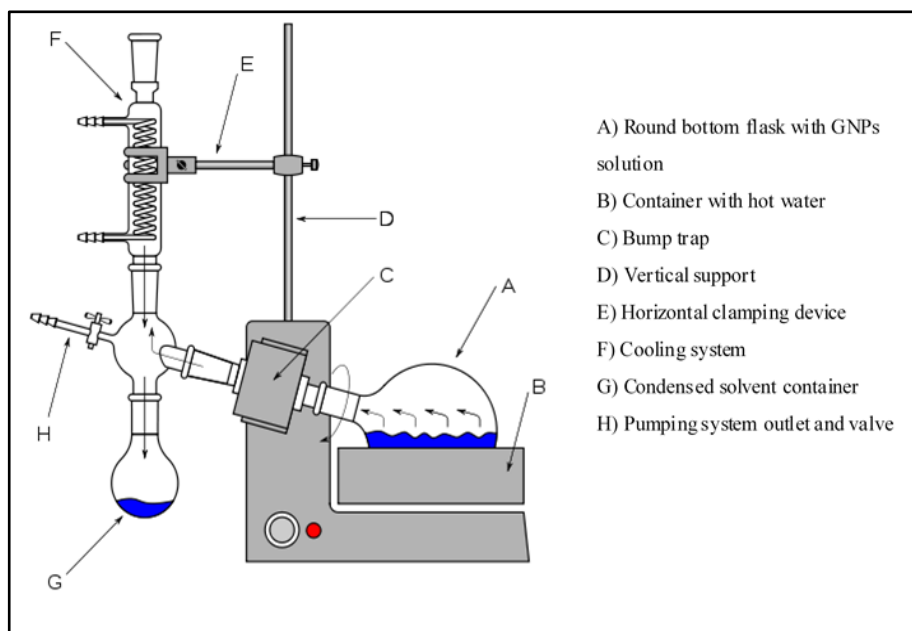
Figure 13 Schematic representation of Rotovap apparatus *[15]*

2.3.3 GNPs dimensional characterization

In order to dimensionally characterize the produced GNPs, a transmission electron microscope (TEM) was utilized. Specifically, both water based- and toluene based-GNPs were characterized by the same TEM. This machine is also sometimes defined as conventional transmission electron microscopy or CTEM and implies a beam of electrons which is transmitted through a specimen to form an image. In order for this specimen to be crossed by the beam, it has to be characterized by an ultrathin section which is often less than 100 nm. Alternatively, a grid can be utilized as a support for the suspension to be analyzed. As the beam is transmitted through the specimen, the interaction of electrons with the sample produces the final image which is then magnified and focused onto an imaging device such as a fluorescent screen, a layer of photographic film, or a sensor like a charge-coupled device. [16]

The higher resolution which is provided by a TEM compared to an optical microscope, is due to the smaller de Broglie wavelength of electrons. In fact, the maximum resolution d that can be obtained with a light microscope has always been limited by the photons wavelength and the numerical aperture (NA) of the system according to the following relation where n is the index of refraction of the medium in which the lens is working and α is the maximum half-angle of the cone of light that can enter the lens.

$$d = \frac{\lambda}{2n \sin \alpha} = \frac{\lambda}{2NA}$$

In order to calculate the electrons wavelength, it must be remembered that it is related to their kinetic energy by the de Broglie equation. However, an additional correction must be made to account for relativistic effects, since in a TEM an electron's velocity approaches the speed of light. In the following expression, h is the Plank's constant, m_0 is the rest mass of an electron and E is the energy of the accelerated electron.

$$\lambda_e = \frac{h}{\sqrt{2m_0 E \ (1 + \frac{E}{2m_0 c^2})}}$$

The electron beam can be produced in two different ways, namely by thermionic or field electron emission. More precisely, the emission source can be a tungsten filament or needle, or a lanthanum hexaboride (LaB$_6$) single crystal. In both cases, the gun is connected to a high voltage source (i.e. 100-300 kV) and thanks to the application of a sufficient current the gun will emit electrons by one of the two mentioned processes into the vacuum. Moreover, a so-called Wehnelt cylinder provides preliminary focus of the emitted electrons into a beam and the upper lenses of the TEM focus the electron beam to the desired size and location. Figure 14 shows two different electron beam sources while figure 15 illustrates a whole TEM apparatus. [16]
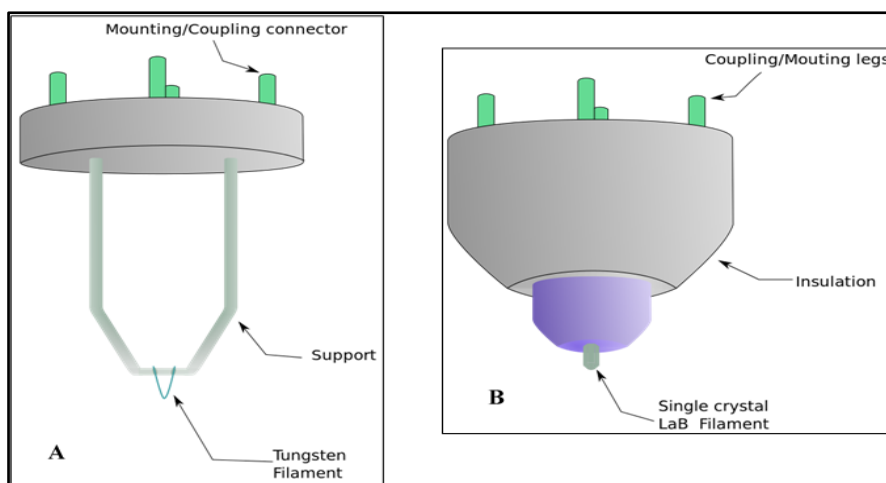
Figure 14 Tungsten filament electron beam source (A) and single crystal LaB$_6$ electron beam source (B) *[16]*

To provide the desired manipulation of the electron beam, two physical effects can be exploited. First, magnetic fields are useful to cause electrons to move according to the left-hand rule. Second, electrostatic fields can be used to deflect electrons through a constant angle. The formation of a shift in the beam path is obtained by coupling two deflections in opposing directions, resulting in an easy control over the beam path. After the beam crosses the sample, it contains information about electron density, phase and periodicity and it is thus useful to produce the image.

Sample preparation for a TEM observation is not trivial. In fact, as previously asserted, in order for the image to be produced, the electron beam needs to be transmitted through the sample. This implies that the sample must be extremely thin and to fulfill this requirement, a specific grid must be utilized. In particular, the mentioned grid is a 3-mm diameter circular support characterized by numerous cells which can host the sample. More precisely, a drop of sample has to be deposited on the grid and the necessary time for the solvent to evaporate needs to be waited. Different grids can be found which can be more or less appropriate for the different samples to analyze. Specifically, regular TEM grids can be made of copper, molybdenum, gold or platinum while more performing grids present a further layer of formvar before a superficial carbon layer. In fact, for the current thesis work, carbon covered grids were used.

With the aim to produce an observable sample, a single drop of GNPs dispersed in water or in toluene was deposited on a grid which was clamped with tweezers. For water based-GNPs it was necessary to wait for about 3 hours for the water to completely evaporate. Oppositely, a drop of GNPs dispersed in toluene dried much more quickly due to the high vapor pressure of toluene. Once the grids were ready, they could be inserted into the TEM apparatus by using the specimen port after having equalized the pressure in the TEM chamber. After the sample was located into the holder and the specimen rod was approached to the TEM, it was necessary to make the vacuum into the TEM chamber before completing the insertion.
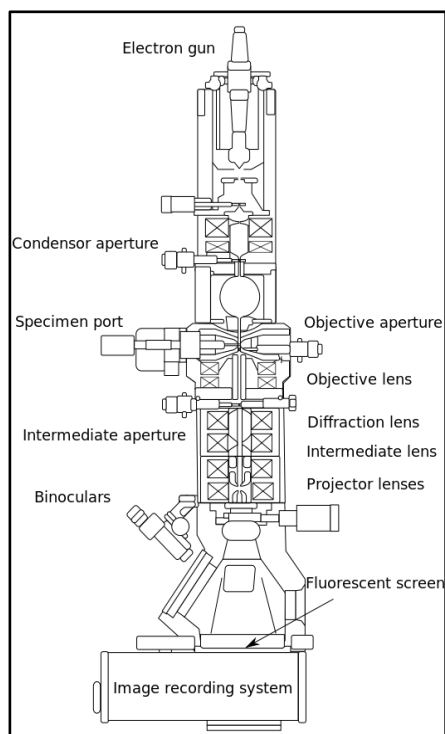
Figure 15 Layout of optical components in a basic TEM
[16]

Once properly inserted, the LaB$_6$ filament could be switched on and thanks to the vacuum the electron beam could properly move along its path. By using specific software and instrumentation to adjust brightness, magnification, focus and sample investigation area, it was possible to capture multiple images of GNPs. Specifically, three different images corresponding to three different areas were kept per each sample. Figure 16 shows an example of a captured image of water based-GNPs (A) and toluene based-GNPs (B).
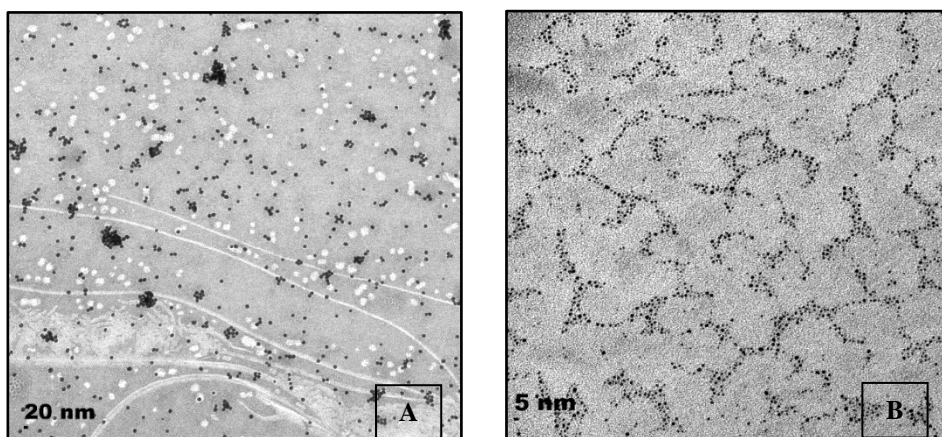
Figure 16 TEM pictures of GNPs dispersed in water produced by Turkevich Method (A)
and GNPs dispersed in Toluene produced by Brust Method (B)

As it can be seen in the previous picture, water based-GNPs present a bigger dimension, namely about 15 nm, compared to toluene based-GNPs which dimension is around 3 nm as it will be reported and discussed later. This different dimension makes much more difficult to take a picture of GNPs dispersed in toluene than in water. In fact, it is not easy to combine brightness and magnification in order to clearly distinguish GNPs which at low magnification appear simply as cloudy and blurry areas.

In order for the dimensional characterization to be performed, the captured images were used and elaborated by the software *Image J.* In fact, it allows to import the image, set a scale in pixels which corresponds to the picture scale (i.e. 20 or 5 nm) and to draw

22

lines along the diameter of GNPs which can consequently be measured instantaneously. About 150 GNPs were measured per each picture corresponding to a certain area on the grid. Next, the dimensions of the 150 GNPs were averaged among them and the three averages were further averaged among them. Figure 17 (A) illustrates the applied procedure to define GNPs dimension by *Image J* and specifically it is applied to GNPs dispersed in toluene. Figure 17 (B), instead, shows a dimensional distribution which was calculated for the specific sample LC1-090.
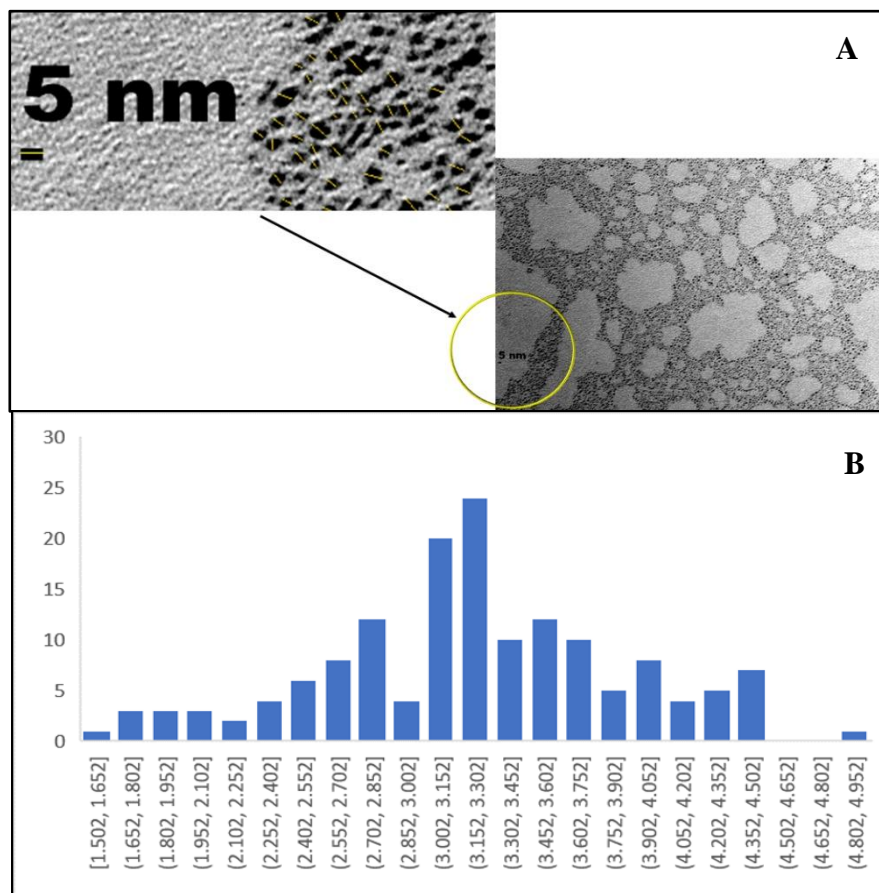
Figure 17 Applied procedure to calculate GNPs size by Image J (A) and dimensional distribution in sample LC1-090 (B)

As said above, the first step consists in imposing that a certain number of pixels, selected by drawing a line along the scale bar, corresponds to 5 nm (or 20 nm). At this point, the software is equipped with a correspondence between pixels and nm. As a consequence, every time a line is drawn it is possible to know how many nm it corresponds to. Therefore, 150 lines were drawn along the GNPs diameter to define its length as visible in the zooming situated in the left corner of the picture.

As far as water based-GNPs are concerned, the obtained dimension was about 14 nm with a standard deviation of about 2.6. The latter high value was probably caused by an inexperienced use of the software Image J and by an inaccurate drawing of the lines along the diameter of GNPs. However, it must be underlined how simple it is to tune the GNPs dimension by simply varying the amount of added sodium citrate. In fact, if more stabilizer is added, a thicker layer of negative charges will be present on the surface of GNPs resulting in a lower aggregation and a lower final GNPs dimension. On the contrary, if a small amount of sodium citrate is added, GNPs are more likely to aggregate and their dimension results to be increased. Figure 18 (A) shows a schematic of a layer of negative charges around GNPs which can be made thinner or thicker by varying the quantity of sodium citrate which is added during the synthesis procedure. However, water based-GNPs were not considered as useful as toluene based-GNPs for the current thesis work. Therefore, only the latter were finally produced and characterized systematically. Specifically, the obtained diameter dimension was always between 2 and 3 nm and the standard deviation was around 0.6 reflecting a better experience in the use of Image J and a good sample monodispersity. The dimensional control of GNPs dispersed in toluene is not as easy as in the case of GNPs dispersed in water. In fact, Brust method is based upon the addition of the reducing agent $NaBH_4$ after the stabilizer

dodecanethiol has already been added. In fact, the reduction is controlled and finally arrested by the dodecanethiol. However, its quantity is not as effective as the one of sodium citrate in defining the final dimension which tunability results consequently arduous. Nevertheless, GNPs present a very high interaction with the thiol group (i.e. -SH) which can be easily connected to the surface in order to functionalize it. As it will be illustrated later, thiol-functionalized GNPs are extremely versatile and useful for the current thesis work because a good connection with QDs can be established. In figure 18 (B) an example of GNPs stabilized by dodecanethiol is shown together with an example of their versatility demonstrated by the connection with chains characterized by a thiol extremity and a variable second extremity (red or green). [17]
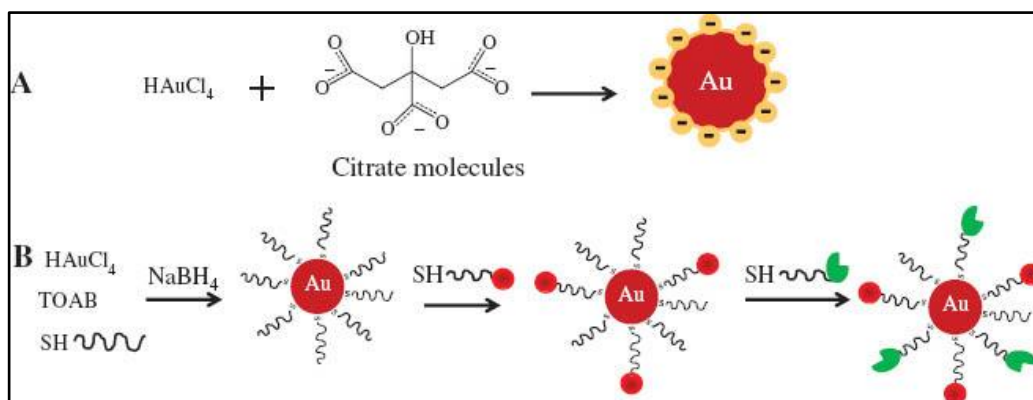
Figure 18 Sodium citrate stabilized GNPs in water (A) and dodecanethiol stabilized GNPs in toluene (B) *[17]*

2.4 SOLID HYBRYD LAYER OF QDs AND GNPs

The present paragraph is devoted to explaining how the hybrid layer of QDs and GNPs was produced and studied. In particular, different approaches were investigated and will be listed in a chronological way starting from the first and most random attempt until the last and most appropriate one. This variety of approaches derived from an initial uncertainty about the best way to study the interaction between fluorescent QDs and plasmonic GNPs leading to an observable enhanced fluorescence as illustrated in the Appendix. Despite the mentioned plurality of approaches, the same chemical principle can explain the connection between QDs and GNPs. In fact, as previously anticipated, the TTC group present at the apex of the petal-like structure around each QD can be cut by the action of a reducing agent such as hexylamine. As a result, the thiol terminated-PS chains which are obtained, can be utilized to establish a connection between QDs and GNPs. Regardless of the amount of hexylamine, the instant when it was added and the ratio between QDs and GNPs which all varied according to the applied approach, the mechanism leading to an interaction between the two components is the same and it is illustrated in figure 19.

In particular, the single bonds between carbon and sulfur in the TTC group, highlighted in red in the previous figure, are cut when hexylamine is added. Subsequently, sulfur atoms complete their octet by adding a Hydrogen atom coming from the hexylamine itself. As a result, each quantum dot results to be surrounded by thiol (i.e.-SH) terminated PS chains which can establish an effective connection with GNPs. Thus, when the latter are added, a hybrid material is generated which is composed of fluorescent QDs and plasmonic GNPs. As it was already explained, distance plays a fundamental role in determining the resulting effect of their interaction as well as the amount of added plasmonic component. Farinha et al. reported a theoretical DLS-derived z-average hydrodynamic diameters of the QDs (i.e. Dh) of 45 ± 0.2 nm providing an average PS shell thickness, and thus a mean QD-GNP distance, of ~20 nm. However, they asserted that the individuated interparticle distance was overestimated because of two reasons. First, since the polymer chains are not rigid, the intrinsic conformational flexibility leads to a minimum QD-GNP distance which is considerably lower than the mean value.
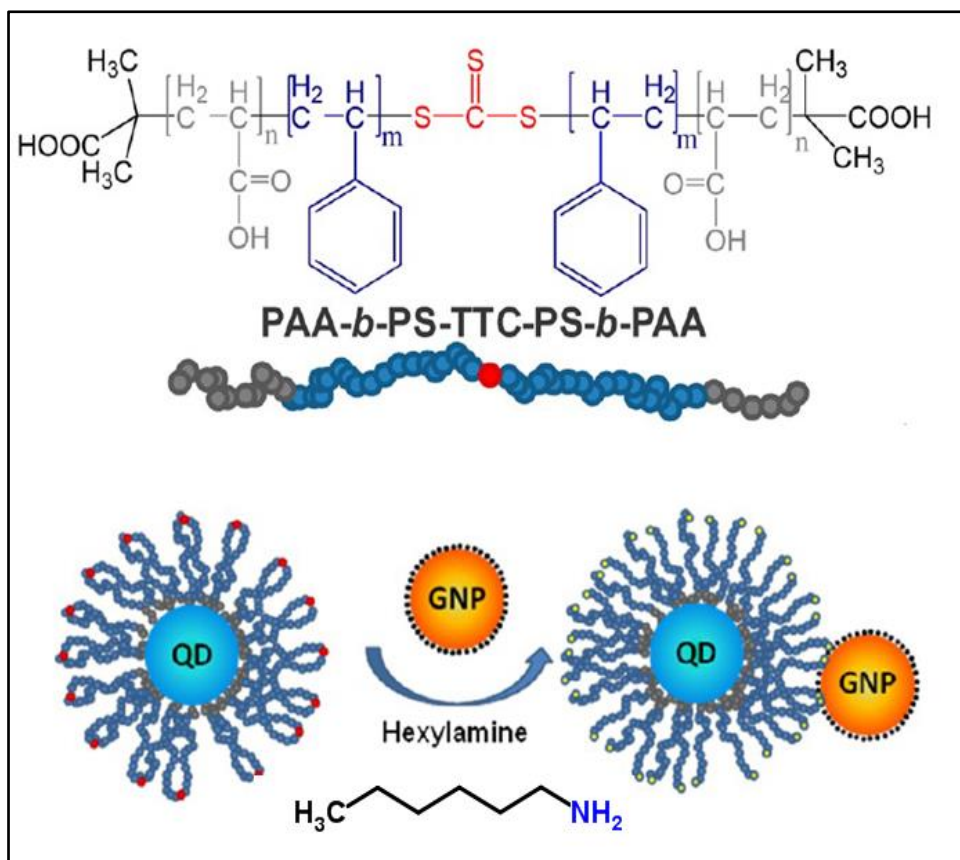
Figure 19 Hexylamine role in establishing QDs-GNPs connection *[4]*

Second, as a mean value, the z-average diameter obtained with DLS reflects the higher end of the size distribution and therefore it results to be oversized. In conclusion, a more accurate value of QD-GNP distance, even though slightly influenced by solvent evaporation, was determined by TEM and it was ~3 nm. [4] Even if a specific study on the reciprocal distance between the two components was not carried out in the present thesis work, the relation between GNPs concentration and QDs-GNPs distance will be hypothesized in the following chapters.

As far as samples nomenclature is concerned, it will be presented step by step when the different research approaches will be considered. However, the general rule that was applied is based upon the utilized laboratory book. In fact, each sample is identified with the initials of the author of the present work (i.e. Luca Ceresa), a number corresponding to the personal laboratory book and a number corresponding to the page where that specific sample was reported. This rule was applied to PS-CdS samples, Gold Nanoparticles and hybrid solid layers on glass substrate. It follows a schematic example of the described nomenclature procedure.
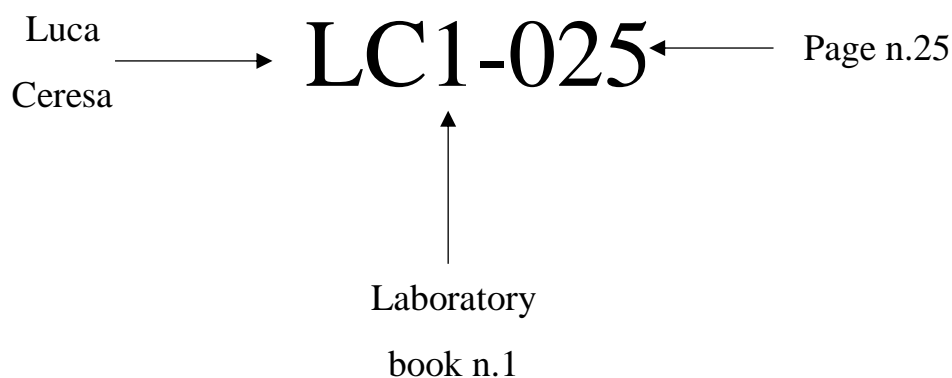
2.4.1 Approach n.1: "Water based-GNPs and THF action"

The first approach to study QDs – GNPs interaction was based upon the realization of a PS-CdS layer spread over a squared glass substrate by spin coating. After a drying step, the original idea was to dip the substrate into Hexylamine to obtain the opening of the TTC groups. Finally, the action of different amounts of THF had to be investigated by submerging the glass substrates with PS-CdS into different solutions of water based-GNPs characterized by an increasing percentage of THF. Specifically, the main objective of the present study was to understand how the action of THF could have been effective in swelling the PS chains by consequently increasing the distance between fluorescent and plasmonic component. This would have been useful to explain the role of distance in a hybrid layer of QDs and metal NPs. However, several problems appeared during the samples realization and analysis. Firstly, as it will be quantitatively explained in Chapter 3, the first applied method to produce a layer of PS-CdS QDs, or rather spin-coating, revealed to be unable to generate a layer thick enough to be clearly distinguished by UV-vis. Spin-coating was performed by using the specific apparatus visible in figure 20. First and foremost, it was essential to fix the glass substarte on a central holder situated beneath the circular cover which can be seen in the figure. This was done by activating a pump which sucked air and kept the substrate in position during the rotational step. The latter was subsequently started, and the desired parameters could be adjusted by the LCD screen on the front face of the spin coating machine. Precisely, the RPM value was set on 3000 while the total rotation time was set on 97.5 s.

Figure 20 Spin coating machine

In order for the right speed to be reached it was necessary to wait about 30 s after which the rapid dropping of the PS-CdS solution was performed by an adjustable pipette. The remaining time was necessary to allow a good spread of the deposited solution over the whole substrate surface.

Moreover, beside the insufficient absorption achievable by UV-vis, due to the scarce thickness of the deposited layer, an almost non-existent connection between QDs and GNPs was reported. In fact, after the spin coating of PS-CdS, different approaches were investigated to provide the opening of the TTC groups mediated by Hexylamine. Unfortunately, after these steps, the contact with water-based GNPs didn't result in any sort of connection between QDs and GNPs because no clear evidence of absorption peaks at 520 nm were observable by UV-vis or in the excitation spectrum done by fluorometer.

With the aim to solve the two mentioned problems several attempts have been conducted. Precisely, to face the low signal deriving from the spin coating step, different values of deposited volumes, rotational speed and rotation time have been attempted. However,

no significant change was obtained until when the spin coating step was substituted by ***drop casting***. In fact, as it will be explained later, this last method resulted to be consistently more effective in providing a thicker layer of PS-CdS QDs able to absorb the incoming radiation with reproducible results at UV-Vis and fluorometer. As far as the interaction between QDs and GNPs is concerned, instead, it was observed that the addition of Hexylamine onto the deposited layer of PS-CdS was not effective. On the contrary, it caused a dissolution of the underlying layer resulting in absence of connection between fluorescent and plasmonic components. Therefore, different paths were explored, including the drop casting of a solution of Hexylamine and GNPs over a previously drop casted layer of PS-CdS and the preparation of an initial layer containing PS-CdS and Hexylamine followed by immersion into a GNPs solution. However, no encouraging and reproducible results were obtained, and a procedural change appeared to be absolutely necessary. Indeed approach n.2 was hypothesized and applied for the next experiments.

2.4.2 Approach n.2: "QDMs and GNPs drop casting and Solvent Annealing"

The second approach had the main objective of maintaining all positive characteristics of the previous one, by simultaneously solving some crucial identified problems. Specifically, the most important advantage typical of spin coating was the achievable smoothness that was absolutely unrealizable by drop casting. On the other hand, drop casting was definitely better than spin coating in reaching the necessary layer thickness to obtain a good result at UV-vis and fluorometer. Therefore, an intermediate method was selected which could simultaneously guarantee the advantages coming from both methods. The so-called ***solvent annealing*** procedure is based upon deposition (i.e. drop casting) of a desired solution and solvent evaporation in a situation of reduced vapor pressure. More specifically, the glass slides were positioned on a support inserted into a glass jar and the solution was carefully dropped onto them by using an adjustable pipette. Moreover, the bottom of the jar was filled with the same solvent utilized to synthesize the dropped solution and the jar was sealed with aluminum foil. Thus, a closed chamber was created which caused a slower evaporation of the solvent from the deposited solution onto the glass slides. This was due to the high amount of solvent vapor in the atmosphere all around the samples in the jar. Consequently, a smooth solid layer of deposited solution could be created once the solvent resulted evaporated. This technique, under the name of Solvent Vapor Annealing, was studied by Sinturel et al. who reported that a slow evaporation rate can lead to an ordered organization of the deposited layer. [18] In fact, in order for this to happen, different amounts of time were tested, and 24 hours was considered the minimum necessary time to produce a stable layer. Figure 21 reports the utilized apparatus consisting in a glass jar, a support for the glass slides and a metallic stick useful to insert and extract the support.

Beside the described method to create a solid layer, a suitable way to obtain a good interaction between QDs and GNPs had to be identified. Therefore, a so-called Quantum dot micelles (QDMs) and Gold Nanoparticles (GNPs) solution was previously synthesized and later deposited on the glass slides. More precisely, as it will be reported in Chapter 3, different solutions were prepared, namely a pure PS-CdS solution, a PS-CdS + Hexylamine solution, a PS-CdS + GNPs solution and finally a PS-CdS + Hexylamine + GNPs solution. This was useful to test how the presence of exclusively Hexylamine or GNPs affected the QDs absorption and emission. Moreover, the connection effect derived from the opening of the TTC groups could be studied by comparing the different samples. In addition, different ratios of GNPs and QDMs were tested by adding different amounts of GNPs. As a consequence, the role of GNPs' density could be studied in terms of auto absorption effect, scattering and field effect.

Furthermore, it has to be mentioned that, since the second approach involved the deposition of an already synthesized QDs-GNPs solution, a good miscibility between the solvent of both components was required. Thus, it was no longer possible to operate with water based-GNPs, but toluene based-ones had to be synthesized. Consequently, Turkevich method was abandoned, as previously anticipated, and Brust method was always applied. In addition, an accurate washing procedure of the glass slides was considered necessary to establish a durable and reliable connection between them and the deposited solution. In particular, they were washed

by 10 minutes sonication in methanol, chloroform, toluene and acetone. After, they were dried in vacuum oven for 3 hours at 65°C. As it will be illustrated in Chapter 3, the proximity between the glass slides in the jar of figure 21 often caused the overflow of the deposited solution with a consequent contamination of samples among each other. For this reason, it was crucial to ensure a good interaction between deposited solution and glass slides during the solvent annealing step.
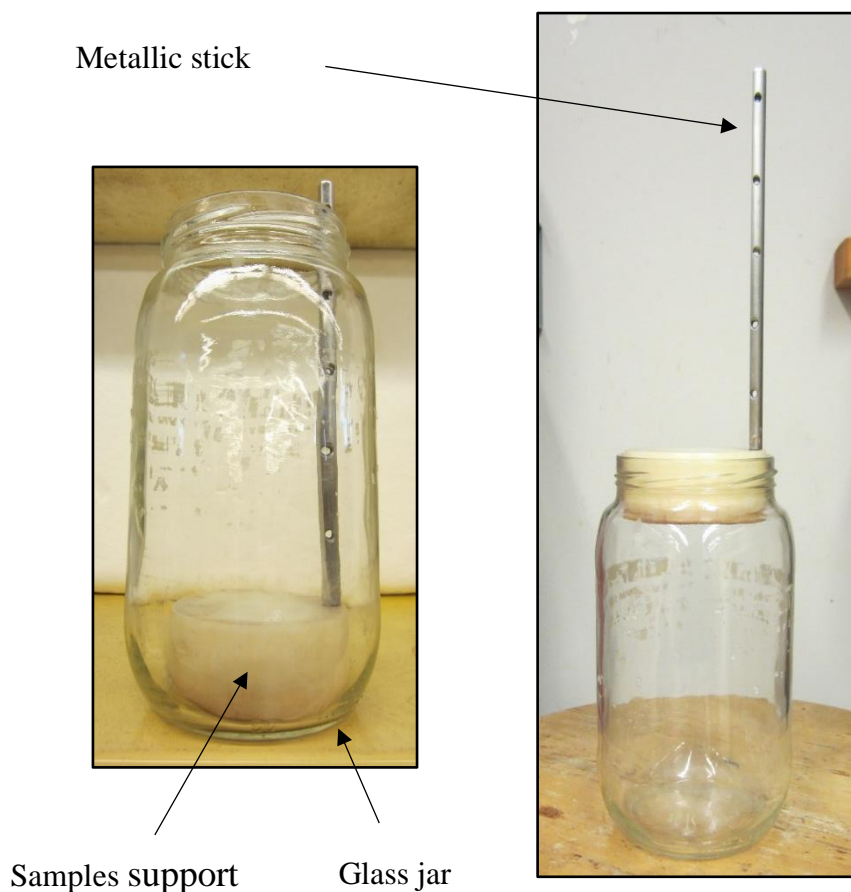
Figure 21 Solvent annealing apparatus

2.4.3 Solid hybrid layers characterization

In order to characterize the obtained solid hybrid layers of QDs and GNPs, mainly UV-vis and fluorometer were used. Specifically, the techniques' working principles are the same which have already been explained for single QDs and GNPs solutions characterization. However, the present paragraph is simply devoted to clarifying that a specific apparatus was necessary to hold glass slides instead of a cuvette. As far as UV-vis is concerned, the cuvette holder was easily removed and substituted by a glass slides holder constituted by a plane surface with a hole to let the light cross the sample and reach the detector. The same is valid for the fluorometer and figure 22 shows the utilized sample holder (A) together with a schematic of the light path (B). In regard to this last point, a further consideration needs to be provided. In fact, light comes from the Xe lamp and hits the sample on the coated side (i.e. front face analysis). At this point, some of the incoming light is directly reflected towards the detector, while some is absorbed and re-emitted by QDs as previously thoroughly explained. However, all the reflected radiation needs to be discarded because it is not interesting for the experimental analysis. In order to do that, a white paper was positioned between sample and detector and the Xe lamp set on 500 nm emission. Therefore, an evident green spot was observable on the white paper because light was directly reflected by the sample. By acting on the screw of the sample holder illustrated in figure 22 (A) it was possible to tune the incidence

angle between light and glass slide by moving the green spot away from the central area of the detector. In particular, the green spot exited completely from the detector area when the angle reached the value of 60°. Indeed, this angle was kept constant and utilized during all fluorometer experiments.
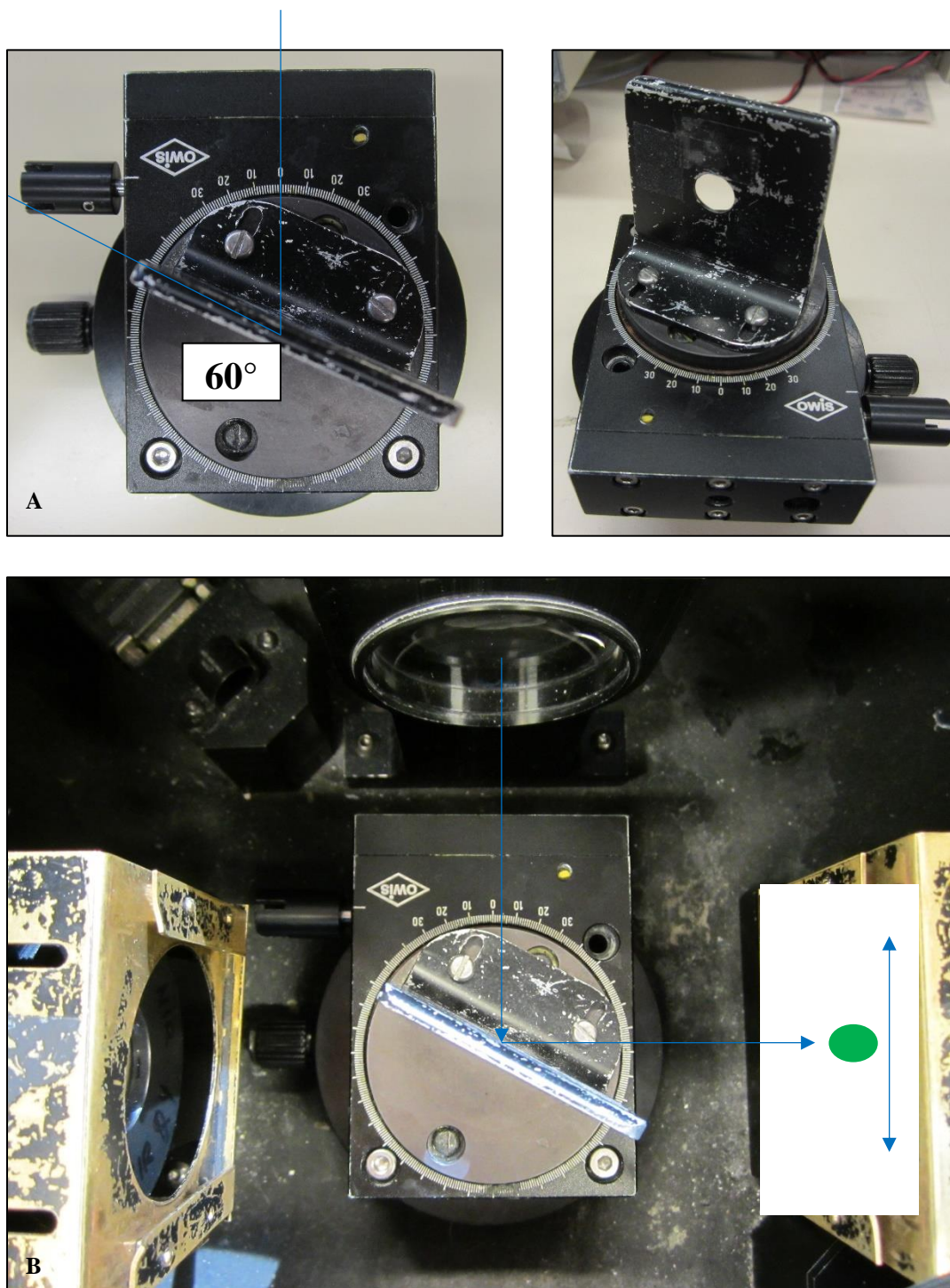
Figure 22 Fluorometer glass slides holder (A) and light path (B)

CHAPTER 3

EXPERIMENTS AND RESULTS

INTRODUCTION

The present chapter is devoted to listing all the experiments that were conducted by following the two previously mentioned approaches. In particular, a specific nomenclature will be reported and explained for each sample. Preparation, analysis and main results will be explained to justify the next step or the identified possible improvement.

3.1 APPROACH N.1: WATER BASED-GNPs AND THF ACTION

This paragraph will present all the experiments conducted during the first period of the current thesis work. As it was explained in the previous chapter, approach n.1 was based upon the utilization of the spin coating technique to produce a first layer of PS-CdS followed by the contact with Hexylamine to open the TTC groups to connect QDs and GNPs. Moreover, the THF capability of swelling the PS chains had to be investigated in order to find and report a correlation between QDs-GNPs distance and resulting performance in fluorescence emission. However, as already anticipated, numerous problems had to be solved and a different approach was finally considered as necessary.

3.1.1 Hexylamine addition: Drop Casting vs. Spin Coating

3.1.1.1 Sample LC1-033: BLC0, BLC1 and BLC2

The first realization attempt of a hybrid material composed of QDs and GNPs involved an initial ***spin coating*** step to create a first layer of PS-CdS. As explained in Chapter 2, spin coating was performed by setting the machine on 3000 RPM for a total time of 97.5 seconds.

The second step was the ***addition of Hexylamine***. Therefore, samples LC1-033, or rather BLC1 and BLC2 where B stands for "back" and it was necessary to identify the non-coated side, were removed from the spin coating machine and left in the vacuum oven to dry at 65°C. After the complete dioxane evaporation, the samples were allowed to cool down and the addition of Hexylamine was performed in two different ways. Specifically, 1 µl of a 0.3 M solution of Hexylamine and toluene was dropped on BLC1 which was put again in the oven to achieve toluene evaporation. Instead, BLC2 was spin coated with 1 µl of pure Hexylamine and dried in the oven as well. The only possible observation was that apparently in BLC1 a small amount of the surface was effectively reached by Hexylamine. BLC2, instead, didn't show any remarkable sign.

The last step was the ***GNPs addition*** and it was performed by dipping BLC1 and BLC2 into a water-based GNPs solution where they remained for 1 h. After this time and a rinsing in D.I. water, the two samples were dried and visually observed. No change in

the appearance before and after dipping into the GNPs solution was noticed suggesting that Hexylamine probably didn't properly succeed in cutting TTC groups to connect gold NPs.

In order to verify the current hypothesis, a "control sample" called BLC0 was created by spin coating 50 µl of the same previous solution with exactly the same parameters as BLC1 and BLC2. After the usual drying step, Hexylamine was added as in BLC1 and it was noticed that the area that was effectively reached by Hexylamine was still very small. Therefore, it was concluded that probably, Hexylamine spin coating didn't work very well because an excessively small amount of reducing agent effectively reached the TTC groups. On the other hand, Hexylamine dropping was not functional either because the final affected area seemed to be very restricted and a central white spot appeared on samples BLC1 and BLC0.

Since the obtained results were discouraging, a different way to add Hexylamine was hypothesized and it was applied in sample LC1-043.

3.1.1.2 Sample LC1-043: BLC0-6c and BLC0-6d

First attempt

This sample had the objective of investigating a different procedure to provide a good contact between TTC groups and Hexylamine leading to a more functional connection between QDs and water based-GNPs.

Therefore, two different series of samples were created which are reported in table 1. Specifically, the so-called "BLCc" series was prepared by spin coating an as-produced PS-CdS solution with the same parameters which were employed for the previous samples. In fact, "c" stands for concentrated and distinguishes this series from the diluted one referred to as "BLCd". More precisely, seven glass slides were prepared by spin coating 50 µl of concentrated PS-CdS solution (i.e. BLC0-6c) and seven glass slides were spin coated with the same amount of a 10 % V/V PS-CdS solution in dioxane. Subsequently, all samples from 1 to 6 were dipped into pure hexylamine for about two seconds each and let dry for 1 h. Next, they were washed in methanol to remove the excess Hexylamine. In fact, its role was only to cut TTC groups and to open PS chains without taking part into following steps. After, all samples were dried together in vacuum oven. Moreover, different vials were prepared with different respective amounts of GNPs and THF from 100% GNPs – 0% THF to 87.5 % GNPs -12.5 % THF.

Each sample was dipped into the corresponding vial (i.e. BLC1c and BLC1d were put into the first vial with 100% GNPs and 0% THF and so on) and let submerged for 1 h. This last time was too long because when the samples were removed from the respective vials the PS-CdS layer had been stripped by the THF.

Second attempt

Since the previous attempt resulted to be a failure because of the excessive immersion time into THF, the same series of samples was produced again. In particular, the first two steps were performed as before while the third step of immersion into GNPs and THF solution lasted only 30 s before the samples to be dried out of oven. However, the final result was still negative since all samples appeared totally transparent and no GNPs remained attached on the surface. This is observable in figure 23 where four glass slides belonging to sample LC1-043 are shown. Precisely, BLC0c, BLC0d, BLC3c and BLC3d are visible and no difference is observable between samples with and without GNPs.

3.1.1.3 Sample LC1-047: B50, B100 and B200

Since it was clear that it was not functional and effective to produce the hybrid material following the described procedure, a "pilot device" was created to effectuate and follow the production step by step. In fact, in order to verify if each step was properly carried out, an intermediate analysis was required.

SAMPLE NAME	GNPs %	THF %
BLC0c	0	0
BLC1c	100	0
BLC2c	97.5	2.5
BLC3c	95	5
BLC4c	92.5	7.5
BLC5c	90	10
BLC6c	87.5	12.5
BLC0d	0	0
BLC1d	100	0
BLC2d	97.5	2.5
BLC3d	95	5
BLC4d	92.5	7.5
BLC5d	90	10
BLC6d	87.5	12.5

Table 1 LC1-043 concentrated and diluted samples
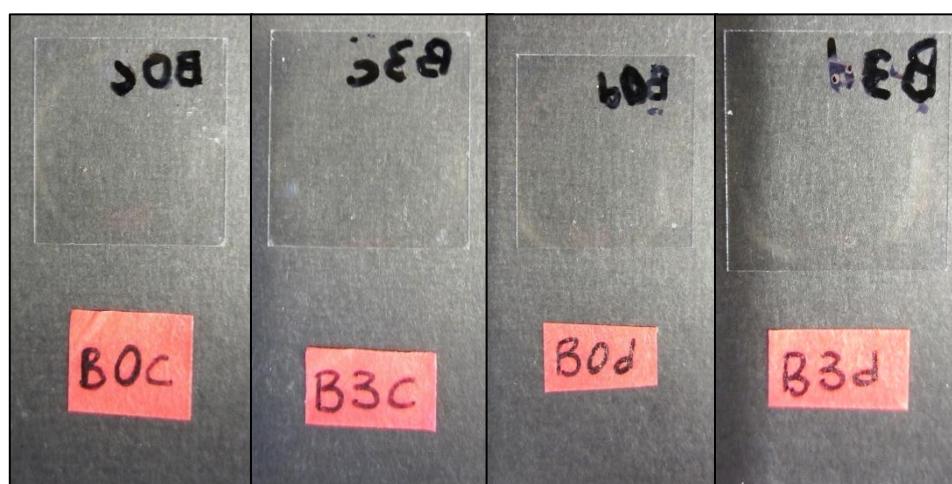
Figure 23 Samples BLC0c, BLC3c, BLC0d, BLC3d belonging to LC1-043

Therefore, 50, 100 and 200 µl of PS-CdS solution were spread over glass substrates by spin coating to create respectively sample B50, B100 and B200. Subsequently, after a night in the oven to get dry, a UV-vis absorption spectrum was obtained which is reported in figure 24 (A). Next, the three samples were differentiated as follows. B50 was dipped into a solution 50% Hexylamine – 50% MeOH, rinsed in pure MeOH and then in D.I. water and finally dried into the oven. Specifically, each of the previous steps was conducted quickly (i.e. 3 seconds). B100, instead, was dipped into pure Hexylamine, then rinsed in pure MeOH and water and dried into the oven. Finally, B200 was dipped into pure Hexylamine for a longer time (i.e. 30 seconds) then washed in MeOH and water and dried in the same way. Figure 24 (B) shows the obtained UV-vis absorption spectrum of the hybrid material after the contact with Hexylamine. In particular, B50 and B100 show a similar pattern before and after the Hexylamine addition, indicating

that the PS-CdS layer was not removed. On the contrary, the UV-vis spectrum of B200 shows no more absorption signal probably due to the excessive contact time with Hexylamine which dissolved the already thin layer of PS-CdS previously spin coated on the glass substrate. Therefore, exclusively samples B50 and B100 were dipped into a GNPs solution with 0% THF for 30 s to investigate the effectiveness of connection between the opened PS chains and GNPs. However, the UV-vis spectrum obtained after this step didn't show any clear sign of absorption between 500 and 600 nm which would have meant the presence of gold. This result is illustrated in figure 24 (C).
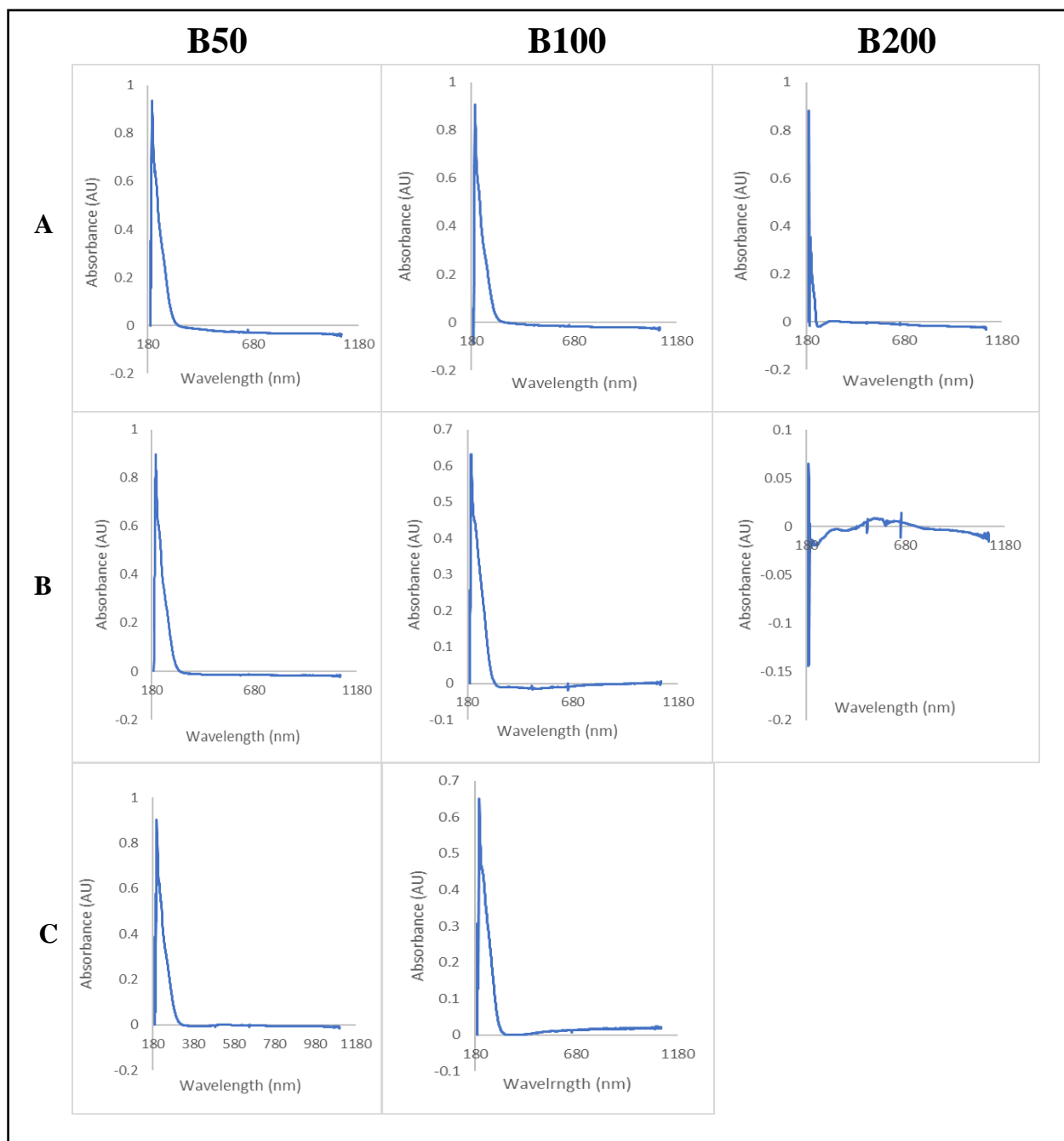
Figure 24 Absorption spectra of samples B50, B100 and B200. UV-vis absorption of as-produced PS-CdS (A), after Hexylamine contact (B) and after immersion into GNPs solution (C)

Actually, sample B100 seemed to show a slight increasing trend after 500 nm but this couldn't be considered as a clear sign of the presence of Gold. Consequently, also this sample was considered bad-performing and another series had to be prepared.

3.1.1.4 Sample LC1-051: B100A, B100B and B100C

Since the most promising sample until now was B100, three other samples were prepared by spin coating 100 µl of PS-CdS solution, namely B100A, B100B and B100C. Specifically, after the spin coating was effectuated, the first sample was dipped into Hexylamine for 2 seconds and immediately washed in MeOH and water. Unlike the previous series, B100A was immersed in a water based-GNPs solution without the intermediate drying step described in paragraph 3.1.3 and finally it was left into the oven for 1 hour. Instead, B100B was dipped into Hexylamine for 2 seconds and left overnight to dry out of oven before undergoing the same procedure applied for B100A. Last, B100C was dipped into Hexylamine and left overnight to dry out of oven like B100B. However, the day after, it was put into the oven to complete the drying process without any rinsing in water and MeOH. Subsequently, sample B100A was tested with UV-vis absorption but still no gold could be observed. Samples B100B and B100C, instead, were tested with UV-vis before being dipped into the same water based-GNPs solution used for B100A, and a final UV-vis spectrum was later obtained. Unfortunately, still no clear presence of gold was detected as observable in figure 25 where the absorption spectra of the three final samples are shown.
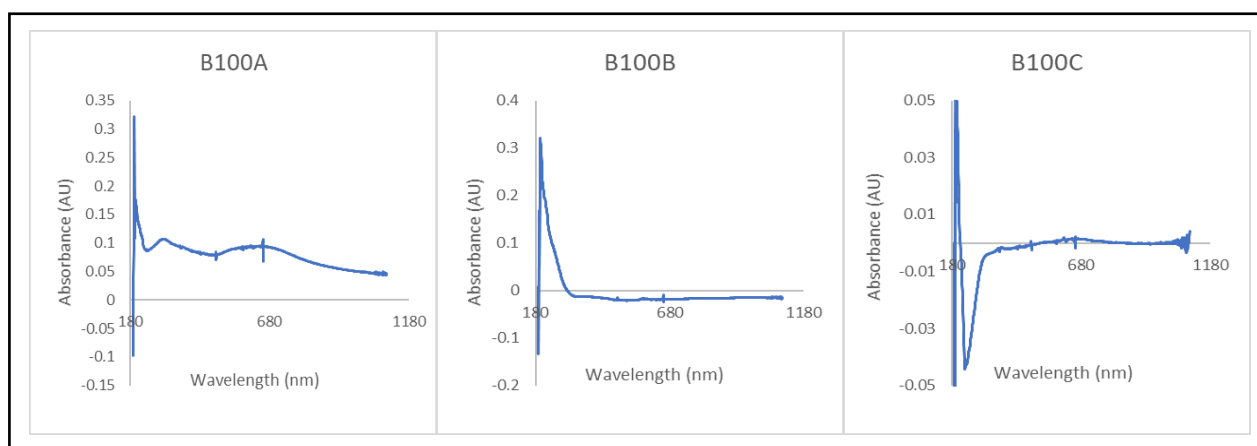
Figure 25 Absorption spectra of final sample LC1-051

Even though the result was generally negative, B100A seemed to provide a little more evident signal. In fact, this was taken into account for the realization of the next sample.

3.1.1.5 Sample LC1-052: B100D, B100E, B100F – B50D, B50E, B50F

Two series of glass slides were produced which belong to sample LC1-052. In particular, three of them were prepared with 100 µl of PS-CdS solution (i.e. B100D, E and F) and other three with 50 µl of the same solution (i.e. B50D, E and F) by maintaining the usual parameters of rotation and time. After, the six samples were dried in vacuum oven for 1 hour and tested with UV-vis absorption. A good absorption signal was detected only in sample B50D, by confirming the presence of the spin coated layer of PS-CdS, while all other samples didn't show the typical absorption spectrum of PS-CdS. Figure 26 (A) compares the absorption spectrum of sample B50D which shows the usual trend and B50E as a representation of non-properly absorbing samples. Later, samples B100D, E and F were quickly dipped into pure Hexylamine, pure MeOH and finally water before being left in the water based-GNPs solution overnight. Differently, B50D, E and F were dipped into a 50% solution of MeOH and Hexylamine, and washed in pure MeOH and water before being dipped into the GNPs solution for only 30 seconds and dried in the oven for half an hour. In

figure 26 (B) the UV-vis spectra of the final samples can be observed which are still completely discouraging because no presence of gold was detected clearly.
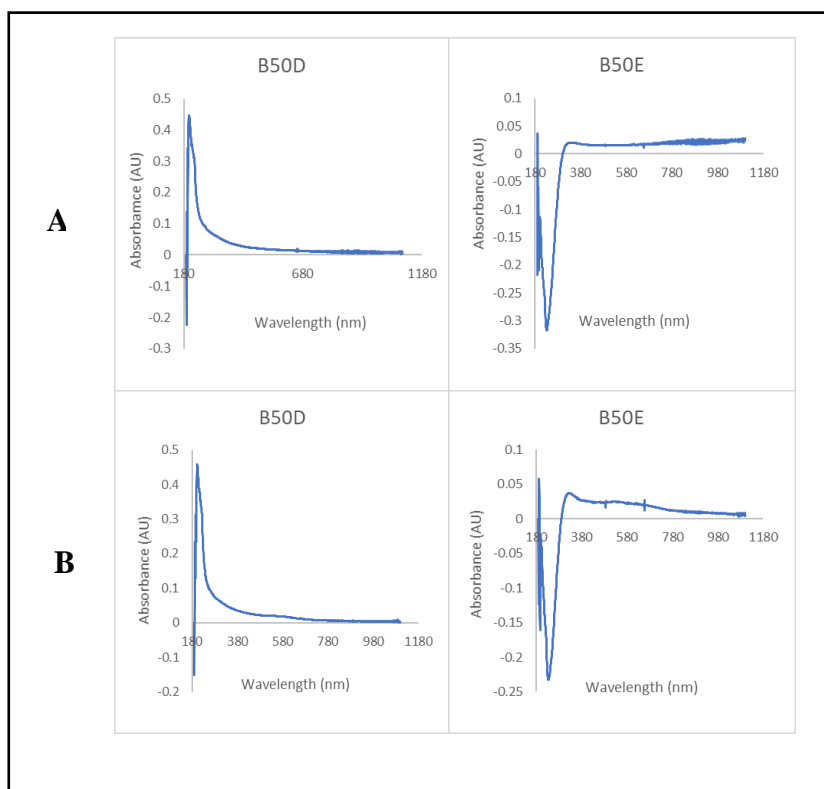
Figure 26 Absorption spectra of B50D and B50E before (A) and after (B) dipping into GNPs solution

3.1.2 Drop Casted samples with *a priori* mixing of GNPs and Hexylamine

3.1.2.1 Sample LC1-054: Dr1, Dr2 and Dr3

At this point, it was clear that a more functional technique had to be individuated to deposit a first layer of PS-CdS which absorption was reproducible and easily detectable. Therefore, spin coating was suspended and **drop casting** was tested. As it was already explained, the main goal which was attempted by spin coating was the realization of a smooth layer of PS-CdS ensured by the action of a considerable centrifugal force. This was impossible to realize by drop casting. However, three glass slides were prepared by drop casting 100 µl of PS-CdS solution (i.e. Dr1, Dr2 and Dr3) which were dried out of oven. Subsequently, Dr2 was drop casted with 100 µl of a solution 50 % water-based GNPs and 50% Hexylamine and MeOH (1:1 volume ratio), while Dr3 was drop casted with 100 µl of a solution 50 % water-based GNPs and 50% Hexylamine and MeOH (1:3 volume ratio). This attempt was conducted to establish whether it was useful to mix GNPs and Hexylamine before the contact with a previously drop casted layer. However, a considerably intense phenomenon of flakes formation affected the drop casted layer and this technique was suspended because apparently not promising. Nevertheless, sample Dr1 was tested at fluorometer and the excitation spectrum reported in figure 27 was obtained. Actually, it was encouraging to observe for the first time an excitation spectrum resembling the one which was obtained during the same test of PS-CdS in solution. This meant that probably, drop casting was the right technique to produce a layer thick enough to be effectively able to absorb the incoming radiation and to be detected by fluorometer. However, because of the flakes formation, drop casting didn't seem to be the right choice and it was temporarily suspended.
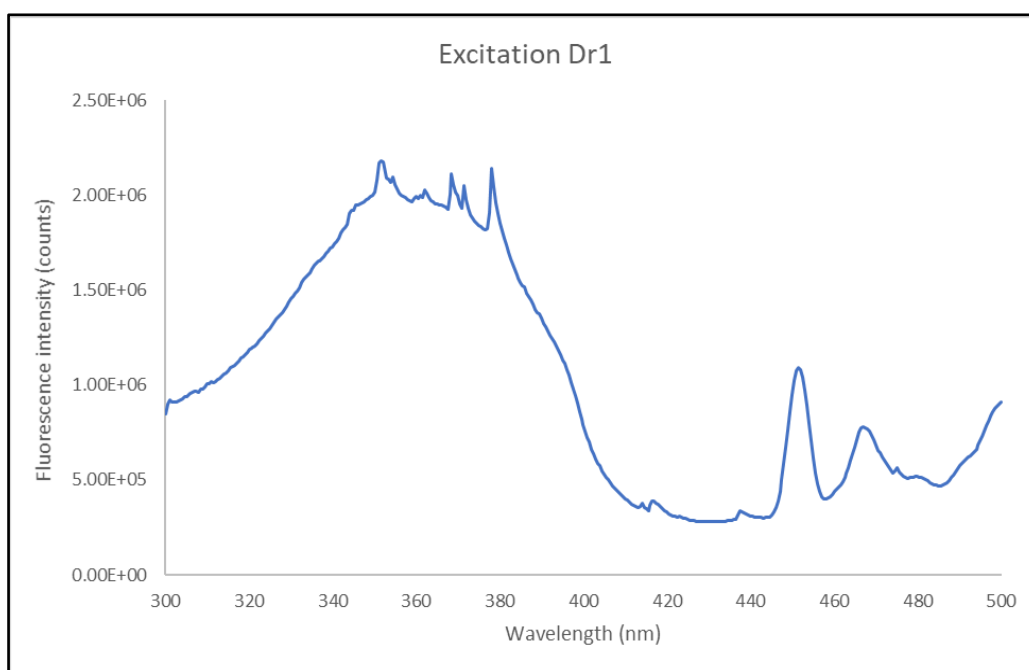
Figure 27 Fluorometer excitation spectrum of sample Dr1

3.1.3 Spin Coating and pre-mixing of QDs and Hexylamine

3.1.3.1 Sample LC1-055: NM1-6

A slightly different procedure was tested with samples belonging to series NM. In fact, this name was assigned to underline that it was a New Method (i.e. NM). In particular, this new procedure was based upon the deposition by spin coating of an already prepared solution of PS-CdS and Hexylamine. This was considered to be a promising method to allow the opening of the TTC groups while simultaneously ensuring the formation of a smooth layer. So, samples NM1, 2 and 3 were prepared first and the following procedure was followed. NM1 was produced by spin coating of 100 µl of an as prepared PS-CdS solution. NM2 and NM3, instead, were produced by spin coating of 100 µl of the so-called S1 and S2 solutions. In particular S1 was a mix composed of 100 µl of PS-CdS and 100 µl of pure Hexylamine, while S2 was a mix of 140 µl of PS-CdS and 60 µl of pure Hexylamine. These different volumes were used in order to test the result of different amount of reducing agent. After 1 hour of drying in the vacuum oven, the three samples were visually inspected, and they appeared to be extremely transparent probably due to the excessive low amount of deposited material. For this reason, no further experiments were conducted. Instead, a new sample defined as NM 4 was prepared by spin coating of 100 µl of PS-CdS solution followed by 0.5 h drying in the oven. Later, 100 µl of S1 solution were deposited by spin coating and the sample was left another 0.5 h in the oven. Finally, it was dipped into a water based-GNPs solution overnight. Meanwhile, two new samples called NM5 and NM6 were prepared by slightly changing the spin coating parameters. Precisely, the speed was reduced to 2200 RPM while the total time was reduced to 77.5 seconds. This was done in order to try to increase the thickness of the deposited layer. Moreover, a double amount of material was deposited compared to the previous NM samples. In particular, 100 µl of PS-CdS were deposited twice with a waiting time of about 5 minutes between the first deposition and the following one. This procedure was envisioned to be more effective than one single deposition of 200 µl of solution with the aim to increase the resulting deposited layer. Subsequently, 100 µl of the same previous S1 solution were deposited by spin coating on samples NM5 and NM6 which were later left 20 h in the oven to dry. Finally, NM5 was dipped into the GNPs solution for 2 h, while NM6 remained in the same solution overnight. Fluorometer analysis of samples NM4, 5 and 6 were performed which unfortunately didn't provide any remarkable result. In fact, beside a very low peak at around 350 nm, which is the typical wavelength

of maximum absorption of PS-CdS QDs, the excitation spectrum appeared very similar before and after dipping into the GNPs solution demonstrating that still no gold was fixed on the glass substrates. Figure 28 shows the obtained excitation spectra for samples NM4, 5 and 6. Precisely, column A shows samples before dipping into the GNPs solution, while column B shows the obtained spectrum after contact with gold. Moreover, figure 29 shows their physical appearance.
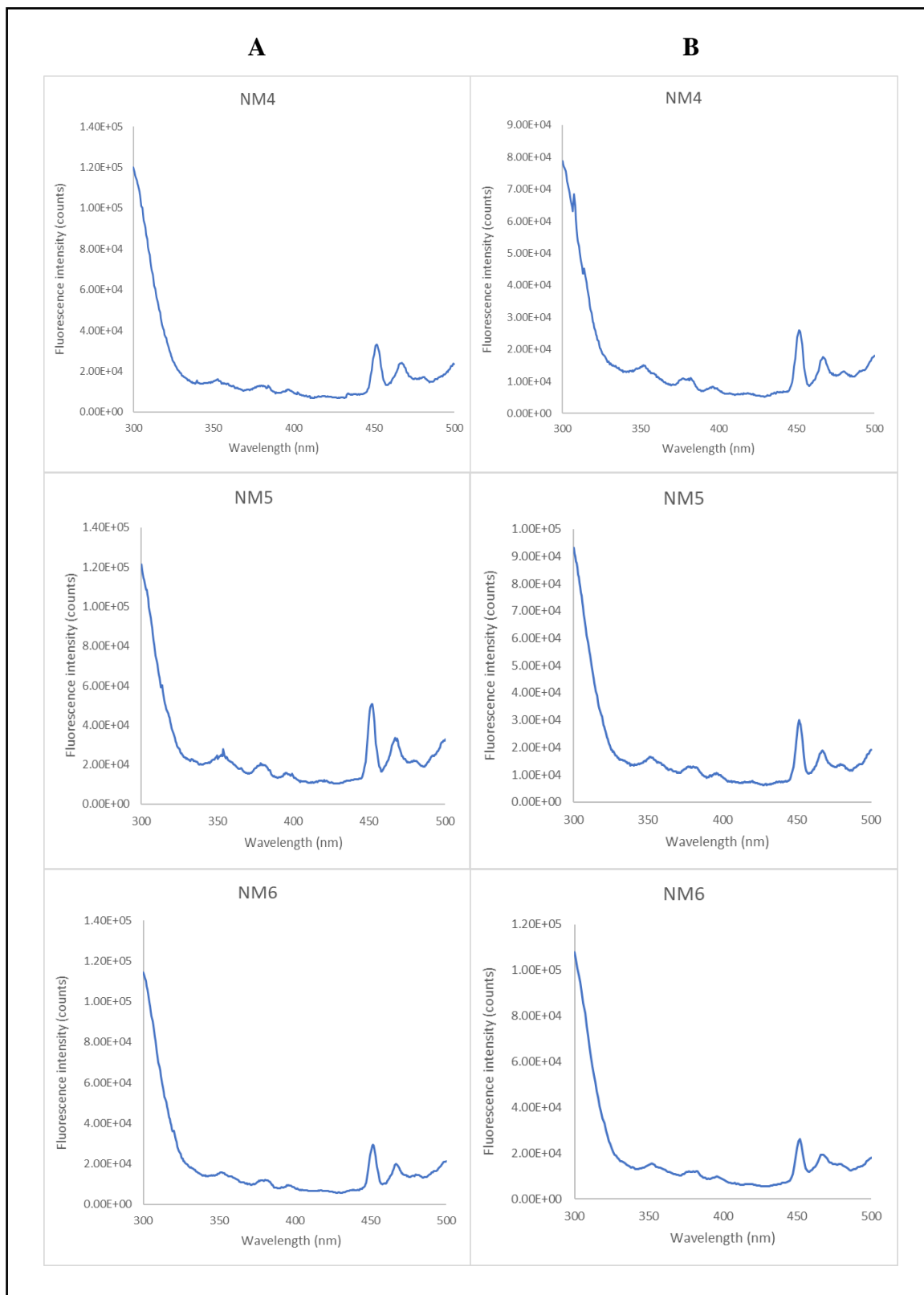
Figure 28 Excitation spectra before (A) and after (B) dipping into GNPs solutions of samples NM4, 5 and 6
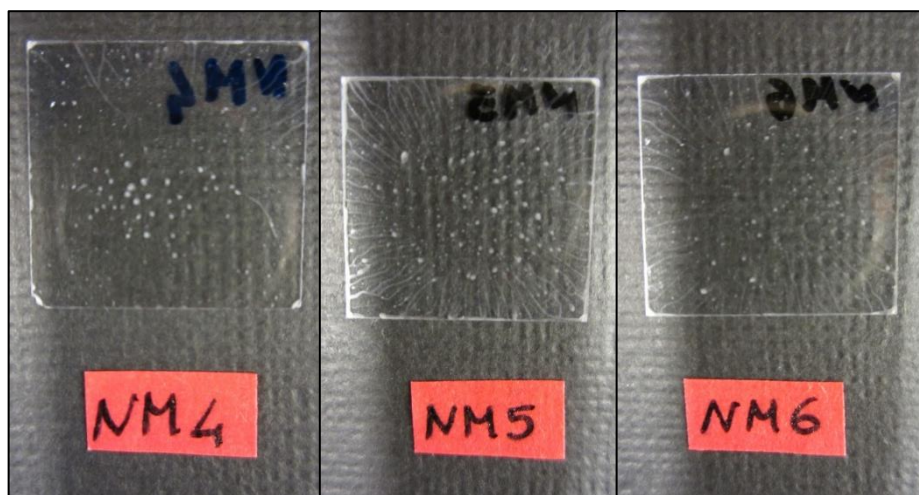
Figure 29 Samples NM4, NM5 and NM6

3.1.4 Drop Casting and pre-mixing of QDs and Hexylamine

3.1.4.1 Sample LC1-058: DS1 and DS2

It has previously been asserted that samples belonging to the series Dr were able to produce a layer that was thick enough to provide absorption and a good excitation spectrum, but they were strongly affected by flakes formation and by an intense exfoliation. On the contrary, samples belonging to NM series were capable of creating a smooth layer not affected by exfoliation, but the signal was extremely low. Therefore, an attempt to combine these two methods was done with samples DS1 and DS2. Basically, they were created by applying the so-called "New Method" to the drop casting deposition technique. In particular, DS1 was produced by drop casting 100 µl of S1 solution (50% PS-CdS and 50% pure Hexylamine), while DS2 was produced by drop casting 100 µl of S2 solution (70% PS-CdS and 30% pure Hexylamine). Moreover, a control sample was produced by drop casting 100 µl of pure PS-CdS. The three samples were left out of oven until almost dry and subsequently DS1 and DS2 were dipped into the GNPs solution for 1 h and then dried out of oven. Figure 30 (A) shows the resulting excitation spectra which were obtained at fluorometer. In particular, it is now possible to observe a well visible peak at 350 nm which is typically the wavelength of maximum absorption for PS-CdS samples. The other appearing peaks are simply due to scattering and this can be affirmed because an evident shift was observed if the wavelength range was modified. Moreover, in figure 30 (B) the emission spectra are reported corresponding to different excitation wavelength (i.e. 350, 370, 390 and 410 nm). As expected, the highest peak corresponds to the excitation wavelength of 350 nm. Furthermore, it is worth noticing that the control sample, which didn't undergo immersion into GNPs solution, provided a consistently higher peak of emission than samples DS1 and DS2. The lower emission observed in DS1 and DS2 is probably due to the auto absorption effect caused by the presence of GNPs which absorb the same wavelength which is emitted by QDs (i.e. 520 nm). Moreover, a higher emission was obtained for sample DS2 with respect to DS1 and this can be attributed to the fact that more Hexylamine was used to produce sample DS1. In fact, a higher amount of reducing agent could have caused a more significant connection between QDs and GNPs resulting in a more evident auto absorption effect and a lower emission. In conclusion, samples DS1 and DS2 where drop casting was applied to deposit a solution of PS-CdS and Hexylamine, and dipping was applied to create a connection with GNPs, demonstrated that the addition of GNPs reduced the detected radiation because part of it was reabsorbed before the detector was reached. This hypothesis will be investigated later by a different approach which will be explained in the following paragraph.
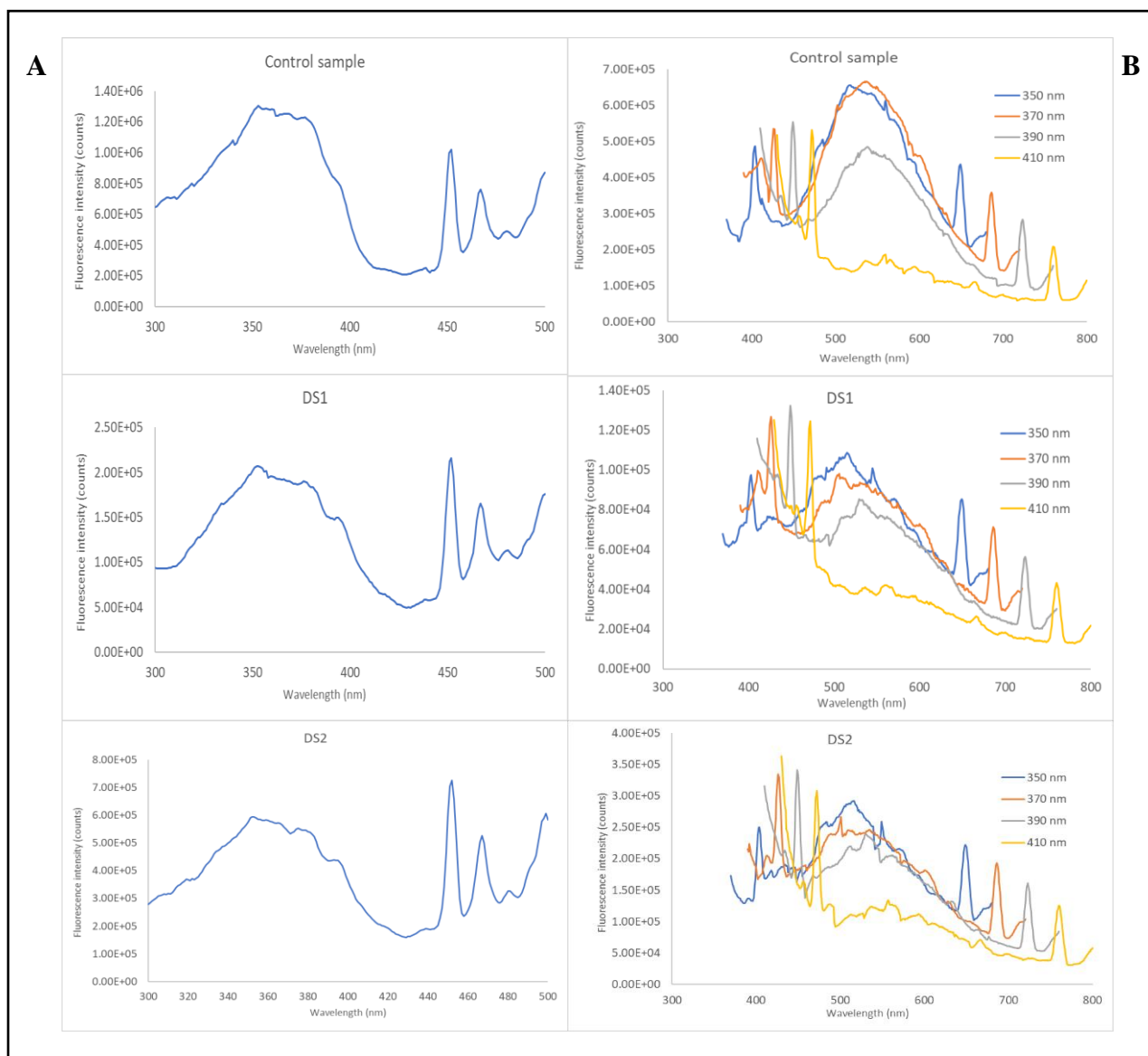
Figure 30 Excitation (A) and emission (B) spectra of samples DS1, DS2 and control

3.2 APPROACH N.2: QDMs AND GNPs DROP CASTING AND SOLVENT ANNEALING

This second approach is based upon the deposition by drop casting and solvent annealing of an already prepared solution of PS-CdS QDs (i.e. QDMs) and toluene based-GNPs. Therefore, the main difference compared to the previous method is that gold is no more attempted to be connected to the already deposited layer of PS-CdS but rather a single layer is deposited which already contains gold. More precisely, different layers have been compared which were respectively composed of pure PS-CdS, PS-CdS + Hexylamine, PS-CdS + GNPs and PS-CdS + Hexylamine + GNPs. In fact, this comparison was useful to understand the role of Hexylamine in opening the TTC groups resulting in a closer proximity between GNPs and QDs and consequently in a variation of the detected fluorescence emitted by QDs. As it will be explained in this paragraph, different samples were produced until when the ideal procedure was individuated and applied to obtain the most meaningful result of the current thesis work.

Despite the variety of procedures and steps applied to carry out approach n.2, its main goal was always to compare the signal emitted by QDs in presence and absence of gold and/or Hexylamine. Specifically, the main idea was to understand whether a layer of pure

PS-CdS could present an enhanced fluorescence when gold was added, and which was the difference when also Hexylamine was utilized.
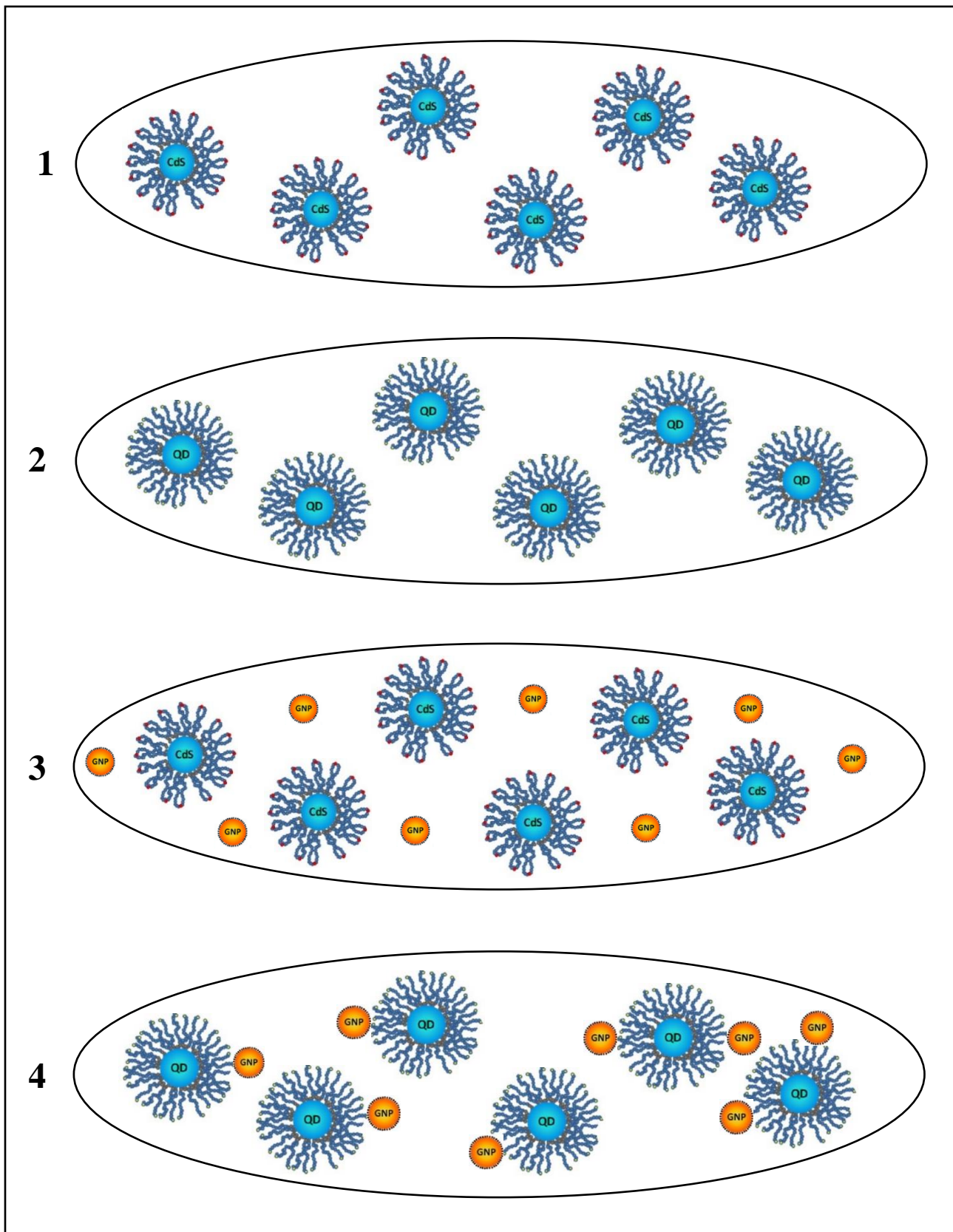
Figure 31 Schematic of sample layers of pure PS-CdS (1), PS-CdS + Hexylamine (2), PS-CdS + GNPs (3), PS-CdS + Hexylamine + GNPs (4)

Figure 31 clarifies this concept by showing four different layers deposited on glass slides. Specifically, the first one is characterized by pure PS-CdS where the PS chains are still "petal" like; the second one shows PS-CdS which PS chains have been cut by the addition of Hexylamine; the third one shows PS-CdS with uncut PS chains with GNPs added; the fourth one shows open PS-CdS with GNPs. After measuring the signal emitted by the pure PS-CdS layer, the fundamental objective was to individuate whether an appreciable difference was reportable between the signal emitted by the third and the fourth sample which presented respectively a condition of randomly dispersed GNPs among QDs and a closer proximity between the two components. In other words, the scope of the current approach was to establish if the reduced distance between QDs and GNPs, due to the addition of Hexylamine, could somehow modify the measured fluorescence intensity.

As it was anticipated in Chapter 2, the applied method to produce the mentioned samples was the so-called drop casting followed by solvent annealing. In particular, it was able to provide a layer thick enough to obtain a good absorption and an easily observable fluorescence emission. In order to do that, the apparatus shown in figure 21 was used for all samples.

As it has been done in paragraph 3.1, all samples created according to approach n.2 will be presented here by following a chronological order of preparation and analysis. Specifically, problems and issues encountered sample by sample will be explained and the applied specific solution will be motivated.

3.2.1 Sample LC1-063

The main objective of the present sample was to verify the capability of drop casting and solvent annealing to produce a smooth layer able to properly absorb the incoming radiation and to emit a detectable fluorescence. Moreover, the action of different amounts of Hexylamine had to be tested to establish the best ratio to be used for the realization of the following samples. Therefore, six glass slides were properly washed (ref. 2.4.2) and prepared as it is shown in figure 32. Specifically, slides 1 and 2 on the first row were made of pure PS-CdS, slides 3 and 4 on the second row were drop casted with a 30% V/V solution of Hexylamine in PS-CdS and slides 5 and 6 were drop casted with a 10 % V/V solution of Hexylamine in PS-CdS
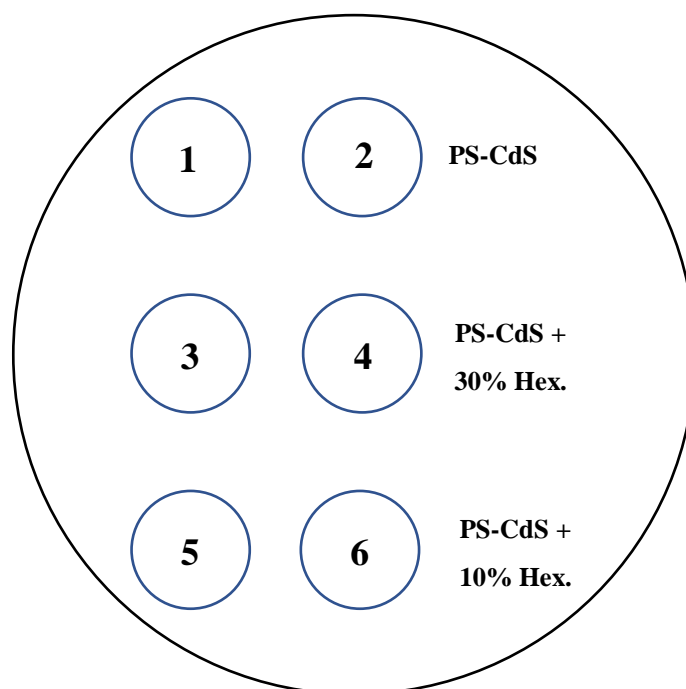
Figure 32 Layout of drop casting and solvent annealing for sample LC1-063

In particular, the circular support was risen by using the metal stick and the six glass slides were positioned so that their reciprocal distance was maximized. Moreover, as illustrated in the previous figure, the squared glass slides utilized until now were substituted by circular ones which perfectly fitted the fluorometer sample holder visible in figure 22. By using an adjustable pipette, 100 µl of the right solution were drop casted on each slide making sure that the solution was deposited slowly enough not to overflow. Subsequently, the support was gently re-inserted into the jar which bottom was filled with 10 ml of dioxane. Finally, the jar was sealed with aluminum foil to create a closed chamber characterized by a dioxane-saturated atmosphere. After 3 days, slides 3, 5 and 7 were removed from the jar and dried in vacuum oven overnight. Differently, slides 2, 4 and 6 remained into the jar for 6 days after which they were dried in vacuum oven for 3 h. Excitation and emission fluorometer test were conducted on slides 1 to 6 and the resulting spectra are respectively reported in figure 33 (A) and (B). As far as excitation is concerned, it is possible to assert that the typical trend of PS-CdS QDs is respected. Likewise, the emission spectra corresponding to the reported wavelengths is coherent with the fact that 350 nm is the maximum absorption wavelength.
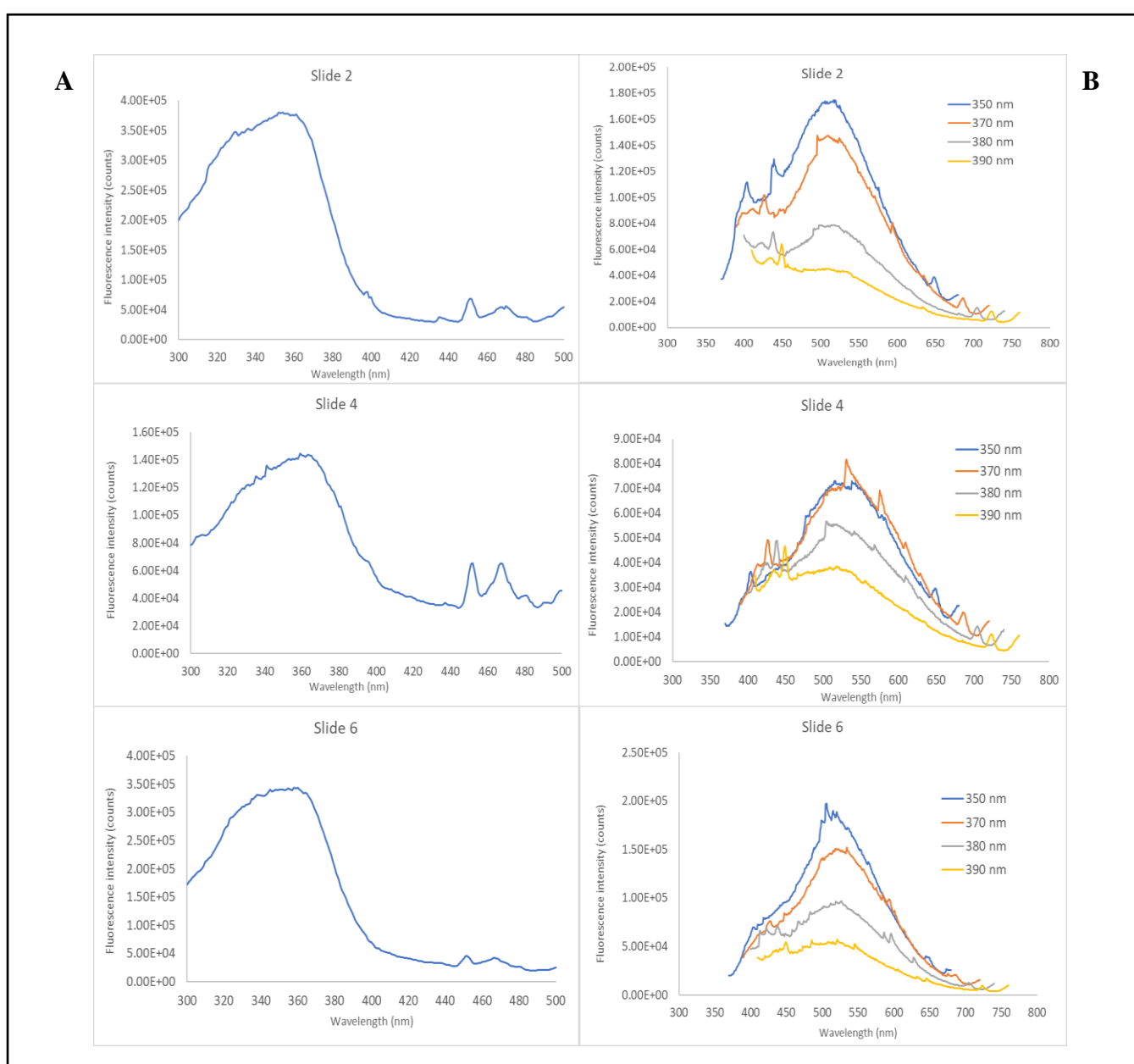
Figure 33 Excitation (A) and emission (B) spectra of sample LC1-063

Moreover, it is worth noticing that an apparently unjustified variation in the excitation and emission spectra is observable. In fact, even if the addition of Hexylamine shouldn't have caused any excitation and emission change, this was actually reported, and it could be attributed to intrinsic oscillations due to the experimental apparatus. More specifically, the intensity of radiation emitted by the Xe lamp, as well as the detected one emitted by QDs could be affected by the environmental temperature. This means that even if obtained spectra present different intensities this is not always due to a realistic phenomenon. For this reason, as it will be explained later, fluorometer measurements of a certain sample will be always conducted on the same day. This reduces results oscillation due to experimental conditions variation.

3.2.2 Sample LC1-069

After having verified the functionality of the previously described method in depositing a layer of PS-CdS with and without Hexylamine, a more structured procedure was applied to realize sample LC1-069. In fact, for the first time, all categories of glass slides, namely pure PS-CdS, PS-CdS + Hexylamine, PS-CdS + GNPs and PS-CdS + Hexylamine + GNPs were produced, tested and compared. Specifically, figure 34 shows how the glass slides were arranged on the jar support.
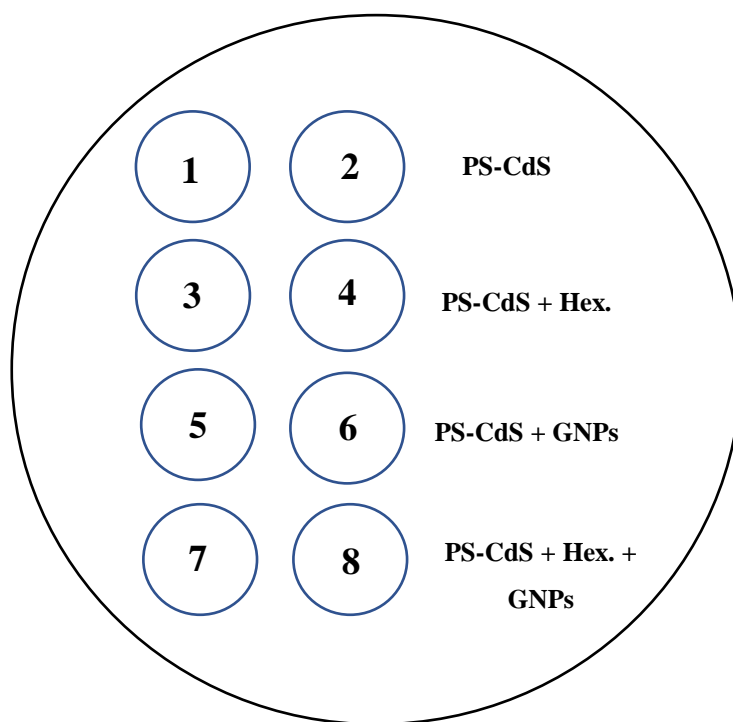
Figure 34 Layout for drop casting and solvent annealing of sample LC1-069

In order to produce the glass slides, four corresponding solutions were previously prepared in separated vials. Specifically, a volume of 1000 μl of each solution had to be produced. So, for slides 1 and 2, 1000 μl of pure PS-CdS were inserted into the first vial which was labelled as S 1 and S 2.

With the aim to determine the amount of Hexylamine to be added, the work by Farinha et al. was considered and followed. Specifically, 1.25 equivalent of Hexylamine per TTC group had to be used. Therefore, it was essential to remind that each chain is characterized by 1 TTC group per each 34 groups of COOH or rather PAA. Indeed, the first essential step was to calculate the number of moles of TTC groups which corresponds to the number of moles of the initially added raft copolymer during the synthesis of PS-CdS QDs.

$$n_{polymer} = n_{TTC} = \frac{Mass_{polymer}}{MW} = \frac{0.0306g}{27,000} = 1.133 \cdot 10^{-6}$$

$$n_{Hex.} = n_{TTC} \cdot 1.25 = 1.416 \cdot 10^{-6}$$

Once the moles of Hexylamine were calculated, it was easy to obtain its mass and corresponding volume by the following procedure.

$$Mass_{Hex.} = n_{Hex.} \cdot MW = 1.416 \cdot 10^{-6} \cdot 101.9 = 1.433 \cdot 10^{-4}g$$

$$Vol_{Hex.} = \frac{M_{Hex.}}{d} = \frac{1.433 \cdot 10^{-4}g}{0.77g/cm^3} = 1.86 \cdot 10^{-4}cm^3 = 1.86 \cdot 10^{-7}\,l = 0.186\ \mu l$$

Next, the Hexylamine had to be added in the form of a 0.03 M solution in Toluene and consequently the solvent volume had to be calculated as follows.

$$0.03M = \frac{n_{Hex.}}{Vol_{Tol.}} \rightarrow Vol_{Tol.} = \frac{n_{hex}}{0.03\ mol/l} = \frac{1.416 \cdot 10^{-6}mol}{0.03\ mol/l} = 4.72 \cdot 10^{-5}\,l = 47.2\ \mu l$$

The obtained values correspond to the necessary Hexylamine and Toluene for the total volume of synthesized PS-CdS solution (i.e. $5.95 \cdot 10^3\ \mu l\ of\ Dioxane + 158.16\ \mu l\ of\ MeOH + 8.11\ \mu l\ of\ MeOH\ and\ water = 6116.27\ \mu l$ in total). Since it was necessary to produce only a smaller amount (i.e. 1 ml of PS-CdS + Hex. solution to be drop casted on glass slides n. 3 and 4) the following proportion was established.

$$47.4\ \mu l : 6116.27\ \mu l = X : 1000\ \mu l$$

$$X = 7.75\ \mu l$$

To sum up, in order to produce the solution for samples n. 3 and 4, 1000 µl of pure PS-CdS had to be mixed with 7.75 µl of the so-called *Bulk H solution* which, in turn, was made of 0.186 µl of Hexylamine and 47.2 µl of Toluene. As already said, since these quantities were small and difficult to be accurately measured, the actual utilized amounts were 18.6 µl of Hexylamine and 4720 µl of Toluene.

As far as slides 5 and 6 are concerned, it was necessary to establish a certain ratio GNP/QDM and consequently it was fundamental to apply the following series of steps as it was reported by Farinha et al. in the supporting information section of their work [4]. First of all, the exact number of gold atoms per each gold nanoparticle had to be calculated. So, the average diameter of GNPs was used which had been defined by TEM as previously explained. It follows a numeric example involving GNPs belonging to sample LC1-065 which dimension was reported to be 3.23 nm. An easy volume calculation was performed by supposing a spherical shape of the GNPs and the mass was determined by considering a density of 19.7 g/cm³.

$$V_{GNPs} = \frac{4}{3}\pi r^3 = 1.764 \cdot 10^{-20}cm^3$$

$$Mass_{GNPs} = V_{GNPs} \cdot d = 3.475 \cdot 10^{-19}g$$

The number of gold atoms per each GNP was calculated by multiplying the number of moles of gold in one particle by the Avogadro's number.

$$N_{Au} = \frac{Mass_{GNP}}{MW_{Au}} \cdot N_A = \frac{3.475 \cdot 10^{-19} g}{196.97 g/mol} \cdot 6.022 \cdot 10^{23} = 1062 \, atoms$$

The following step was the calculation of the number of SH groups in each QDM. So, it was necessary to use the QDs' dimension previously found by UV-vis. Specifically, sample LC1-041 had a mean diameter of 2 nm and consequently the volume of a single QD was $0.4188 \cdot 10^{-20} cm^3$. Accordingly, the mass was calculated by knowing that CdS density is 4.82 g/cm^3 and the obtained value was $2.02 \cdot 10^{-20} g$.

Subsequently, the number of Cd^{2+} ions in each micelle had to be defined by multiplying the number of moles of CdS molecules in one micelle by the Avogadro's number.

$$N_{Cd^{2+}} = \frac{Mass_{QD}}{MW_{CdS}} \cdot N_A = \frac{2.02 \cdot 10^{-20} \, g}{144.48 \frac{g}{mol}} \cdot 6.022 \cdot 10^{23} = 84 \, Cd^{2+}$$

Considering that each Cd^{2+} ion can get connected with 2 COO$^-$ groups (coming from COOH), the number of COO$^-$ groups can be calculated by doubling N_{Cd}^{2+}. Therefore, 168 COO$^-$ were calculated. At this point, it had to be remembered that each polymer chain has 34 COOH groups and consequently the number of polymer chains present in each micelle could be established as follows.

$$Chains_{micelle} = \frac{Total \, COO^-}{COO^- per \, chain} = \frac{168}{34} = 5 \, chains/micelle$$

Since each polymer chain originates 2 SH groups, 10 SH groups can be found per each CdS QD micelle. On the other hand, the total number of polymer chains can be calculated by multiplying the moles of initially added raft copolymer by the Avogadro's number and the number of micelles can be found by dividing the total number of chains by the chains per micelle.

$$Chains_{tot} = \frac{Copolymer \, mass}{MW} \cdot N_A = \frac{0.0306 \, g}{27,000 \frac{g}{mol}} \cdot 6.022 \cdot 10^{23} = 6.825 \cdot 10^{17} \, chains$$

$$N_{micelles} = \frac{Total \, chains}{Chains \, per \, micelle} = \frac{6.825 \cdot 10^{17} \, chains}{5 \, chains/micelle} = 1.365 \cdot 10^{17} micelles.$$

Finally, an appropriate proportion had to be established to identify the number of micelles which were contained in only 1000 µl of PS-CdS solution.

$$1.365 \cdot 10^{17} micelles : 6116.27 = X : 1000$$
$$X = 2.23 \cdot 10^{16} micelles$$

Now, it is easy to establish the desired GNP/QDM ratio. In fact, to realize the current sample, a ratio equal to 0.77 was employed. Since 0.77 is equal to 1/13, it means that one GNP will be present each 13 QDMs. So, to calculate how many GNPs to be added, the following proportion was used.

$$1\ GNP : 13\ QDMs = X\ GNPs : QDMs\ in\ 1000\mu l$$
$$X = \text{1.71} \cdot \text{10}^{15}\ GNPs$$

Therefore, knowing that this was the necessary number of GNPs to be added, an appropriate bulk solution of GNPs in Toluene was prepared. In particular, the required mass was obtained from the number of GNPs as follows.

$$M_{GNPs} = Moles\ of\ GNPs \cdot MW = \frac{N_{GNPs}}{N_A} \cdot MW = 2.84 \cdot 10^{-9} \cdot MW = \text{5.6} \cdot \text{10}^{-7} g$$

Since the volume of Toluene to be added to the GNPs had to be simultaneously large enough to be easily measurable and low enough not to significantly alter the concentration of the original PS-CdS solution, 10 µl were considered as the ideal volume. Thus, the molarity of the solution to be added was calculated as follows.

$$M = \frac{n\ GNPs}{Vol\ Tol} = \frac{2.84 \cdot 10^{-9}}{10\ \mu l} = 2.84 \cdot 10^{-4}$$

At this point, by choosing a comfortable amount of GNPs to be measured, e.g. 0.020 g, the volume of Toluene to produce the so-called *Bulk G* solution could be easily determined, passing through the imposed molarity, which was 336 µl.
In conclusion, to prepare the Bulk G solution, 336 µl of Toluene were mixed with 0.020 g of GNPs and to prepare the vial for slides 5 and 6, 1000 µl of PS-CdS were mixed with 10 µl of Bulk G solution.

Finally, to produce slides 7 and 8, a fourth vial was prepared which contained 1000 µl of PS-CdS, 7.75 µl of Bulk H solution and 10 µl of Bilk G solution.

After the preparation of the four vials, 100 µl of each solution were drop casted on the corresponding glass slides and the solvent annealing apparatus was prepared as previously explained. Subsequently, slides 1, 3, 5 and 7 were removed from the jar after 2 days, dried in vacuum oven at 65°C for 2 h and tested at fluorometer. Instead, slides 2, 4, 6 and 8 were removed after 3 days, dried and tested in the same way. As already reported, excitation and emission spectra were run to verify that the maximum absorption wavelength was around 350-360 nm and that the emission spectra obtained with different excitation wavelengths were coherent. Surprisingly, the obtained absorption spectrum presented an unusual trend with a peak at 330 nm and, accordingly, the emission spectrum with the highest intensity was obtained when the excitation wavelength was exactly 330 nm. Figure 35 (A) shows the absorption spectrum provided by slide 1 (i.e. pure PS-CdS) with the aforementioned peak at 330 nm, figure 35 (B) illustrates the compared emission spectra of slides 1, 3, 5, and 7 and figure 35 (C) shows the compared emission spectra of slides 2, 4, 6 and 8.
As it can be observed, in figure 35 (B), the emission intensity of pure PS-CdS is higher than the emission intensity given by the GNPs and Hexylamine-containing sample (i.e. slide 7). Oppositely, slide 3, or rather PS-CdS + Hexylamine presents a higher intensity which is only overpassed by the intensity of slide 5 or rather PS-CdS + GNPs. These obtained results are apparently conflicting with the previously provided theoretical background.
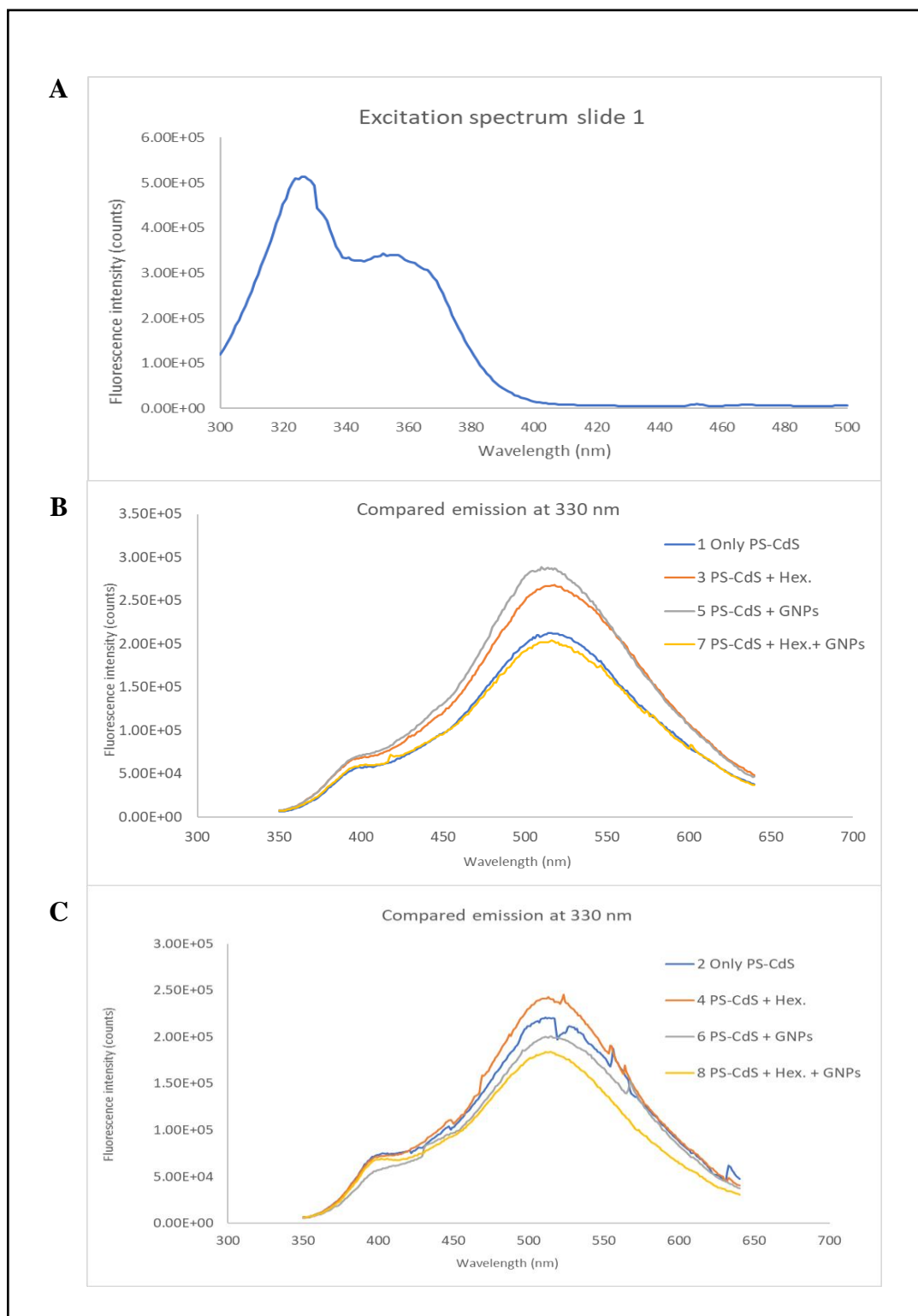
Figure 35 Absorption spectrum of sample LC1-069 slide 1 (A), compared emission of slide 1 (PS-CdS), 3 (PS-CdS + Hexylamine), 5 (PS-CdS + GNPS), 7 (PS-CdS + Hexylamine + GNPs) (B) and compared emission of slide 2 (PS-CdS), 4 (PS-CdS + Hexylamine), 6 (PS-CdS + GNPS), 8 (PS-CdS + Hexylamine + GNPs) (C)

In fact, it seems that a random dispersion of GNPs is able to increase the signal while a close proximity between QDs and GNPs, which was thought to increase the detected fluorescence, rather caused its decrease. A possible explanation is that the proximity could enhance the so-called auto absorption effect while a random dispersion of GNPs is more likely to enhance the detected radiation due to scattering or field effect.

47

Differently, slides 2, 4, 6 and 8 provided a series of spectra where the signal of PS-CdS + Hexylamine is the highest and the fluorescence radiation of sample PS-CdS + GNPs is even lower that the sample with pure PS-CdS. In other words, the even series of samples provided a result according to which the presence of GNPs is always reducing the detected emission.

In conclusion, since the obtained results were conflicting and not totally sound, a new sample was produced with the same procedure which was employed for sample LC1-069.

3.2.3 Sample LC1-075
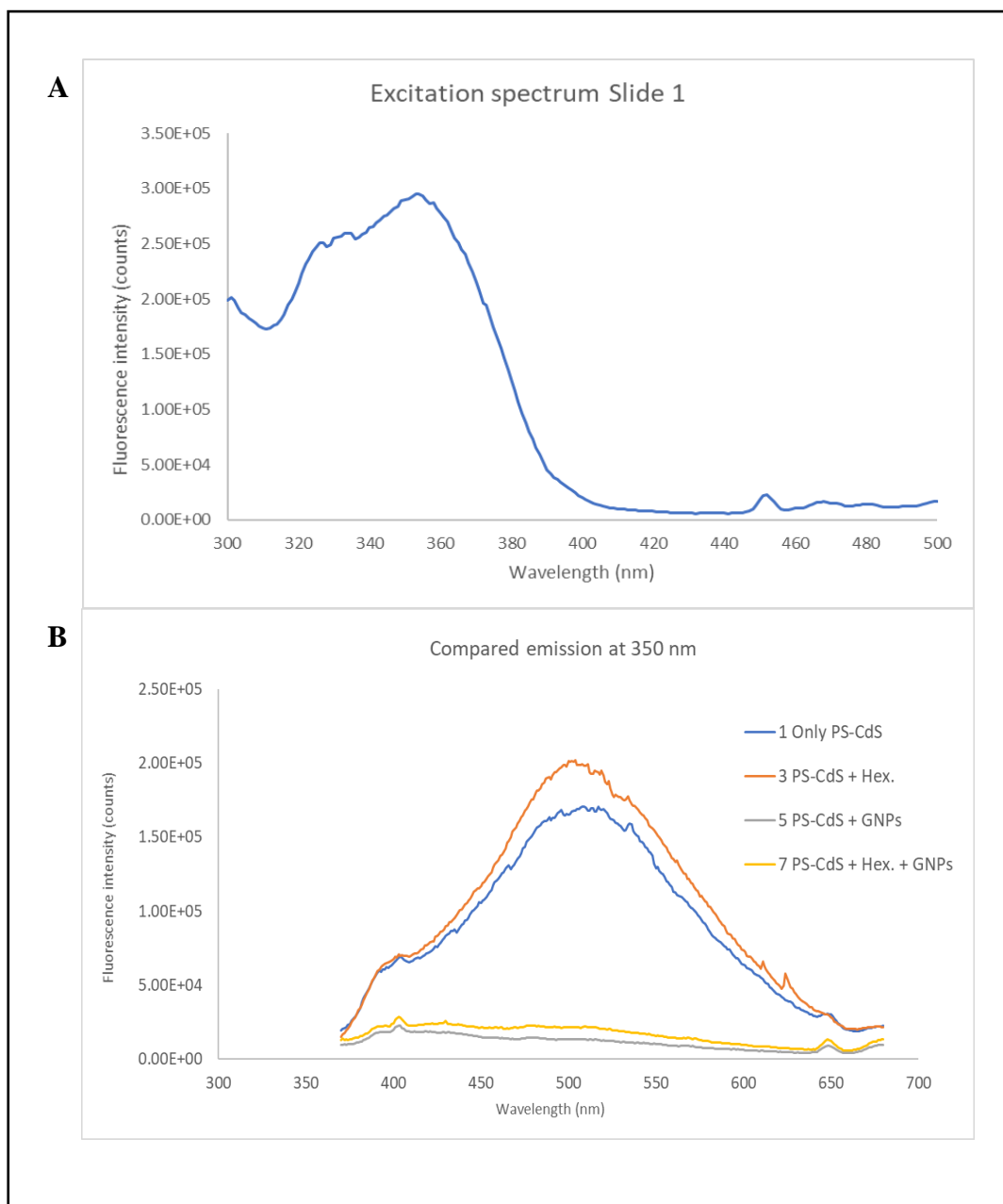
Figure 36 Excitation spectrum of sample LC1-075 slide1 (A) and compared emission of slide 1 (PS-CdS), 3 (PS-CdS + Hexylamine), 5 (PS-CdS + GNPS) and 7 (PS-CdS + Hexylamine + GNPs) (B)

This sample was prepared with the same previously explained procedure except for the drop casted volume which was reduced to 75 µl to prevent solution overflow which occurred more than once when 100 µl where deposited by compromising all the results because of general contamination. The solvent annealing procedure was carried out in the same glass jar with the same amount of

dioxane. However, a shorter time of solvent annealing was tested with slides 1, 3, 5 and 7 which were left into the jar for only 24 hours and then dried in vacuum oven at 65°C for 4 hours. Differently, slides 2, 4, 6 and 8 were solvent annealed for 2 days and then dried in vacuum oven at the same temperature and for the same time. First and foremost, it is worth mentioning that odd and even series of samples provided an identical result demonstrating that it was useless to spend a solvent annealing time longer then one day. Moreover, the obtained excitation spectrum showed a clear peak at 350 nm which confirmed to be the most absorbed wavelength as visible in figure 36 (A) which is referred to slide 1. Finally, different compared emission spectra were obtained with respect to sample 069 as visible in figure 36 (B). In fact, the signal provided by PS-CdS + Hexylamine continued to be the highest, followed by pure PS-CdS. However, in this case, the less emitting slide was the one containing only PS-CdS + GNPs while slide 7, which contained also Hexylamine, provided a slightly higher signal as if the close proximity reduced the auto absorption effect. However, this result was conflicting with the previous one and an unequivocal explanation was still impossible to be hypothesized. At this point, the main objective was to try to identify a procedure providing at least coherent results. Therefore, the following sample was produced with the same parameters to compare all obtained results.

3.2.4 Sample LC1-083

This sample was prepared exactly like LC1-075 and the same volume of 75 µl of solutions was deposited on properly washed glass slides. Slides 1, 3, 5 and 7 were left under solvent annealing for 1 day and subsequently were dried in vacuum oven for 4 h at 65°C. The same drying procedure was applied to slides n. 2, 4, 6 and 8 which were solvent annealed for 2 days. Figure 37 (A) illustrates the obtained excitation spectrum for slide n. 1 where the usual trend is observable which presents the typical peak at about 350 nm. As reported for sample LC1-069, the emission spectra provided by the odd series of samples (B) is rather different compared to the even series (C). In particular, odd samples provided the same result which was already observed in the even series of sample 069. However, the emission given by slides 5 and 7 are here almost indistinguishable. More interestingly, the even series of the present sample 083 resulted to be particularly encouraging. In fact, it can be observed that the emission intensity of pure PS-CdS (i.e. slide 1) is higher than the emission provided by the GNPs-containing sample (i.e. slide 5). A possible explanation for the current behavior is that when gold is randomly dispersed among QDs, the dominant occurring phenomenon is the auto-absorption effect according to which GNPs reabsorb some of the radiation emitted by QDs. In fact, the produced CdS QDs mainly emit at 520 nm which is also the most absorbed wavelength by GNPs. Oppositely, when only Hexylamine is added, apparently without a univocal reason, the reported emission is increased. Moreover, when GNPs and Hexylamine are added together, the observed emission reached the highest value. The obtained result was encouraging because it seemed that the addition of the reducing agent could provide an effective close proximity between QDs and GNPs in such a way that the dominant occurring phenomenon was the field effect resulting in an example of metal enhanced florescence. Therefore, it was concluded that when GNPs are randomly dispersed among QDs they caused mainly the auto-absorption effect while when they are approached to QDs they effectively worked as antennae to concentrate the electric field around themselves by consequently improving the absorption and quantum efficiency of QDs. This last described finding was effectively matching the theoretically expected result. However, the inconsistency between the different series was not an acceptable point and consequently further investigation was required.

3.2.5 Sample LC1-087

This sample was prepared by the same procedure which was previously established but a further point was added. In fact, it was realized that the apparent inconsistency between odd and even series could have been caused by already mentioned intrinsic issues related to fluorometer apparatus.
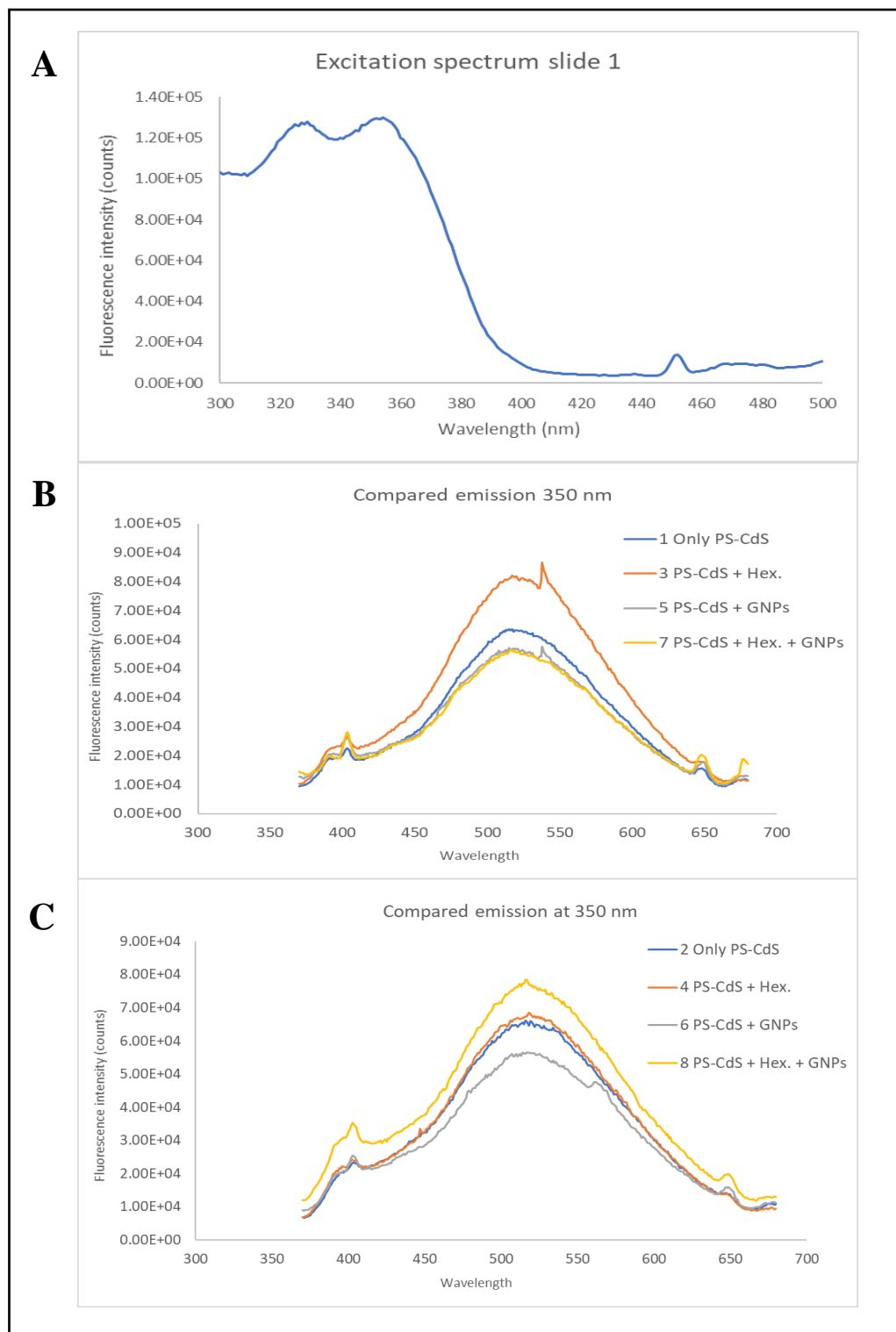
Figure 37 Absorption spectrum of sample LC1-083 slide 1 (A), compared emission of slide 1 (PS-CdS), 3 (PS-CdS + Hexylamine), 5 (PS-CdS + GNPS), 7 (PS-CdS + Hexylamine + GNPs) (B) and compared emission of slide 2 (PS-CdS), 4 (PS-CdS + Hexylamine), 6 (PS-CdS + GNPS), 8 (PS-CdS + Hexylamine + GNPs) (C)

Therefore, instead of preparing two slides per each category (i.e. 8 slides total) and to separately plot the provided excitation and emission results, three slides per each category were produced and the corresponding results were averaged before being plotted. In other words, 12 slides were produced in total and four plots obtained, one per each triplicate. Moreover, the three series were

simultaneously produced, and the solvent annealing time was the same for each glass slide (i.e. 24 h). This allowed for the realization of three series of samples where the objective was to minimize differences among the slides belonging to the same category. Figure 38 shows the layout for the current sample where it is possible to see the 12 glass slides. A crucial point needs to be underlined which is related to the difficulty represented by the low inter-slide distance. This will be often mentioned for the following samples as an element increasing the probability of overflowing. As far as nomenclature is concerned, in order to differentiate the three replicates, alphabetic labels were utilized. More specifically, letters A, B and C were utilized to identify the first, second and third replicate of each category.
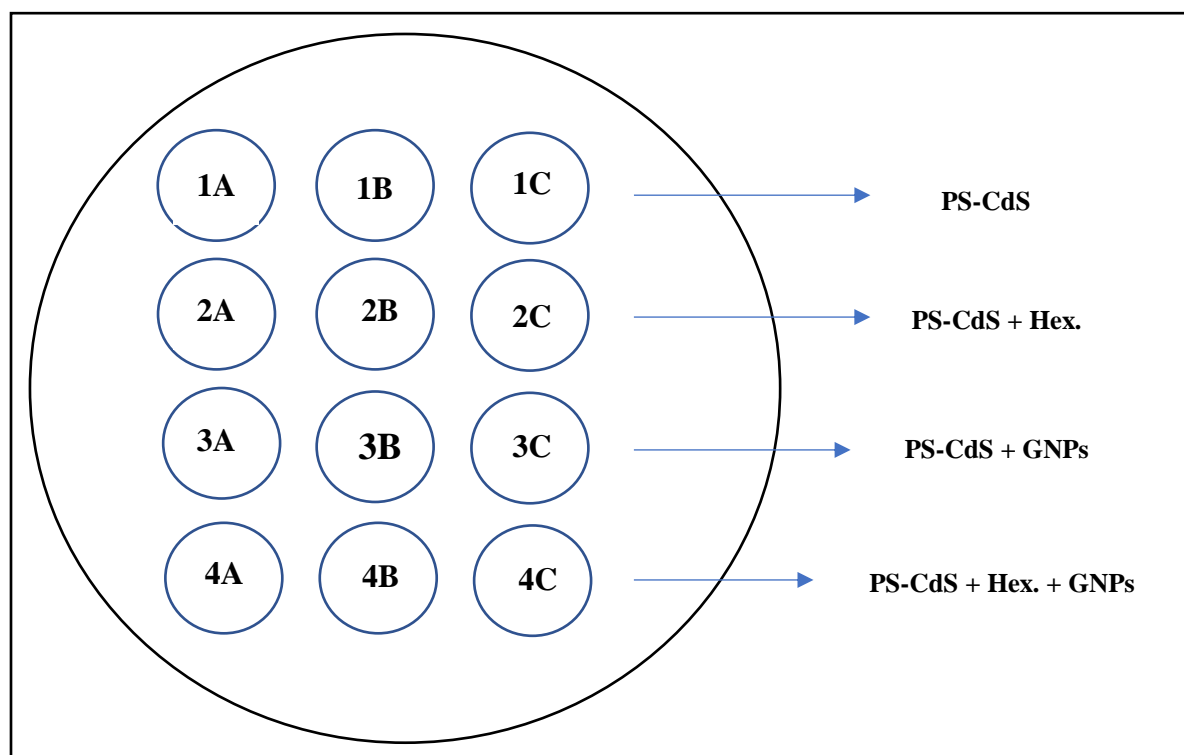
Figure 38 Layout for drop casting and solvent annealing of sample LC1-087

The tested ratio of GNP/QDM was in this case lowered to 0.001 which means that 1 GNP was present each 665 micelles. The same volume of 75 µl of solutions was dropped on all samples which were dried overnight in vacuum oven at 65°C after 24 h of solvent annealing.

As reported in figure 39, a comparison among the excitation and emission spectra obtained from the four categories of slides is illustrated. Specifically, this was done by using an excitation wavelength of 360 nm since it resulted to be the most absorbed wavelength. Like in sample LC1-083, the emission of pure PS-CdS was higher than the emission of PS-CdS + GNPs. This confirmed the dominance of the auto absorption effect occurring when GNPs are randomly dispersed which reduces the detected emission. On the contrary, the addition of Hexylamine seemed to confirm the achievement of a good connection between fluorescent and plasmonic components resulting in the highest emission signal. What remains apparently without any clear explanation is the higher emission of the sample containing PS-CdS and Hexylamine compared to pure PS-CdS.

Moreover, since each plot results from the average of three different glass slides, it is interesting to consider the single plots to provide an idea of how spread the results were. In particular, since the most significant spectra to compare are those obtained from slide 3 (i.e. PS-CdS + GNPs) and slide 4 (i.e. PS-CdS + Hexylamine + GNPs), a graph illustrating all six plots is reported in figure 40. As it can be seen, there is not a considerable difference among slides 4A, 4B and 4C which makes the result reliable. Slides 3A, 3B and 3C, instead, are slightly more spread. However, since the highest plot belonging to slide 3 (i.e. 3B) is clearly below the

lowest plot belonging to slide 4 (i.e. 4C), it is possible and correct to assert that the signal emitted by glass 3 without Hexylamine is lower than the signal emitted by slide 4 with Hexylamine.
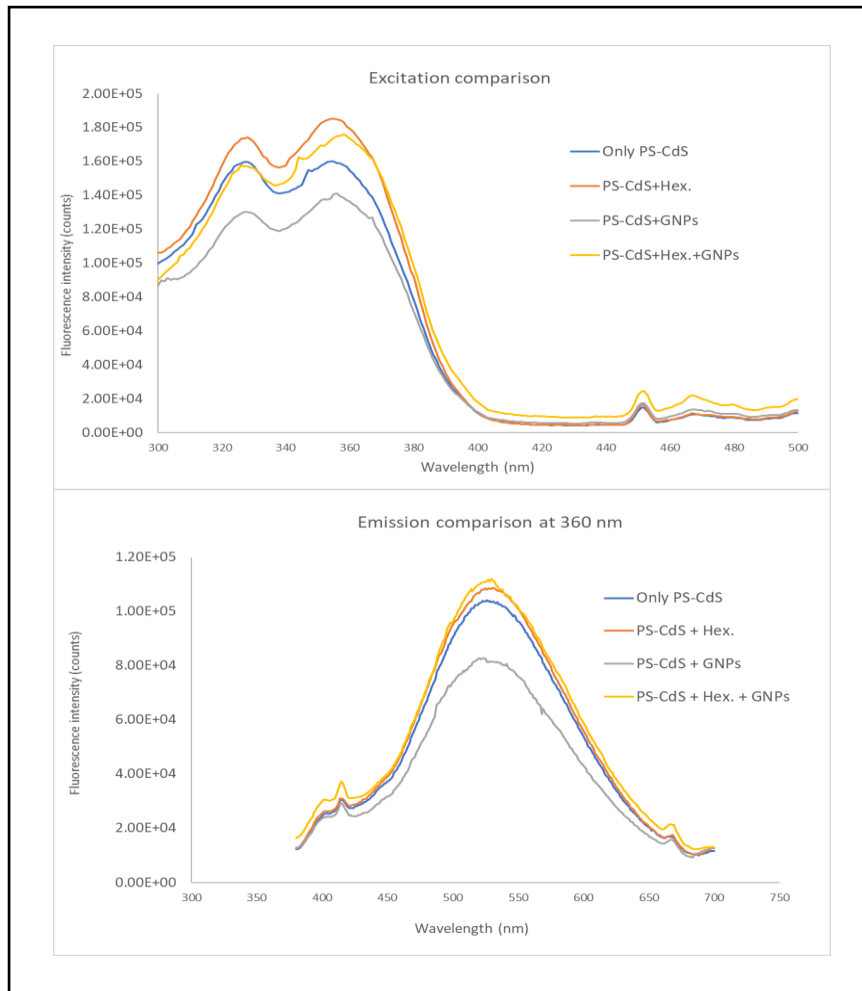
Figure 39 Excitation and emission comparison in sample LC1-087
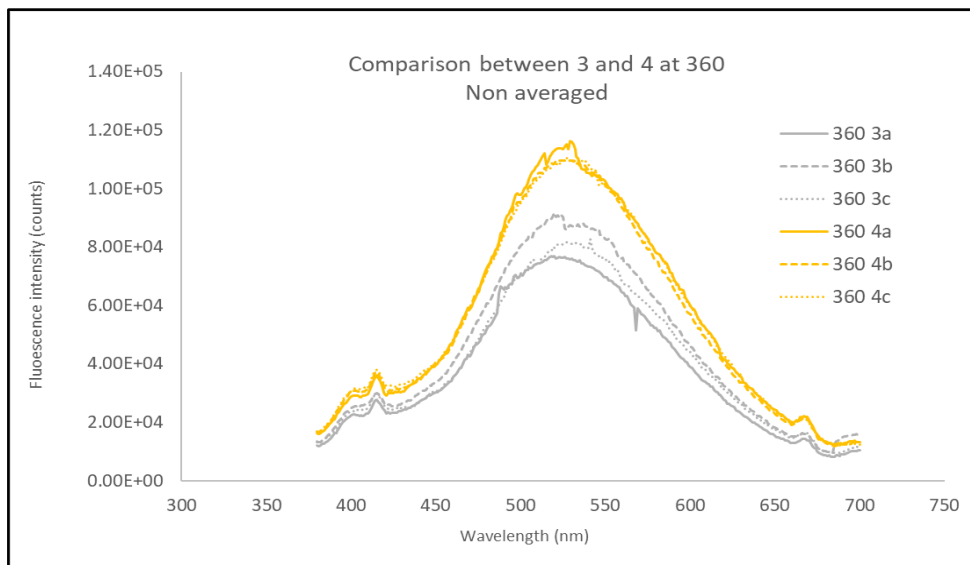
Figure 40 Compared emission of slides 3A, 3B, 3C and 4A, 4B, 4C

With the aim to obtain a confirmation of the result provided by sample LC1-087 also in slightly different conditions, LC1-088 was prepared.

3.2.6 Sample LC1-088

The same procedure applied to realize sample LC1-087 was utilized for sample LC1-088 except for the increased GNP/QDM ratio that in this case was risen to 0.007. In other words, 1 GNP was now present each 133 micelles. Theoretically, the expected result was a similar plot to LC1-087 but the effect of enhanced photoluminescence provided by the close proximity between QDs and GNPs was expected to be more pronounced. However, when LC1-088 was tested after the same solvent annealing procedure and drying utilized for LC1-087, a conflicting result appeared as it can be seen in figure 41. In fact, the pure PS-CdS sample showed an emission intensity which was higher than both samples with gold with and without Hexylamine. Consequently, it seemed that the presence of Hexylamine was not really effective in increasing the detected PL. However, it was still true that the emitted PL was higher in the case on simultaneous presence of GNPs and Hexylamine compared to the case where only GNPs were added. The fundamental difference is that in LC1-087, the effect of Hexylamine was intense enough to provide a stronger signal than pure PS-CdS, while in LC1-088 the action of the reducing agent was only able to increase the detected radiation compared to the sample with PS-CdS + GNPs.
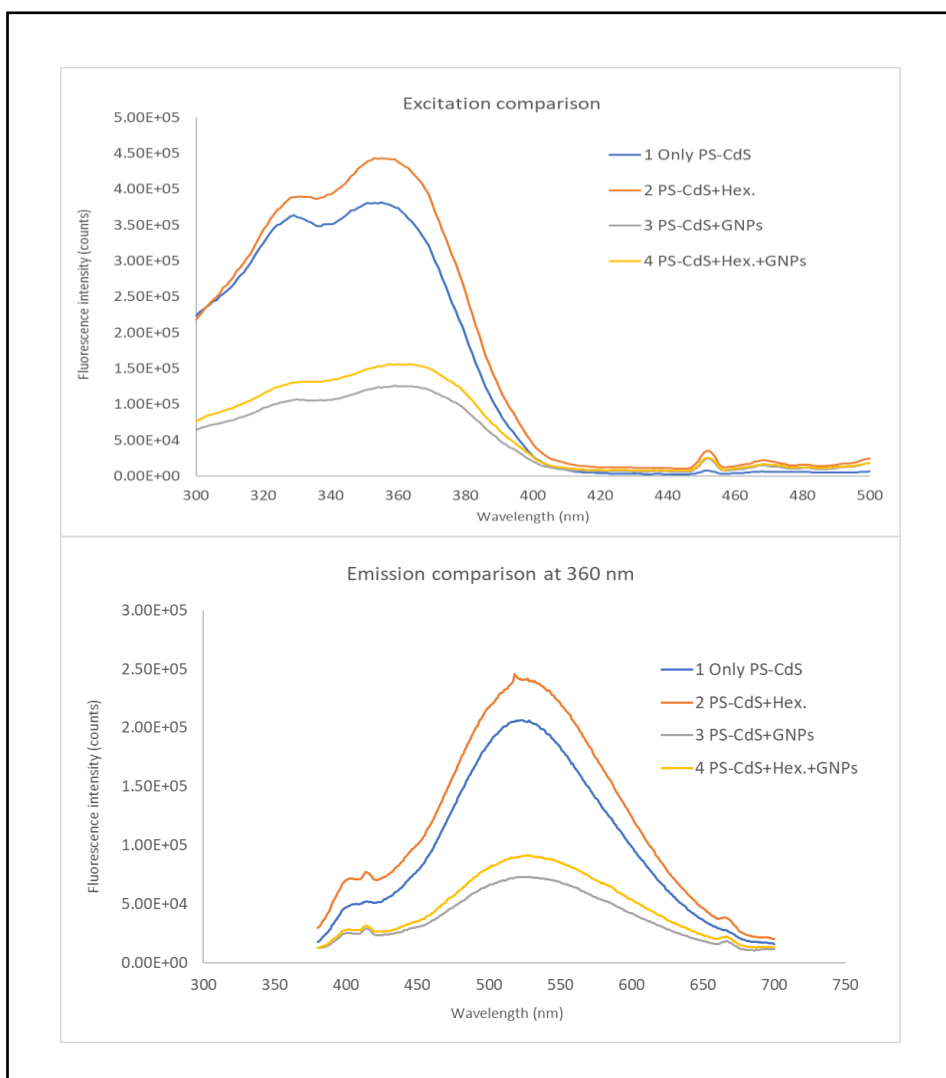
Figure 41 Excitation and emission comparison in sample LC1-088

At this point, it appeared useful to consider exclusively a comparison between the signal emitted by PS-CdS + GNPs and PS-CdS + Hexylamine + GNPs and to compare the obtained increase in the last two considered samples, namely LC1-087 and LC1-088. In regard to this, figure 42 shows the achieved compared result.

It can easily be noticed that the blue plots (i.e. sample LC1-087) are separated by a larger gap compared to the red plots (i.e. sample LC1-088). In other words, it was observed that when the added amount of gold was lower, which was the case of sample LC1-087, the achieved increase in PL after the addition of Hexylamine was more significant. This phenomenon was tried to be explained by hypothesizing that a low amount of gold could effectively be connected to QDs providing a visible field effect able to enhance the detected PL. Oppositely, when the added amount of gold reached excessive values, the auto absorption effect was more likely to dominate, and the PL increase was reduced. Therefore, with the aim to demonstrate the validity of this assertion, a different ratio GNP/QDM, which was even lower than 0.001, was tested in the next sample.
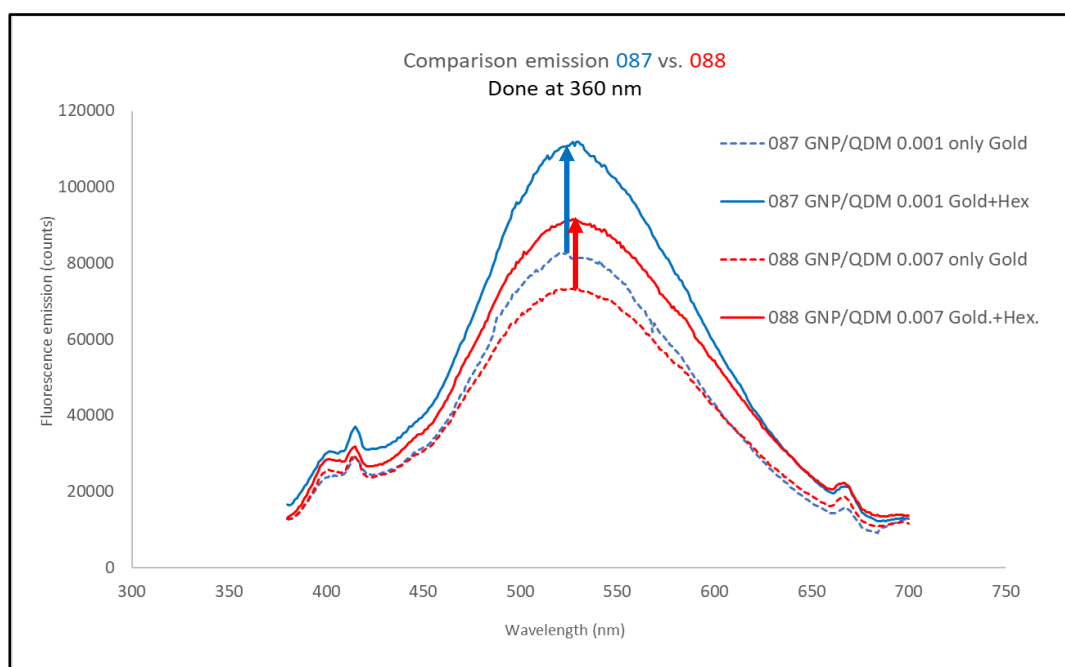
Figure 42 Inter-sample compared emission of PS-CdS+GNPs and PS-CdS+Hexylamine+GNPs in samples LC1-087 and LC1-088

3.2.7 Sample LC1-092 and LC1-094

A GNP-QDM ratio of 0.0007 was tested in sample LC1-092 to identify whether a lower amount of GNPs compared to sample LC1-087 could have been more effective in providing a PL enhancement when QDs and GNPs were approached by the addition of Hexylamine. More specifically, in this case, the investigated ratio corresponded to 1 GNP each 1410 micelles. It is important to remind that, during the production of this sample, the previously mentioned phenomenon of overflowing occurred by causing a general contamination and unreliability of results. In particular, few hours (e.g. 2-3 h) after the drop casting step, during the solvent annealing procedure in the sealed glass jar in saturated dioxane atmosphere, the deposited solution flew over the edges of a glass slide by causing a chain reaction among almost all the other slides and imposing a necessary new setting up. This effect was probably due to a poor interaction between the glass surface and the deposited sample solution. In fact, the previously described washing procedure constituted by four different steps of sonication in methanol, chloroform, toluene and acetone, intended to increase the affinity between surface and solution, could have lost its effect due to the long storage time of the washed glass slides before their effective usage during sample realization. Therefore, a further washing before proceeding to drop cast the different solutions was

identified as necessary and it was performed by using chloroform and acetone. More precisely, this washing step was then repeated every time the glass slides had received the main washing treatment more than 24 hours in advance, before effectuating the drop casting and solvent annealing procedure.

Indeed, after the first unsuccessful attempt to realize sample LC1-092, the further washing allowed for the creation of a good sample which compared excitation and emission done at 360 nm are reported in figure 43.
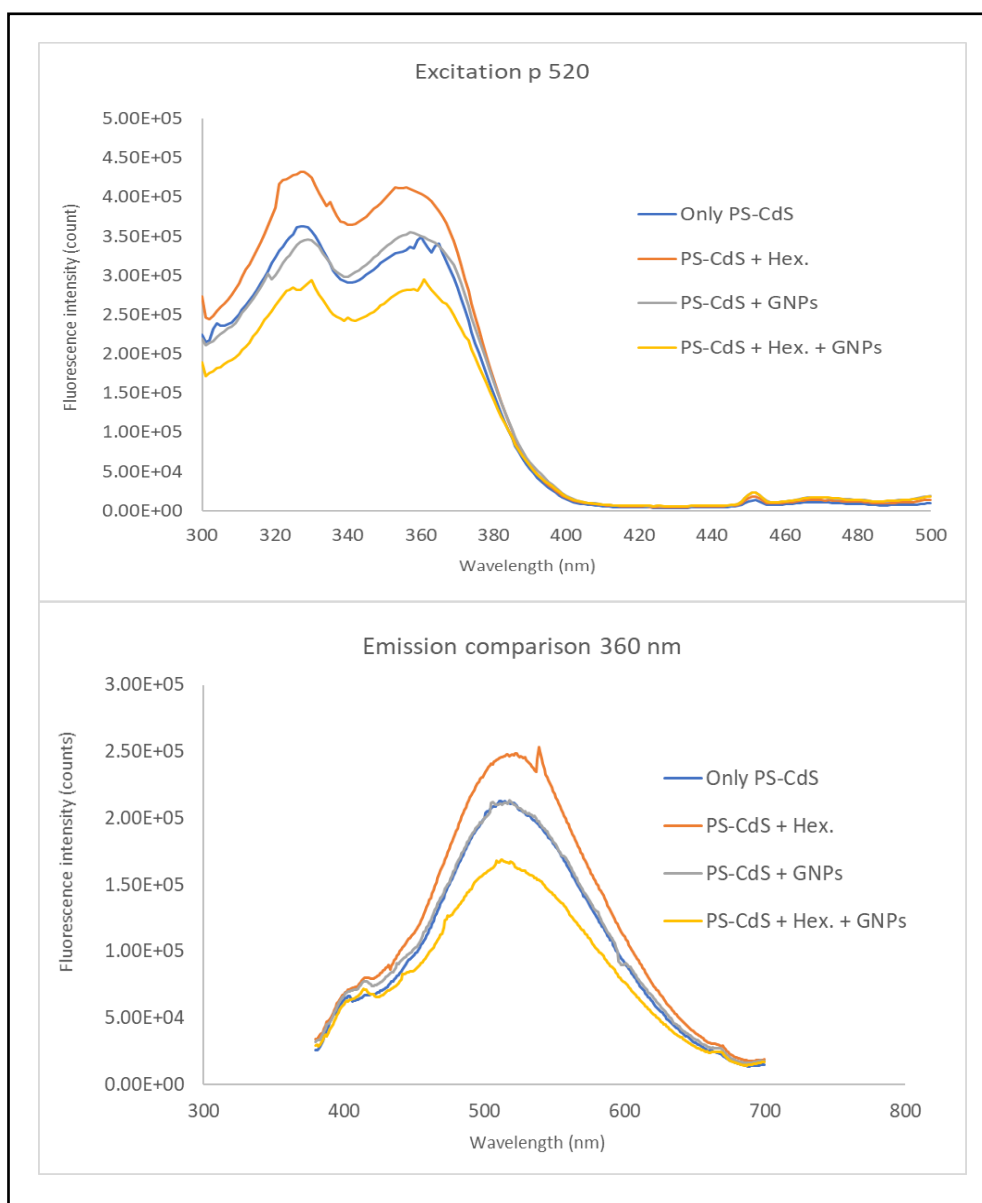
Figure 43 Excitation and emission comparison in sample LC1-092

Unfortunately, an unexpected and apparently inexplicable result was obtained. In fact, as visible in the previous figure, the PL signal emitted by slides 4 (i.e. PS-CdS + Hexylamine + GNPs) was lower than slide 3 (PS-CdS + GNPs) as if the proximity between QDs and GNPs induced by the reducing agent were enhancing the auto absorption effect in contrast with what observed in samples LC1-087 and LC1-088. Figure 44 clarifies the mentioned behavior by showing the compared emission of the last three samples in presence and absence of Hexylamine. Specifically, the same blue and red positive gaps indicated in figure 42 can be seen together with the resulting negative gap of sample LC1-092 highlighted in green.
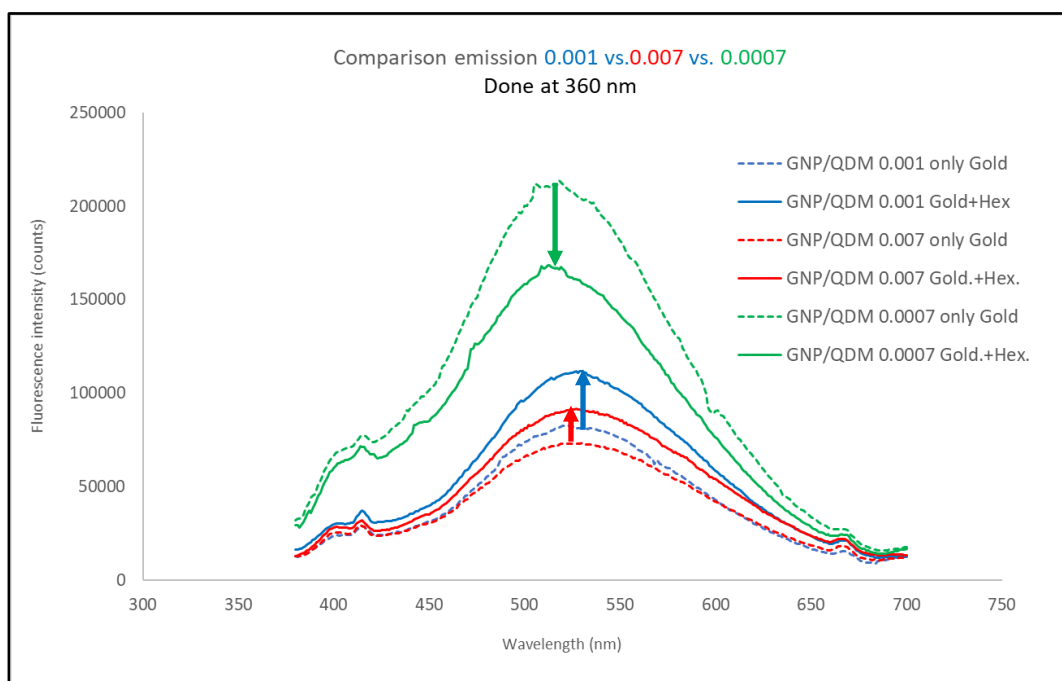
Figure 44 Inter-sample compared emission of PS-CdS+GNPs and PS-CdS+Hexylamine+GNPs in samples LC1-087, LC1-088 and LC1-092

In order to gain more evidence on the reliability of the previous results, another sample was produced and tested. In particular, this was identified by the name of LC1-094 and it was characterized by an intermediate GNP/QDM ratio with respect to samples 087 and 088, or rather 0.004. In other words, 1 GNP was present each 250 micelles. Since both samples 087 and 088 had provided an enhanced PL in the case of combined presence of GNPs and Hexylamine with respect to GNPs alone, also for sample 094 the expected result was the same. However, surprisingly enough, a trend similar to sample 092 was reported and it is shown in figure 45 in the form of a negative gap highlighted in yellow.
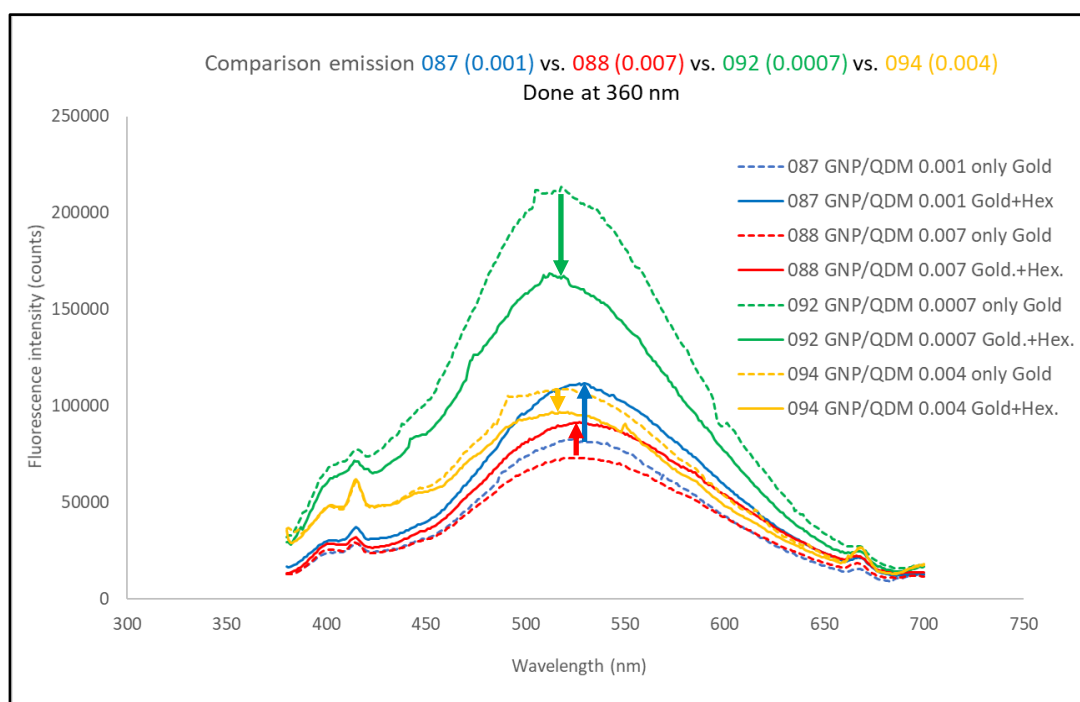
Figure 45 Inter-sample compared emission of PS-CdS+GNPs and PS-CdS+Hexylamine+GNPs in samples LC1-087, LC1-088, LC1-092 and LC1-094

To sum up, as indicated in table 2, for the GNP/QDM ratios of 0.001 and 0.007 corresponding to sample 087 and 088, a positive PL enhancement was reported when Hexylamine was present together with GNPs. Oppositely, for ratios of 0.0007 and 0.004 corresponding to sample 092 and 094, a decrease in PL was caused by the combination of GNPs and Hexylamine compared to the case of GNPs alone.

Sample name	GNP/QDM	Micelles per each GNP	Gap GNPs+Hex / GNPs alone
LC1-087	0.001	665	⬆
LC1-088	0.007	133	⬆
LC1-092	0.0007	1410	⬇
LC1-094	0.004	250	⬇

Table 2 General comparison among samples 087, 088, 092 and 094

In conclusion a clear trend of the relationship between detected PL and GNP/QDM ratio was impossible to be individuated. After the realization of sample LC1-094 it was clear that the identification of a coherent and reproducible pattern was hard to obtain. Moreover, it was confirmed that the oscillations due to intrinsic issues related to the fluorometer apparatus played a fundamental role. In fact, since the different samples 087, 088, 092 and 094 had been tested on different days, it was impossible to consider their comparison as reliable. In fact, if it was out of discussion that each couple of spectra was related exactly by the mentioned positive or negative gap, what was not certain was the respective position of the different samples. Moreover, a new batch of PS-CdS and GNPs had been produced each time to realize each solid sample and consequently many different parameters could have affected the actually detected PL. In other words, it was impossible to trust the relative intensity of the four dashed trends among each other as well as that of the continuous trends. Therefore, in order to produce more reliable samples a slightly different procedure was applied which is described in the following paragraph.

3.2.8 Final successful approach: "The ratios method"

The final part of the present thesis work provided better results because the main method which was applied to test the different samples was radically modified and improved. Specifically, the most important issues which had been identified in the previous approach are listed below:

1) Poor reliability of results due to intrinsic oscillations deriving from the fluorometer apparatus itself. In fact, as it was specified before, the emitted radiation by the Xe lamp could suffer from intensity variation. Likewise, the detector could report a different result according to the current condition in terms of environmental temperature and other external factors. The mentioned variations were tolerable as long as the measurements were taken during the same session, while they

caused totally unreliable results if the fluorometer was switched off and turn on again. To explain it better, once the Xe lamp was activated and warmed, all the measurements had to be performed without turning the lamp off. It was demonstrated that the same sample could provide different emission and excitation spectra if the measurements were taken repeatedly during the day after a cycle of cooling and warming of lamp and detector. Since an unacceptable variation was reported if measurements were taken on the same sample at a relatively short distance of time (e.g. one during the morning and another one during the afternoon) it was clear that spectra obtained on different days were definitely impossible to be reliably compared. On the contrary, it was considered acceptable to compare results obtained on samples which were tested at a maximum temporal distance of about 6 h as it will be reported later.

2) Poor reliability due to different batches of PS-CdS and GNPs. In fact, each time a new series of glass slides had to be prepared, a new batch of PS-CdS was produced. As far as GNPs are concerned, multiple batches were produced even if the quantity produced per batch allowed for a longer durability than PS-CdS and consequently the same batch of GNPs could be used to produce different samples. However, dimension variations occurred because of slightly different synthesis results or because of particles aggregation and it was not reliable to compare glass slides which were produced with different sized-particles. In fact, as it was demonstrated before, sizes are important to determine emission and absorption wavelengths and could consequently strongly affect the result of the interaction between fluorescent and plasmonic components.

In order to solve the aforementioned problems, a better procedure was hypothesized to carry out a new series of experiments which were still conducted according to approach n.2.

1) Production and analysis of 5 different ratios GNP/QDM in the range 0.001-0.01.
   1) Sample 1: GNP/QDM = 0.001
   2) Sample 2: GNP/QDM = 0.0025
   3) Sample 3: GNP/QDM = 0.005
   4) Sample 4: GNP/QDM = 0.0075
   5) Sample 5 GNP/QDM = 0.01

2) Production of two different cases per each sample.
   1) Case A: PS-CdS + GNPs
   2) Case B: PS-CdS + Hexylamine + GNPs

3) Production of three identical samples per each case in order to do triplicate measurements.
   1) Case Ai, Aii, Aiii
   2) Case Bi, Bii, Biii

4) Production of two reference samples with three identical slides per each sample.
   1) Sample 0i, 0ii, 0iii = only PS-CdS
   2) Sample 00i, 00ii, 00iii = PS-CdS + Hexylamine

Therefore, a total set of samples was constituted by 36 glass slides as it is shown in table 3 and as it is illustrated in figure 46 which shows a utilized box to keep the samples ordered and safe from photobleaching. On each sample, it was necessary to run an excitation spectrum in the usual range of 300 nm – 500 nm and an emission spectrum at 360 nm. It is remarkable that all measurements had to be run during the same day in order to ensure a good consistency of results. In regard to this, the total duration of an analysis

session lasted about 6 hours and minor results oscillations, deriving from the fluorometer during this period of time, were considered as acceptable. Furthermore, PS-CdS and GNPs employed for the realization of a complete series of samples had to come from the same batch. In this way, it was possible to reliably compare different GNP/QDM ratios and to identify the action of an increasing amount of gold. Moreover, it was possible to investigate the role of Hexylamine in enhancing QDs fluorescence properties by ensuring a closer proximity to GNPs.

Sample name	GNP/QDM	PS-CdS	Hexylamine	GNPs	Replicates
1 A	0.001	x		x	3
1 B	0.001	x	x	x	3
2 A	0.0025	x		x	3
2 B	0.0025	x	x	x	3
3 A	0.005	x		x	3
3 B	0.005	x	x	x	3
4 A	0.0075	x		x	3
4 B	0.0075	x	x	x	3
5 A	0.01	x		x	3
5 B	0.01	x	x	x	3
0	0	x			3
00	0	x	x		3
					Tot: 36

Table 3 Typical organization of last series of samples

More specifically, with the aim to effectively compare the signal obtained from the different glass slides, a method based on ratios establishment was conducted. In particular, three main ratios were defined.

1) Ratio R = B/A

This is the ratio between the maximum emission (i.e. at 520 nm) of samples with GNPs + Hexylamine and samples with only GNPs (i.e. B/A) and it was useful to study the effect of the reducing agent on an increasing amount of gold NPs.

2) Ratio R1 = A/0

This is the ratio between the maximum emission (i.e. at 520 nm) of samples with GNPs and samples with only PS-CdS (i.e. A/0) and it was useful to investigate the effect of GNPs addition and increase while in absence of Hexylamine.

3) Ratio R2 = B/0

This is the ratio between the maximum emission (i.e. at 520 nm) of samples with GNPs + Hexylamine and samples with only PS-CdS + Hexylamine (i.e. B/00) and it was useful to investigate the effect of GNPs addition and increase while in presence of Hexylamine.
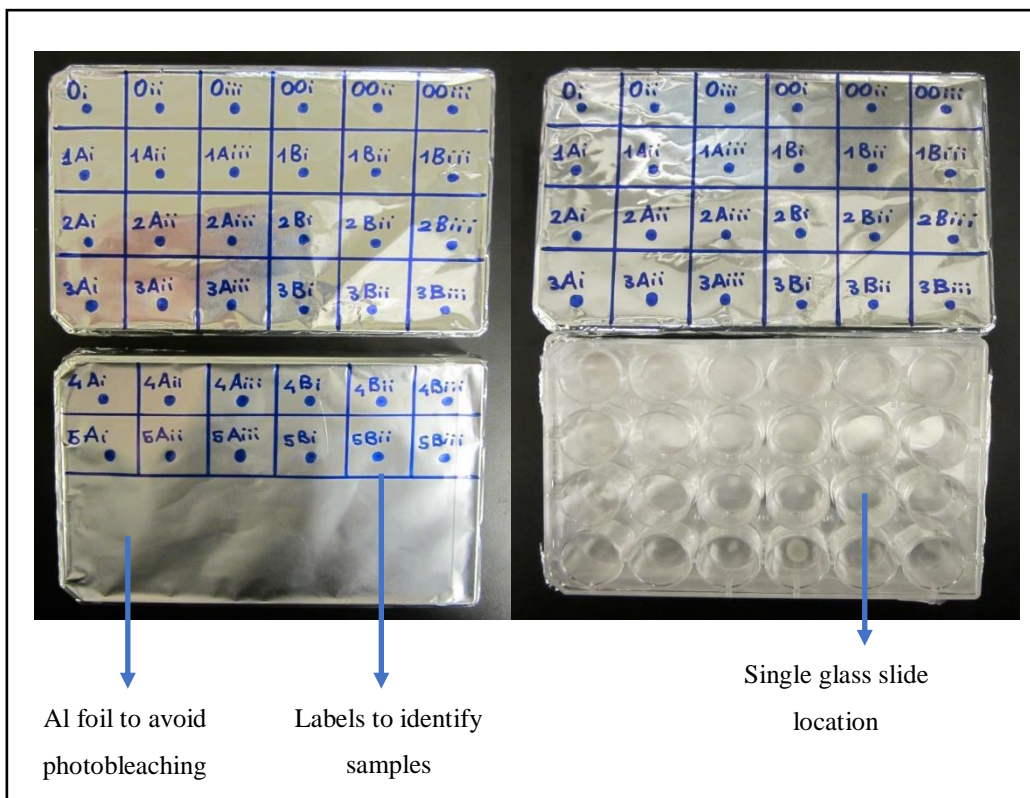
Figure 46 Samples boxes with single glass slide locations, specific labels and aluminum foil protection

The present procedure provided positive results because it was able to overcome the problem represented by the intrinsic signal variation due to the fluorometer apparatus. In fact, if different samples had been produced and orderly tested, the signal emitted by the first tested sample would have been hardly comparable with the signal emitted by the last sample because the fluorometer parameters could have been slightly changed as said before. Instead, by establishing and calculating ratios, possible artifacts deriving from long time separated measures would have been less likely to affect the final result. More precisely, all samples illustrated in figure 46 were tested in the following order: 0i – 00i – 1Ai – 1Bi – 2Ai – 2Bi – 3Ai – 3Bi – 4Ai – 4Bi – 5Ai – 5Bi. Subsequently, replicate ii was tested in the same order and finally replicate iii. Later, all replicates were averaged among each other in order to obtain a total of 12 values. For instance, 0i, 0ii and 0iii were averaged so that a single final value was achievable for slide "0". The same was done for all glass slides and then all ratios were calculated and plotted. The main advantage represented by the described method is that the long time elapsing between the first and the last sample, or rather 0i and 5Biii, didn't represent a problem since all samples belonging to replicate "i" were tested near in time and the same for replicates "ii" and "iii". As it will be discussed in Chapter 4, this procedure allowed to find interesting and sound results about the action of GNPs and Hexylamine in terms of field effect, scattering and auto absorption effect.

3.2.8.1 Sample LC1-099

LC1-099 was the first sample which was produced according to the aforementioned procedure. Specifically, 12 vials had to be prepared before proceeding to perform the usual drop casting and solvent annealing steps. Therefore, 12 5-ml vials were filled with 1 ml of PS-CdS solution each. They were labelled and filled as follows.

- Sample 0: 1 ml of pure PS-CdS
- Sample 00: 1 ml of pure PS-CdS + 7.83 µl of Bulk H solution (45 µl of Hexylamine and 11.574 ml of pure dioxane)

- Sample 1A: 1 ml of pure PS-CdS + 10 µl of Bulk G1 solution (0.005 g of GNPs and 28.86 ml of toluene). GNP/QDM = 0.001
- Sample 1B: 1 ml of pure PS-CdS + 7.83 µl of Bulk H solution + 10 µl of Bulk G1 solution
- Sample 2A: 1 ml of pure PS-CdS + 10 µl of Bulk G2 solution (0.005 g of GNPs and 12.83 ml of toluene). GNP/QDM = 0.0025
- Sample 2B: 1 ml of pure PS-CdS + 7.83 µl of Bulk H solution + 10 µl of Bulk G2 solution
- Sample 3A: 1 ml of pure PS-CdS + 10 µl of Bulk G3 solution (0.005 g of GNPs and 6.41 ml of toluene). GNP/QDM = 0.005
- Sample 3B: 1 ml of pure PS-CdS + 7.83 µl of Bulk H solution + 10 µl of Bulk G3 solution
- Sample 4A: 1 ml of pure PS-CdS + 10 µl of Bulk G4 solution (0.005 g of GNPs and 4.26 ml of toluene). GNP/QDM = 0.0075
- Sample 4B: 1 ml of pure PS-CdS + 7.83 µl of Bulk H solution + 10 µl of Bulk G4 solution
- Sample 5A: 1 ml of pure PS-CdS + 10 µl of Bulk G5 solution (0.005 g of GNPs and 3.20 ml of toluene). GNP/QDM = 0.01
- Sample 5B: 1 ml of pure PS-CdS + 7.83 µl of Bulk H solution + 10 µl of Bulk G5 solution

It is essential to highlight the order with which the different components were added. Firstly, all 12 samples were filled with pure PS-CdS. Later, sample 00 and all samples belonging to category B were added 7.83 µl of Bulk H solution and finally, all samples belonging to categories A and B were added the corresponding Bulk G solution. The order actually matters for samples B because it is important to add Hexylamine before GNPs so that when they are added they can find already open TTC groups and the connection can be immediately established.

Another important point which needs to be specified is that the solvent annealing apparatus could fit a maximum of 12 glass slides so that they could be separated by a sufficient distance to prevent reciprocal contamination due to solution overflow. As a consequence, the 36 glass slides had to be split in three production sessions. In other words, all samples belonging to replicate i were produced together and the same was valid for replicates ii and iii.

Once all glass slides belonging to replicate i were properly arranged on the support, 75 µl of the corresponding solution were drop casted. After, the glass jar was filled with 10 ml of dioxane and it was adequately sealed with Al foil. As previously asserted, the solvent annealing procedure lasted 24 hours before removing the glass slides from the jar and drying them in vacuum oven at 65°C overnight. After the extraction of replicate i from the jar, replicate ii was started immediately. In this way, while replicate i was in the oven, the next replicate could undergo the solvent annealing procedure.
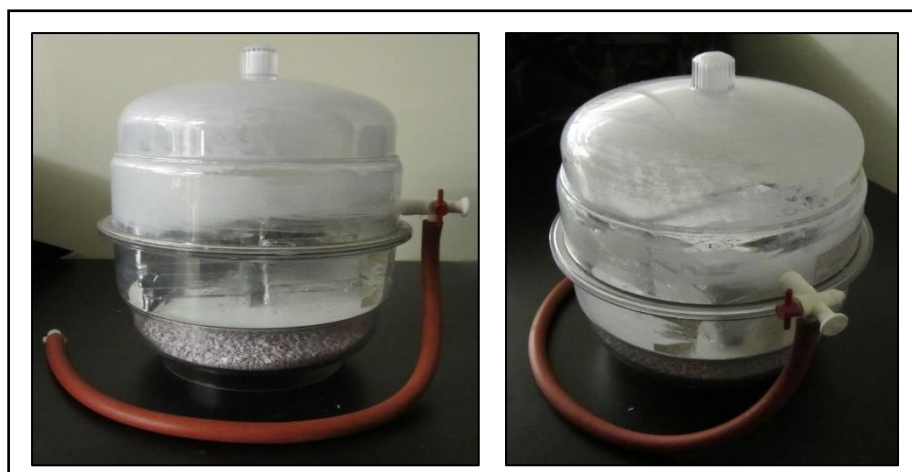
Figure 47 Desiccator used to store ready replicates while producing the next ones

After 24 h, when also replicate ii was ready to be removed from the jar and to be dried in the oven, replicate i was momentarily stored in the desiccator visible in figure 47. Simultaneously, series iii could be prepared and could undergo its solvent annealing procedure at the end of which the glass slides were dried and series ii was kept in the desiccator together with series i. In this way, after three days, all samples were ready and could be tested at fluorometer to provide excitation and emission spectra.

The intrinsic drawback of this three day-involving procedure is that series i, ii and iii were probably affected by serious inequalities due to the different day when they were produced. In fact, different values of humidity or temperature could affect the solvent annealing procedure and different features could appear in the deposited films after their solidification upon drying. Figure 48 shows the entire series of slides belonging to sample LC1-099. A curious turbidity can be observed on samples belonging to replicate ii which seemed to be attributable to humidity which was probably trapped during the solvent annealing step.
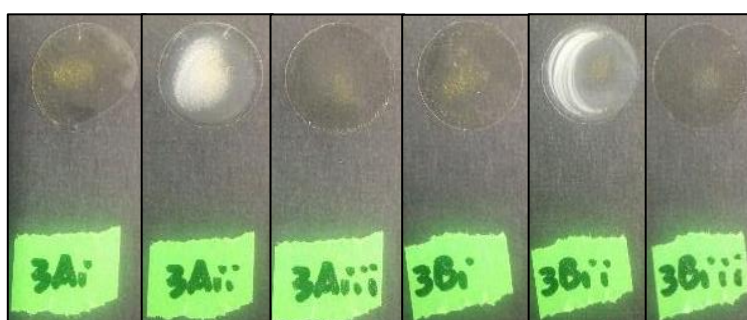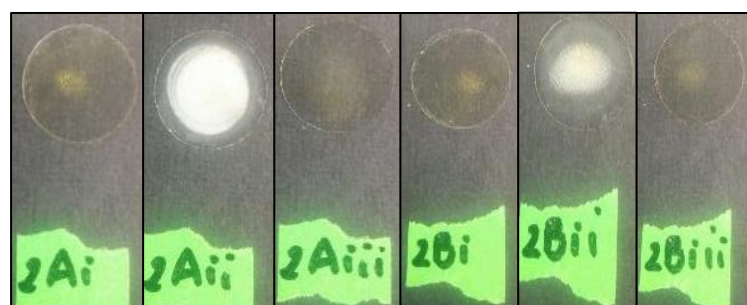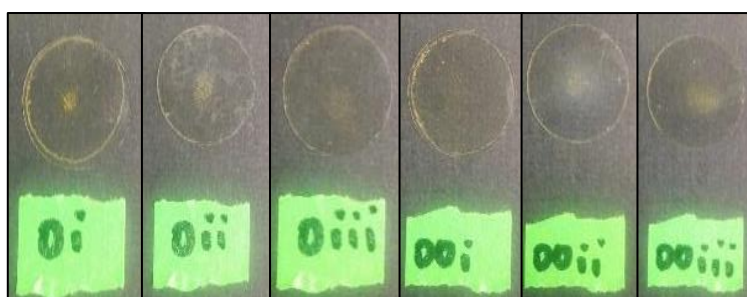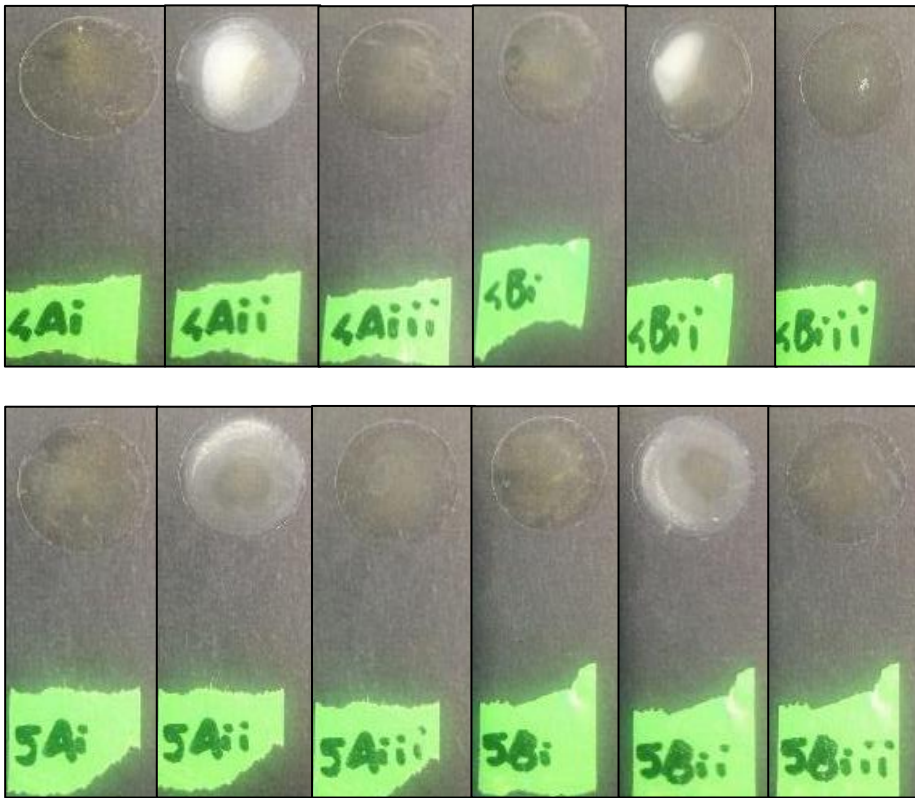
Figure 48 Physical appearance of sample LC1-099

Once all glass slides were ready, they were tested at fluorometer as explained in the previous paragraph. In particular, excitation and emission spectra were obtained for all slides and the emission at 520 nm was utilized to establish the previously mentioned three ratios, namely R, R1 and R2. The following step was to obtain a single spectrum per each sample by averaging the results deriving from the three replicates. For example, sample 0i, 0ii and 0iii presented respectively these emission intensity values:

$$0i = 2.82 \cdot 10^5$$
$$0ii = 2.74 \cdot 10^5$$
$$0iii = 3.34 \cdot 10^5$$

As it is easily observable, even if these samples were theoretically identical, the resulting emission intensity was slightly different. As previously asserted, this could be due to many different reasons among which different temperature and humidity conditions during samples synthesis, different solidification procedure, different sample ages (i.e. replicate i was two days older than replicate iii) and intrinsic issues regarding the emitted and detected light by the fluorometer apparatus.

Therefore, beside the average value which is provided below, the standard deviation was also reported.

$$Average \ intensity = 2.96 \ \cdot 10^5$$
$$Standard \ deviation = 3.24 \ \cdot 10^4$$

Indeed, once these two values were calculated, it was possible to define the so-called percentage relative error by dividing the standard deviation by the average intensity and by multiplying the result by 100 as it follows.

$$\%Error = \frac{Standard \ deviation}{Average \ intensity} \cdot 100 = \frac{3.24 \ \cdot 10^4}{2.96 \ \cdot 10^5} \cdot 100 = 10.94\%$$

This relative error was used to draw the error bars which appear in figures 49 and 50 which depict the three aforementioned ratios, namely R, R1 and R2. In particular, to define the right error associated to the ratio between two values, an error propagation procedure was applied which provided the right value to utilize in the plot. For instance, considering slide 1A, it was possible to conduct the same procedure already reported for glass slide 0. In this way it was possible to obtain the error associated to this slide, or rather 4.73%. At this point, the error associated to the ratio A/0 could be achieved by multiplying the biggest error among those involved in the calculation by the effective intensity ratio R1 = A/0 and by dividing the result by 100. Table 4 reports the utilized value with the final error.

Rel. Err. 0 (%)	Rel. Err. A (%)	Ratio R1 (A/0)	Error
10.94	4.73	8.75E-01	0.09

Utilized Relative Error

$$Final\ Error = \frac{Utilized\ Relative\ Error \cdot R1}{100}$$

Table 4 Final Error calculation example

Figure 49 (A) illustrates the resulting ratio between the emission of samples with and without Hexylamine, with GNPs (i.e. R = B/A). It has to be reminded that, in this case, the so-called R ratio was obtained by averaging three signals coming from three glass slides of category B and three of category A. In other words, ratio R for sample 1, or rather R = 1B/1A was calculated as follows.

$$R = \frac{Average\ (1Bi, 1Bii, 1Biii)}{Average\ (1Ai, 1Aii, 1Aiii)}$$

Therefore, the reported error bars obtained by the previous series of steps are useful to provide an idea of how spread the results were. In fact, relative errors were calculated by involving the standard deviation which is able to indicate how much the obtained results are different from the average value. Moreover, with the aim to provide a clearer idea of the exact position of the three ratios, the plot in figure 49 (B) is reported. Precisely, this indicates the position of all calculated ratios. For instance, for sample 1, it shows ratio 1Bi/1Ai, 1Bii/1Aii and 1Biii/1Aiii.

The general trend which can be individuated in the previous spectra is a significant increase between sample 1 and sample 3 which is later followed by a decrease with sample 4 and a new slight increase with sample 5. Even if a clearer trend will be available with the following samples, what is already understandable by sample LC1-099 is that the increase in the amount of GNPs allowed for an increase of the ratio between the signal emitted by the sample with GNPs + Hexylamine and by the one without Hexylamine. Specifically, this trend was observed until sample 3, or rather until a ratio GNP/QDM equal to 0.005. In other words, the addition of the reducing agent seemed to provide an evident field effect observable in the enhanced signal of samples B compared to the one of samples A until when a limit of added GNPs was reached. In fact, after sample 3, a decrease was observed, and the ratio reached a value lower than 1, meaning that the sample with Hexylamine was emitting less than the one without.

It could be concluded that until a ratio of 0.005, the field or plasmonic effect was dominant, while when more gold was added, the Hexylamine was no more effective in establishing a preferential close proximity between GNPs and QDs. In other words, when too much GNPs are present, it exists no more difference between a random dispersion and a selective positioning. As a consequence, the auto absorption effect seems to become dominant. Finally, the apparent increase observed in sample 5 could have been caused by scattering which is likely to become significant when a considerable amount of gold is added. However, this effect should be

restrained because of the intrinsic nature of the current measure. In fact, calculations based on ratios allowed to cancel the action of those components which are equally present.
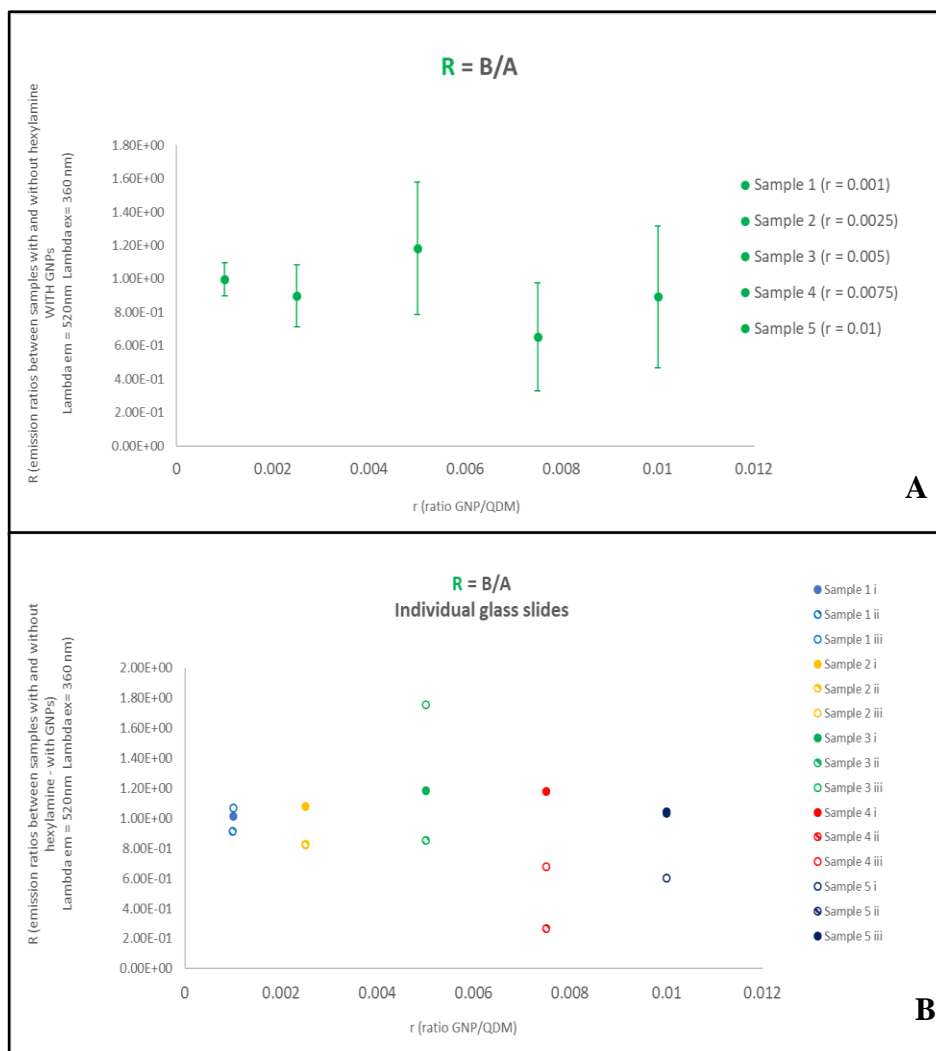
Figure 49 Plot of ratio R averaged (A) and for individual glass slides (B) for sample LC1-099

This means that, since the same quantity of GNPs is present both in sample B and A, the action of gold should not affect the result which, on the contrary, only reflects the change deriving from the addition of Hexylamine.

Moreover, figure 50 reports the obtained R1 (A) and R2 (B) ratios which respectively represent the ratios between emission with GNPs and without GNPs in absence and presence of Hexylamine. As far as R1 is concerned, a general decrease is observable which reflects the PL reduction due to the addition of GNPs. As said before, by dividing A by 0 all parameters are canceled except the action of GNPs which effectively absorb some of the emitted radiation by giving raise to the auto absorption effect. Coming to R2, the same trend is observable confirming the previous comment.

It needs to be admitted that the extended error bars did not permit to formulate a certain theory about the observed behavior. The hypothetic origin of such extended error bars was connected with the mentioned turbidity visible in figure 48 and mainly affecting samples belonging to replicate ii. In fact, among the three replicates, ii was the one presenting the highest signal and was consequently broadening the error extension. With the aim to investigate the result which would have been obtained if the three replicates had been more similar to each other, a temperature annealing step lasting 24 h in vacuum oven was attempted on replicates ii. Unfortunately, no change in appearance occurred at the end of this step.
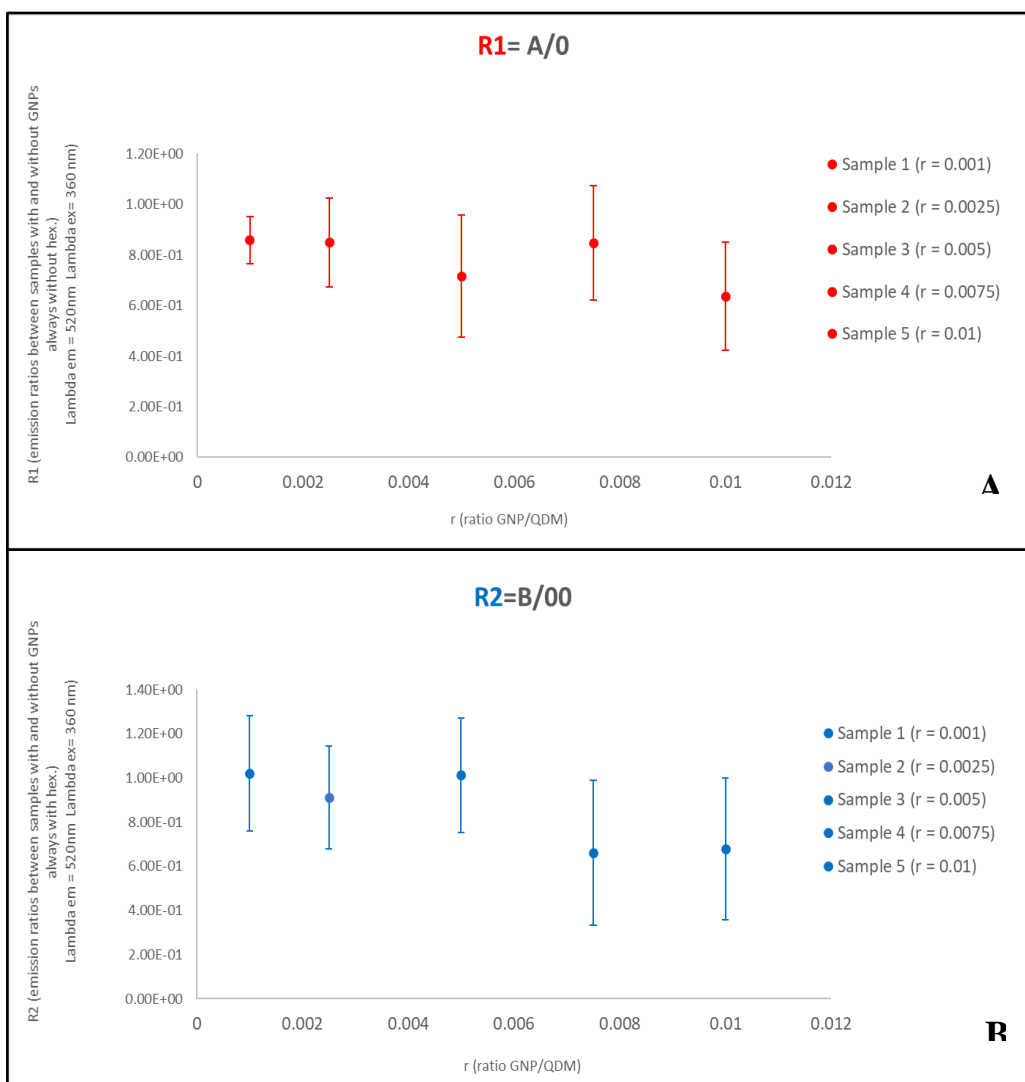
Figure 50 Plot of ratio R1 (A) R2 (B) for sample LC1-099

Moreover, since the samples were irremediably compromised, LC1-099 was archived and the following sample was prepared.

3.2.8.2 Sample LC1- 107

The procedure described for sample LC1-099 was used to realized sample LC1-107. Therefore, 36 glass slides were produced which covered a GNP/QDM ratio ranging from 0.001 to 0.01. A fundamental point which needs to be highlighted is that the 75 µl deposited on the previous sample resulted to be too much to prevent the overflowing phenomenon which occurred twice during the realization of the current sample. Therefore, it was considered necessary to reduce the dropped volume of solution to 60 µl. This point will be more thoroughly analyzed in the next chapter.

Once the 36 glass slides belonging to replicates i, ii and iii were ready, the usual 6 h fluorometer measurement was conducted in order to collect information during the same session. As previously done, excitation and emission spectra were obtained and the wavelength of maximum emission, or rather 520 nm, was used to establish the three ratios R, R1 and R2. Figure 51 (A) reports ratio R while figure 51 (B) and (C) illustrate ratios R1 and R2. As far as R is concerned, the previous comment can be confirmed. In fact, from sample 1 to sample 3 a signal increase can be observed despite the extended error bar associated to sample 3 and mainly due to the considerable large distribution of the three results associated to replicates 3Bi, 3Bii and 3Biii. However, the general observed trend suggests the occurrence of field effect until the ratio GNP/QDM equal to 0.005, while auto absorption dominance appears as

soon as this ratio is overpassed. About ratios R1 and R2, it can be seen that the detected signal decreases as the amount of added GNPs increases. Specifically, this is valid until sample 3 and it could be attributable to auto absorption. On the contrary, the following increase observable in sample 4 and 5 can be related to scattering which is likely to be more evident with high amount of GNPs.
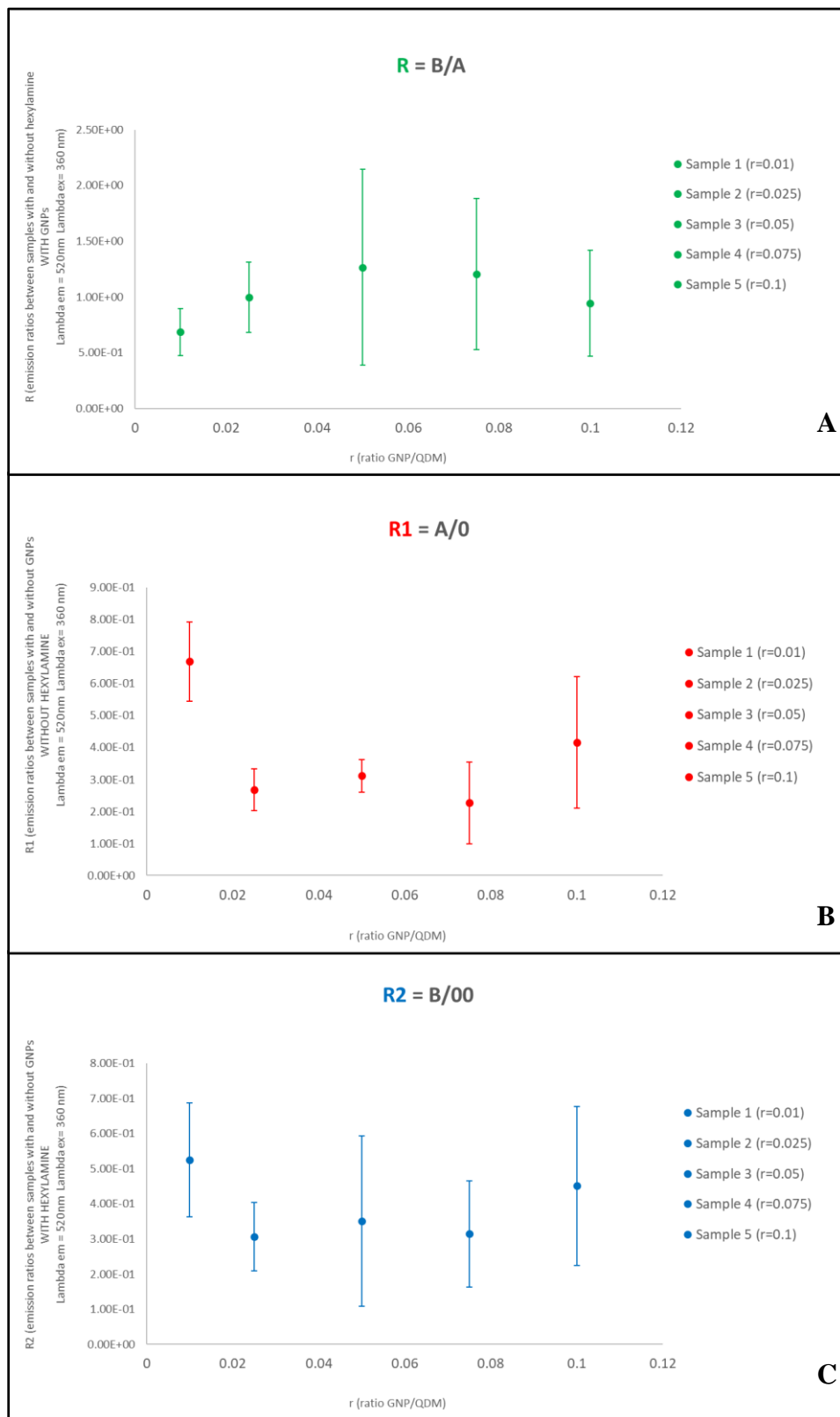
Figure 51 Ratios R (A), R1 (B) and R2 (C) for sample LC1-107

A further interesting point is represented by the comparison between ratio R1 and R2. In particular, it is useful to relate the amount of GNPs with the respective position of the ratios to evaluate the role of Hexylamine and the possible difference arising from its addition. Figure 52 shows a comparison between these ratios and the same trend can be observed even if different gaps can be noticed between ratio R1 and R2 within the different samples. In fact, sample 1 presents a larger difference between the two ratios compared to the other samples. Moreover, the marker associated to R1 is higher than the marker associated to R2. For all other samples this is not the case and this suggests that since the GNPs amount is kept very low, Hexylamine is effective in ensuring a close proximity between GNPs and QDs resulting in a more evident auto absorption effect. Instead, when GNPs are added in a greater amount, they are still able to reduce the detected signal because of auto absorption but this occurs in a less evident measure. Nevertheless, even though the still large error bars preclude from establishing a certain theory, what was observed seems to be coherent with the theoretical study presented in the Appendix.
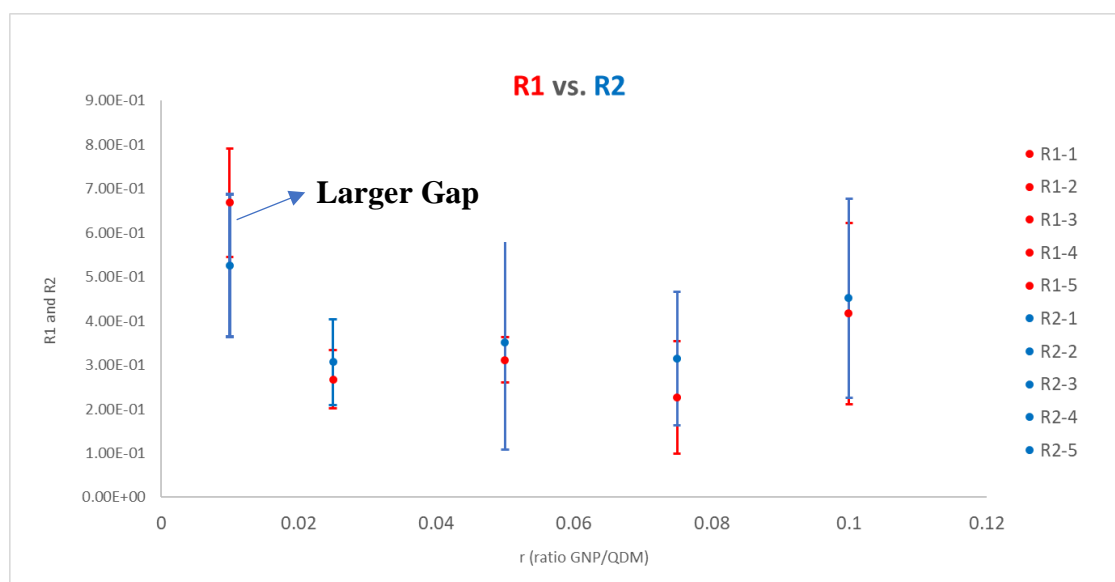
Figure 52 Comparison between R1 and R2 in sample LC1-107

3.2.8.3 Samples LC1-114 and LC1-116

The current couple of samples was produced to achieve two main goals. First of all, sample LC1-114 was produced by adding a double Hexylamine amount compared to LC1-107 and it was useful to confirm the previously explained behavior. Moreover, sample LC1-116 was utilized to confirm the theory according to which the addition of the Homopolymer should have enhanced the observed effects. In the present paragraph, sample LC1-114 will be discussed first, followed by sample LC1-116 and their comparison.

As far as sample LC1-114 is concerned, the same solutions produced for sample LC1-107 were used with the addition of another 6.4 µl of Hexylamine solution (i.e. Bulk H) to vials corresponding to samples 00, 1B, 2B, 3B, 4B and 5B. In fact, the increased amount of reducing agent was believed to be able to increase the observable field effect or auto absorption effect. Next, 60 µl of each solution were deposited on each glass slide as previously illustrated and replicate i, ii and iii were finally prepared and tested at fluorometer. Figure 53 (A) illustrates ratio R obtained by averaging the signals coming from the three glass slides and figure 53 (B) shows the three plots corresponding to the three replicates. A trendline was added to better see the trend.
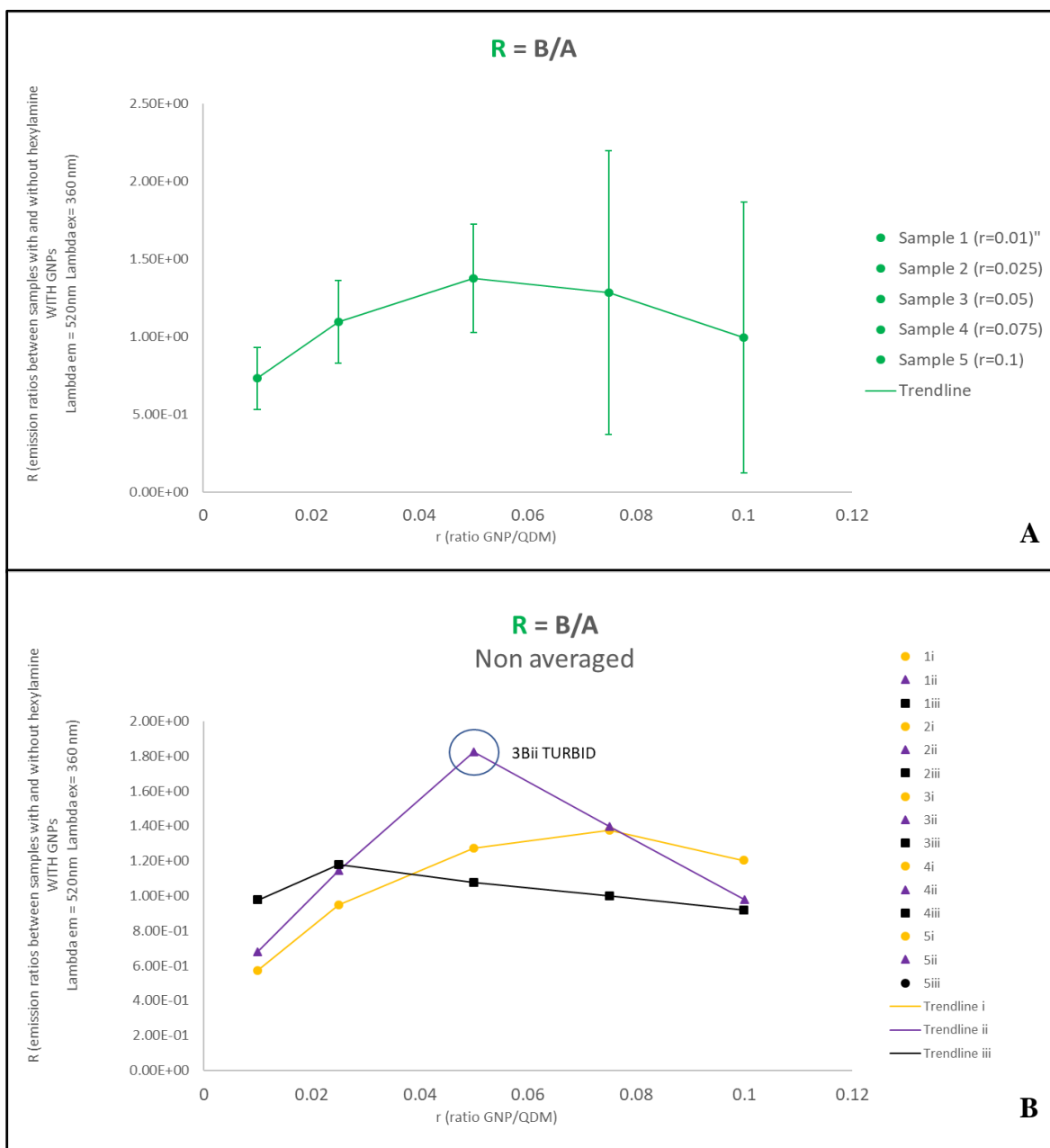
Figure 53 Ratio R averaged (A) and non-averaged (B) for sample LC1-114

As it can be seen, the usual ratio increase occurred from sample 1 to sample 3 as a consequence of the field effect caused by the proximity between QDs and GNPs induced by Hexylamine. As previously asserted, when more GNPs were added, Hexylamine was no more able to establish a consistent difference between a random dispersion of GNPs among QDs and a preferential close proximity, resulting in a dominant auto absorption effect and a ratio decrease. As it can be observed in figure 53 (B), there is a substantial difference among the three replicates, especially for sample 3. In fact, sample 3Bii was seen to be turbid meaning that scattering could have occurred resulting in an increased signal and a higher B/A ratio. This explains the ambiguous position of ratio R for replicate ii of sample 3. Instead, the large error bar appearing in sample 4, is the result of a large error deriving from the multiplication of the relative B error (i.e. 71 %) and the ratio B/A. Differently, for sample 5, the large error bar was caused by a large error relative to A (i.e. 87 %). However, even if the last two samples are somehow difficult to be explained, sample 1-3 suggest a clear field effect.

As previously done, also ratio R1 and R2 were obtained which comparison is shown in figure 54. The same trend identified in paragraph 3.2.8.2 is observable also here. Specifically, R1 shows a clear decreasing trend from sample 1 to 4 while a slight increase

occurred in sample 5 which was probably due to scattering. R2 showed a similar pattern with a slight increase for sample 3 and 5. Due to the large error bars which are often superimposed, it is hard to formulate a certain theory. However, as said before, the main result is represented by sample 1 where the difference between R1 and R2 is more appreciable. In other words, the obtained first ratio is already lower in the case where Hexylamine is added. This could be explained by saying that if Hexylamine is added and a small amount of GNPs is present, the occurring auto absorption effect is more evident.
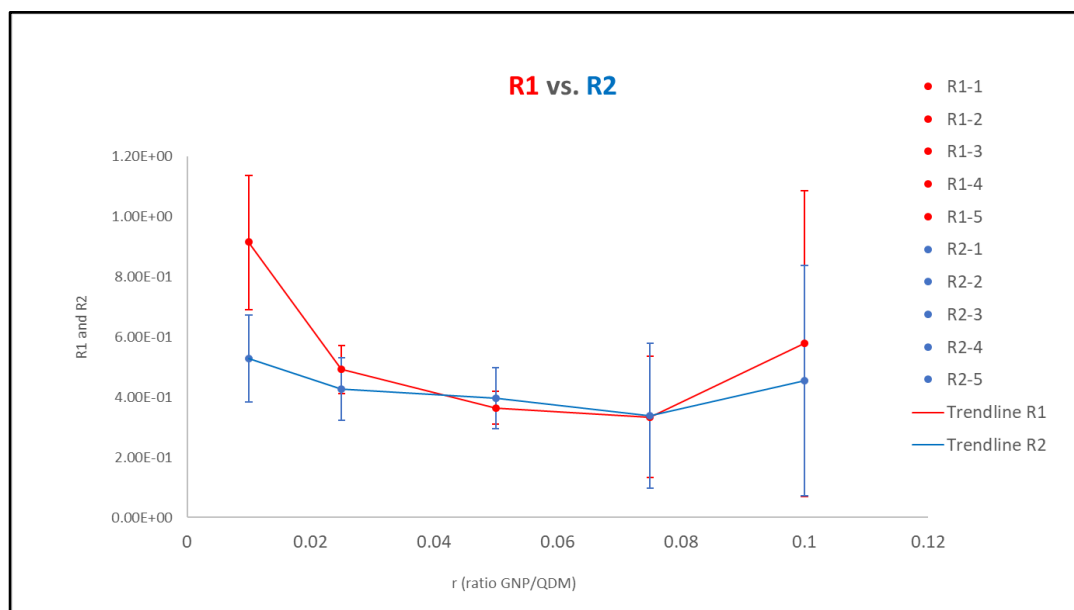
Figure 54 Comparison between R1 and R2 in sample LC1-114

Subsequently, with the aim to confirm the current theory, sample LC1-116 was produced with the same amount of Hexylamine used for sample LC1-114 and with the addition of *Polystyrene Homopolymer* in a percentage of 50% w/w with respect to the added raft copolymer. The Homopolymer addition was thought to be useful to provide an initial larger distance between QDs and GNPs resulting in a more evident effect of Hexylamine. In other words, if the theory according to which Hexylamine is able to approach and connect QDs and GNPs had been sound and right, the addition of Homopolymer would have enhanced its effect and the gap between B and A, or rather the R ratio would have been higher. On the contrary, the R1 and R2 ratios should have been lower since the occurring auto absorption effect was expected to be more evident due to the larger interparticle distance caused by the addition of PS Homopolymer (HP).

Therefore, except for the HP addition, sample LC1-116 was prepared according to the usual procedure and 60 µl were dropped on each glass slide. Ratio R was plotted with the average values and is reported in figure 55 (A). Moreover, the three single replicates were plotted and appear in figure 55 (B). It is easy to recognize the same trend already discussed for sample LC1-107 where the field effect due to the addition of Hexylamine is clearly evident from sample 1 to 3. As far as ratios R1 and R2 are concerned, figure 56 confirms the previously presented theory according to which Hexylamine addition enhanced the observed auto absorption effect which caused a substantial signal decrease from sample 1 to 3 and a following increase probably due to the scattering determined by the large amount of gold.

Even if slightly less visible here than in sample LC1-114, sample 1 is still the one where the gap between R1 and R2 is the largest. This confirms that when the added amount of GNPs is kept low, the Hexylamine effect in causing auto absorption effect is more evident. However, if some HP is added, the mentioned effect can be lightly concealed as confirmed by the plot. In fact, unlike sample LC1-114, here the error bars associated to sample 1 are slightly superimposed.
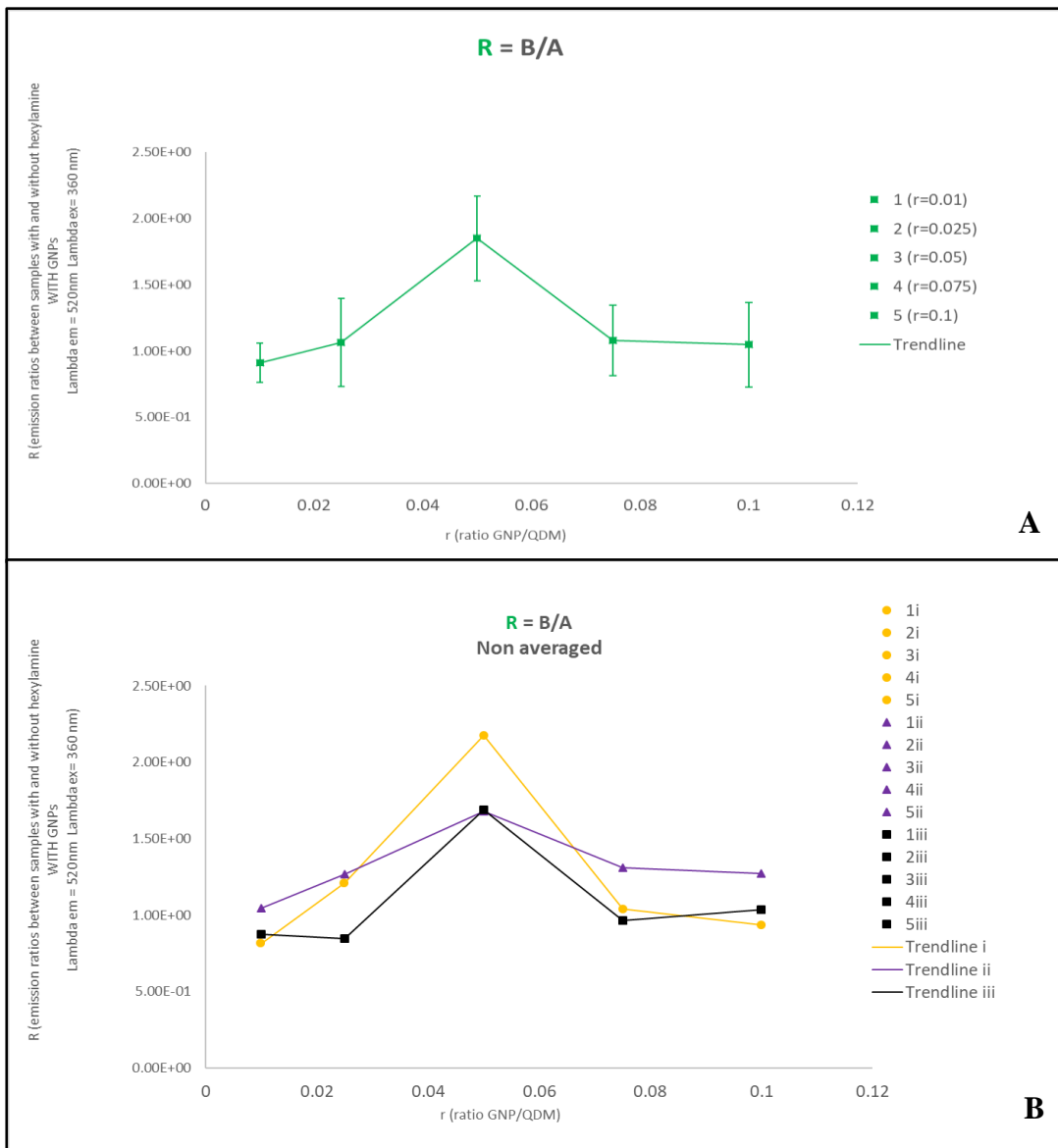
Figure 55 Ratio R averaged (A) and non-averaged (B) for sample LC1-116
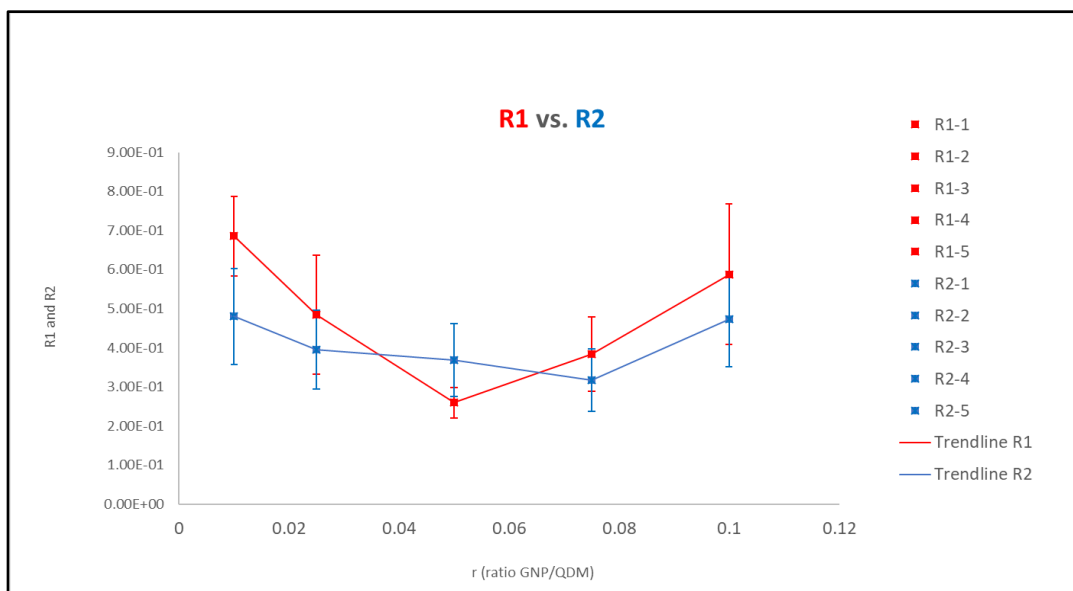
Figure 56 Comparison between R1 and R2 in sample LC1-116

Finally, after having confirmed the trends identified with sample LC1-114, it is useful to compare the results with and without the addition of HP to find a correspondence with the previously presented theory. In regard to this, figure 57 shows a comparison between ratio R (A), R1 (B) and R2 (C) of samples LC1-114 (without HP) and LC1-116 (with HP).
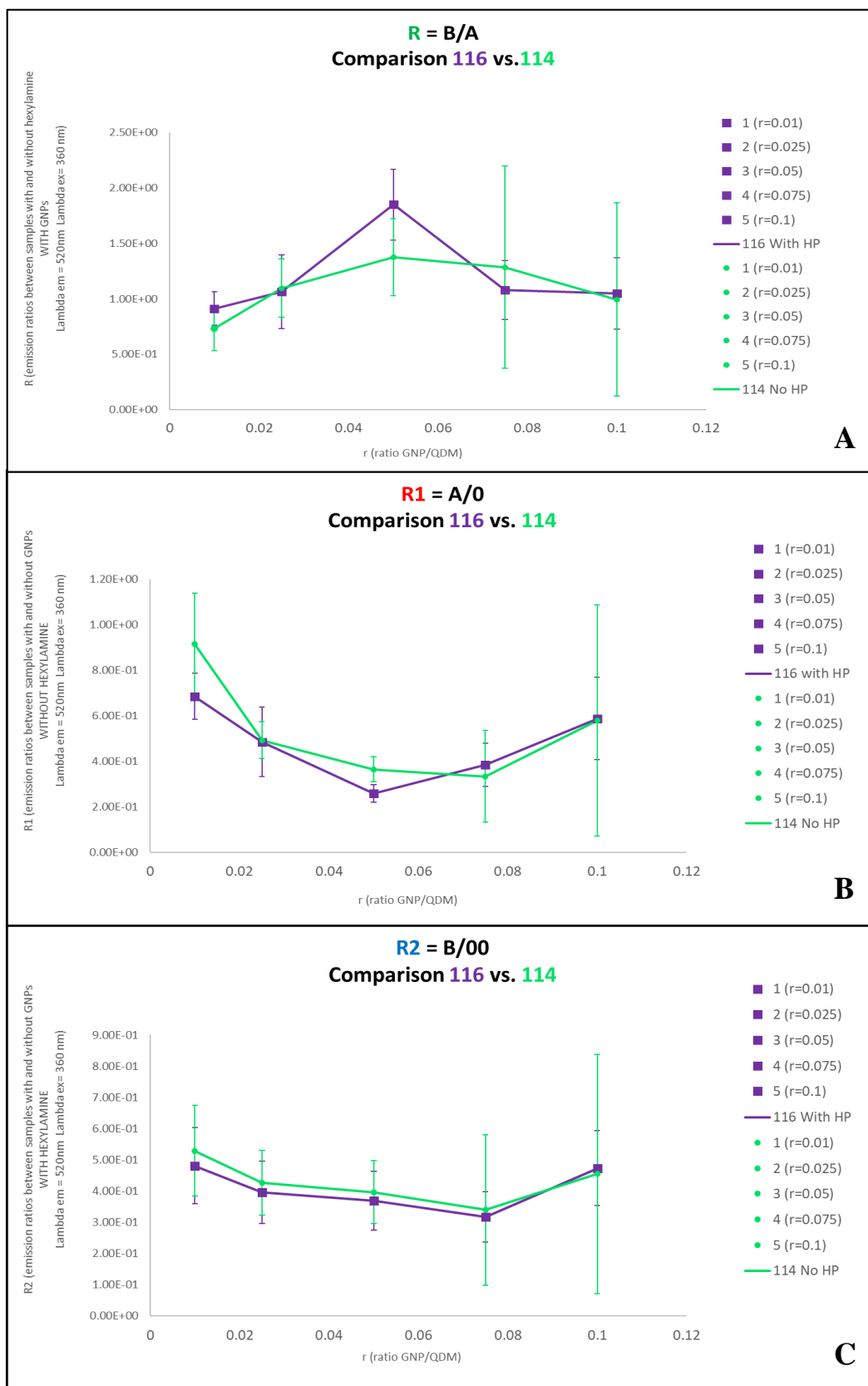
Figure 57 Comparison of ratio R (A), R1 (B) and R2 (C) between sample 116 with HP and 114 without HP

As far as ratio R is concerned, a confirmation of the previous theory was obtained because a more consistent field effect was observed from sample 1 to 3. In fact, the purple plot corresponding to the sample with HP reaches a maximum with sample 3 which is higher than the one obtained in the case without HP. In other words, when the HP is added, the initial interparticle distance between QDs and GNPs is enlarged and consequently, the action of Hexylamine in approaching and connecting them is more evident. In particular, this evidence is observed by the higher R ratio which means a larger gap between the signal of B (with Hexylamine) and the signal of A (with no Hexylamine).

About R1 and R2, instead, it is easy to notice that the addition of the HP lowers the ratios. In fact, this means that the signal difference between A and 0 (for ratio R1) and between B and 00 (for ratio R2) is more pronounced since the emission of sample A and B is further decreased. In other words, an enhancement of the auto absorption effect was observed for almost all the GNPs amounts.

3.2.8.4 Samples LC1-119

As it will be discussed in the next chapter, one of the most important drawbacks affecting the current procedure, involves the prolonged series of steps to have all the three replicates ready. In fact, as explained before, two days passed from the moment when the first and the last replicates were effectively ready to be analyzed. Even if the desiccator was properly employed to prevent surface alteration together with a safe box providing one single spot per each glass slide, some modifications could have occurred which could have been the cause for the reciprocal difference among the three replicates belonging to the same sample. For this reason, a last sample was produced where all 36 glass slides were prepared together. However, the obtained result was not as favorable as expected mainly as far as ratio R = B/A is concerned. In fact, the latter was characterized by an almost irregular trend not showing the clear field effect which was visible in the previous samples. On the contrary, about ratios R1 and R2, the typical auto absorption effect was observable which confirmed the theory according to which GNPs absorb the radiation emitted by QDs. Furthermore, the same comparison between sample LC1-114 (without HP) and sample LC1-116 (with HP) was repeated by substituting the latter with sample LC1-119. As reported in figure 58 (A) the aforementioned irregular trend for ratio R of sample LC1-119 is observable. Moreover, a clearly less evident field effect can be deduced, represented by the lower level of the trend compared to sample LC1-114. Finally, the R1 and R2 ratios comparisons appear in figure 58 (B) and 58 (C) respectively. As it is noticeable, a more evident auto absorption effect is provided by the sample with HP, confirming the previously expressed theory. Further considerations will be provided about these results and about the applied technique's properties in Chapter 4.
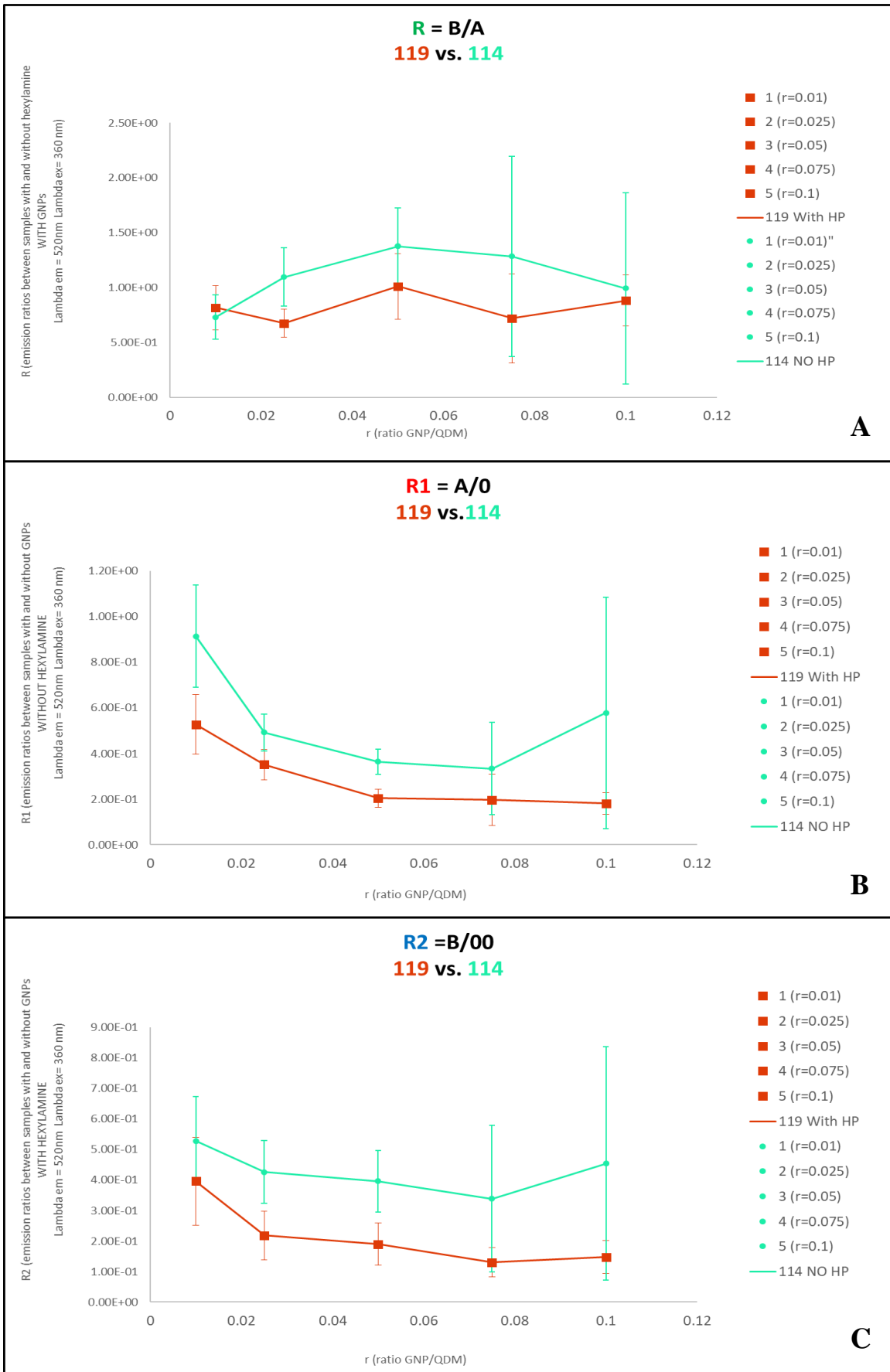
Figure 58 Comparison of ratio R (A), R1 (B) and R2 (C) between sample 119 with HP and 114 without HP

CHAPTER 4

DISCUSSION AND FINAL REMARKS

INTRODUCTION

This last chapter presents the main objective of reporting the fundamental advantages and drawbacks related to the applied procedure to realize and test samples from LC1-099 until LC1-119. In fact, these samples have been identified as the most promising ones, while the previous attempts didn't give any optimistic perspectives. Specifically, the already briefly explained results will be more thoroughly considered here with the aim to individuate what was properly done and what should have been done in a more effective manner. Finally, even if this is above the objective of the present thesis work, some possible applications will be considered.

4.1 Advantages deriving from Approach n.2 with Ratios

As previously explained, a substantial improvement was provided to the current thesis work when the so-called approach n.2 was applied. In fact, a series of inconsistent and discouraging results were obtained by utilizing approach n.1. The main reason why the latter didn't work could probably be attributed to the high difficulty in establishing a connection between QDs and GNPs when the first component was already in the solid state. In fact, even though different strategies were attempted, when the PS-CdS layer was deposited on the glass slides, the Hexylamine didn't manage to be effective enough to open the TTC groups in order to establish a good connection with GNPs. On the contrary, the main observed phenomenon was a consistent dilution of the deposited layer once the reducing agent was added. As a consequence, the immersion into the GNPs solution was not effective in providing a connection between QDs and GNPs.

Before considering the essential reason why approach n.2 was more functional in terms of procedure and analysis, it is important to highlight which are the motivations which caused the choice of such an approach. Beside what was mentioned above about Hexylamine incapability to prepare the deposited PS-CdS layer to get connected to GNPs, an important factor needs to be remembered. In fact, it was reported that the two main methods to deposit a layer of solution on a glass slide were drop casting and spin coating. The interesting point is that both these methods present an advantage and a drawback which make them impossible to be effective alone. In particular, drop casting was observed to be able to guarantee a deposited thickness high enough to be adequately detected during the analysis. However, a huge roughness and surface irregularity were visible by a quick AFM measurement, combined with a recurring flakes formation. On the other hand, spin coating was very efficient in ensuring a particularly smooth layer, but the low deposited amount of material caused difficulties during the analysis sessions. In fact, a spin coated layer was hardly visible. Therefore, the application of an intermediate method was required which was able to provide both the advantages by minimizing the drawbacks. Indeed, drop casting with solvent annealing was used which was able to give a consistent thickness in order for the sample to be easily detectable, together with a good surface smoothness provided by the lowered

vapor pressure of the deposited Dioxane induced by the saturated atmosphere. In other words, a reduced velocity during the evaporation process provided the sample with a good surface regularity.

However, the most important reason why approach n. 2 was so interesting resides into the *ratios establishment step*. As it was reported in Chapter 3, one of the most serious problem affecting the fluorometer measurements was a frequent results inconsistency mainly due to oscillations in fluorometer emissions or detections. Indeed, to solve the current problem, the best way was establishing and comparing ratios among measurements and not measurements itself. For example, samples LC1-087, LC1-088, LC1-092 and LC1-094, which were compared in table 2, presented inconsistent results mainly due to fluorometer issues which were restrained by using the new approach. Moreover, another important issue affecting samples prior to LC1-099 was their dimensional variability. In fact, as it was said, an impossible comparison among the action of different amounts of GNPs was reported due to the fact that both QDs and GNPs were characterized each time by a slightly different dimension since they belonged to different batches. This complication was annulled when samples after LC1-099 were produced with the same batch.

Finally, what was defined as *auto correction property* needs to be explained and highlighted. In fact, when establishing the three ratios R, R1 and R2, the action coming from the component equally present at the numerator and at the denominator, is deleted and other interesting effects can be observed. In other words, as far as ratio R is concerned, when the signal emitted by sample B is divided by the signal emitted by sample A, the common presence of GNPs doesn't play a role anymore. On the contrary, only the action of Hexylamine can be highlighted in different samples with an increasing amount of Gold. Therefore, it can be hypothesized how Hexylamine behaves in the various conditions and there is an auto correction effect for the GNPs presence. Differently, with ratio R1 and R2, the signal of samples with and without GNPs can be investigated and specifically the occurring phenomenon can be studied both in absence and presence of the reducing agent. As before, in ratio R2, the action of Hexylamine is not directly visible since it is present either at the numerator and at the denominator, but actually, the behavior of Gold can be observed when also Hexylamine is present. As a consequence, a hypothesis can be formulated according to which Hexylamine can increase the achieved auto absorption effect.

4.2 Drawbacks deriving from Approach n.2

Even if the approach involving the establishment of ratios R, R1 and R2 seems to be promising and well-working, there are some drawbacks which must be considered, and which are mainly related to the samples production steps.

First and foremost, the problem of overflowing needs to be mentioned since it caused a change of the spread volume among different samples. In fact, LC1-099, and LC1-107 were prepared by drop casting 75 µl, while from sample LC1-114 to LC1-119 60 µl was considered as the best amount to spread because a larger one caused repeated overflowing phenomena. To be more precise in regard to this, the mentioned phenomenon occurred after few hours (e.g. 2-3) of solvent annealing. Specifically, the glass slides were deposited on the support and the right volume was spread. Next, the support was gently inserted into the jar taking care to avoid overflowing. Subsequently, the glass jar was adequately sealed with Al foil to generate a close chamber containing a dioxane saturated atmosphere. At this point, apparently without a specific reason, one or more glass slides underwent overflowing by contaminating the other slides with their solution. Since it was clearly impossible to trust such slides, new ones were produced with a lower amount of solution (i.e. 60 µl instead of 75 µl) in order to reduce the chances of overflowing. Effectively, the last considered amount of solution never caused the phenomenon which is being discussed. Different explanations were hypothesized all involving the low interaction between the glass slide and the dropped solution. In fact, glass slides were properly washed with different solvents in order to provide a good surface wettability by the main solvent (i.e. dioxane) but it is possible that the extended amount of time elapsing from the cleaning steps to the drop casting step could have reduced the established compatibility and tendency to remain connected. However, the last hypothesis is far from being accurate since all glass slides were accurately stored under vacuum

after being washed and before being utilized. Moreover, other factors could have influenced the reciprocal bounding tendency between solution and surface such as consistent temperature variations occurring in the laboratory. In fact, these could have slightly modified the solution viscosity and eventually could have reduced it by favoring the observed overflowing.

Another significant factor which needs to be underlined is that a consistent variability among the three mentioned replicates was always observed. In fact, the applied drop casting technique is very likely to cause inequalities among samples since it is performed by human hand. Although it is true that a precise graduated pipette was employed, it is also true that the exact position from where the solution was dropped was not always the same. In fact, the tip was approached as much as possible to the slide and then the solution released but a different spreading dynamic was extremely probable. This could have ended in an uneven thickness of the obtained slides either belonging to different replicates of the same sample or to different samples. As a consequence, the reported signal could have been affected by the actual pattern which was far from being consistent among all samples. Furthermore, after having performed the drop casting step, the solvent annealing procedure could have been the cause of further inequalities. In fact, samples production took place on three different days which respective temperature, humidity and pressure conditions were probably different. However, although the mentioned problems were actually present, it is also true that slides belonging to sample LC1-119 were produced together and even more appreciable differences were encountered among different replicates belonging to the same sample. Figure 59, for example, shows the extremely different plots obtained for ratio R = B/A. Anyway, it must be underlined that the apparatus used for the realization of the current sample was not as professional as the previous one. Therefore, the obtained difference could have still been eliminated if the three replicates had been produced with a well-performing single apparatus.
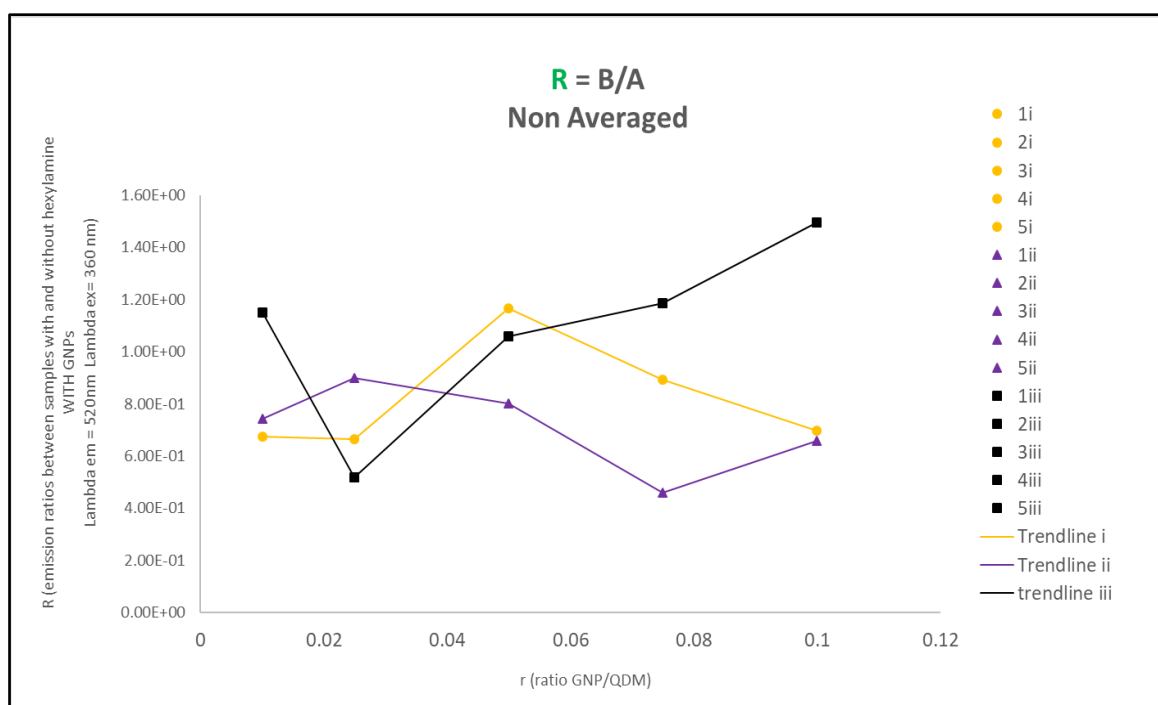
Figure 59 Ratio R non-averaged for sample LC1-119

Related to the previous issue, is the mentioned appearance of turbidity on some samples. In fact, this problem could be related to an increased amount of humidity eventually present during the solvent annealing procedure. In turn, this could have been caused by a higher level of air humidity combined with a non-perfectly sealed glass jar. Figure 60 (A) reports the obtained ratio R1 for sample LC1-114 which is particularly representative since the clearly higher values obtained for slides 4 and 5 of replicate ii were probably caused by the evident turbidity observable in figure 60 (B). In fact, a turbid slide (i.e. 4Bii and 5Bii in this case) are more likely to

be affected by scattering which in turn makes the B signal extremely higher than the A signal by consequently increasing the observed R ratio.
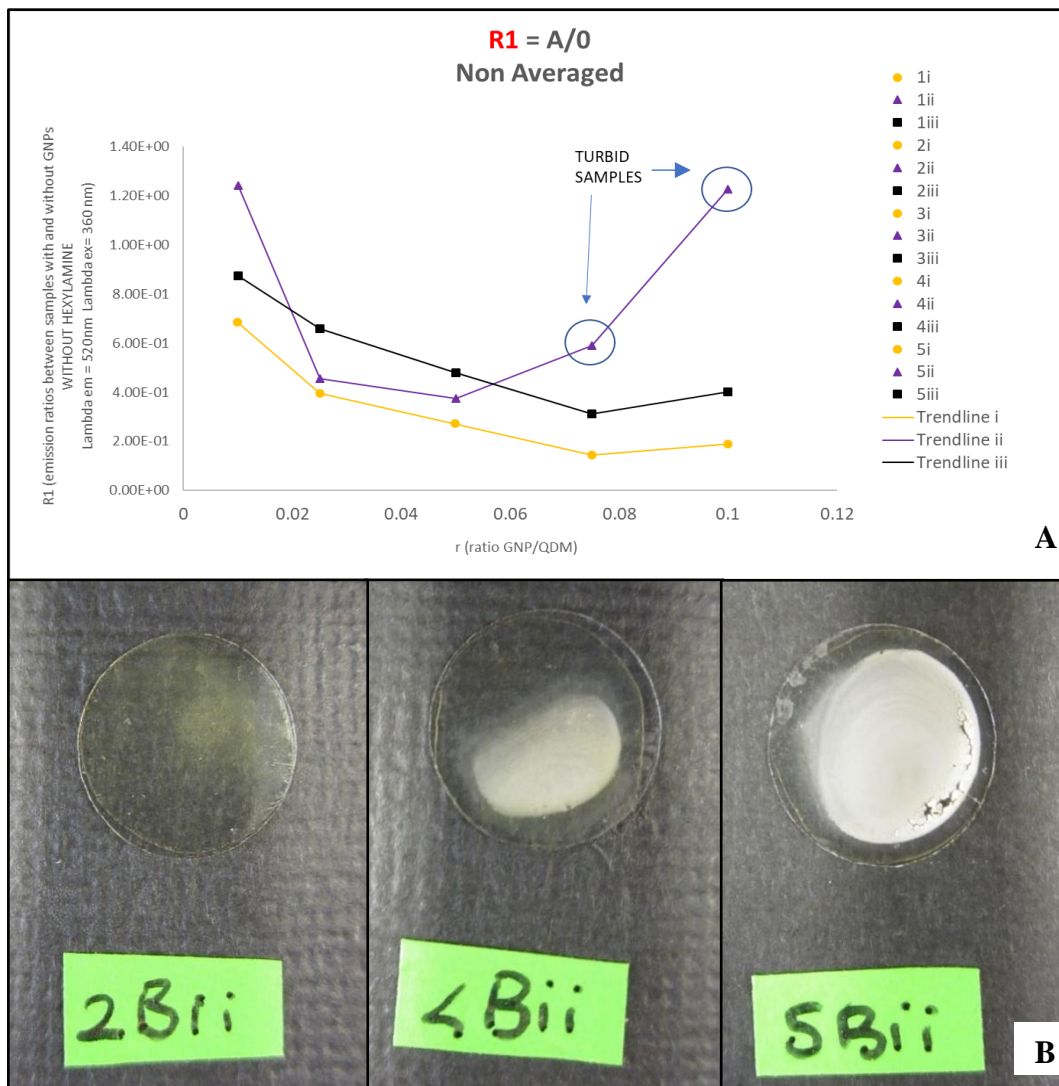
Figure 60 Ratio R1 non-averaged (A) and physical appearance of slides 2Biii, 4Biii and 5Biii for sample LC1-114

However, unfortunately, the previous theory was not always verified and sometimes, even if samples appeared as turbid, the obtained signal was not higher. For this reason, a procedure involving the discard of turbid samples was not considered as applicable because it would not have been always reliable. Oppositely, all replicates were taken into account to achieve a result which was as much realistic as possible.

4.3 The final theory

This paragraph has the main objective of making a sound conclusion based on the conducted research to explain the actual interaction between QDs and GNPs. Since the only promising approach was the so-called approach n.2 with Ratios establishment, this will be the only considered one.

First and foremost, it needs to be reminded that the interaction between GNPs and PS-CdS has been observed to be effectively provided by the addition of Hexylamine. [4] Therefore, the elaborated theory is based upon the close proximity between the two components induced by the addition of the reducing agent. Since the most representative sample without HP was LC1-114, this will be considered to elaborate the current theory.

Figure 61 (A) reports the obtained R ratio, while figure 61 (B) illustrates a direct comparison between R1 and R2. As far as R is concerned, a clear increase from slide 1 to 3 can be seen. More specifically, slide 1 gave a ratio which value was lower than 1. This means that the emission of slide B (with Hexylamine) was lower than the emission of slide A (without hexylamine). Oppositely, slides 2 and 3 provided a ratio which value was higher than 1 with an increasing trend. This means that the emission of slide B became higher than the emission of slide A. Therefore, it could be concluded that since the quantity of GNPs is low, the close proximity induced by Hexylamine manly causes the auto absorption effect visible in a ratio R < 1. Oppositely, when the amount of GNPs is increased until a GNP/QDM ratio of 0.005, the close proximity seems to provide a clear field effect observable in a ratio R > 1. About slides 4 and 5, it is hard to formulate any theory. However, it is probable that the high amount of Gold enhanced the scattering effect which could have been more consistent for slides belonging to category A which could have reduced the R ratio. Furthermore, the increased scattering could be the cause for the large error bars.
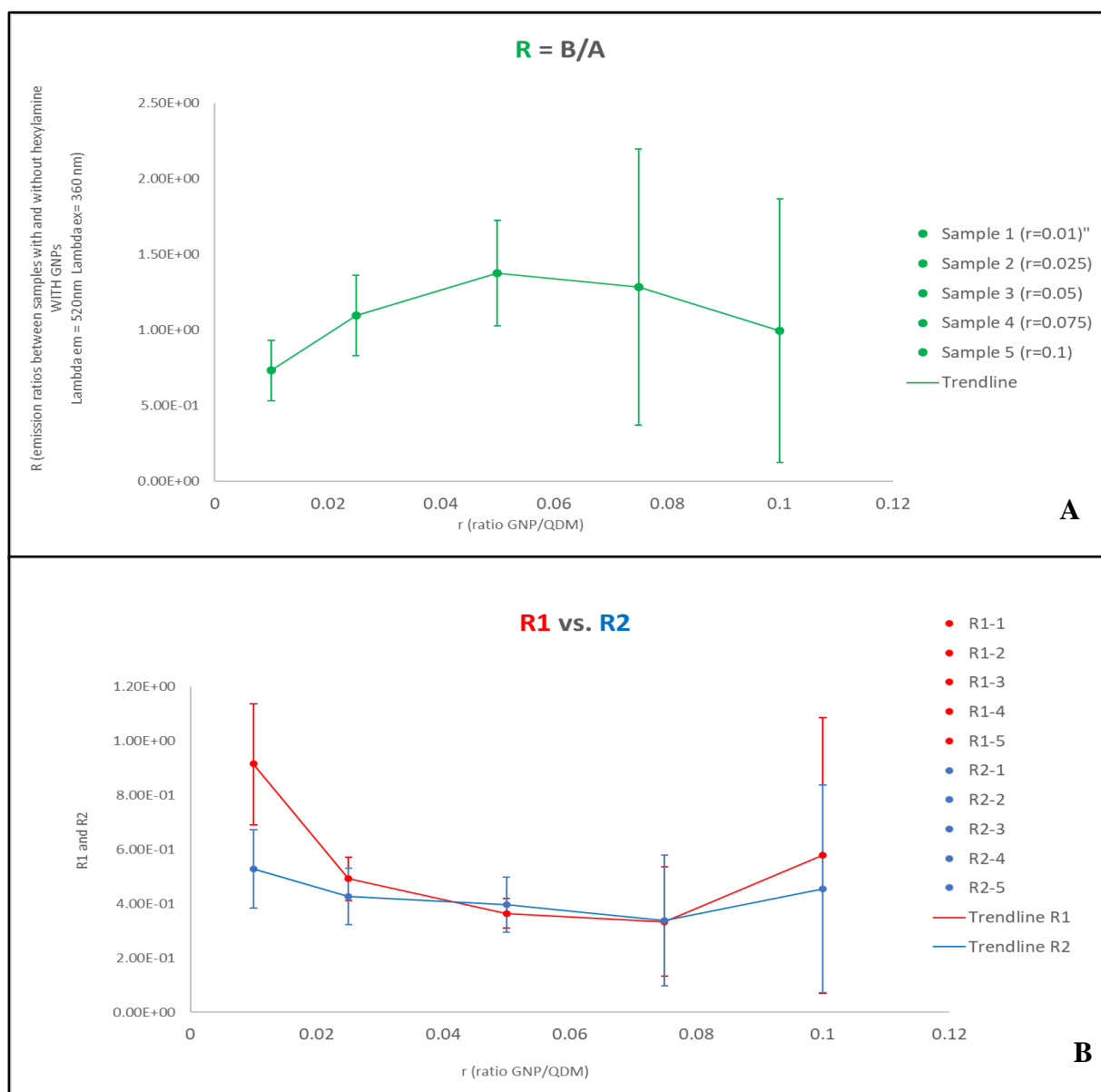
Figure 61 Ratio R (A) and comparison between ratios R1 and R2 (B) for sample LC1-114

In fact, scattering is a very unpredictable phenomenon which could have caused different effects in the different samples. Instead, about R1 and R2, the general decreasing trend suggests that GNPs can effectively absorb the radiation emitted by QDs, or rather provide auto absorption effect. Specifically, R1 decreases until slide 4 by confirming that a higher amount of GNPs can absorb more efficiently, while slide 5 gave a slightly higher ratio probably due to scattering. However, the obtained R1 ratios are all abundantly below 1 meaning that slides A are emitting less than slide 0 because of the mentioned auto absorption. Finally, the obtained trend for R2 is very similar and the previous explanation can be applied. However, the consistent gap existing between ratio R1 and R2 for slide 1 suggests that when a low amount of GNPs is used, the close proximity enhances the auto absorption effect. In other words, when few GNPs are present, if Hexylamine is added, they can more efficiently absorb part of the radiation emitted by QDs. Similarly, with the addition of Hexylamine, a stronger auto absorption effect is observable with few GNPs. This confirms the observation reported with ratio R according to which auto absorption dominates with few GNPs while field effect becomes more important as the amount of GNPs increases.

As far as the addition of the Homopolymer is concerned, sample 116 can be considered to formulate a theory.

First of all, it must be remembered that the theoretical role of the HP is to increase the initial distance between QDs and GNPs with the result of enhancing the Hexylamine's observed action. In fact, by comparing the obtained R ratios for sample 114 and 116, a more evident effect of the reducing agent can be noticed in the higher final R which is achieved for slide 3 of sample 116 (with HP). Moreover, also slide 1 of sample 116 provided a higher ratio compared to sample 114, indicating that the field effect was already more likely to happen even if the amount of GNP was low. In other words, the addition of HP forced QDs and GNPs to be initially more far apart which was useful to enhance the observed action of Hexylamine in moving them closer by causing a more evident field effect. As said before, slides 4 and 5 remain hard to be interpreted because of the high tendency of scattering to occur. Figure 62 shows the already reported comparison between ratios R of samples 114 and 116
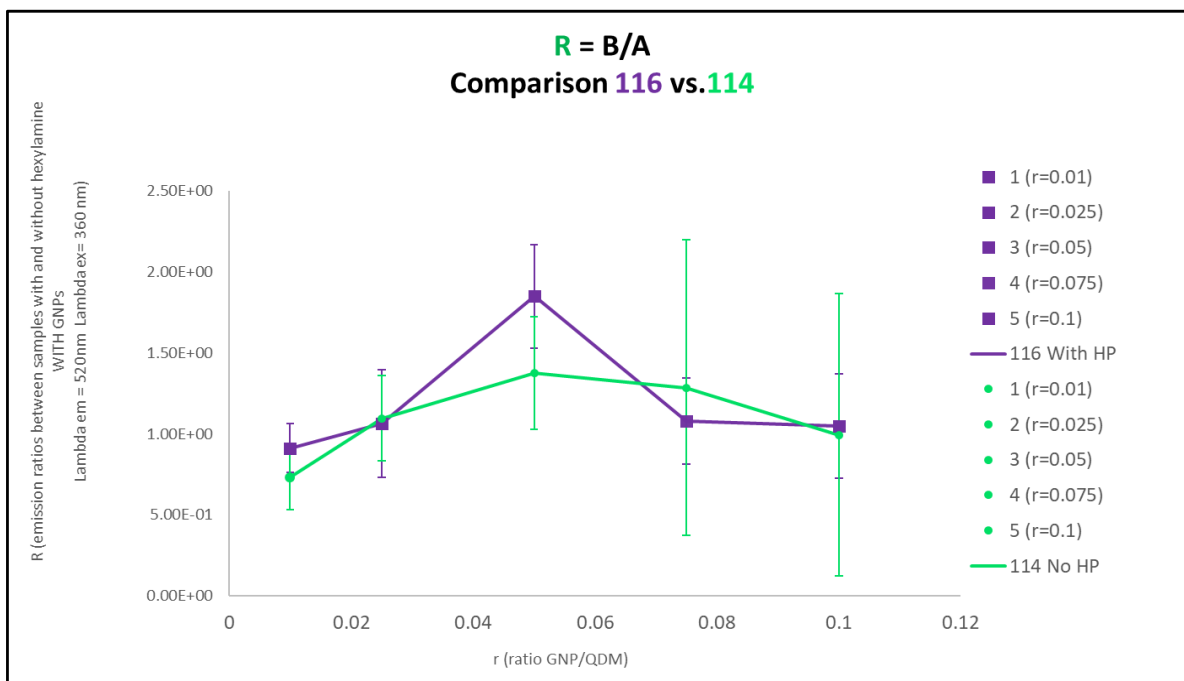
Figure 62 Comparison of ratio R between samples 116 with HP and 114 without HP

As far as ratios R1 and R2 are concerned, the addition of HP was useful to enhance the behavior already observed in sample 114. In fact, the decreasing trends indicating the occurrence of the auto absorption effect are also visible in sample 116. However, sample

116 showed lower values of both R1 and R2 for almost all the tested slides by confirming that the auto absorption effect occurred even more intensely.

Therefore, it can be concluded that the addition of the HP was extremely useful to confirm the observed behavior of sample 114. Moreover, the elaborated theory in regard to the dynamic of interaction between QDs and GNPs can be reinforced. It can finally be asserted that when the role of Hexylamine is investigated, its action is mainly the enhancement of the auto absorption effect until when the added amount of GNPs is kept low. On the contrary, when the latter is increased, the main action of the reducing agent begins to be the field effect which is important to enhance fluorescence properties of QDs. In addition, if the action of Gold itself is tested, auto absorption is clearly more and more identifiable as the Gold amount increases. Furthermore, when also Hexylamine is present a stronger effect is observable even when the amount of Gold is low. Figures 63 (A) and (B) illustrate the comparison of ratio R1 and R2 between samples 116 and 114.
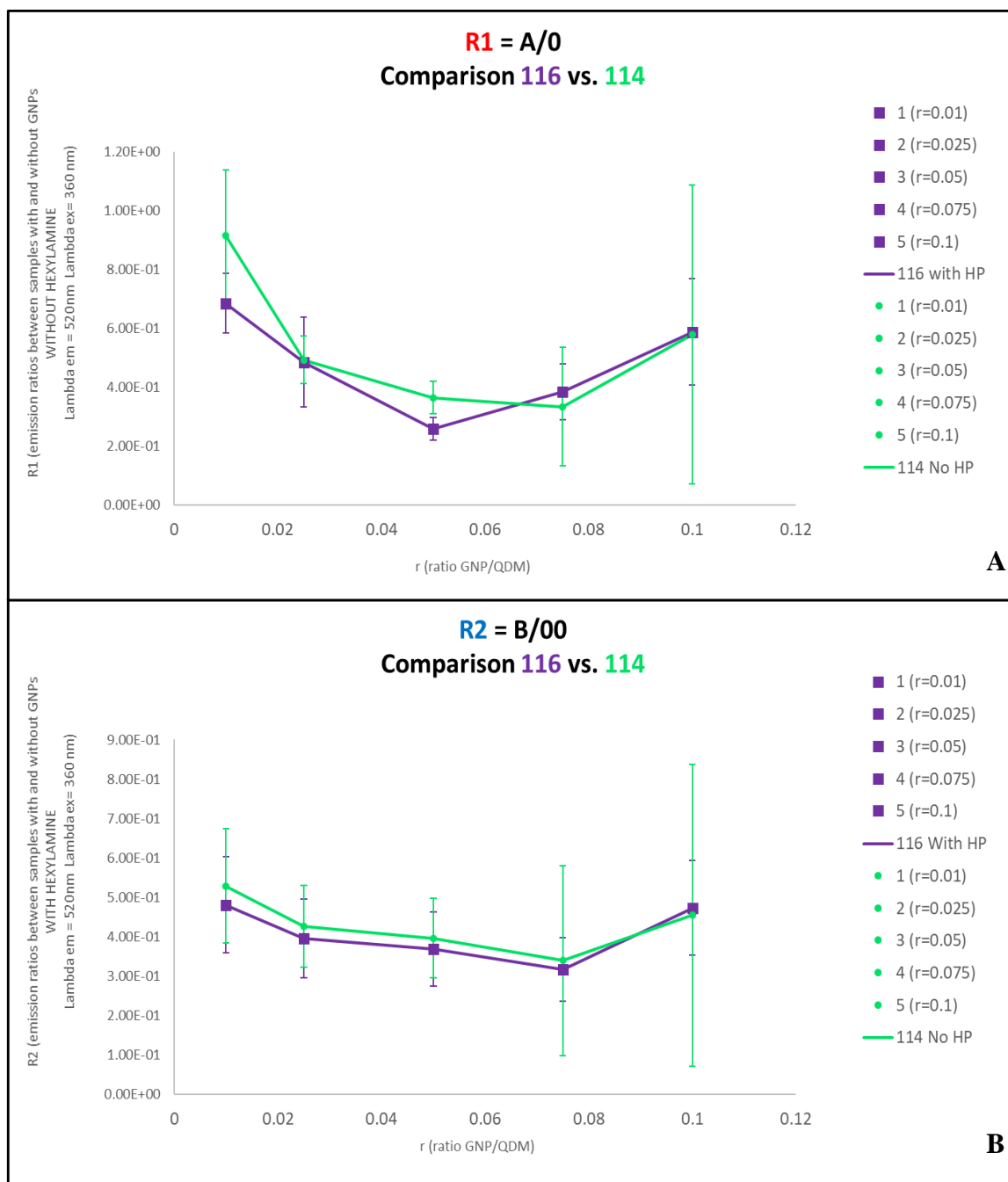
Figure 63 Comparison of ratio R1 (A) and R2 (B) between samples 116 with HP and 114 without HP

4.4 Possible improvements and perspective studies

As reported in paragraph 4.2 some fundamental drawbacks could be identified in the applied approach. Therefore, a more accurate and precise procedure could eventually be able to provide better results which could confirm the hypothesized theory.

In particular, the fundamental problem affecting samples produced according to approach n.2 with Ratios establishment was the low reproducibility of slides belonging to the same category. In other words, the three produced replicates were often too different among each other which ended up in large error bars. In turn, these prevented from formulating a totally reliable and sound theory about the interaction between QDs and GNPs. Three main improvements could be listed which have the objective to reduce the observed inequalities.

First and foremost, all 36 glass slides should have been produced together. In fact, the extremely pronounced difference in terms of daily temperature, humidity and pressure must have affected the three replicates which were produced during three different days. Even though an attempt was conducted to produce all the slides simultaneously, with sample LC1-119, the utilized apparatus was not as performing as the one reported in figure 21 and used to prepare a maximum of 12 glass slides. In fact, it was basically a glass container with a large petri dish positioned upside down in order to arrange the 36 slides on the external surface of its bottom. In addition, an Al foil sealing was attempted which was not really effective. Thus, in order to reduce undesired inequalities, a better chamber for solvent annealing should have been employed which should have been equipped with a large support and a good sealing apparatus.

Secondly, a better interaction between glass slides surface and spread solution should have been acquired. In fact, if this had been the case, no overflowing would have occurred, and the same amount of solution would have been deposited on all glass slides without cases in which, for instance, 75 µl resulted to be an excessive volume to be dropped. In order to do so, a more efficient washing procedure could have been conducted followed by a surface functionalization able to provide a better interaction between glass and PS-CdS solution. However, a functionalization could have resulted in a prevented capability of CdS to effectively be connected to GNPs. Therefore, probably, surface cleaning aimed to increase surface wettability by dioxane is still the best solution. However, different sonication times could have been tested and eventually other solvents could have been tried to further increase the desired wettability.

Finally, in order to obtain more comparable glass slides, a more efficient spreading technique should have been applied to create identical and evenly distributed film thickness all over the glass slide. In fact, as said before, it could have happened that some glass slides had a thicker or thinner deposited film where the fluorometer radiation hit. As a consequence, a different detected radiation was probably obtained which was only due to an uneven thickness rather than to real optical phenomena.

In conclusion, a perspective study which should be applied to verify the hypothesized theory involves the TEM observation of a microtomed sample. In particular, by applying this technique, it would be possible to verify the physical proximity between QDs and GNPs caused by the addition of Hexylamine. Specifically, by observing a sample without HP with and without Hexylamine it would be possible to verify if the addition of the reducing agent is effectively able to move fluorescent and plasmonic components closer. Moreover, by repeating the observation with HP-containing samples, it would be possible to doublecheck the mentioned behavior.

4.5 Eventual applications of the current study

The main applications of Metal Enhanced Fluorescence have already been broadly investigated in literature and can be substantially divided into two main fields. The first one involves functional optoelectronic devices and sensors and finds its main application in photonic crystals where the QDs photoluminescence is increased thanks to the presence of the plasmonic components, such as Gold

or Silver NPs. The second one, instead, is more related to the biological world and to the imaging procedure. For instance, fluorescent cancer biomarkers could be created by using fluorescent QDs which PL intensity could be increased by the metal. [4]

As far as the application as a sensor is concerned, the first approach of the current thesis work was actually intended to suggest a device able to recognize different samples, acting, in turn, as a sensor. In fact, the original idea was to deposit a layer of PS-CdS and later to open the TTC groups by adding Hexylamine. At this point, different water based GNPs solutions have been created with different amount of THF. Theoretically, since THF is able to swell the PS chains around the QDs, different amounts of this solvent should provide different swelling conditions and consequently different distances between GNPs and QDs. As a consequence, different PL intensities could be collected corresponding to the different cases. Accordingly, it would be possible to identify the percentage of THF based upon the obtained signal. Consequently, if different types of solvent were used instead of different percentages of the same solvent, it would be theoretically possible to individuate the present solvent based on the obtained PL. This is exactly a sensor which could be used to find the main solvent present in a solution which is tested. Specifically, the sensor could be designed to respond with a certain PL to the presence of dangerous solvents. In this way, it would be possible to detect them and to prevent their storage in dangerous places like airplanes or trains. Figure 64 shows an illustration of this hypothetical application.

About biological applications, the main goal is to bind fluorescent components to certain proteins which need to be individuated to find the presence of a certain disease. More specifically, if the body is affected by a certain disease, specific biomarkers are present. The goal is to make them more visible by using photoluminescent components. The addition of Metal NPs could be useful to enhance their properties and to make them even more performing in revealing the presence of a certain biomarker corresponding to a certain illness. As reported by Fang Xie et al., the two most important complications are related to low intensities and photo stability, which is particularly evident in the case of near infrared fluorophores. However, according to them, these problems can be effectively restrained by providing fluorophores with a metallic component causing MEF [1]. Nevertheless, as it is a reported in the Appendix, semiconductor QDs usually present a higher PL intensity and a better photo stability compared to organic fluorophores. Unfortunately, they seem to be barely applicable for biological aims because of their high toxicity. In regard to this, the current thesis work plays a promising role since the produced QDs are safely covered with a thick enough layer of PS which would make them rather compatible with the human body.

To sum up, the studied combination of PS-CdS and GNPs seems to be promising also in the biological field even if it is true that some unaddressed problems remain essential, such as the necessity to expel the fluorescent substance from the body after the clinical exam by avoiding undesired accumulation of intrinsically toxic material. Alternatively, sensors based upon microfluidics could be envisioned where a blood sample could interact with a QDs-GNPs solution which could effectively signaling the presence of specific biomarkers.
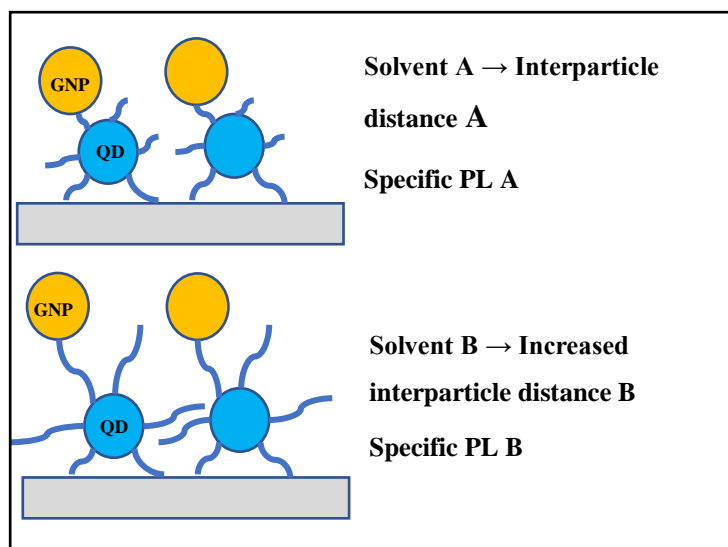
Figure 64 Schematic illustration of a sensor application

APPENDIX

PRELIMINARY CONCEPTS

INTRODUCTION

This Appendix presents the main objective to describe some of the most important concepts involved in this work. First of all, some general considerations about polymer science will be reported followed by an accurate analysis and explanation about self-assembly of block copolymers. This first topic has a crucial role in understanding the behavior of the Polystyrene layer around the quantum dots to prevent the quenching effect eventually observable between quantum dots and gold nanoparticles. Subsequently, a description of the behavior of quantum dots will be provided, together with an insightful explanation of the fluorescence effect. Moreover, a general overview on cadmium sulfide quantum dots will be presented and will comprise information about the production of colloidal solutions of this material and the possibility of giving rise to hierarchical structures. Later, it will follow a general outlook about gold nanoparticles and, more specifically, about the different existing types and the most common production methods. Finally, some information about the metal enhanced fluorescence phenomenon observed in solution will be listed with the aim to introduce the same phenomenon observed in a solid layer. For this reason, an accurate explanation of the procedure adopted for the realization of the sample will be reported at the end of the present Appendix.

A.1 BASIC CONCEPTS OF POLYMER SCIENCE

The following paragraphs have been mainly extracted by the book "Introduction to Polymers" by R.J Young and P.A. Lovell and from "Polymer Chemistry" by Paul C. Hiemenz and Timothy P. Lodge.

A.1.1 Basic definitions and nomenclature

As reported by R.J. Young and P.A. Lovel in their book "Introduction to polymers" a "polymer is basically a substance composed of molecules which have long sequences of one or more species of atoms or groups of atoms linked to each other by primary, usually covalent, bonds". They decided to emphasize the term "substance" in this definition to highlight that even though the words polymer and macromolecule are used as synonyms, the latter specifically defines the molecules of which the former is composed. Consequently, it is possible to assert that a polymer is made of many macromolecules that are, in turn, formed by linking together monomer molecules through chemical reactions. This procedure is known with the term of polymerization. For example, polymerization of ethylene gives rise to polyethylene, a sample of which could contain molecules characterized by 50000 carbon atoms linked together in a chain. It is this long chain nature which makes polymers unique among all the other materials and provides them with their characteristic properties. [19]

A.1.1.1 Skeletal structure

The previously reported definition of polymers implies that they present a linear skeletal structure that can be represented by a chain with two ends. However, there are many non-linear skeletal structures like those shown in figure 65. In particular, *branched polymers* present side chains, or branches, characterized by a considerable length and bonded to the main central chain at branch points, also called junction points. These polymers are classified in terms of the number and size of their branches. *Network polymers,* instead, present a three-dimensional structure in which all chains are connected among each other and are defined as crosslinked. Consequently, it is possible to define a crosslink density, or degree of crosslinking, which is related to the number of junction points per unit volume. Non-linear polymer may essentially be formed by standard polymerization or by linking already existing chains. [19]
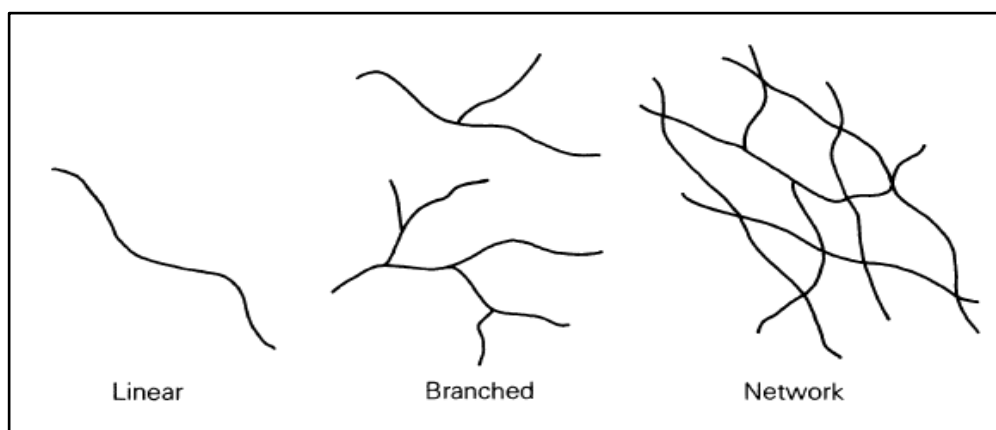
Figure 65 Skeletal structure of linear and non-linear polymers *[19]*

It is important to consider that variations in the skeletal structure give rise to differences in properties. For example, a linear polyethylene presents a melting point about 20°C higher than a branched homonymous polymer. Moreover, it is worth remembering that unlike linear and branched polymers, network polymers cannot be melted upon heating or be dissolved. This behavior is due to the presence of the aforementioned chemical or physical crosslinks. However, they may considerably swell when put in contact with compatible solvents. [19]

It follows a classification of polymers that results of crucial importance in understanding the nature of the substances used in the present work. In particular, the category of copolymers covers a fundamental role and will be thoroughly analyzed in the next section.

A.1.1.2 Polymer classification

The present classification is established based on two different aspects. The first one involves the physical characteristics of polymers and their consequent behavior. The second one, instead, focuses more on the polymer chains aspect and it is the most important for the considerations that are made in the present thesis.

As far as the first classification is concerned, polymers can be sorted in *thermoplastics*, *elastomers* and *thermosets*. The first can be further organized in amorphous and crystalline and are often referred to as plastics. This kind of polymers presents a linear or branched structure and can be melt upon the application of heat. Consequently, they can be molded repeatedly into virtually any shape by using many different techniques among which extrusion and injection molding are the most known and used. They are the most commonly used polymers in industries. Although their crystallization is a rare process, because it requires a considerable

ordering of the highly coiled and entangled macromolecules present in the liquid state, it can sometimes happen. However, not a perfect crystal is formed but rather some crystalline regions alternated to some other which are amorphous. The final structure is therefore referred to as semi-crystalline. The crystalline part is characterized by a melting temperature (Tm) while the amorphous part has its own glass transition temperature (Tg). This is a temperature, or rather a temperature range, at which the polymers transform from a hard-glassy state to a soft-rubbery state. It can be inferred that semi-crystalline polymers present both their Tm and Tg while completely amorphous polymers only have a Tg. [19]

Elastomers are low crosslinked rubbery polymers that can be highly stretched and that can easily recover their previous shape as soon as the applied stress is released. This entropy driven process is ensured by the crosslinks which act as a spring and make the polymer elastic in the sense that permanent flow upon deformation is prevented. [19]

Finally, thermosets are rigid materials and are network polymers where chain motion is strongly obstructed by the high degree of crosslinking. Unlike thermoplastics, both elastomers and thermosets are intractable once formed and degrade rather than melt if heat is applied. [19]

If the second classification is applied, polymers can be placed in the category of Homopolymers and Copolymers. The definition of the former is a polymer derived from one species of monomer, even if the same name is often widely applied to polymers which structure can be represented by multiple repetition of a single type of repeat unit which might contain one or more species of monomer unit. As a general way to represent a homopolymer, the repeat unit is enclosed by brackets. Therefore, the hypothetical homopolymer composed by the repeat unit A, ~A – A – A – A – A – A – A – A – A – A ~, is shorten by – $[A]_n$ – where n stands for the number of repeat units linked together to give rise to a macromolecule. Talking about the nomenclature, a name is assigned to a polymer by placing the prefix "poly" before the name of the repeating monomer. [19]

The last considered category, and the most important one for the current thesis, are the copolymers. These substances derive from more than one species of monomer and, as discussed for homopolymers, it is common practice to use a structure-based definition. Therefore, the word copolymer is commonly used to describe polymers which molecules contain two or more different types of repeat unit. [19]

Different types of copolymers can be identified based on the arrangement of the repeat unit along the polymer chain. As it is reported by Young and Lovell, and by the majority of the literature about polymer science, the letters A and B will be used here to refer to two different units. However, more complex copolymers could be contemplated, characterized by a higher number of repeat units. [19]

The first type of copolymers is called *statistical copolymers* and presents a sequential distribution respecting some known statistical laws. This category turns into *random copolymers* when the distribution of repeat units is completely random. An example of random copolymer is represented below. [19]

~ A – A – B – A – B – B – B – A – B – A – A – B – B – A – A – A – A – B ~

The second copolymer category is referred to as *alternating copolymers* where the two different types of repeat units are ordered alternately along the polymer chain as it is illustrated here.

~ A – B – A – B – A – B – A – B – A –B – A – B – A – B – A – B – A – B ~

The copolymers reported until now generally have properties that are intermediate to those of the corresponding homopolymers. Therefore, one single material could be designed to combine the desirable properties of the homopolymers.

Even more important for the thesis in object is the group of *block copolymers* which are linear copolymers in which the repeat unit is organized into long sequences or blocks. Indeed, for example, letter A will appear connected to another A before connecting to a

B. The reason why this happens will be clarified later when an explanation about the likelihood of monomers to mix will be provided. Two common structures of block copolymers are reported below, the first one of which is referred to as *AB di-block copolymer* and the second one as *ABA triblock copolymer*. [19]

~ A – A – A – A – A – A ~ A – A – A – B – B – B – B – B – B – B – B – B ~

~ A – A – A – A – A – A – B – B – B – B – B – B –A – A – A – A – A – A ~

Finally, less important for the present work but still covering a fundamental role in the polymer science field, *graft copolymers* can be imagined as branched block copolymers. In fact, they generally present, in their simplest form, a main homopolymer chain with branches of a different homopolymer as illustrated below.

B – B – B – B – B
|
B
|
~ A – A – A – A – A – A – A – A – A – A – A – A – A – A – A – A – A – A ~
|
B
|
B – B – B – B – B
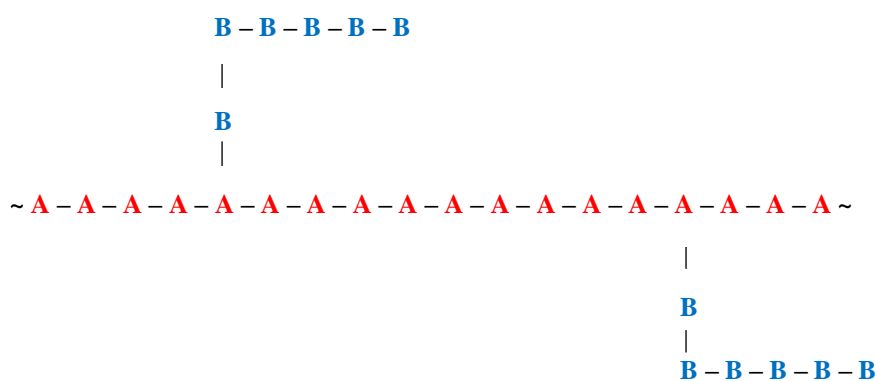
Unlike the previously described categories of copolymers, block and graft copolymers usually show characteristics that are typical of each of the constituent homopolymer. Moreover, they present unique properties deriving from the chemical linkage between the homopolymer sequences with the result that they are prevented from behaving totally independently of each other. [19]

To conclude this paragraph, a nomenclature example is reported that refers directly to the current thesis. Although the effectively used block copolymer being more complex than a simple di-block copolymer, what follows is merely an example of the rules applied to assign a name. In particular, if the repeat units are, for example, poly acrylic acid (PAA) and polystyrene (PS), the consequent di-block copolymer will be referred to as poly acrylic acid – block – polystyrene or rather PAA-b-PS. More detail about the real utilized substance is provided in Chapter 2.

A.1.1.3 Molar mass and degree of polymerization

The present paragraph has the fundamental role of providing insight about polymers molar mass which is important to understand how numerous properties of polymers show a strong dependence upon the size of polymer chains. Consequently, the characteristics of composite materials where polymers are present, can vary according to the structure of the latter. Therefore, it is essential to characterize the chains' dimensions, and this is usually done by measuring the molar mass of a polymer that is simply the mass of one mole of substance. The units that are used to refer to the molar mass, always indicated with M, are g mol^{-1} or kg mol^{-1}. If the case of a homopolymer is considered, it is easy to understand that its molar mass is related to the degree of polymerization, usually referred to as x and indicating the number of repeat units in the polymer chains. As a consequence, the molar mass can be expressed as $M = x \, M_0$ where the last term stands for the molar mass of the repeat unit. [19]

As it was previously explained, polymers consist of macromolecules which are characterized by a certain range of molar masses. Since the molar mass varies by intervals of the entity of M_0, it follows that its distribution shows a discontinuous trend. However,

for the majority of polymers the mentioned intervals are greatly smaller than the total range of molar mass and so the final distribution can be assumed to be continuous as illustrated in figure 66. [19]
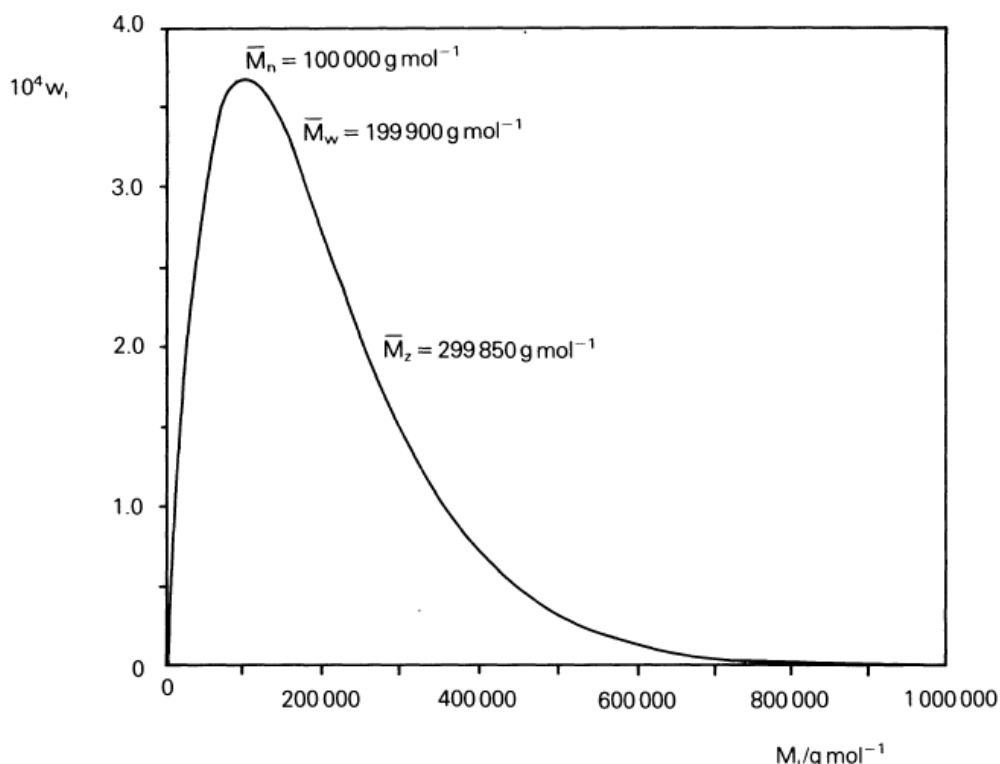
Figure 66 Typical molar mass distribution curve *[19]*

In order to acquire a complete knowledge about the molar mass distribution, it is useful to organize it in molar mass averages. These are usually defined by considering the discontinuous character of the macromolecules distribution. In fact, macromolecules exist in discrete fractions *i* containing N*i* molecules of mass M*i*. Therefore, it is possible to define three different kinds of molar mass that are represented in figure 66.

First, the *number-average molar mass ($\bar{M}n$)* is defined as "the sum of the products between the molar mass of each fraction and its mole fraction". Consequently, the number-average molar mass can be expressed as follows.

$$\bar{M}n = \sum X_i M_i \qquad (1.1)$$

In the previous formula, the term X_i stands for the mole fraction of molecules characterized by a mass M_i and it can be alternatively expressed by the ratio between N_i and the total number of molecules, as shown in the following equation.

$$\bar{M}n = \frac{\sum N_i M_i}{\sum N_i} \qquad (1.2)$$

It is easy to see that this average is the arithmetic mean of the molar mass distribution. However, during laboratory measurements procedures, it is often more convenient to refer to weight fraction rather than numbers of molecules. For this reason, the weight fraction w_i is defined as the mass of molecules with a molar mass M_i divided by the total mass of all the considered molecules, as illustrated here.

$$w_i = \frac{N_i M_i}{\sum N_i M_i} \qquad (1.3)$$

88

Second, considering the last reported equation, it is possible to define the *weight-average molar mass ($\bar{M}w$)* which is defined as "the sum of the products between the molar mass of each fraction and its weight fraction".

$$\bar{M}w = \sum w_i M_i \qquad (1.4)$$

By combining equation 1.3 and 1.4 it is easy to obtain the expression of the weight-average molar mass in terms of number of molecules.

$$\bar{M}w = \frac{\sum N_i M_i^2}{\sum N_i M_i} \qquad (1.5)$$

Once $\bar{M}n$ and $\bar{M}w$ are obtained, the polymer can be characterized in terms of its polydispersity. In fact, the ratio $\bar{M}w/\bar{M}n$ is called polydispersity or heterogeneity index and it provides a measure of the broadness of the molar mass distribution. A perfect monodisperse polymer, characterized by identical macromolecules, presents an index equal to 1.00. However, this is never observed because of unavoidable inefficiency during the synthesis. On the contrary, a typical range value of the polydispersity index is 1.50 – 2.00.

Third, *z-average molar mass($\bar{M}z$),* deriving from different methods of molar mass measurements (e.g. sedimentation equilibrium) is defined as follows.

$$\bar{M}z = \frac{\sum N_i M_i^3}{\sum N_i M_i^2} = \frac{\sum w_i M_i^2}{\sum w_i M_i} \qquad (1.6)$$

However, this is beyond the purpose of the current introduction that is only necessary to explain how the molar mass can be calculated and represents an important factor to establish behaviors and properties of polymers or polymer-based composite materials. In fact, when the polymers used in the current thesis work were illustrated, the molar mass of the obtained structure was mentioned. [19]

A.1.2 Polymer Synthesis

The present paragraph has the main role of introducing the polymerization reactions and to deeply explain what is the theory supporting the concept of copolymerization. The latter is particularly important to lead to the following topic of RAFT copolymerization that results of fundamental importance for the current thesis work.

A.1.2.1 General classification of polymerization reactions

One of the fundamental concepts to understand the polymerization procedure is the polymer functionality. It is possible to think about is as the ability of the monomer to be linked to another monomer. Consequently, if the objective is the realization of a chain, the desired value of functionality has to be at least two. In other words, each monomer should present at least two points where another monomer could link. As a result, a linear chain can be created. Moreover, as it can easily be imagined, an increase in the polymer functionality, allows for the creation of a more complex structure as the previously presented ones. [19]

As far as the polymerizations classification is concerned, polymer science has until now relied on the work of Carothers who identified two main processes through which the polymerization can occur. In particular they are named *condensation* and *addition* polymerizations. In the first one, the repeat units possess less atoms than present in the monomers. This is allowed by the elimination of a molecule occurring during the chemical reaction. In the second one, instead, the number of atoms constituting the repeat units and the monomer are exactly the same. [19]

However, the classification provided by Carothers turned out to be unsatisfactory when some condensation polymerizations were individuated which presented some typical features of addition polymerization and vice versa. Consequently, a more precise classification was provided based upon the polymerization mechanism. *Step-growth* polymerizations are those where each species can react among each other. Namely, if for instance two monomers react to create a dimer, subsequently the latter can react with a monomer or another dimer. Moreover, a trimer derived from the reaction between a monomer with a dimer, in turn, can react with a monomer, a dimer or another trimer. In other words, it can be affirmed that the chains grow step-wise. On the contrary, if the only allowed reaction is the one between monomers and so between the growing chain and the next monomer, the polymerization is referred to as *chain-growth*. This usually needs an initial reaction between the first monomer and a molecule called initiator. The main features of the presented reactions involve the degree of polymerization. In fact, in step polymerization, this increases steadily, during the reaction, but the polymer is quickly consumed at the very beginning of the reaction. Young and Lovell reported, for instance, that if the degree of polymerization is $\overline{x_n} = 10$, "less than 1% of the monomer remains unreacted". Oppositely, in chain polymerization, the polymer is consumed steadily, and high degrees of polymerization are obtained at low monomer conversions. [19]

Step polymerization

Among the step polymerization processes, the two categories that could be identified are *linear* and *non-linear* step polymerization. The first one could be further subdivided into *polycondensation*, e.g. the formation of a linear polyesters and *polyaddition*, e.g. the reaction occurring when polyurethanes are produced. Specifically, while the first one involves the elimination of small molecules, the second one doesn't show this feature. As far as non-linear step polymerization is concerned, this is the process through which network polymers are generated e.g. formaldehyde-based resins or epoxy resins. [19]

Chain polymerization

More significant in relation to the present thesis work, is the chain polymerization reaction. In particular, it is possible to individuate three different sub-categories of this synthesis method, namely free-radical, anionic and cationic polymerization.

Free radical polymerization is the most diffused and utilized method of polymerization and it is almost only applied to obtain a polymer from a monomer presenting the general structure $CH_2=CR_1R_2$. What is defined as a free radical, is an "independently-existing species" which is characterized by the presence of an unpaired electron. Consequently, its reactivity is high and its lifetime short accordingly. Each growing chain has a terminal reactive site i.e. the free radical molecule, that is also referred to as active center and ensures the bonding with the next monomer. In fact, when a monomer is added, it becomes part of the growing chain and the active center is transferred to the new chain extremity. [19]

Three different sub-steps occur during a free radical polymerization, namely initiation, propagation and termination. Within the first, the formation of the free radical from an initiator and the addition of the formed free radical to a monomer are the two sub-steps occurring. In other words, the initiator is fundamental to obtain the free radical species that, subsequently, interacts with the first monomer of the future chain and creates the reactive site. Immediately after, propagation occurs during which monomers are connected to the growing chain. Finally, thanks to the termination step, the growth of a chain is arrested. In particular, this can happen following two different paths. The first one is called combination and it involves the coupling of two growing chains resulting in their growth arrest. The second one is called disproportionation and it is based upon the subtraction of a hydrogen atom

from one growing chain by another. It is useful to remember that combination yields the formation of a final head-to-head linkage and the resulting chain is characterized by two initiator fragments at both its extremities. Oppositely, disproportionation generates two chains the first one of which presents a saturated end-group and the second one of which has an unsaturated end-group. [19]

A very important concept to be explained is the chain transfer phenomenon. As reported in literature [19], this affects the degree of polymerization that, in turn, is defined as follows.

$$\overline{x_n} = \frac{Moles\ of\ monomer\ consumed\ in\ unit\ time}{Moles\ of\ polymer\ formed\ in\ unit\ time} \qquad (1.7)$$

In particular, the real experimentally obtained values of $\overline{x_n}$ are lower than those calculated by the previous equation because of secondary reactions that arrest the growth of a chain radical. These are referred to as chain transfer reactions and could be represented by the following schematic.

$$M^{\cdot}_i + T - A \rightarrow M_i - T + A^{\cdot}$$
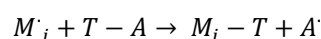
Specifically, T and A are the components of a hypothetical molecule TA. The chain radical separates the T-A molecule by subtracting $T^{\cdot}$ and giving rise to a "dead" polymer molecule and a new radical $A^{\cdot}$. The latter, in turn, can react with another monomer to cause the growth of a new chain as illustrated here.

$$A^{\cdot} + M \rightarrow AM_1^{\cdot}$$
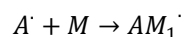
Ionic polymerization i.e. *cationic* or *anionic*, according to the features of the reacting species, is the second kind of chain polymerization and it is a process characterized by the absence of an inherent termination step. Consequently, this is the typical procedure applied to develop the so-called living polymerization. In regard to it, the absence of chain transfer reactions allows the chains to maintain their active end-groups and to further grow when additional monomer is added after complete conversion of its initial quantity.

However, considering the introductory character of the present paragraph, this topic will not be thoroughly covered. Nevertheless, what is worth remembering is that, as far as cationic polymerization is concerned, an electrophile species is fundamental to provide the first reacting monomer with a proton H^+. In particular, sulphuric acid (H_2SO_4) or perchloric acid ($HClO_4$) are used as initiator and can make the monomer a cationic active center. On the other hand, anionic polymerization initiation involves dissociation of a certain species and the following addition of the generated ion to the first reacting monomer. [19] In addition, even if in literature it is common to find the same vocabulary referring to the polymerization steps (i.e. initiation, propagation and termination) for both free-radical and ionic polymerization, it is important to remember that these are quite different in these two categories. Just to name a reason, termination by combination is not possible in ionic polymerization because it would prevent the character of the previously illustrated living polymerization. [20]

A.1.3 Copolymers

What follows is an insight about copolymers that presents the aim to go further in depth compared to the previous paragraph. In fact, some general features about copolymers will be provided here, together with the most important synthesis methods. Furthermore, the concept of Reversible Addition-Fragmentation Transfer (RAFT) will be presented and analyzed. This part has a

role of great importance because the considered procedure has been applied during the production of the polymer that was utilized for the current thesis work.

First and foremost, it is important to introduce that copolymerization can take place in two different ways, namely step and chain copolymerization. Furthermore, as reported in literature [19], both can yield to statistical copolymers and block copolymers. In particular, the description of the first way will be rapid because non-fundamental for the present thesis work. Oppositely, chain copolymerization will be covered in detail.

Step copolymerization yielding statistical copolymers

Copolymers are simply formed by the simultaneous polymerization of two or more different monomers. In particular, as far as the category of step copolymerization is concerned, the goal is to obtain copolymers with high molar masses. Consequently, the process has to be taken to high extents of reaction. In addition, it is fundamental to distinguish between the overall composition of the copolymer and the sequence distribution of the different repeat units. If the former corresponds to the composition of the comonomer mixtures that are utilized to produce the final copolymer, the latter strictly depends on differences in monomer reactivity. It follows that, if the functional groups (i.e. A and B) present the same reactivity for each monomer, the prevalence of one monomer over the other to react is dictated by the mole fraction of functional groups that it would guarantee. If these conditions are present, *random copolymers* are generated.

Oppositely, when monomers present the same type of functional groups, but characterized by different reactivity, the polymerization procedure acquires a more complex character and do not yield random copolymers. In particular, the more reactive monomer (i.e. the one containing the more reactive functional group) is preferentially incorporated into the new forming polymer. In other words, the initial oligomeric chain is richer in the more reactive monomer. On the other hand, the precipitation of the less reactive monomer is increased as the more reactive is consumed by this "preferential reaction". In conclusion, the resulting copolymers present "significant sequences of the same repeat units" or rather a "blocky" structure. [19]

Step copolymerization yielding block copolymers

The step polymerization process can be tuned to generate alternating block copolymers. In particular, this is possible by using low molar mass prepolymers with terminal functional groups in the role of comonomers. When this kind of step copolymerization is applied, it is usual to refer to the blocks as *segments* and to the copolymers as *segmented copolymers*.

A.1.3.1 Chain copolymerization

As it was explained for step copolymerization, also in chain copolymerization the different reactivity of monomers can affect the sequence distribution of the repeat units constituting the formed copolymer molecules. For reasons that derive from the nature of chain polymerization, it is possible to observe that high molar mass copolymer molecules are formed early in the reaction. Nevertheless, as seen for step copolymerization, it is still observable that the most reactive monomer is more likely to be incorporated into the forming chain. Consequently, when the extent of reaction is low, the first molecules that form, or rather the ones characterized by high molar mass, might have a considerably different composition compared to the initial comonomer mixture. [19]

With the aim to forecast the composition of a formed copolymer at a certain instant of time during the process of chain copolymerization, it is useful to define a kinetic model. In particular, as Young and Lovell reported in their book, the simplest model is called *terminal model* and its name refers to the fact that the reactivity of an active center only depends upon the terminal monomer unit. The next part will be presented by rigorously following the structure of the current source. [19]

First and foremost, Young and Lovell assumed that only the propagation step must be considered in defining the total amount of consumed monomer. In other words, the contribution of initiation and termination is negligible. The active centers that are responsible for copolymerization of monomer A with monomer B are illustrated as follows, with the asterisk indicating the active center which can be, for instance, an unpaired electron in the case of free radical copolymerization.

--------A* and --------B*

By considering that the only way to yield the active centers propagation is the addition of an A or B monomer, there are four different possible reactions each of which is characterized by its own rate constant K.

--------A* + A $\xrightarrow{K_{AA}}$ --------AA*

--------A* + B $\xrightarrow{K_{AB}}$ --------AB*

--------B* + B $\xrightarrow{K_{BB}}$ --------BB*

--------B* + A $\xrightarrow{K_{BA}}$ --------BA*
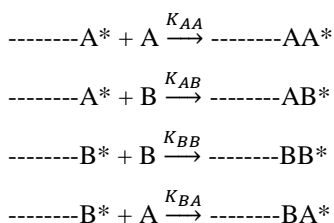
Those reactions that occur between the same monomer, or rather those which present rate constants K_{AA} and K_{BB}, are referred to as *homopropagation reactions*. On the other hand, the reactions between different monomers present mixed rate constant K_{AB} and K_{BA} and are called *cross-propagation reactions*. Indeed, it is possible to define the rate of consumption of monomer A as follows.

$$-\frac{d[A]}{dt} = K_{AA}[A^*][A] + K_{BA}[B^*][A] \qquad (1.8)$$

In the previous equation, [A*] and [B*] are the concentrations of growing chains characterized by A-type and B-type active centers respectively. Likewise, it is possible to illustrate the rate of consumption of monomer B.

$$-\frac{d[B]}{dt} = K_{BB}[B^*][B] + K_{AB}[A^*][B] \qquad (1.9)$$

From the previous equations, it is easy to provide an expression of the ratio of the amount of monomer A and monomer B that are incorporated into the polymer chain at any instant of time. Specifically, this is obtained by dividing the two rates of consumptions as follows.

$$\frac{d[A]}{d[B]} = \frac{[A]}{[B]} \left\{ \frac{K_{AA}[A^*] + K_{BA}[B^*]}{K_{BB}[B^*] + K_{AB}[A^*]} \right\} \qquad (1.10)$$

Furthermore, by dividing the quantities in brackets by the concentration [B*], the same expression reported by Young and Lovell is achievable. [19]

$$\frac{d[A]}{d[B]} = \frac{[A]}{[B]} \left\{ \frac{K_{AA}[A^*]/[B^*] + K_{BA}}{K_{BB} + K_{AB}[A^*]/[B^*]} \right\} \qquad (1.11)$$

The ratio between [A*] and [B*] can be treated by applying appropriate steady state conditions as follows.

$$\frac{d[A^*]}{dt} = 0 \quad and \quad \frac{d[B^*]}{dt} = 0$$

As far as formation and loss of specific active centers is concerned, it is possible to assert that the contribution of initiation and termination is negligible with respect to that of the cross-propagation reactions. Consequently, the following expressions report the variation of concentration of A* and B* in terms of cross-propagation.

$$\frac{d[A^*]}{dt} = K_{BA}[B^*][A] - K_{AB}[A^*][B] \qquad (1.12)$$

$$\frac{d[B^*]}{dt} = K_{AB}[A^*][B] - K_{BA}[B^*][A] \qquad (1.13)$$

Moreover, by applying the previously introduced steady state conditions, the following ratio is achievable.

$$\frac{[A^*]}{[B^*]} = \frac{K_{BA}[A]}{K_{AB}[B]} \qquad (1.14)$$

By substitution of equation (1.14) into equation (1.11), and by further simplification, the copolymer composition equation, in one of its forms, is obtainable. Specifically, r_A and r_B represent the respective monomer reactivity ratios.

$$r_A = \frac{K_{AA}}{K_{AB}} \quad and \quad r_B = \frac{K_{BB}}{K_{BA}}$$

$$\frac{d[A]}{d[B]} = \frac{[A]}{[B]}\left(\frac{r_A[A] + [B]}{[A] + r_B[B]}\right) \qquad (1.15)$$

What is provided by equation 1.15 is the molar ratio between repeat units of type A and B in the copolymer formed ad any instant of time during the copolymerization. However, it is more functional to express compositions as mole fractions. Consequently, it is possible to define the mole fraction f_A of monomer A in the comonomer mixture and the mole fraction F_A of A-type repeat units in the copolymer formed at a specific instant of time as follows.

$$f_A = \frac{[A]}{[A] + [B]} \qquad (1.16)$$

$$F_A = \frac{d[A]}{(d[A] + d[B])} \qquad (1.17)$$

By considering that the maximum mole fraction is 1, the following relationships are true.

$$f_B = 1 - f_A$$
$$F_B = 1 - F_A$$

Finally, it is possible to rewrite equation 1.15 in terms of f_A, f_B and F_A (or F_B) as follows.

$$F_A = \frac{r_A f_A{}^2 + f_A f_B}{r_A f_A{}^2 + 2 f_A f_B + r_B f_B{}^2} \qquad (1.18)$$

94

$$F_B = \frac{r_B f_B{}^2 + f_A f_B}{r_A f_A{}^2 + 2 f_A f_B + r_B f_B{}^2} \qquad (1.19)$$

As indicated in equation 1.15, the monomer reactivity ratios express the ratio between the homopropagation and the cross-propagation rate constants. In addition, it is fundamental to highlight that these ratios are important quantities because, for a certain instantaneous comonomer composition, they establish the composition of the generated copolymer as well as the sequence distribution of the involved repeat units. Specifically, if $r_A > 1$, it follows that the active center --------A* prefers linking to monomer A. Oppositely, if $r_A < 1$, the same active center in more prone to connect to monomer B. In other words, in the first case homopolymerization is the most likely procedure while in the second one cross polymerization dominates. Likewise, the quantity r_B describes the behavior of monomer B.

Figure 67 illustrates the various plots that can be obtained with different r_A and r_B couples. In particular, as reported by Young and Lovell [19], the first category of copolymers is the one where $F_A = f_A$ regardless of the value of f_A. This case is referred to as *random copolymers*, presents $r_A = r_B = 1$ and shows an equal probability for both the active centers to add monomers A or B. This first case appears in figure 67 as the straight line.

More frequent is the condition where one of the monomers presents a higher reactivity compared to the other. If it is assumed that monomer A is most reactive, this will be preferentially added by both the active centers. This situation can be expressed, in terms of reactivity ratios, by asserting that $r_A > 1$ and $r_B < 1$. Obviously, the inverse relation would be true if B were the most reactive monomer. In the figure below, three examples of this relation are illustrated. Specifically, the two cases with $r_A > 1$ and $r_B < 1$ appear as a plot above the straight line corresponding to $r_A = r_B = 1$. Inversely, the case with $r_A < 1$ and $r_B > 1$ is plotted underneath the straight line.

A special sub-case of the previous one is represented by the *ideal copolymerization* and is characterized by $r_A r_B = 1$. This means that $r_A = 1/r_B$ and consequently $k_{AA}/k_{AB} = k_{BA}/k_{BB}$. It is possible to affirm that under these conditions the relative rates at which the two monomers are added to the growing chain is the same. As a consequence, even if $F_A \neq f_A$, the sequence distribution is random.
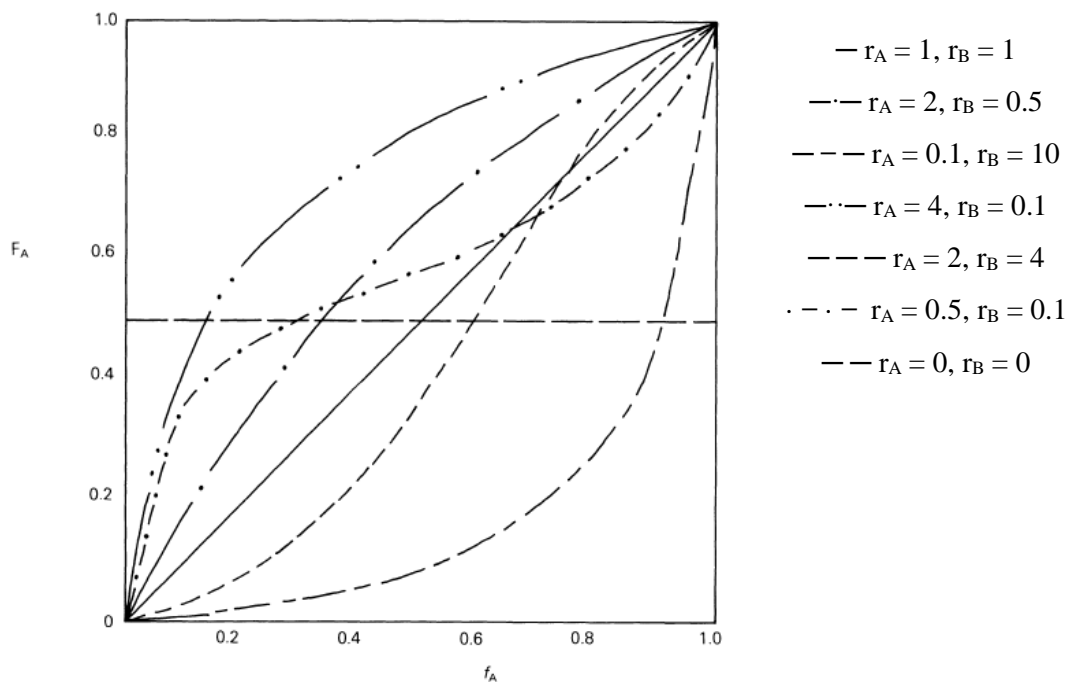

Figure 67 Plots of equation 1.18 illustrating the variation of copolymer composition F_A with comonomer composition f_A for different couples of r_A and r_B *[19]*

More generally, the value of the ratio r_A/r_B gives an idea of the extension of the continuous sequences composed by the same type of repeat unit. In other words, if this ratio is high, it means that there is a strong tendency to generate sequences made of exclusively A-type monomers. On the other hand, the sequences composed of B-type monomers are shorter. The same is true, and exacerbated, if $r_A \gg 1$ and $r_B \ll 1$. In fact, in this case it is possible to observe an extreme situation in which the homopolymerization of the two monomers occurs. Specifically, the sequences that form earlier are almost exclusively composed of the most reactive monomer A. When all this monomer has been consumed, the homopolymerization of monomer B takes place.

Finally, in figure 67 the so-called *azeotropic copolymerization* is shown. This occurs when both r_A and r_B are bigger or smaller than zero. It is observable that when the product $r_A r_B$ decreases, an alternation in the addition of monomer molecules takes place. Furthermore, the extremization of the present case occurs when a perfectly alternating copolymers forms because $r_A = r_B = 0$. In fact, under these conditions, homopropagation is prevented. This last case appears in figure 67 as a horizontal line.

A.1.3.2 Block copolymers and RAFT copolymerization

As asserted by Young and Lovell [19], the most effective way to produce a block copolymer by chain polymerization is through living polymers. This means that it is necessary to generate living homopolymer molecules by performing the polymerization of a first monomer. Subsequently, the polymerization of the second monomer starts from the terminal active sites. In other words, the first step is the creation of a homopolymer composed of monomer A while the second step is the formation of another block made of homopolymer B. Specifically, this result is referred to as AB di-block copolymer. In all the different strategies that can be selected to obtain the aforementioned result, namely ionic, Ziegler-Natta, ring-opening and group transfer methods of chain polymerization, the order of polymerization has a fundamental role. In fact, after the first block is completed, this must be effective in providing the polymerization of the second. This is the reason why the less reactive monomer is always polymerized first. Furthermore, it has been found that anionic living polymerization represents the most effective strategy for the preparation of block copolymers. Specifically, block copolymers with blocks of "pre-defined molar mass, narrow molar mass distribution and controlled stereochemistry" [19] can be produced by applying a precise control of the polymerization conditions.

The outstanding properties of block copolymers have been mentioned by many other researchers and authors. For example, Pan Cai-Yuan and Hong Chun Yan from the department of Polymer Science and Engineering of University of Science and Technology of China, reported how, because of "their distinctive structures, block copolymers have useful and desirable properties". [21] Among their various applications, they mentioned their use in inexpensive adhesive tape where triblock linear copolymers can guarantee pressure-sensitive adhesion. Moreover, polyurethane foams are made of block copolymers referred to as thermoplastic elastomers that are able to provide high temperature resistance by remaining flexible at lower temperatures.

Beside the use of the previously mentioned living polymerization, controlled radical polymerization methods have been developed to produce block copolymers. Moreover, these two techniques have been effectively combined. The main difference existing between ionic and radical synthesis techniques is that in the former the growing species are mutually repulsive while in the latter it is easy to observe bimolecular termination like radical recombination or disproportionation. Recently developed techniques, namely ATRP (atom-transfer radical polymerization) and RAFT (reversible addition-fragmentation transfer) present the common objective of reducing the instantaneous concentration of growing radical species. This is achieved by adding an "excess of covalent dormant species that exists in rapid equilibrium with the growth-active radical species" [21] . The result is that the established dynamic and rapid equilibrium reduces the chances for bimolecular termination and simultaneously makes living and dormant chains equally likely to propagate because of the frequent interconversion between the two species. The final obtained feature is an approximately uniform chain length. However, due to the fact that around 10 % of the growing radicals still suffer from termination during the polymerization process, it is necessary to separate the obtained block copolymer from homopolymer unwanted byproducts. [21]

Since the present thesis work is based on the use of a particular type of block copolymer produced by the so-called RAFT copolymerization, what follows is a detailed analysis of this polymerization procedure.

RAFT copolymerization

Moad and coworkers can be considered as the pioneers in the study of Raft copolymerization. Their work, entitled "Living Free-Radical Polymerization by Reversible Addition-Fragmentation Chain Transfer: The Raft Process" has been published in 1998 and reported the astonishing properties of this polymerization process. [22]. As previously introduced, they asserted that in order to produce a block copolymer with good properties, it was useful to combine the positive effects of both living and free radical polymerizations. In particular, the former provides the possibility to effectively control molecular weight and polydispersity and to produce polymers and block copolymers characterized by a complex architecture. The latter, in turn, presents the virtue of an outstanding versatility. Consequently, combining free radical and ionic polymerization was seen by many researchers as a very promising strategy to synthesize block copolymers. In addition, the already existent methods to merge these two approaches presented numerous drawbacks, namely the scarce applicability limited to a small range of monomers, the necessity of solvents that were expensive or difficult to be removed, the required application of special polymerization conditions (e.g. high reaction temperatures) and the pronounced sensitivity to acid or protic monomers. Beside the already considered ATRP, the other two main mechanism utilized until now to combine ionic and free-radical character are the so-called *polymerization with reversible termination by coupling* and *free-radical polymerization with reversible chain transfer* (also referred to as *degenerative chain transfer*). In figure 68 a schematic of the last procedure is illustrated.
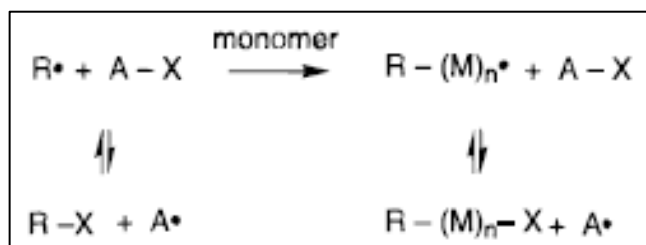
Figure 68: Simplified mechanism for free-radical polymerization with reversible chain transfer *[22]*

Specifically, the species A-X is called transfer agent and it can react with the initiating component $R^\bullet$ or with the propagating radicals ($R - (M)_n^\bullet$) to give rise to a new transfer agent, namely $R - X$ and $R - (M)_n - X$ and a species able to initiate another polymerization step, or rather $A^\bullet$. The RAFT copolymerization, object of the present paragraph, is a specific case of the described process. In particular, in the RAFT case, the reversible chain transfer occurs by an addition-fragmentation sequence.

According to Moad and coworkers [22], this innovative copolymerization procedure can easily be applied to a wide range of monomers and reaction conditions. In addition, unlike previous works (e.g. the polymerization procedure in presence of alkyl iodides to achieve reversible chain transfer by homolytic substitution, studied by Gaynor et al. [23] and which gave a polydispersity never lower than 1.4) can guarantee controlled molecular weight and low polydispersity values (usually < 1.2 and sometimes < 1.1). In particular, the living character of RAFT polymerization is guaranteed by a promptly available class of organic solvents and it is very easy to perform. Specifically, the key point is that the polymerization has to be conducted in presence of the so-called dithio compounds which act as a very efficient reversible addition-fragmentation chain transfer agent. What is shown in figure 69 is the molecular structure of the mentioned dithio compounds with the different Z and R groups that can be contemplated.

As previously anticipated, Moad et al. stressed the point that RAFT polymerization is a very versatile process. In fact, polymerizations can easily be carried out in bulk, solution, emulsion or suspension. Moreover, no significant limitations have been

reported on reaction temperature. Beside its versatility, the living character is one of the most important features of the present synthesis method. Many different factors can highlight this character, namely the narrow polydispersity product, a molecular weight-conversion profile that appears to be almost linear, the easy possibility to predict the molecular weight from the ratio monomer consumed over transfer agent and the capability to increase the molecular weight or to generate blocks by adding additional monomer. [22]
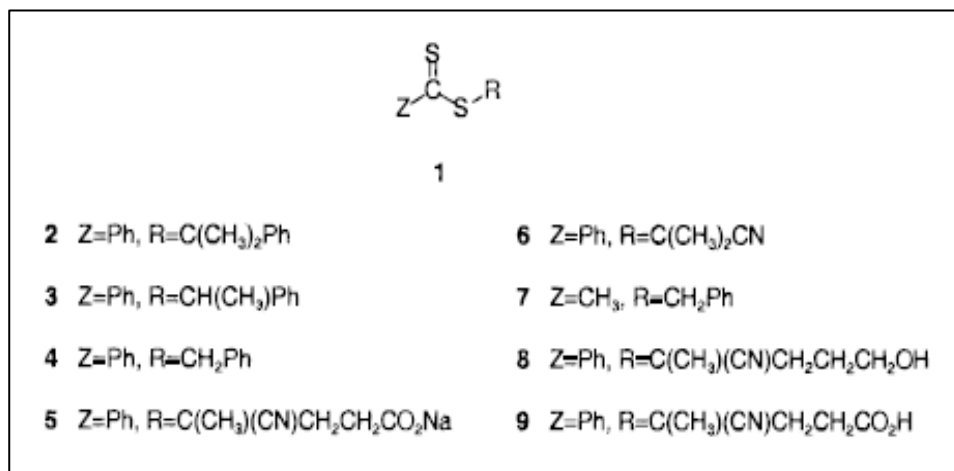
Figure 69: Class of organic solvents conferring the living character *[22]*

As far as the mechanism of RAFT is concerned, this is based upon a reversible addition-fragmentation sequence where the transfer of the group S=C(Z)S- between the active and the dormant chains provides the living character.

Figure 70 reports a schematic of the present mechanism where $R^\bullet, I^\bullet$ and $P_n^\bullet$ are species that can initiate free-radical polymerization.
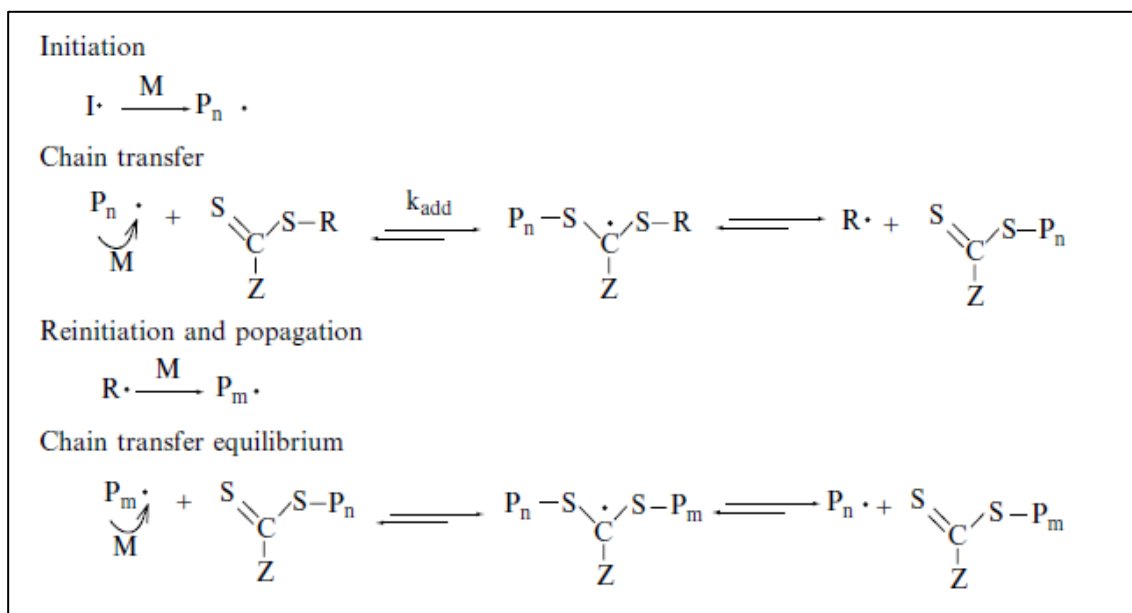
Figure 70: RAFT polymerization procedure *[21]*

In conclusion, what Moad et al. maintain is that the effectiveness of the reagents (1 in figure 69) in providing the fundamental living character is due to the high transfer constant which provides a quick rate of exchange between dormant and living chains. In particular, they assert that the choice of Z and R covers a very important role in ensuring the success of the RAFT procedure. In

fact, Z must "activate the C=S double bond toward radical addition" while R needs to be an effective free-radical leaving group. Moreover, once expelled, $R^{\bullet}$ has to act as a good free radical polymerization re-initiator. Suitable examples of Z groups are aryl and alkyl, while R is often a cumyl or a cyan isopropyl.

A.1.3.3 RAFT Polymerization of PAA-PS-TTC-PS-PAA

What follows is a more precise and specific example of RAFT polymerization applied to produce the polymer employed to conduct the present thesis work. In particular, the polymerization of styrene is achieved through what is defined as macro chain transfer agent.

In 2009, Xiaoguang et al. reported an example of ab initio (unseeded) RAFT emulsion polymerization of Styrene mediated by Poly (acrylic acid-b-styrene) trithiocarbonate by highlighting that this procedure was able to provide simultaneously high colloidal stability (i.e. no coagulum), high polymerization rate with short inhibition period, theoretically predictable number-average molecular weight (M_n) and low polydispersity index [24]. On the contrary, previous studies identified a too low chain transfer agent as the cause for a high polydispersity index. Moreover, Xiaoguang et al. asserted that in an ab initio emulsion polymerization where the RAFT agent is highly effective, colloidal instability, slow polymerization rate with long inhibition period, and uncontrolled polymer molecular weight have been individuated as the main drawbacks.

Xiaoguang et al. produced their Macro-RAFT Agent by a two-step solution polymerization. Subsequently, the produced agent was used to provide the emulsion polymerization of styrene. Unlike the previous amphiphilic macro RAFT agents (e.g. acrylic acid and butyl acrylate) which were often hydrophobic and had to be neutralized with NaOH to dissolve in water before polymerization, their agent presented a hydrophilic head that was completely ionized and consequently characterized by a large dimension due to a strong electrostatic repulsion. What was identified as an interesting advantage, is that a small number of these amphiphilic surfactant molecules was necessary to form a micelle. As a consequence, a high number of micelles could be generated resulting in an increase of the nucleation period.

In 2013, Farinha et al. reported a study about the enhanced photoluminescence from assemblies of Cadmium Sulfide quantum dots and gold nanoparticles in which a symmetric tetrablock copolymer played a fundamental role in ensuring a layer around the dots preventing the phenomenon of quenching due to the contact between quantum dots and metal nanoparticles. [4] In particular, this work results extremely useful in explaining some crucial points involved in the present thesis. For this reason, it is recalled now with the aim to provide an introduction about the production of the mentioned copolymer and it is recalled in Chapter 2 to thoroughly analyze its properties.

A.1.4 Block Copolymer Self-Assembly

In order to produce the structures that were utilized to conduct the present thesis work, it has been taken advantage of the so-called polymer self-assembly capability. The aim of the present paragraph is to provide a quick overview about this interesting feature while a more detailed explanation specific to the used copolymer is presented in Chapter 2.

As reported by Adi Eisenberg et al. [25] block copolymer self-assembly has been a very attracting topic for many decades because it can provide the formation of ordered structures with a wide variety of morphologies. Specifically, it is possible to create spheres, cylinders, bicontinuous structures, lamellae, vesicles and other hierarchical more complex assemblies. Very diffused in nature, self-assembly is common to be observed in the behavior of phospholipids which form membranes of living cells. In addition, self-assembly can be easily reproduced in laboratory to form, for instance, nanoreactors to host chemical reactions and material synthesis. What has already been investigated and thoroughly explained by researchers is that all the molecules able to guarantee a self-

assembly behavior consist of one or more hydrophobic tails and a hydrophilic head and are defined as amphiphiles. Specifically, it is the interaction between the environment and the molecule itself that provides the assembly and the consequent formation of the observable complex structure. With the aim to predict which assembly is more likely to form, a parameter p has been defined as follows.

$$p = \frac{v}{a_0 l_c}$$

In particular, v is the volume of the hydrophobic tail, l_c is its length, and a_0 is the contact area of the head group. According to the value assumed by p, it is possible to predict the shape of the formed structure. When $p < 1/3$, the observed assembly is spherical; if $1/3 < p < 1/2$ cylinders are created; when $1/2 < p < 1$, flexible lamellae or vesicles are generated; if $p = 1$, planar lamellae are produced; finally, when $p > 1$, inverted structures are observed. All the mentioned assemblies can find an explanation if the two main interactions are properly understood. In fact, amphiphiles present simultaneously what is called *hydrophobic attraction* between tails and what is defined as *hydrophilic repulsion* between headgroups. In order to explain them it is easy to consider an aqueous environment where the amphiphiles are dispersed. As far as the former is concerned, it must be noted that during the process of micellization (or rather the micelle formation) the entropy increase associated to the disruption of the water ordered structure around the tails plays a fundamental role. In other words, when the micelle is formed the water around the tails tends to lose its ordered cage-like structure lead by an increase in entropy. Consequently, the water between two tails is excluded and they undergo a reciprocal attraction. On the other hand, it is also possible to note a clear contribution of electrostatic repulsion between adjacent heads. To summarize, the final formed micelle is the result of a compromise between these two components. For instance, when the value of p is low, the assembly that is more likely to appear is the spherical one because a_0 is the dominant parameter. As a consequence, the heads are rather big, and the hydrophilic repulsion dominates by providing the formation of a sphere. On the contrary, when p grows bigger, a_0 becomes less important and the repulsive contribution leaves the field free for the attractive one which provides the formation of planar assemblies. Finally, the inverted micelles appear when the environment is organic. In this case, in fact, the heads tend to stay close among each other and form a hydrophilic nucleus. Oppositely, the hydrophobic tails create a sort of protective layer around the nucleus by solubilizing the amphiphiles in the organic phase. [26]

To conclude, it is worth summarizing that regular micelles are able to stabilize molecules in an aqueous environment while inverted micelles can provide stabilization for molecules in an organic medium. Figure 71 illustrates the composition of a regular micelle.
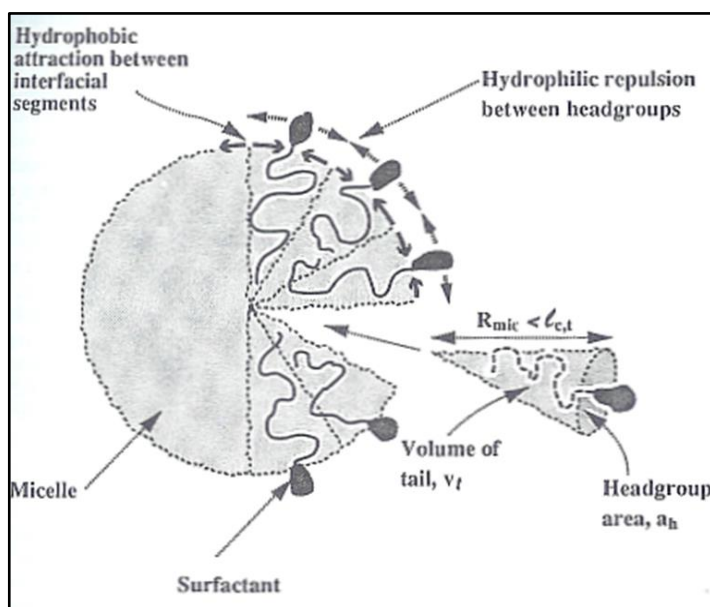

Figure 71 Regular Micelle structure *[26]*

As far as block copolymer self-assembly is concerned, it is possible to see it as if the macromolecules were amphiphiles. In fact, as previously illustrated, block copolymers are made of blocks some of which can present a hydrophilic or a hydrophobic character. Consequently, block copolymers can be treated as amphiphilic molecules able to generate micellar assemblies that vary based upon the value of the p parameter. In Chapter 2, more details about the micellar structure provided by the tetrablock copolymer PAA-PS-TTC-PS-PAA is presented.

A.2 QUANTUM DOTS OVERVIEW

The present paragraph has the main function to present general concepts about quantum dots, namely their functionality as luminous materials and their most common polymer-based production methods. With the role of a preparatory explanation, some information about fluorescence will be provided to differentiate the features of inorganic quantum dots and organic dyes. Finally, a more specific paragraph about Cadmium Sulfide quantum dots will be reported.

A.2.1 Basic organic fluorescence concepts

As it has been reported by Sterling Gleason in 1960, "The world of fluorescence is a world of beautiful color. In the darkness, all the ordinary colors of our daylight world disappear. Only the intensely glowing hues of fluorescent substances touched by the ultraviolet beam shine out with striking clarity". The strong passion emerging from this statement transmits the interest that researchers have been feeling towards the field of materials' luminous characteristics. Luminescence is defined as the radiation emitted by a molecule or an atom after the absorption of a certain amount of energy which, in turn, allowed its electrons to reach higher energy levels. Simply speaking, luminescence is the result of the release of energy by electrons when they move from excited high energy levels back to non-excited lower energy ones. Specifically, the main types of luminescence are fluorescence and phosphorescence.

First of all, it is useful to understand what happens when a material is stimulated by a luminous radiation. As asserted by Bernard Valeur in its book "Molecular Fluorescence: Principles and applications" [27], the Perrin-Jablonski diagram, reported in figure 72, is extremely helpful in explaining all the possible phenomena related to luminescence. In particular, the singlet electronic states are identified through the label S_0 (fundamental electronic state) and S_1, S_2, …. S_n (excited electronic states). Moreover, the so-called triplet states are indicated with T_1, T_2…T_n. Even though the present diagram is mostly referred to organic molecules, it is still useful to understand how fluorescence generally occurs in luminous materials. In fact, the first step is always the absorption which is commonly very fast ($\approx 10^{-15}$ s). As observable from figure 8, the vertical arrows, displaying absorption, start from the lowest energy level where the majority of molecules are situated at room temperature. [27]

After the absorption of a photon, molecules undergo an increase in their energy that is visible as a jump towards higher energy levels. Subsequently, different de-excitation processes can be observed.

First, *Internal Conversion* (IC in the previous figure) can occur and it consists of a non-radiative transition involving two electronic states of the same spin multiplicity. When the sample is in its solution state, internal conversion is followed by vibrational relaxation causing the molecule to reach the lowest vibrational level of the current electronic state. Vibrational relaxation always occurs when a molecule is excited to an energy level higher than the lowest one. For example, if the energy state S_1 is considered, the relaxation from the higher energy level towards the 0-vibrational level occurs with a time scale of $10^{-13} - 10^{-11}$s. However, internal conversion from S_1 to S_0 is not efficient and consequently less likely to happen than conversion from S_2 to S_1.
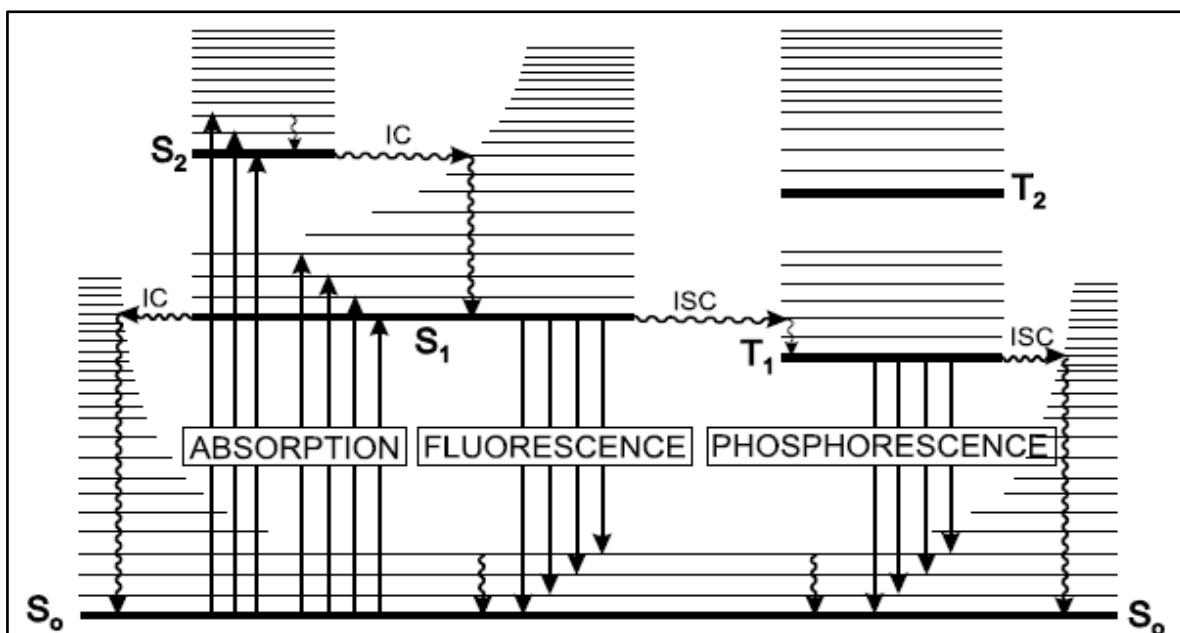
Figure 72 Perrin-Jablonski diagram *[27]*

This is due to the higher energy gap between S_1 and S_0 than between S_2 and S_1. Consequently, while between S_2 and S_1 the most probable event is internal conversion (and vibrational relaxation) internal conversion between S_1 and S_0 is in competition with other two phenomena namely *fluorescence* and *phosphorescence*. As far as fluorescence is concerned, this is defined as the emission of photons associated with the transition of the molecule from S_1 to S_0. What is fundamental to be considered is the Stokes Rule, according to which the emission wavelength related to a fluorescence event is always higher than the absorption wavelength or rather the one that was used to excite the molecule to higher energy levels. In other words, this is a confirmation of the previously explained internal conversion which always competes and accompanies fluorescence, by reducing the energy of the emission radiation. Nevertheless, partial overlaps between absorption and emission spectra have been observed and associated with the presence at room temperature of a small population of molecules in energy levels higher than the zero one. Therefore, at a very low temperature, any deviation from the Stokes rule should be eliminated. Moreover, it must be considered that the time associated to emission is the same as the one associated to absorption ($\approx 10^{-15}$ s). However, excited molecules remain in the S_1 state before the emission of photons for a time varying from a few tens of picoseconds to a few hundreds of nanoseconds. During this time, other phenomena can occur (e.g. internal conversion) which reduce the fluorescence intensity. Specifically, this reduction has an exponential trend and a characteristic time reflecting the average lifetime of the molecules in the S_1 state. [27]

Finally, beside fluorescence, *Intersystem Crossing* can occur, and it consists of a non-radiative transition between two iso-energetic levels belonging to electronic states characterized by different multiplicities. For instance, as visible in figure 72, ISC can involve a molecule passing from the zero-energy level of S_1 to an excited level of T_1. After, vibrational relaxation causes the molecule to reach the lowest energy level belonging to the triplet T_1. If the sample is in solution and at room temperature, a non-radiative event of de-excitation is more likely to occur. On the contrary, when the temperature is lower, or the sample is in its solid state, a radiative emission can be observed. This phenomenon is referred to as *phosphorescence*. [27]

A.2.2 Quantum Dots as fluorescent materials

Quantum dots are tiny particles or nanocrystals of a semiconducting material with diameters in the range of 2-10 nanometers. In fact, they are generally composed of 10-50 atoms. [28] They were first discovered in 1980 and have immediately been considered

as astonishing structures because of their properties, intermediate between those of bulk semiconductors and discrete molecules, due to the high surface-to-volume ratios that characterize them.

Because of their small size, quantum dots present electron confinement in a small space referred to as quantum box. Moreover, when the radius of quantum dots is smaller than the Bohr radius, or rather the average distance between the electron in the conduction band and the hole left in the valence band, quantization of the energy levels can be observed. Figure 73 shows how the aforementioned quantization affects the energy levels, by making them appear different compared to the case of a bulk material. In particular, the continuity characterizing the bulk material's levels disappears. In fact, quantum dots have been nicknamed "artificial atoms" [29] because of their properties relating them more to atoms than to bulk materials.

Another important feature to be considered is the relationship between fluorescence of quantum dots and their dimension. Specifically, as their size decreases, the energy gap present between the lowest conduction band and the highest valence band increases. Consequently, it is possible to assert that the smaller the size, the higher the energy to be provided in order to excite the dot and the energy released during the emission event. Moreover, it is easy to tune the emission wavelength by simply varying the quantum dots dimension. [30] [31]
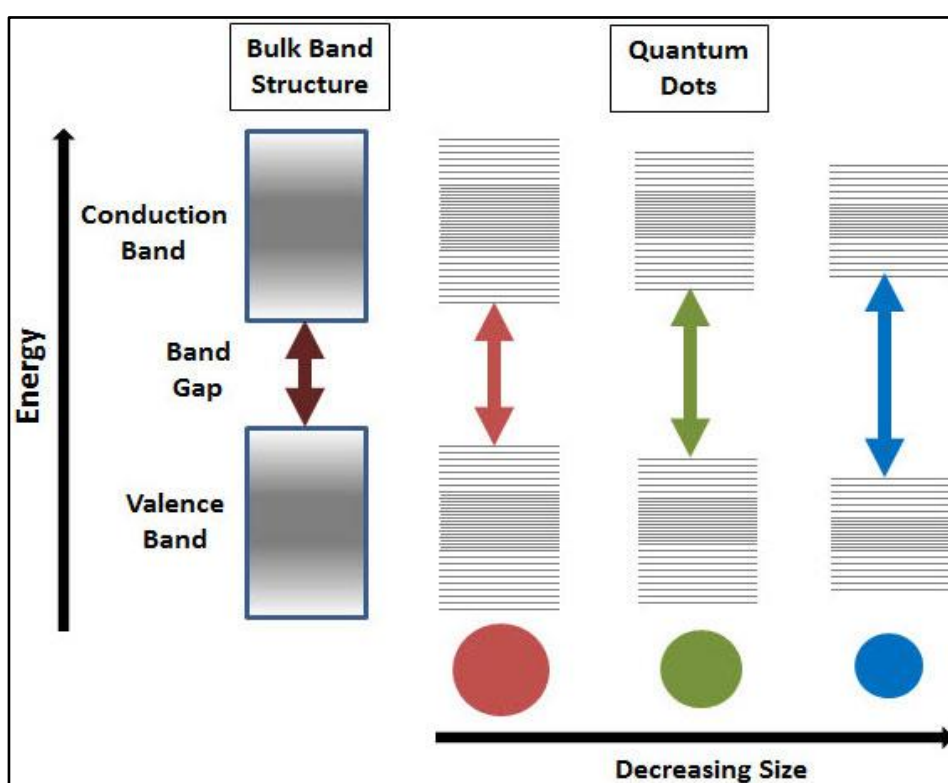
Figure 73 Splitting of energy levels in quantum dots due to the quantum confinement effect and relationship between size and emission wavelength. *[46]*

According to their composition and structure, quantum dots can be classified into three main types. In particular, when they are constituted of a single element and their internal composition is uniform, they are referred to as *Core-Type Quantum Dots*. This first category can be affected by a reduction of fluorescence quantum yield due to non-radiative events. In order to improve the efficiency and brightness of QDs, shells of a different semiconductor characterized by a higher band gap can be grown around the previous dots. The result is a small region of the first material embedded in another one showing a wider band gap and this category is identified with the name of *Core-Shell Quantum Dots*. Finally, it has to be considered that, even though tuning size of QDs has become a crucial step to manipulate and control their properties, this can cause problems in many applications presenting specific size restrictions. Consequently, multi-components quantum dots have been hypothesized as a solution to tune properties without

changing crystallite size. In particular, *alloyed semiconductor quantum dots* with homogeneous or gradient internal structure allow manipulating the properties by simply acting on composition and internal structure without affecting size.

A.2.2.1 Optical Properties of Semiconductor Nanocrystals

With the aim to reach a higher level of detail, the work of Peter Reiss "Synthesis of semiconductor nanocrystals in organic solvents" can be considered here. [32] Specifically, this is the second chapter of the book "Semiconductor Nanocrystal Quantum Dots – Synthesis, Assembly, Spectroscopy and Applications" edited by Andrey L. Rogach. As asserted by Reiss, *absorption* of a photon by a nanocrystal only occurs when its energy is higher than the band gap. A fundamental characteristic to be taken into account is that the position of an absorption peak depends on the band gap and so on the quantum dot's dimension. On the other hand, width and shape of the peaks are determined by the distribution in size and by the form and stoichiometry of the Nano Chrystals (NCs). As a consequence, it can be asserted that if a sample is polydisperse, it only shows a shoulder in the absorption spectrum corresponding to the excitonic transition. Other less pronounced absorption peaks appearing at shorter wavelengths correspond to excited states characterized by higher energy. The extent of polydispersity can be evaluated based upon the resolution of the peaks. In particular, the larger the number of the peaks and the more clearly they are resolved, the smaller the size dispersion of the particles. In figure 74, absorption and normalized photoluminescence spectra of a size series of CdSe NCs are shown. As previously specified, they are shifted according to the Stokes Rule.
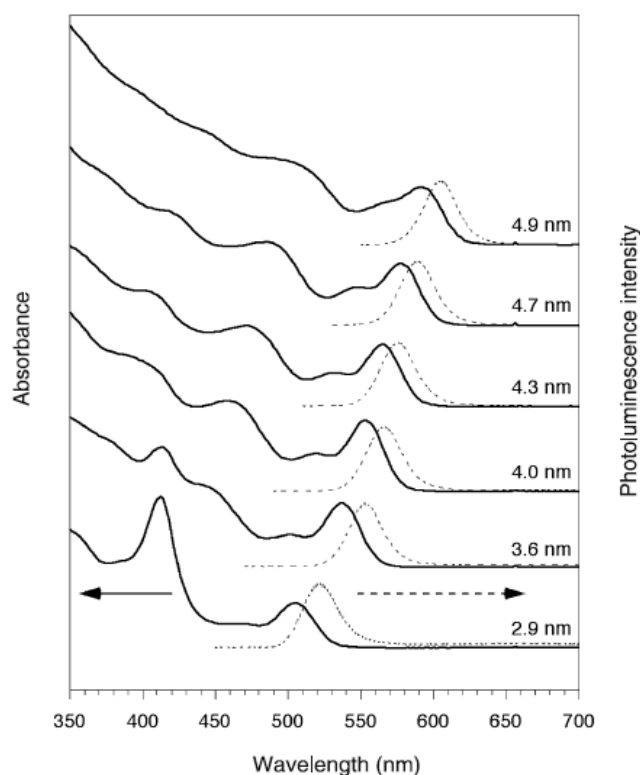
Figure 74 Absorption and normalized photoluminescence spectra of a size series of CdSe NCs *[32]*

As far as *photoluminescence* is concerned, Reiss defines it as "the generation of luminescence through excitation of photons". [32] In particular, as already described for organic materials in paragraph A.2.1, also semiconductor quantum dots present fluorescence and phosphorescence. Specifically, the former is the capability of emitting light at a higher wavelength compared to the absorbed one after the so called "charge carrier relaxation via phonons to the lowest excited state". [32] The interval after which light is emitted is defined as fluorescence lifetime and it is the most representative difference between fluorescence and phosphorescence

which occur otherwise in a similar manner. More precisely, due to its symmetry, the excited state lifetime related to phosphorescence is considerably longer than the one associated to fluorescence. Figure 75 reports the fluorescence phenomenon occurring in a bulk semiconductor. Electrons populating the valence band are excited by a radiation which energy is referred to as $h\nu_e$. This allows them to reach the conduction band as indicated by the red arrow. After the previously mentioned relaxation step via phonons, electrons reach the lowest energy level in the conduction band before jumping back to the valence band with the associated fluorescence emission. This is shown by the green arrow and its energy is $h\nu_f$. As mentioned above, the emitted energy is always less than the absorbed one. In other words, $h\nu_e > h\nu_f$.
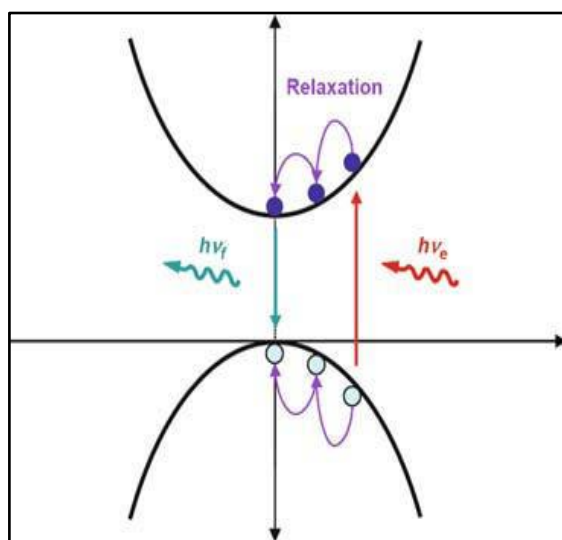
Figure 75 Fluorescence phenomenon in a bulk semiconductor *[32]*

As already explained, what distinguishes a bulk semiconductor from a quantum dot is the typical discretization of the energy levels occurring in the latter. Therefore, the real fluorescence phenomenon happening in a quantum dot is better illustrated by figure 76. Specifically, it shows the exciton states of CdSe QDs involved in absorption and emission processes. [32]

Finally, what Reiss specifies is that efficient room temperature band edge emission can only be observed when NCs are characterized by a proper surface passivation. On the contrary, charge carriers can be trapped in surface states increasing the amount of non-radiative recombination and reducing the radiative emission which is object of experimental observation. In order to properly understand the current point, it is useful to introduce the concept of *blinking phenomenon* and *fluorescence quantum yield*. As far as the first is concerned, it has been observed that when single semiconductor NCs are excited by a continuous radiation, their emission is intermittent.
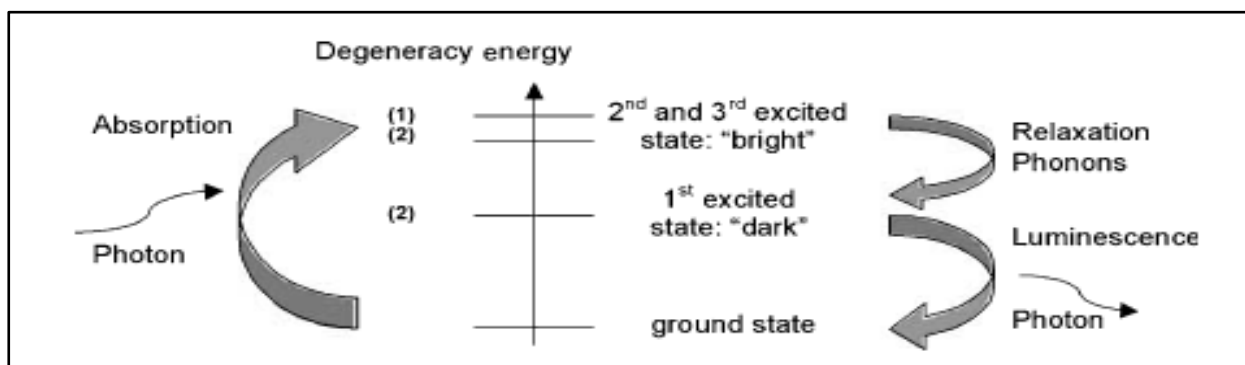
Figure 76 Exciton states of CdSe NCs involved in absorption and emission processes *[32]*

In other words, "on" and "off" periods occur resembling a random telegraph signal. [32] Even though a clear understanding of this phenomenon has not been achieved yet, it has been observed that it affects the final fluorescence quantum yield. In fact, this is defined as the ratio between the number of absorbed and emitted photons. Consequently, it is easy to understand that a value of 1 is hardly achievable because some NCs are in the "off" state. Moreover, as previously asserted, a scarce surface passivation can cause the presence of surface trap states increasing non-radiative phenomena and reducing the resulting fluorescence quantum yield. In conclusion, in order to have a good quantum yield, it is highly desirable to provide a surface passivation which is produced, for instance, by capping the NCs with appropriate ligands. This topic will be subsequently analyzed when a specific case involving CdS QDs will be considered.

A.2.3 Semiconductor NCs – polymer composites

Due to their unique size-dependent photoluminescence properties, semiconductor nanocrystals (NCs) or rather quantum dots (QDs) have been highly investigated and identified as one of the best candidate to develop the field of optics, electronics and biomedicine. However, a strong tendency to agglomerate has been observed. Specifically, this is due to the high surface to volume ratio which causes the highly active surface atoms to considerably alter and deteriorate the physicochemical properties. Consequently, a smart functionalization of quantum dots has been considered as a key point to ensure stabilization and specific desired properties. Among all methods developed up to now to provide a good stabilization, Dayan Wang focused mainly on those based upon the use of polymers. [33] Even though other procedures using alkanes or silica have been object of an intense study, they are beyond the target of the present work. On the contrary, a list of the most diffused polymer-based methods will be provided here.

First and foremost, what Wang clarifies is that NCs stability is determined by a thermodynamic balance between repulsive and attractive interaction. In particular, the former is mainly electrostatic or steric, while the latter is basically represented by van der Waals or hydrophobic interactions. In order to form stable NCs, it is necessary to have repulsive interactions stronger than attractive ones so that the particles can be kept apart. Since electrostatic repulsion has been observed to be particularly sensitive to the size of NCs and to the different surrounding media, steric repulsion has been identified as the best stabilization medium. [33] Specifically, polymers are able to provide an excellent steric hindrance and to impart NCs with a good resistance against environmental variation. Moreover, NCs can inherit the good compatibility, the outstanding processability and the engineering performance typical of polymers. [33] Therefore, stabilization based upon steric hindrance mediated by the use of polymers has been highly investigated and different realization procedures have been hypothesized. In order to summarize them, it is useful to consider the classification reported by Wang who asserts that all synthesis methods can be classified into two categories or rather *chemical synthesis* and *physical blending*.

A.2.3.1 Chemical synthesis of quantum dots – polymer composites

Two main approaches can be distinguished which belong to the current category. In particular, the first one is characterized by the synthesis of quantum dots in the presence of already produced polymers. Oppositely, the second one is based upon the polymerization in presence of quantum dots. Finally, another category can be individuated which is substantially a combination of the previous ones.

Synthesis of QDs in the presence of polymers

This production method is characterized by an ancient tradition and was already used by pigment industries which had the necessity to incorporate ZnO or Fe_2O_3 into polymers. A typical preparation procedure involves the use of organometallic precursors of QDs

that are inserted into polymer matrices in different ways, namely simple mixing, polymerization of monomers in presence of precursors or copolymerization of monomers and precursors if the latter has the capability to polymerize. The obtained mixture is subsequently exposed to chalcogenide solution or gas. The key role is played by the polymer matrices which prevents the infinite crystal growth allowing to form nanometer-sized crystals of semiconductors and yielding a QD-polymer composite. [33]. An example of the described method has been reported by Yang et at. who synthesized new types of monomers and cross-linkers constituted by methacrylate holding Pb, Zn, or Cd. Specifically, atom transfer radical polymerization (ATRP) has been applied to copolymerize the Pb-containing monomers and cross-linkers. Later, the obtained films have been exposed to H$_2$S gas in order to generate PbS NCs embedded within polymer thin films. Figure 77 shows the structure of the resulting film made of polymer and PbS NCs. [34]
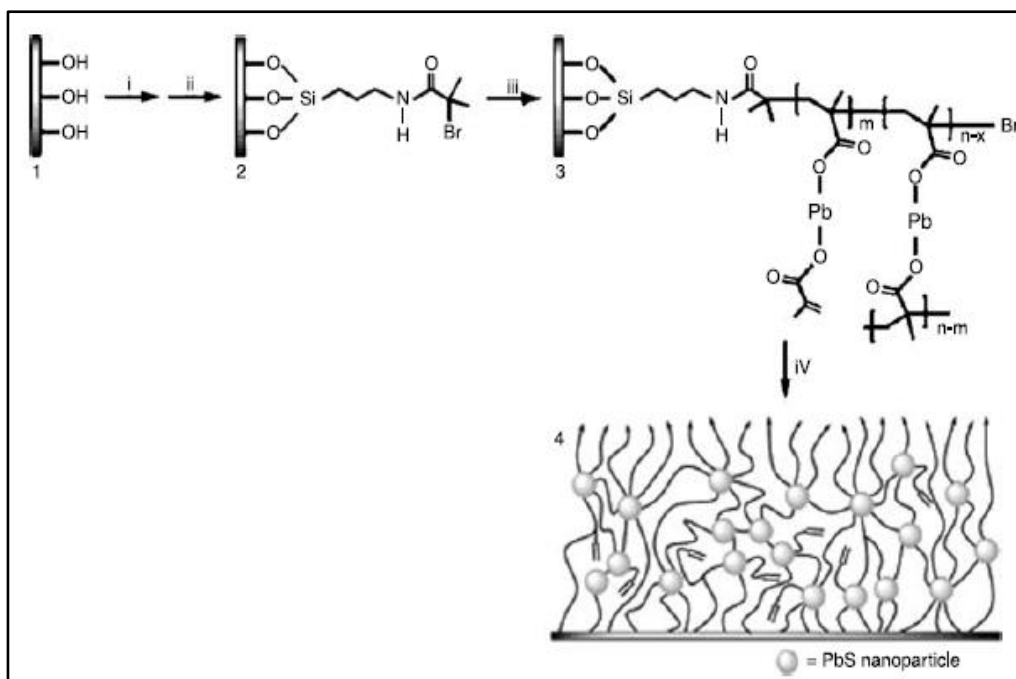
Figure 77 Preparation procedure of PbS NC - polymer composites on a silicon wafer by ATRP of Pb-containing monomers followed by exposition to H$_2$S. The following conditions have been applied: (i) 3-aminopropyltriethoxysilane, toluene; (ii) 2-bromo 2-methylpropionic acid, DCC, DMAP, CH2Cl2; (iii) lead dimethacrylate, p-toluenesulfonyl chloride, Cu(I)Cl, 2,20-bipyridine, DMF; (iv) H2S gas [34]

Polymerization in the presence of QDs

The opposite approach involves the polymerization of monomers in the presence of an already created NC. First and foremost, it is important to underline that NCs can be divided into two categories according to the synthesis environment. Specifically, they can be organic or aqueous. As far as the former is concerned, they are typically prepared by pyrolysis of organometallic precursors in hot organic coordinative solvents followed by capping by ligands with long alkyl chains such as trioctylphosphine oxide (TOPO). About aqueous NCs, instead, the neutralization of metallic ions and chalcogenides in the presence of mercapto-ligands is applied. The matter of surface wettability is managed by using amphiphilic molecules which are eventually able to turn the surface character from hydrophilic to hydrophobic or vice versa. Moreover, the important issue involving NCs – Polymer compatibility has to be taken into account when considering the current method. Firstly, the agglomeration of semiconductor NCs is very likely to occur and it causes an evident quenching of their photoluminescence. Therefore, with the aim to avoid this phenomenon, semiconductor NCs should be dispersed in monomers with which a better compatibility is easily achievable. In addition, it is advisable to cap semiconductor NCs with polymerizable ligands which can create a strong coupling with polymer matrices. Finally, even though the considered procedure can be promising in realizing sculptures of semiconductor NC – polymer composites into microspheres, which

would be extremely interesting and useful as markers for biological detection, a serious drawback has to be mentioned. In particular, free radicals often quench the photoluminescence of the NCs reducing the optical properties of the composite. [33]

Grafting polymers on semiconductor NCs

The previous categories of chemical synthesis are able to produce semiconductor NC – polymer composites which are typically in the form of bulky blocks, thin films and fibers. Nonetheless, they are not able to define and control the separation distance between NCs with a resulting poor control over their interaction and therefore a decrease of their collective properties. In order to overcome this problem, the production of polymer shells with defined and controllable thickness has been applied around NCs. Specifically, this can be performed by coating NCs with polymers (i.e. Grafting-to strategy) or by growing polymer brushes from NCs (i.e. Grafting-from strategy). [33]

As far as organic semiconductor NCs are concerned, *Grafting-to strategy* has the objective to encapsulate them by copolymer through the hydrophobic interaction occurring between polymer and the alkyl chain surrounding the organic semiconductor NCs. Specifically, an intense study has been conducted on encapsulating organic NCs into the hydrophobic cores of block copolymer micelles. In fact, this allows an efficient phase transfer of organic NCs into aqueous media with a promising potential applicability in biomedicine. Following the strategy of a simple mix of hydrophobic NCs with copolymer in a common solvent followed by its evaporation, Dubertret et al. have been able to insert a ZnS-overcoated CdSe NC into the hydrophobic core of micelles constituted of PEG, phosphatidylethanolamine, and phosphatidylcholine. Figure 78 shows a schematic illustration of the applied procedure where it is possible to distinguish solvent evaporation and water addition to end with the formation of the quantum dot containing - micelle. [33] [35]
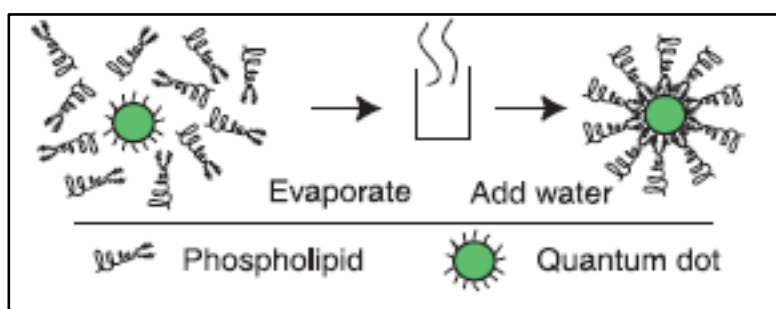
Figure 78 Schematic illustration of QD encapsulation into the micelle core *[35]*

Moreover, it has to be mentioned that grafting-to strategy has been applied to coat aqueous semiconductor NCs with polymers. Unlike organic NCs, aqueous NCs are usually negatively or positively charged because of protonation or deprotonation of the capping ligand. For example, Yang et al. reported a study in which they were able to coat negatively charged CdTe NCs with positively charged polymers through electrostatic interactions. [33]

A number of advantages related to grafting-to strategy can be listed. First of all, it is possible to modify NC solubility without damaging the layer of ligands around it. This results in a good preservation of NC photoluminescence. Moreover, the hydrophobic intermediate layer of block-copolymer guarantees a good hydrophobic barrier preventing NCs from attacks coming from the surrounding aqueous medium. This provides an excellent resistance against, for instance, acid. In addition, it is easy to add many different functionalities into the block-copolymer coating without deteriorating the NC. Finally, it is simple to encapsulate different NCs into polymer capsules resulting in multifunctional biological labels. However, the most important drawback is the limited capability to ensure the encapsulation of exactly one NC per micelle. [33]

The second category of grafting techniques is referred to as *Grafting-from strategy*. This has been developed because it was clear that agglomeration of NCs could have been reduced by growing polymers directly from NCs. In addition, to implement the current technique it is simple to cap NCs with polymerizable ligands, e.g. vinyl groups, following by polymerization carried out by initiators. Moreover, a complementary strategy of grafting polymer brushes has been studied. In particular, this is a surface-initiated polymerization by capping initiators on NCs and it was encouraged by the development of living radical polymerization techniques among which RAFT played a key role. Different groups reported studies on grafting-from strategies via surface-initiated living polymerization [36] and the most important drawback that was individuated comes from the maximal grafting density that is possible to obtain around a NC. In fact, due to this maximal grafting density, polymer brushes are forced to adopt a stretched conformation resulting in an alteration of their physicochemical properties. For instance, the stimuli-response behavior observable in certain polymers in their state of free polymer chains can be suppressed. [33]

A.2.3.2 Physical synthesis of quantum dots – polymer composites

A different approach with respect to the previous one is the physical confinement of semiconductor NCs in polymers. As asserted by Wang "incorporation of as-prepared NCs into polymer matrices should be the most straightforward way especially for the large-scale industrial use". [33] In fact, a physical blending of polymer and NCs is easily realizable as long as there is a good compatibility between these two components. This is ensured by capping semiconductor NCs obtained from pyrolysis of organometallic precursors with hydrophobic alkyl chains. However, in order to obtain a better structural stability of semiconductor NC – polymer composites further interactions between NCs and the polymer host matrices may be required. These are, for instance, electrostatic interaction or even covalent bonding.

An intense study has been conducted on physical synthesis of NCs – polymer composites to realize high performance LEDs. For instance, spin-coating has been applied to create thin films with tunable electroluminescence and photoluminescence arising from variation of size of NCs and molecular weight of the conjugated polymer. A key point was represented by the realization of a good transferring of electrons across the NC/polymer interface. This can be realized if a good compatibility between NCs and polymer matrices is ensured. In turn, a good compatibility derives from the alkyl capping of the NCs which guarantees a good interaction with the polymer matrices. On the contrary, the removal of the surface-capping ligands of semiconductor NCs usually brings to a phase separation of NCs and polymer. In most cases this is negative because it prevents the realization of homogeneous and transparent composites for optical applications. However, Greenham et al. reported a case in which a phase separation was rather advisable. In fact, they observed that the removal of TOPO capping from the surface of NCs, e.g. CdSe or CdS, enforced the segregation from MEH-PPV. In turn, this created a large interface for charge separation and provided a way for electrons and holes to travel towards the appropriate electrode without being recombined. Moreover, by removing the TOPO, the photoluminescence of the MEH-PPV was quenched and, consequently, the quantum efficiency of the semiconductor NC – polymer composites improved. Figure 79 shows a schematic illustration of MEH-PPV/NC composites with (a) and without (b) TOPO capping ligand. [33] [37]

Finally, other physical methods to produce semiconductor NCs – polymer composites have been investigated which will not be covered in the present work. Specifically, they are the so-called Layer-by-layer assembly which has been reported to be applicable to both planar and curved substrates, and the use of solid or hollow microspheres to encapsulate as-prepared NCs. Instead, a method combining physical blending and chemical reactions, involving the in-situ production of QDs inside polymer micelles, has been used to conduct the present thesis work and is presented in Chapter 2.
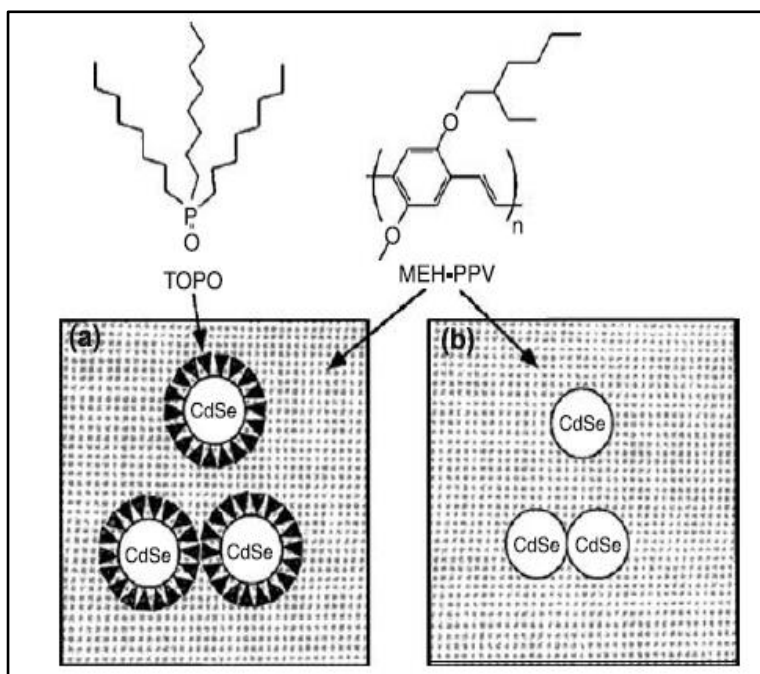
Figure 79 Schematic illustration of MEH-PPV/NC composites with (a) and without (b) TOPO
capping ligand *[33]*

A.2.4 A specific case: CdS QDs

The present paragraph has the main objective to introduce the specific case of CdS quantum dots which have been employed in the current thesis work. Specifically, a short analysis involving the issue introduced in paragraph A.2.2.1 about surface trap state will be conducted.

The uniqueness of these quantum dots arises from their size dependent optical and electronic properties and flexible processability. In turn, their size can effectively be tuned by changing the utilized synthesis conditions. Typical CdS quantum dots are inorganic semiconductors characterized by an outer surface coating of organic ligands to reduce charge recombination and quantum yield reduction. Moreover, these ligands provide stability, solubility, and processability in solution. Unlike organic dyes, quantum dots present a broad absorption with finite emission positions. As a consequence, quantum dots can be excited over a broad range while emitting at a finite position, yielding true color emission. The emission potential of the quantum dots strongly depends on the quality and size distribution of the nanocrystals in solution.

As reported by Tachibana et al. [38] quantum dots surface modification is very likely to create surface or interfacial trap states that bring to a reduction in the number of exciton states or energy due to non-radiative charge recombination. With the aim to avoid these trap states a common and diffused procedure is coating QDs by a ligand or a shell. However, even though thicker shells have been observed to improve photoluminescence quantum yields, they can also isolate a core exciton state. Consequently, the interaction between an exciton state and other materials which receive an electron or hole from the core state results to be decreased. In their study, Tachibana et al. tried to investigate the origin of trap state emission. Specifically, their main objective was to clarify the relationship between CdS QDs surface structure and trap state photoluminescence. Moreover, they have been able to investigate size dependent photoluminescence with comparison between exciton and trap states.

The quantum dots used for their study [38] have been obtained by a non-injection method yielding sizes of < 3.2 nm by setting the heating temperature between 90° and 210°. On the contrary, sizes > 3.3 nm have been obtained by adding the same amount of precursors without purification and by using a temperature in the range 210° - 250°. As a confirmation of the previously explained

"quantum size effect" which relates size and exciton peak position, Tachibana and his group observed that as the QD size increases, the first exciton peak shifts to longer wavelengths, namely towards the red color emission. Accordingly, figure 80 reports the absorption spectra of CdS quantum dots with different diameters ranging from 1.4 to 4.3 nm where it is possible to observe that the bigger the QD, the longer the emission wavelength.
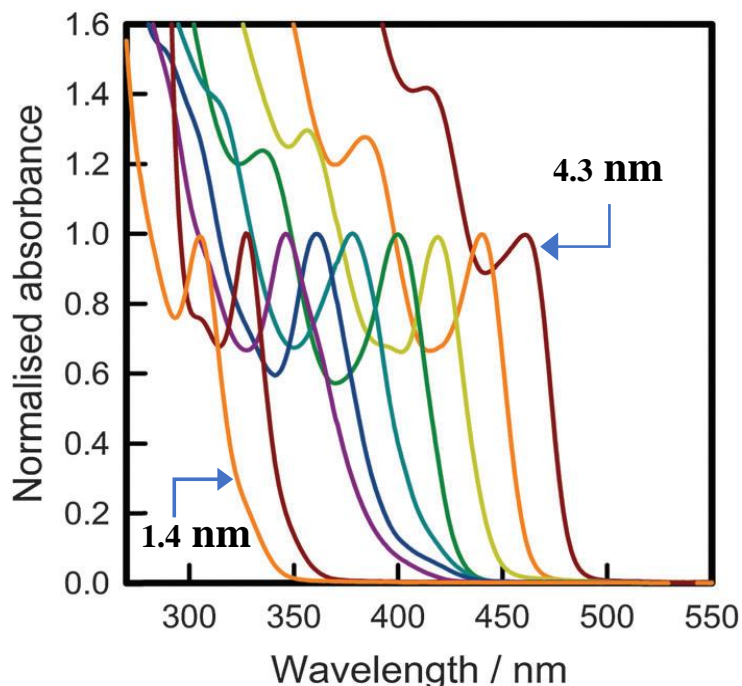

Figure 80 Absorption spectra of CdS QDs with different diameters *[38]*

The optical characterization performed on the previous quantum dots is reported in figure 81. In particular, it is possible to see the absorption spectra in black and the emission spectra in red for four different quantum dots sizes from 3.1 nm to 4.3 nm. As far as the emission spectra are concerned, they provided a very interesting result. In fact, two different peaks have been resolved. The higher energy narrow band has been associated with band edge emission and it is indicated by the green spotted line, while the lower energy broad band derives from trap states and it is pointed out by the blue line. As it is easy to notice, as the QD size increases, the trap state emission intensity decreases, while the band edge emission increases. This observation was used by Tachibana et al. to conclude that trap state emission increases with the increase of the surface area per unit volume or rather with the surface area to volume ratio. In turn, this means that trap states mainly originate from surface states when the surface is not well passivated.

In addition, time-resolved photoluminescence decays have been observed and the main result was that as the QD size increases, the photoluminescence lifetime increases as well. More specifically, two decay components have been individuated, namely τ_F or rather faster decay component, and τ_S or rather slower decay component. Interestingly, they observed that the faster decay component dominates for larger QDs, while the slower one is dominant for smaller QDs.

In order to relate the QD surface structure with the origin of trap states, Tachibana e al. performed XPS measurements and realized that a larger amount of Cd atoms was present in a quantum dot compared to S atoms. Consequently, all prepared QDs had a surface enriched in Cd and experiments about binding energy revealed the existence of surface Cd with sulfur vacancy. Moreover, the ratio of Cd with sulfur vacancy i.e. Cd_{SV} to total Cd atoms becomes bigger with the decrease of the QD radius. Therefore, by considering that the smaller the QD the more significant the trap state emission, and the bigger the ratio Cd_{SV}/Cd , Tachibana and his group concluded that trap state emission can be attributed to "surface trapped electrons at the surface Cd with sulfur vacancies". [38]
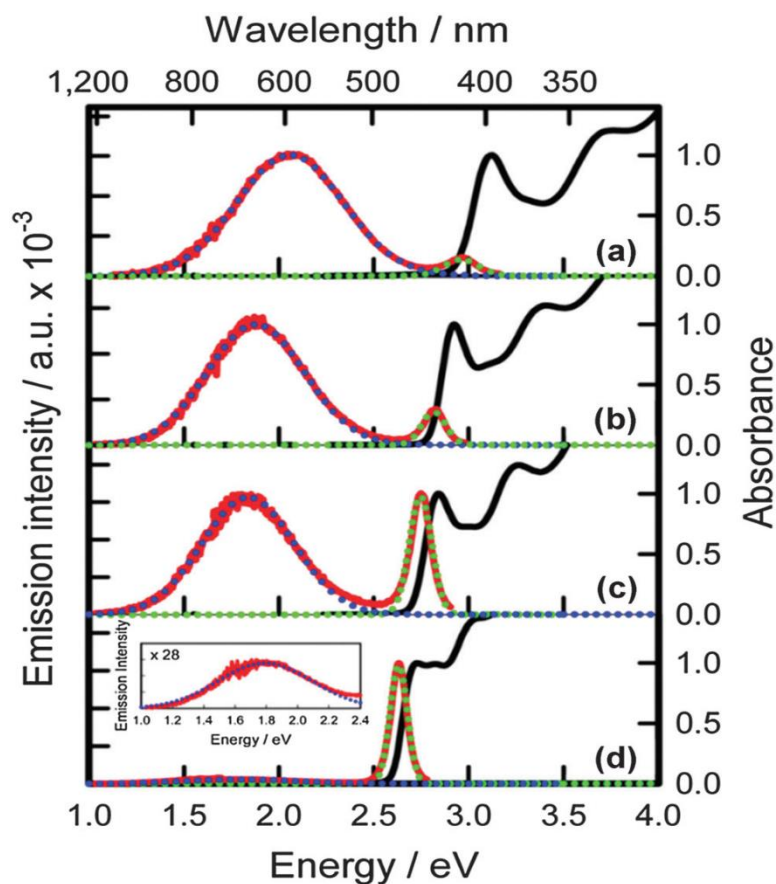
Figure 81 Absorption and emission spectra of CdS QDs with diameter ranging from 3.1 to 4.3 nm *[38]*

A.3 GOLD NANOPARTICLES OVERVIEW

This short paragraph has the main objective of presenting the fundamental features of gold nanoparticles. Specifically, general information will be provided followed by a distinction between water and organic solvent based nanoparticles. Finally, some considerations about optical properties will be reported.

A.3.1 Gold nanoparticles basic concepts

Gold nanoparticles (GNPs) have been discovered and used since a long time ago. In fact, the first example of their application dates back to the 4th century when the famous Lycurgus Cup was manufactured. This interesting object owes its fame to its amazing characteristics due to the presence of gold nanoparticles imparting to the cup the ability to change color depending on the location of the light source. As it often appears in literature, gold nanoparticles are commonly defined as colloidal gold. This name refers to a colloidal suspension of nanoparticles in water or in an organic solvent. Nowadays, GNPs represent a very up-to-date topic and have been intensively investigated as an innovative material to be used in different applications, namely electronics, optics and electromagnetics. The relation existing between GNPs size and their absorption spectra has been studied together with resonance Rayleigh scattering and resonance non-linear scattering. [39] The properties observed in colloidal gold nanoparticles, and thus their applications, strongly depend on their size and shape. In turn, size and shape can be tuned and controlled during the synthesis procedure.

A.3.2 Gold nanoparticles synthesis methods

Different procedures have been developed to produce gold nanoparticles. The common point to them all is the presence of a solvent in which they are dispersed so that gold nanoparticles usually appear as a solution which color varies according to the particles dimension and the type of solvent. Generally speaking, all the liquid chemical methods, i.e. those methods implying a liquid to synthesize the particles, are based upon the reduction of chloroauric acid (H[AuCl$_4$]). Specifically, the typical procedure is characterized by dissolution of chloroauric acid, vigorous stirring and addition of a reducing agent. The first reaction occurring is the reduction of Au^{3+} to Au$^+$. After, a disproportionation reaction occurs according to which 3Au$^+$ give origin to Au^{3+} and 2Au^0 and the letter works as a center of nucleation for the further reduction of gold. A fundamental step is the addition of a stabilizing agent which plays a crucial role in avoiding the GNPs aggregation. This agent can vary according to the adopted method as it will be illustrated below. [40] Even though numerous synthesis methods can be found in literature, this chapter is only devoted to present two of them. Specifically, the Turkevich method and the Burst method, respectively using water and toluene as solvents will be briefly reported because important for the present thesis work.

Turkevich synthesis method

Pioneered by J. Turkevich et al. in 1951 and refined by G. Frens in the 1970s, this is considered as the simplest available method and a very versatile one. It allows to produce GNPs dispersed in water with diameters generally around 10-20 nm even if bigger particles are also realizable. The achievable monodispersity is generally good but it decreases as the particle size increases. [40] . The synthesis procedure involves the reaction of small amounts of hot chloroauric acid with small amounts of sodium citrate solution which covers the role of both a reducing agent and a capping agent. In particular, a capping agent is used to stop particle growth and aggregation. In order to do so, it must have a high affinity with the new nuclei so that it will bind to them by reducing their surface energy and preventing them from aggregate with other nuclei. [40] As previously asserted, the Turkevich method is provided with a very good versatility. In fact, it is possible to change the dimension of the produced NPs by simply varying the amount of added sodium citrate solution. For instance, as reported by G. Frens, it was possible to produce GNPs with diameters varying from 16 nm to 150 nm by varying the concentration of sodium citrate during the nucleation of the particles. [14] As far as the practical series of steps is concerned, the two solutions of H[AuCl$_4$] and Na-citrate have to be prepared. Subsequently, the former is brought until its boiling point and the latter is added. During the next 25 seconds, the solution turns into blue because of nucleation occurs and after 70 s the color becomes red because of the formation of monodisperse spherical particles. As it is reported, after 5 minutes, neither further addition of citrate nor more heating is useful to produce any substantial change. As said above, to vary the dimension of the GNPs, it is sufficient to modify the amount of sodium citrate. However, it has been said that when the levels of citrate are kept low to generate big NPs, the results are less reproducible, and the reaction demands for longer times to be completed (i.e. 30 minutes).

Burst synthesis method

This is specifically the method that was mainly applied during this thesis work. Therefore, what it is reported here is simply an introduction to the method that is better explained and analyzed in chapter 2. This synthesis procedure was discovered by Brust and Schiffrin in the early 1990s and can be used to produce gold nanoparticles in organic solvents that are normally immiscible with water (e.g. toluene). The raw material is the same as for the previous method, or rather chloroauric acid. However, in this case, this is mixed with tetraoctylammonium bromide (TOAB or TOABr) and with sodium borohydride (NaBH$_4$), in the role of phase transfer catalyst and reducing agent respectively. Sometimes TOABr is also used as a stabilizing (i.e. anticoagulant) agent. However, its binding with GNPs is not particularly strong resulting in the aggregation of GNPs over the course of about two weeks after the

synthesis. In order to avoid this phenomenon, other stabilizing agents can be utilized like a thiol which ensures a good interaction with GNPs and allows for a longer durability. For instance, dodecanethiol is often utilized. [40]

Figure 82 shows a series of steps typical of this synthesis method. By following the round path, it is easy to see that the first step is the mixing of water solution of chloroauric acid with TOAB dissolved in toluene. A stirring of two hours allows for the phase separation and the gold chloride is moved into the organic phase. After water phase discard, a solution of NaBH$_4$ in water is added which acts as reducing agent bringing to the formation of nanoparticles. As said above, dodecanethiol would be useful as a stabilizing agent and, in fact, it has been used for the current thesis work. [41]
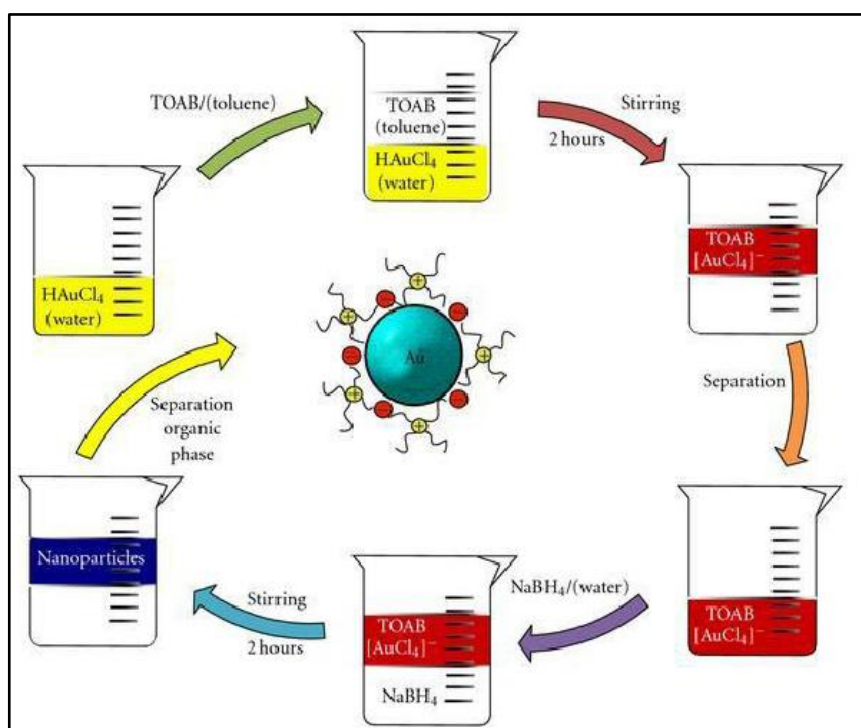
Figure 82 Schematic of Burst synthesis method [41]

The GNPs usually produced by this method present a smaller dimension compared to the Turkevich method. Specifically, the diameters are around 5-6 nm or even smaller. However, a lower level of control on the resulting dimensions is achievable.

A.3.3 Gold nanoparticles optical properties

The interest devoted to GNPs mainly arises from their interaction with visible light. In fact, they are known to absorb and scatter light with a good efficiency. Because of their unique optoelectronic properties, GNPs have been object of an intense research and "have been utilized in high technology applications such as organic photovoltaics, sensory probes, therapeutic agents, drug delivery in biological and medical applications, electronic conductors and catalysis". [42]

The factors influencing gold nanoparticles' interaction with light are mainly the environment around them and their size and physical dimension. Specifically, the main responsible for the mentioned interaction are the conduction electrons situated on the surface of the nanoparticle. In fact, when a light ray propagating near a colloidal NP interacts with these electrons it follows a mutual oscillation of electron charge in resonance with the visible light. This resonant oscillation is referred to as **localized surface plasmon resonance**

(LSPR) and it is the cause for the typical coloration characterizing GNPs. Moreover, the observable color depends on the absorbed wavelength and, consequently, on the reflected one. Specifically, if the GNPs are small (e.g. 30 nm) and monodisperse, the absorption caused by the LSPR is in the range of blue-green color (i.e. 450 nm). As a result, the observable color will correspond to the reflected wavelength or rather the red one (i.e. 700 nm). On the contrary, when the considered particle size increases, the absorption wavelength is red-shifted and the reflected light or rather the color of the solution results to be blue – purple. Figure 83 shows different colors of gold NPs solutions arising from different diameters. [42]

Figure 83 Typical colors displayed by GNPs with increasing diameters *[42]*

Furthermore, if the particle diameter is increased beyond, the absorption wavelength moves towards the IR region and the resulting color turns to be clear or translucent.

As already mentioned for QDs, stabilization is a crucial matter for metal NPs as well. In fact, because of their high surface to volume ratio and their consequent high activity, the tendency to form aggregates is extremely high. Therefore, in order to avoid aggregation, different strategies have been studied. For instance, the use of polymers or small molecules is highly diffused and guaranteed by the versatile surface chemistry of GNPs. The effect of aggregation of GNPs is similar to the one due to the increase of their diameter. Therefore, as previously described, whenever aggregation is not prevented, the resulting color is likely to turn to clear or translucent. This phenomenon is observed, for instance, when excess salt is added to the solution. In fact, the added salt causes the surface charge of the GNPs to become neutral enhancing the aggregation effect. [42]

A fundamental word related to GNPs is **Scattering.** In fact, as it was previously introduced, gold nanoparticles present a very high efficiency in scattering the incoming radiation. Actually, the previous concept of localized surface plasmon resonance is strictly related to the scattering phenomenon. In order to understand this last point, a brief description of the scattering event has to be provided.

The best example of everyday life scattering phenomenon is observable when a light ray crosses a dark room where some dust particles are dispersed in the air. In fact, the immediate effect is an evident brightness of the mentioned particles which become visible by naked eye. In reality, not the real particles can be distinguished, but rather the light that is scattered by them. As reported by Paul C. Hiemenz and Raj Rajagopalan [26] particles interact with the light striking them and deflect some of this light from the original direction. The resulting light is defined as "scattered". Many are the parameter influencing the intensity of scattered light, namely the wavelength of the incident light, the shape and size of the scattering particles, the optical properties of the scatterers and finally the observation angle. [26] Figure 84 shows a schematic of the scattering phenomenon.

The nature of the scattered light has to be looked for in the interaction between an electric field and a charge which is allowed to move with the field. In fact, when the charge interacts with the field, it experiences a force which accelerates it. In particular, if the field is oscillating, as it is in a light radiation, the acceleration experienced by the charge will be oscillating as well. As classical electromagnetism dictates, when a charge is accelerated, the emission of a radiation occurs, and this is referred to as scattered light. In addition, another point needs to be clarified. In fact, when the charge is put under oscillation by the action of the field, a dipole moment μ is induced which is useful to explain why the scattered light is emitted in every direction. If a substance is isotropic, the

induced dipole moment and the field are simply related by the polarizability which is a measure of how likely a charge separation occurs.
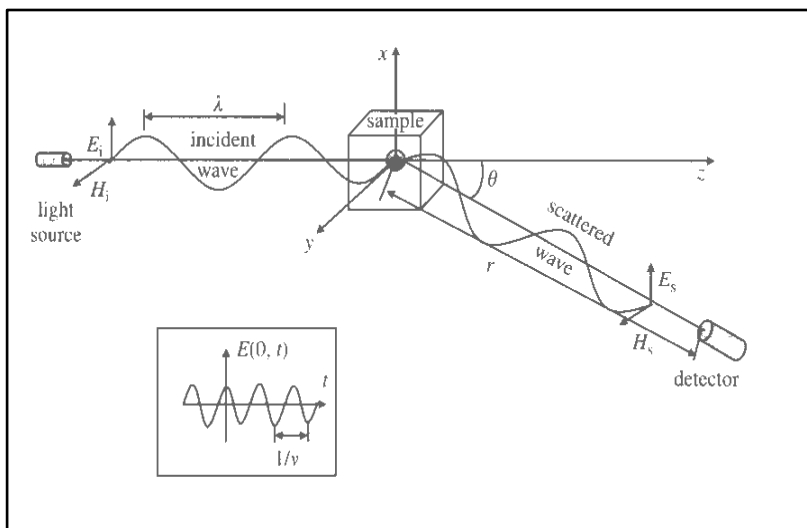
Figure 84 Schematic of scattering phenomenon *[26]*

The mentioned relation is expressed by the following formula where α is the polarizability and E_0 the electric field. [26]

$$\mu = \alpha E_0$$

Different scattering theories have been formulated according to the scatterers' dimensions. Specifically, the so-called Rayleigh scattering theory is the one applied to small particles. More precisely, this is applied whenever the diameter of the scattering center is less than $\lambda/20$, where λ stands for the wavelength of the incoming radiation. Oppositely, when the diameter increases and eventually reaches a value of $\lambda/4$, the Debye theory is applied. Finally, if the diameter further increases, the Mie theory best fits the case.

Figure 85 Different scattering theories according to diameter dimension *[26]*

Figure 85 shows how the light is scattered in the three cases. In particular, the most important condition for the current thesis work is the Rayleigh one. In fact, GNPs are small enough to belong to this category. As it is observable, in this case light is scattered isotropically. [26]
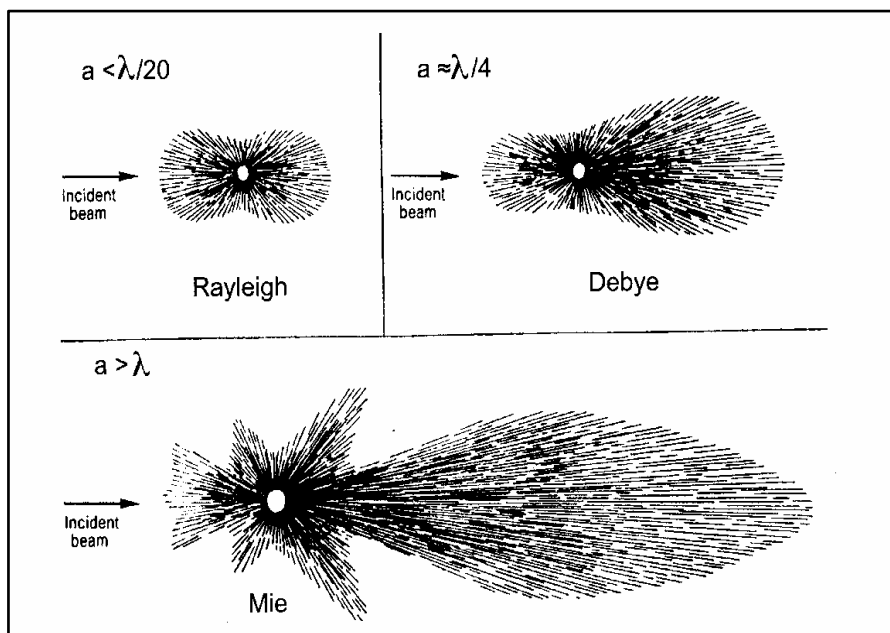
To conclude this paragraph, the interesting study by Shao Pu Liu is worth being mentioned. [39] What they investigated was the relation between GNPs dimension and the resulting absorption spectra. Moreover, the absorption was also studied in relation with the concentration of gold. Finally, resonance Rayleigh scattering (RRS) and resonance non-linear scattering like second order scattering (SOS) and frequency-doubling scattering (FDS), have been analyzed and their relationship with gold concentration and dimension investigated. First of all, the previously introduced sodium citrate reduction method was applied to realize GNPs with different diameters. Specifically, the reported dimensions are 12, 19, 24, 33 and 41 nm. Such nanoparticles have been utilized to study the variation of the absorption peaks position according to the NPs dimension. Specifically, as the diameter increases from 12 to 41 nm, the absorption peak (i.e. λ_{max}) is observed to shift from 520 nm to 530 nm. Therefore, as introduced above, the absorption peaks shift red when the diameter of GNPs is increased. Moreover, when the size of gold is constant, the observed absorption results to be proportional to the concentration of gold. In figure 86 the different absorption spectra for the increasing diameters can be observed. [39]
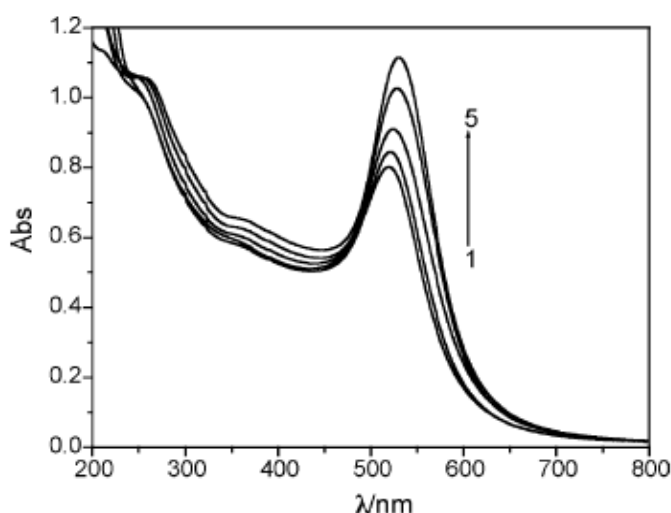

Figure 86 Absorption spectra of gold nanoparticles: (1) 12 nm; (2) 19 nm; (3) 24 nm; (4) 33 nm; (5) 41 nm [39]

As far as the scattering investigation is concerned, what Shao Pu Liu et al. observed was that the scattering peaks of RRS, SOS and FDS, do not change their position according to the particle diameter and are situated respectively at 286 nm, 480 nm and 310 nm. However, their intensity increases linearly with the diameters of gold nanoparticles when their concentration is kept constant. On the other hand, when the particle diameter is constant, the three scattering intensities result to be directly proportional to the concentration of gold nanoparticles.

An important consideration to be done is that particles' dimension varies between 12 and 41 nm and so it is clearly much less than the incident wavelength. Consequently, the main scattering phenomenon occurring is Rayleigh scattering. Moreover, since GNPs present a second absorption peak at 300 nm and the scattering is located near this absorption band, Rayleigh scattering undergoes resonation with absorption light and the result is a resonance enhanced Rayleigh scattering, or rather RRS.

A.4 INTERACTIONS BETWEEN FLUORESCENT QDs and MNPs

As it was anticipated in the paragraph introducing the scope of the current thesis work, the interaction between fluorescent QDs and GNPs represents the heart and the most interesting point of this research. Specifically, the role of distance between QDs and GNPs,

arising from a different added amount of gold, will be considered. In order to properly understand the conducted research, the following paragraph is useful to explain the state of the art about interaction between QDs and plasmonic component (i.e. GNPs). In particular, a general introduction about the main events occurring between metal NPs and fluorescent components will be reported followed by a short reference to an energy transfer experiment and a quick review about studies in solution. Finally, some examples of solid layers of a hybrid material composed of QDs and GNPs, similar to the one produced for the current thesis work, will be presented.

Before the specific analysis of effective events occurring when QDs and MNPs are approached, it is useful to broach a general background. In fact, when analyzing the proximity of the mentioned components three main events are likely to occur and need to be considered. First of all, as introduced in the previous paragraph about GNPs, **scattering** is always present when they are stimulated by an incoming radiation. This is a fundamental point as far as the experimental section of this thesis is concerned. In fact, as it will be better explained later, when the emission of a hybrid material composed of QDs and MNPs is measured, it is crucial to consider that MNPs are actually scattering light and it is necessary to find a way to distinguish the scattered light from the actual emission coming from QDs. Moreover, it is important to take into account that the measured emission can be both increased or decreased by the action of the scattering components (i.e. MNPs). In fact, if a direct measure of a layer is performed (i.e. front – face analysis) the revealed signal is likely to be increased by the action of the metal. Therefore, the detector will receive a higher intensity compared to the one exclusively coming from the QDs. On the contrary, if a back – face analysis is conducted, the scattering action of MNPs is more likely to reduce the detected signal because the scattering direction is mainly opposite with respect to the detector's position.

Secondly, the so-called **auto absorption effect** plays a fundamental role in the field of QDs-metal NPs interaction. In fact, if the emission wavelength of QDs is similar to the absorption wavelength of MNPs, some of the radiation emitted by QDs will be stolen by MNPs and the detected signal will be lowered. Even though this is simply an introductory paragraph, an example is useful to understand the current point. Indeed, GNPs characterized by a diameter of 3-5 nm present a main absorption wavelength of 520 nm. In turn, similar sized QDs emit mainly at the same wavelength. Therefore, the auto absorption effect can occur and some of the emitted radiation coming from QDs will be retained by GNPs before reaching the detector.

Finally, the **plasmonic effect** or **field effect** is a very interesting phenomenon which is able to increase the signal coming from QDs. This effect gave origin to the topic of **Metal Enhanced Fluorescence** (i.e. MEF) where the term "enhanced" has been used to say that the presence of metal is able to strengthen the signal emitted by the fluorescent component (i.e. QDs). The MEF phenomenon has been explained by asserting that when metal nanoparticles are stimulated by a radiation, a local enhancement of the electric field around them takes place and consequently, a more efficient excitation of QDs occurs. In other words, MEF is caused by an increased excitation rate due to the enhanced local field experienced by QDs or fluorophores and the electromagnetic coupling with the metal NP situated nearby. [1] As a result, the fluorescence detected signal results to be increased.

In their review, Fang Xie et al. focused on MEF and its current and future application in biotechnology. [1] As they asserted, nowadays the most diffused labelling technique in bio sensing and bio imaging is represented by the use of fluorescent molecules. However, problems like low intensity emission and low photo stability often limit their applicability. In this regard, MEF is paving the way towards a better detection sensitivity and image enhancement. In fact, much lower concentrations of biomarkers can be detected thanks to the MEF effects, or rather an increased fluorescence quantum yield, a decreased lifetime and a better QD or fluorophore photo stability.

In conclusion, when the interaction between QDs and plasmonic components is studied, either in solution or in solid physical state, the three mentioned events of auto absorption, scattering and plasmonic effect should be considered and their contribution to the final detected emission needs to be estimated. Figure 87 reports a schematic representation of the induced surface charge oscillations in a metal NP caused by an external radiation.

Moreover, the three main responses are shown, namely absorption, scattering and MEF. In addition, the previously explained LSPR is displayed which is thought to be responsible for another phenomenon referred to as surface enhanced Raman scattering (i.e. SERS)
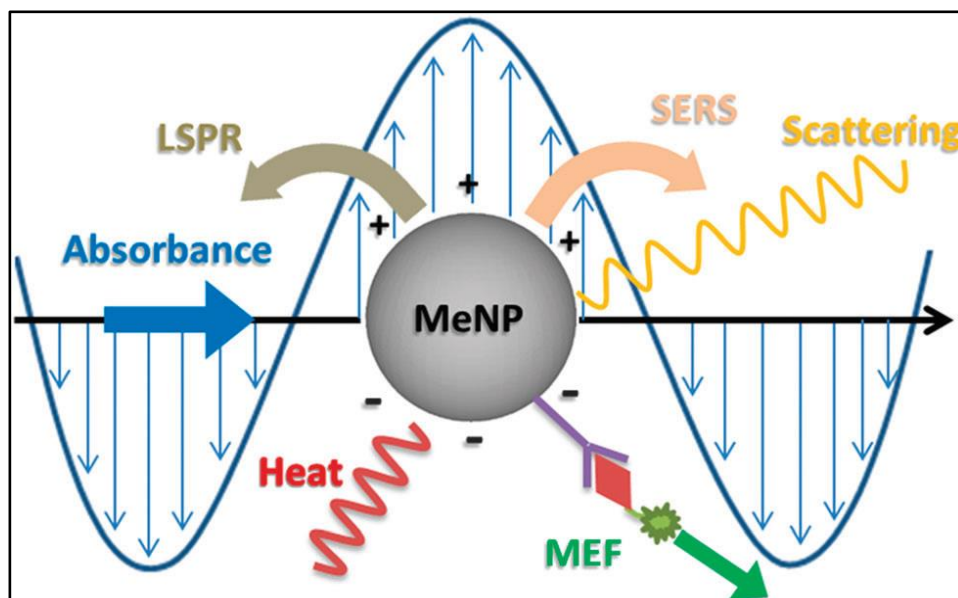

Figure 87 Induced surface charge oscillations in a MNP with possible spectroscopic responses *[1]*

A.4.1 Energy transfer from QDs to metal NPs

As affirmed by Andries Meijerink, "energy transfer between QDs and metal nanoparticles is a hot topic" [43] Even though numerous publications exist about studies on QDs-metal NPs interaction, a clear understanding of the behavior of excitons in QDs in the proximity of a metal nanoparticle is still missing. What has been reported is that the distance between a semiconductor nanowire (NW) and a gold nanoparticle can be probed with a nm accuracy by measuring the influence of plasmonic coupling on the exciton life time. Even if this information is strictly about NWs and not QDs, it is still useful to understand the physics controlling the energy transfer phenomenon. In fact, whenever a metal nanoparticle is situated near to a semiconductor NW an energy transfer event occurs which causes the exciton life time to be shortened. The mentioned transfer is regulated by a distance dependence which trend is R^{-6}. Consequently, as the metal nanoparticle approaches the wire, the exciton life time is shortened, and the emitted wavelength shifts to the blue. Oppositely, the exciton life time is increased, and the wavelength shifted to the red as the nanoparticle is moved away. [43]

In order to verify the mentioned behavior, the study reported by Andries Meijerink results to be very interesting. Specifically, a molecular spring assembly was created as illustrated in figure 88. A NW of CdTe was linked to a gold NP via PEG-aB-PEG string where aB stands for an antibody. To induce the expansion of the string, an antigen (i.e. aG) was added which bound to the aB. Following the chain expansion and the consequent increase of the NW-NP distance, the exciton lifetime was observed to increase, due to a less efficient energy transfer, and the emission shifted to the red. On the contrary, when free aB was added which competed with the aG in establishing a link with PEG, the aG was released by causing a shrinkage of the string. The observed consequence was a reduction of the exciton life time and an emission shift to the blue. [43]
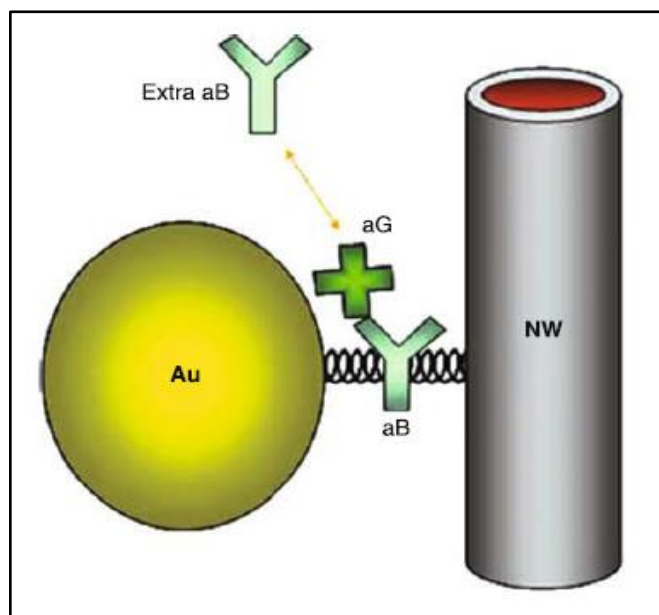
Figure 88 Schematic illustration of spring assembly composed of GNP, string and CdTe NW *[43]*

A.4.2 QDs-MNPs interaction analysis in solution

The present paragraph has the main objective of presenting some examples of interaction between QDs and Metal NPs. In particular, it is exclusively dedicated to the investigation conducted on samples in solution. The goal of these studies is to understand the role of MNPs when these are located near to fluorescent quantum dots. More specifically some conclusions will be made as far as the role of distance between the two components is concerned. In this regard, it is essential to refer to the previously considered problem of stability of QDs and MNPs. In fact, as it has been said, because of their high surface to volume ratio, due to their small size, either QDs and MNPs present a strong tendency to aggregate. Therefore, to maintain their properties, they have to be stabilized and this is done by functionalizing their surface. In addition, the mentioned surface functionalization is not only useful to keep QDs or MNPs apart. In fact, it is also fundamental to establish a binding between them without allowing them to touch. This proximity without contact is necessary to induce the MEF effect and to prevent the phenomenon of **quenching** which occurs when fluorescent and plasmonic components get into physical contact. If this happens, a reduction of the radiation emission is observed and the MEF effect is extinguished.

In their work, Huang et al. synthesized ZnCdSeS QDs-gold NPs hybrid in aqueous solution by using a bi-functional linker mercaptoacetic acid (MPA). [44] Here, the gold NPs are described as isolated metallic nanostructures in which the LSPR is excited because of the collective oscillations of free electrons. As a consequence, the electric field is enhanced as described above and the distance between metal and QD is reported to play an important role in varying the fluorescence enhancement. However, a drawback is described about studies conducted in solution. In fact, highly control is required on uniformity and dispersibility of nanoparticles which sometimes can be difficult to achieve. First of all, oleic acid (OA)-capped ZnCdSeS quantum dots in chloroform were synthesized. Subsequently, by using mercaptoacetic acid (MPA) as a bifunctional linker, MPA-capped ZnCdSeS quantum dots were produced. Because of the character of the functional groups, the QDs resulted to be positively charged, while water soluble GNPs, synthesized by reducing gold chloride with sodium citrate in water, were negatively charged due to the citrate ions absorbed on the surface of GNPs. As a result, the two components established a good connection upon mixing the two solutions. Both water and chloroform-dispersed QDs have been observed to show the peak of absorption at 520 nm. Likewise, GNPs showed their absorption

peak at the same wavelength. Later, to investigate the role of the amount of GNPs on the LSPR effect, different hybrids have been created with an increasing quantity of GNPs from 0 to 120 µl. The reported absorption spectra showed the same trend for GNPs, QDs and hybrid materials. However, as visible in figure 89, the intensity of the absorption peak related to QDs resulted to increase as the amount of gold increased.
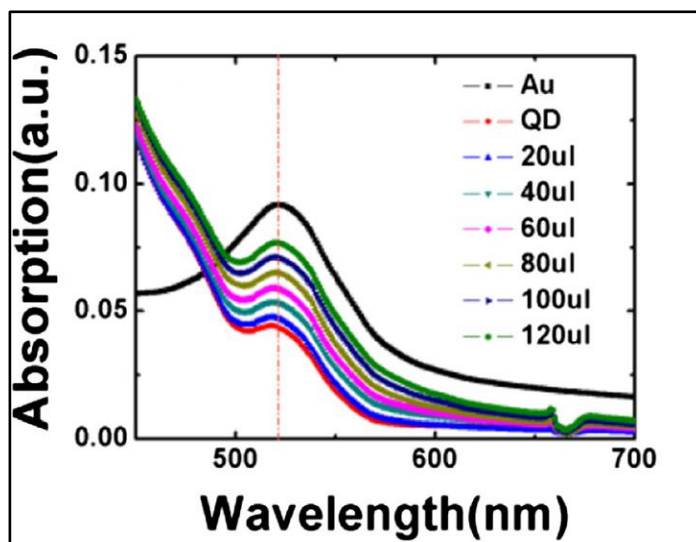

Figure 89 Absorption spectra of GNPs, QDs and hybrid materials *[44]*

About the PL spectra, it is shown in figure 90 that the emission wavelength is located at 540 nm regardless of the presence of gold. Interestingly, a clear fluorescence enhancement was observed only until the added amount of 60 µl of GNPs solution. In fact, when further gold was added, the result was a reduction of the fluorescence intensity. Therefore, Huang et al. affirmed that two mechanisms were competing. On the one hand, the PL enhancement due to the increase of absorption and radiative rate caused by LSPR and dominating only until the added amount of 60 µl of GNPs solution. On the other hand, PL quenching occurring when GNPs and QDs got into physical contact. This last phenomenon is attributed to energy and charge transfer between gold and QDs. Specifically, according to Yin et al. the main reason for this phenomenon is the reverse charge transfer occurring from semiconductor to the metal at the interface. [3] [44]
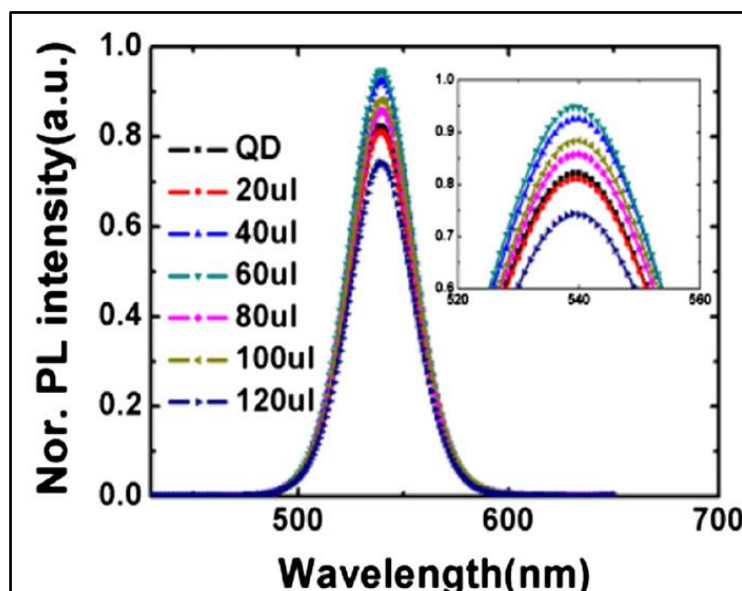

Figure 90 PL spectra of QDs and hybrid material *[44]*

To conclude, it is clear that until when GNPs are under a certain amount, their action is intended to increase the PL because of the LSPR and field effect. As soon as a limit is reached, a contact between GNPs and QDs occurs which causes the quenching to happen. The study reported by Farinha et al. [4] provided an inspiration and a guide line for the current thesis work. By using a solution of tetrablock copolymer chains of poly (acrylic acid)-b-polystyrene-TTC-polystyrene-b-poly (acrylic acid), where TTC represents a single trithiocarbonate group, they induced micellization upon the addition of cadmium sulfide. Specifically, transient micelles were formed which were characterized by a poly (cadmium acrylate) core. Subsequently, through the addition of sodium sulfide, the formation of a single CdS quantum dot was observed inside a flower-like micelle which corona was composed of polystyrene and a TTC group per each "petal". The described structure takes the name of quantum dot micelle (QDM) and results to be very interesting because the addition of a reducing agent can effectively cut the TTC group giving rise to thiols which can, in turn, connect to the surface of GNPs. Therefore, a hybrid structure composed of GNPs and QDs in solution can be easily prepared. Moreover, the PS chains connecting QDs and GNPs provided a good obstacle against PL quenching and a precise location control of embedded NPs. Different amounts of GNPs have been added in order to study their action on photoluminescence and emission lifetime. In particular, the molar ratio of GNPs to QDMs has been defined as R_{GNP} and its investigated values have been 0.001, 0.007, 0.011, 0.015 and 0.077. A good colloidal stability has been observed and only a small increase of the hydrodynamic diameter of the conjugates following the GNPs increase has been reported.

As far as the photoluminescence analysis is concerned, Farinha et al. reported how GNPs can absorb some of the excitation radiation and also reabsorb some of the light emitted by QDs (i.e. auto absorption effect) by hiding the fluorescence enhancement given by the field effect. Therefore, in order for the latter to be visible, a correction needs to be applied on the measured emitted radiation. In figure 91 it is possible to see an uncorrected plot of fluorescence intensity with different amounts of GNPs where it is easy to notice that a higher quantity of gold reduces the measured radiation.
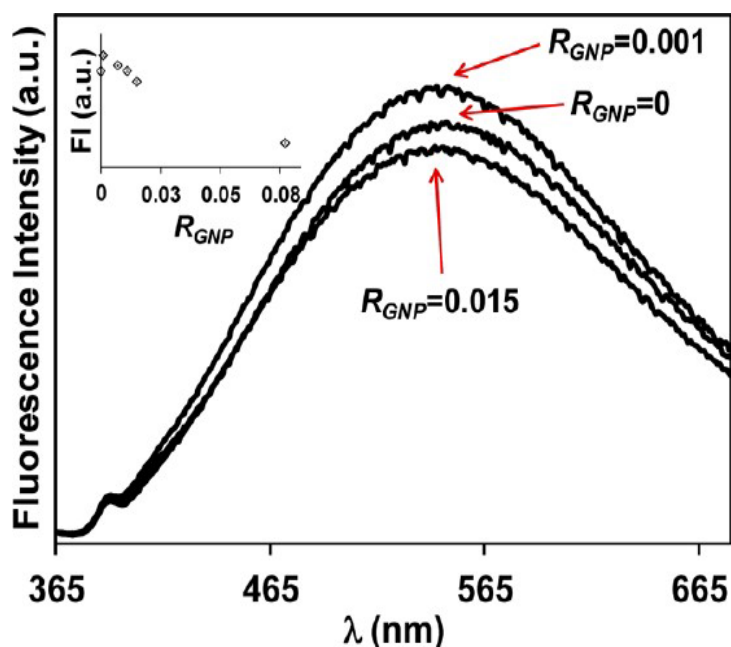
Figure 91 Uncorrected plot of emission spectra of QDM and QDM-GNP assemblies
with $R_{GN\ P}$= 0.001 and 0.015 with λ_{ex} = 350 nm. *[4]*

Oppositely, figure 92 shows a corrected plot in which the field effect can be observed which causes an increase of the QDs photoluminescence. Moreover, an average emission amplification (i.e. EA) has been calculated by dividing the corrected emission intensity corresponding to each QDM-GNP by the intensity of the QDMs alone. The EA has been reported to increase as the R_{GNP} and the excitation wavelength increase.

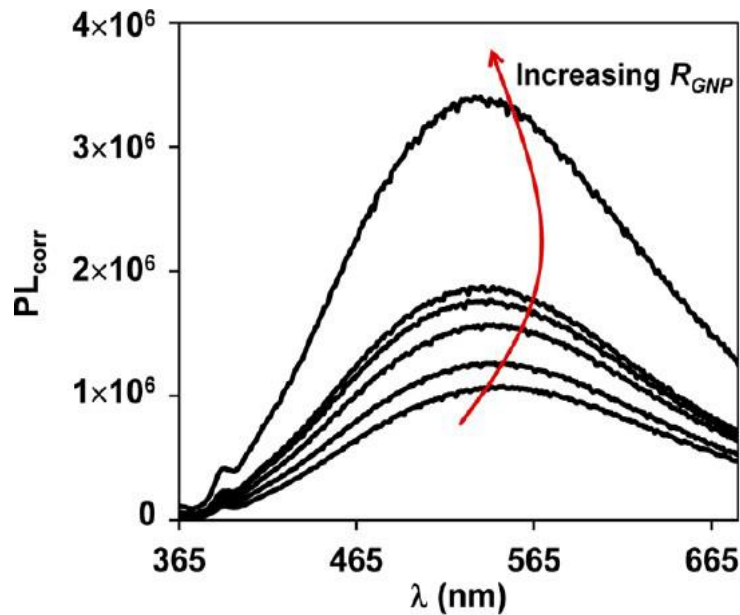Figure 92 Corrected emission spectra of QDM and QDM-GNP dispersions with increasing R_{GNP} *[4]*

Finally, Farinha et al. asserted that no significant change in the emission lifetime was observable, meaning that the interaction between QDMs and GNPs does not cause a significant change in the relaxation pathways of QDs. Moreover, they demonstrated that the observed enhancement was not determined by a simple scattering by GNPs. Instead they affirmed that GNPs act as antennae for the incoming radiation. Specifically, when excited at their LSPR, they become surrounded by an enhanced electromagnetic field able to optimize QDs excitation. [4]

A.4.3 QDs-MNPs interaction analysis in deposited films

Since the current thesis work is mainly devoted to investigating the interaction between QDs and GNPs in hybrid solid structures (i.e. deposited films), the present paragraph plays a fundamental role. The same mechanism to explain the MEF effect that was presented in the previous paragraph is still valid for solid structures as Lidong Li et al. reported in their review. [5] More precisely, they affirmed that the excitation rate of a fluorophore or a QD can be increased by the enhanced local field caused by the excitation of the LSPR. In addition, the nonradiative decay is accelerated resulting in an increased quantum yield and a decreased fluorescence lifetime. Another issue that was introduced for the study in solution and that is particularly crucial for hybrid film of QDs and MNPs in the control over their reciprocal distance. In fact, the fluorescence emitter (i.e. QD) has to be near enough to the plasmonic component since the field effect presents a nearly exponential decrease with distance from the metallic surface. On the other hand, an excessively short distance or even a contact, can result in an undesired PL quenching. Therefore, a spacer interlayer is necessary to separate QD and MNP and a linker needs to be used to bridge them. The advisable distance has been reported to be between 5 and 30 nm [5]. In order to realize such spacer/linker, different materials have been utilized, among which silica, synthetic polymers, DNA and proteins. Furthermore, different procedures can be applied to realize these hybrid nanostructures. For instance, lithographic techniques can provide nanopatterns characterized by high order and "precisely controlled sizes, shapes and interparticle separations". [5] However, this technique results to be expensive, time-consuming and not applicable to large area devices. In spite of being particularly difficult to apply, it has been used by Xiaoying et al. to create hybrid nanostructures of well-organized arrays of colloidal QDs and a self-assembled layer of GNPs. [6] Firstly, they produced lithographically generated nanoscale patterns with tailored surface chemistry in order to achieve a high selectivity and a precise confinement of QDs into well-organized arrays. After, a monolayer of close-packed GNPs was added to introduce the plasmonic component as a fluorescence

enhancer. This strategy, and its effect providing a good lateral confinement and vertical stacking, is shown in figure 93. In particular, a polymer brushes layer is effective in binding QDs only on those areas that were lithographically created.
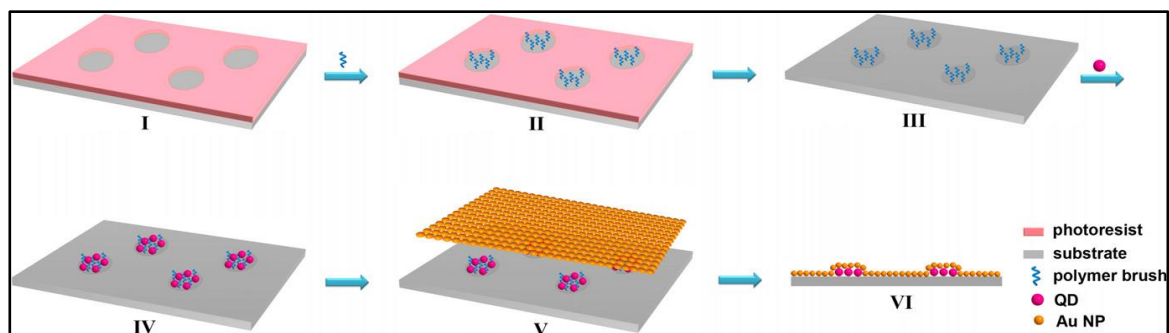

Figure 93 Lithographic technique to generate well-organized arrays of colloidal QDs *[6]*

SEM observations of the described structure confirmed the precise location of QDs only on the so-called anchor spots while no QDs have been observed in the inert regions of the silicon substrate. Moreover, a confocal microscope has been used to investigate the PL enhancement provided by the GNPs. Figure 94 is a fluorescence image obtained with a confocal microscope of a square lattice of anchor spots occupied by QDs. By comparing figure 94 (a) and (b) it is noticeable that the size of the bright spots becomes larger with the increase of the pre-pattern spot size. Moreover, a clear enhancement of fluorescence intensity provided by GNPs is visible by comparing figure 94 (e - without GNPs) with 94 (f - with GNPs).
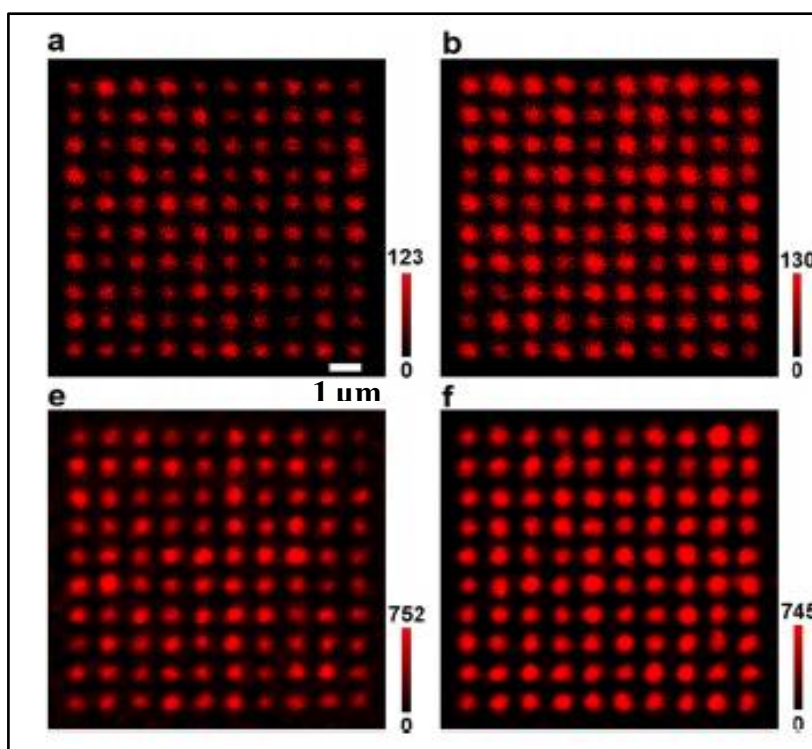
Figure 94 Fluorescence images of red QDs arrays: (a) and (b) QD arrays
only; (e) and (f) QD/Au composite structure *[6]*

The same experiment has been conducted for red, yellow and green QDs and the calculated average enhancement factors for the three colors red, yellow and green were respectively, 4.6, 5.3 and 4.8. As far as green QDs are concerned, a clear auto absorption effect has been observed. In fact, green QDs emit at 520 nm which is also the absorption wavelength associated to LSPR of about

5 nm sized GNPs. A further investigation has been conducted by Xiaoying et al. who produced Silica-covered CdSe QDs and used them for the same experiments previously described. Beside a higher induced local strain in the hybrid film compared to the case without Silica, a larger average enhancement factor of 11 has been reported. About the distance between QDs and GNPs, in the case without Silica its value has been calculated by summing the functionalization of both components and approximated to 6 nm. Differently, upon Silica encapsulation, the measured distance was 11 nm which seems to be the optimal one to achieve the highest enhancement factor.

Beside the described lithographic method, other procedures to realize hybrid films of QDs and MNPs have been developed which are shown in figure 95. The common point to all these synthesis processes is the necessity to establish a good connection between the fluorescent and the plasmonic components by simultaneously controlling and tuning their reciprocal distance in order to vary the resulting fluorescence properties. In particular, the role of spacer can be taken by a dielectric layer, a Langmuir-Blodgett film, a polymeric structure or a biomolecular layer. [5] Specifically, the current thesis work is based upon the use of a polymeric layer which, in turn, results to be a very widespread and versatile method.
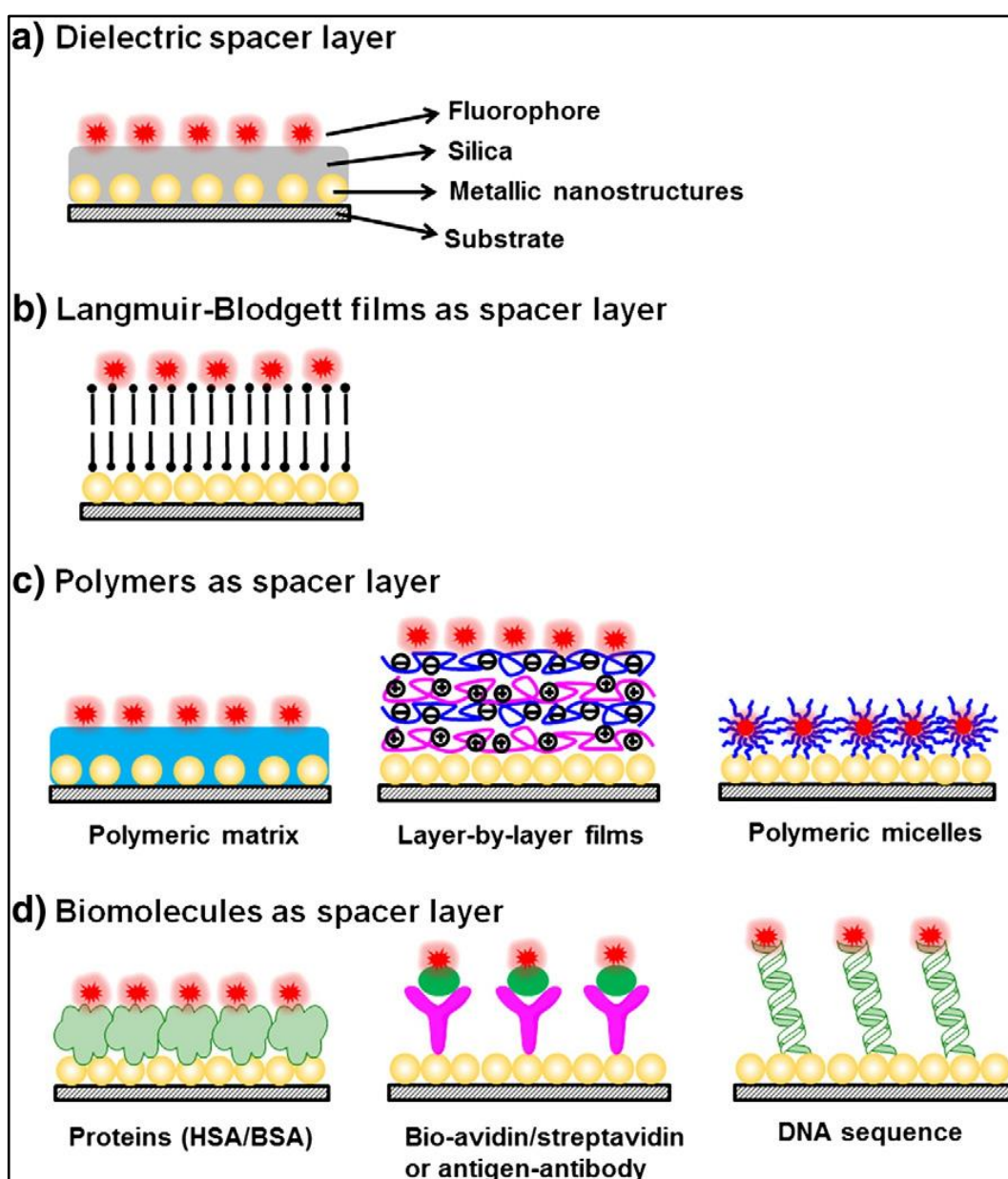

Figure 95 Schematic representation of the common production methods for the spacer layer in QDs-MNPs hybrid materials *[5]*

The application of polymeric materials as spacers has been allowed by the development of the spin-coating technique which permitted to prepare a polymeric matrix in the nanometer range. In fact, sometimes, the polymers not only serve as spacers, but also as a matrix for the QDs/fluorophores or MNPs to be embedded. [5] An interesting example is the work reported by Chen et al. [7] who deposited both CdSe QDs and GNPs on elastomeric polydimethylsiloxane (PDMS) and were able to tune the distance between the two components by simply applying an external stress on the PDMS film. Initially, the excessively close proximity between QDs and GNPs caused a fluorescence quenching. However, as the separation distance increased, under a higher external stress, the measured intensity increased accordingly, and a maximum was reached at the distance of 12 nm which is coherent with previously mentioned results. [6]

The use of block copolymers (BCPs) as spacers found numerous applications in the field of interaction between QDs and MNPs. In fact, as previously described, BCPs have been observed to be able to independently form ordered structures with diverse morphologies which can represent an ideal template to create large scale arrays for nano-photonic applications. Moreover, these structures can behave as plasmonic arrays because they can easily host QDs and MNPs which reciprocal position can be effectively tuned and controlled. For example, M. Haridas and J.K Basu have varied the density of GNPs and CdSe QDs independently inside a BCP matrix in order to investigate the role of these parameters on the final optical properties of the hybrid array. [8] [9] CdSe QDs capped with pyridine have been synthesized according to the method suggested by Peng et al. [10] and based upon the use of CdO as precursor instead of the normally utilized $Cd(CH_3)_2$ to produce CdSe, CdTe or CdS QDs. Moreover, thiol terminated polystyrene (PST) capped GNPs have been produced according to the method reported by Sutton et al. and based upon the reduction of gold chloride in the presence of PST. [11] In this case, the thiol group at the extremity of the PS chains allowed for a good interaction with GNPs. Furthermore, arrays of CdSe QDs and hybrid arrays of CdSe QDs and GNPs have been prepared using a BCP template composed of polystyrene and poly vinyl pyridine (PS-P4VP). Specifically, this BCP is known to form hexagonal arrays of cylinders of P4VP in the PS matrix. In addition, the selective interaction between pyridine ligands at the surface of the CdSe QDs and the P4VP in the BCP allows for the QDs to be located exclusively into the P4VP cylinders while the PST capped GNPs remain inside the PS region. This simplicity in precisely controlling location and dispersion of particles allows to independently control density and interparticle distance. The volume fraction of QDs was 0.0135 for all samples belonging to series C3L, while it was doubled to 0.027 for all samples of series C3H. In addition, the volume fraction of GNPs was varied from 0.0019 to 0.0056 in all samples. As it can be seen in figure 96 (a), the PL emission increases as the amount of gold increases. However, this effect is less pronounced in sample C3H than in C3L and this is because C3L samples have a lower amount of QDs and consequently more GNPs per QDs are available and their effect in enhancing the PL is more visible. On the contrary, PL lifetime measurements (figure 96 b) reveal a lifetime decrease as the gold is increased, and this effect is more pronounced in C3H samples. The reason for this counter-intuitive event has been attributed by M. Haridas et al. to the lower interparticle distance of samples C3H compared to samples C3L, this resulting in a more efficient energy exchange among QDs mediated by GNPs. Moreover, the existence of two different lifetimes has been hypothesized. The first shorter one, or rather τ_1, originates from collective interaction among QDs, while the second longer one, or rather τ_2, is related to radiative electron hole recombination in isolated QDs. It has been observed that the first one becomes the dominant relaxation mode when the quantity of gold is increased, and it is much more affected than τ_2. In fact, this demonstrates the real interaction between QDs and plasmonic component. [9]

Finally, it is worth mentioning that, because of the variety of phenomena occurring when QDs and MNPs are approached, it is intrinsically difficult to differentiate the amount of PL intensity attributable to metal scattering, auto absorption effect and field effect. However, different studies have been conducted to gain more information in this regard, especially by implying silver islands films (SIFs) as plasmonic component together with organic fluorophores. For example, Maliwal et al. [45] studied the properties of a monolayer of labeled avidin molecules near SIFs and observed an increase of the fluorescence intensity of between 18 and 80 with one photon excitation. Moreover, a many hundredfold increase has been measured with two-photons excitation. In addition, a better

photo stability and a dramatic lifetime decrease has been reported. All the mentioned spectral changes have been attributed to increased rates of excitation near the SIFs and increased rates of radiative decay.
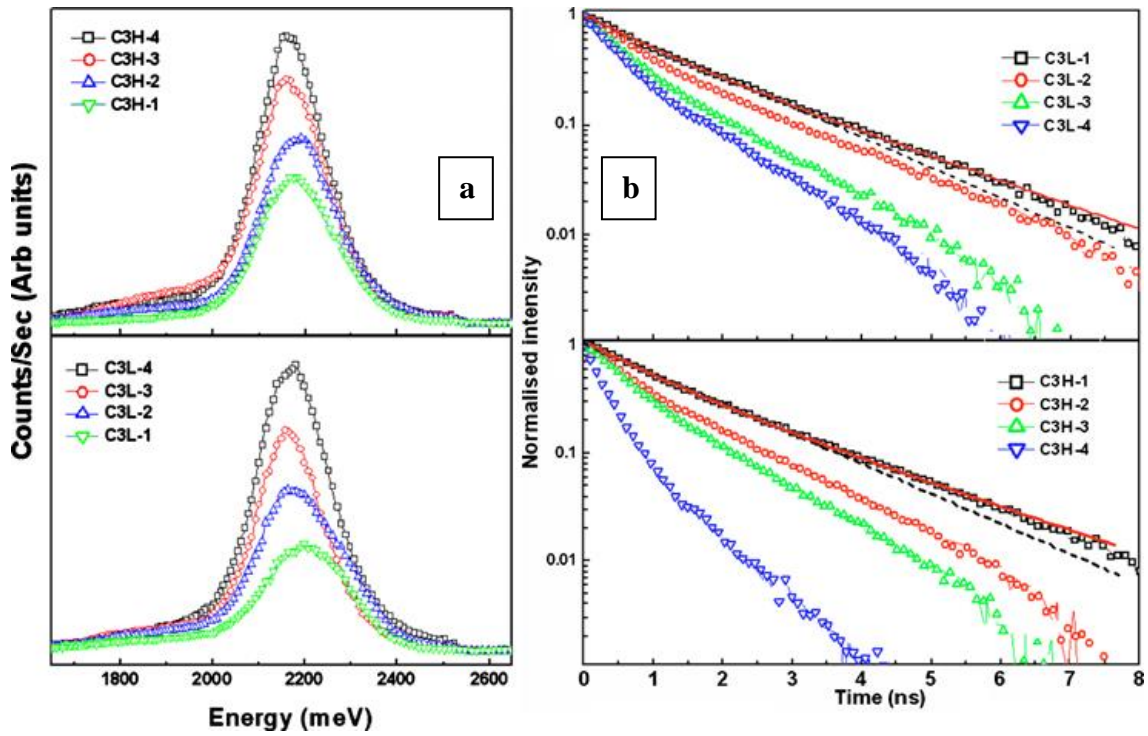

Figure 96 PL (a) and lifetime (b) measurements of sample C3H (1-4) and C3L (1-4) *[9]*

More specifically, the presence of MNPs can affect a fluorophore in two different ways. First of all, the already discussed field effect can be observed and Maliwal et al. defined a ratio called excitation rate enhancement factor, or rather the ratio of the enhanced excitation intensity in the presence of metal particles (I_{enh}) and the excitation intensity of fluorophores alone (I) (i.e. $G_{exc} = \frac{I_{enh}}{I}$). Secondly, the non-radiative (K_{nr}) and radiative (Γ) deactivation rates can be influenced by the interaction between the plasmon band and the fluorophore dipole and corresponding enhancement factors N_{nr} (non-radiative) and N_r (radiative) can be defined. It follows that, if one photon excitation is performed and lifetimes are measured, the observed fluorescence enhancement simultaneously depends on two variables, namely G_{exc} and N_r. In other words, it is impossible to affirm if the measured enhancement is due to field enhancement (G_{exc}) or to the emissive rate enhancement (N_r). Therefore, two-photons excitation can be applied which provides the so-called fluorescence enhancement for two photons excitation (i.e. $G_{fl}^{(2)}$). Since two-photons excitation brings to the same excited state as one photon excitation, the final real field enhancement can be calculated by dividing the fluorescence enhancement for two-photons excitation by the one for single photon excitation (i.e. $G_{exc} = \frac{G_{fl}^{(2)}}{G_{fl}^{(1)}}$). Thus, an effective way to evaluate all enhancement factors in the presence of metal NPs has been individuated. Although the described procedure goes beyond the objective of the current thesis work, it is interesting because it provides a rough idea of the inherent complexity of the studied field.

AKNOWLEDGEMENTS

References

[1]   A. C. a. D. D. Fang Xie, "Plasmonic fluorescence enhancement by metal nanostructures: shaping the future of bionanotechnology," *Physical Chemistry Chemical Physics,* pp. 15709-15726, 2013.

[2]   J. C. J. Z. J. P. W. L. a. Z. Z. Qianqian Huang, "Enhanced Photoluminescence Property for Quantum Dot-Gold Nanoparticle Hybrid," *Nanoscale Research Letters,* 2015.

[3]   C. Y. Y. Z. C.-H. C. J. L. H.-C. K. Z. W. J. L. Y. F. a. C. C. Jun Yin, "Effect of the surface-plasmon–exciton coupling and charge transfer process on the photoluminescence of metal–semiconductor nanostructures," *Nanoscale,* pp. 4436-4442, 2013.

[4]   M. M. T. R. a. T. P. J.P.S. Farinha, "Enhanced Photoluminescence from Micellar Assemblies of Cadmium Sulfide Quantum Dots and Gold Nanoparticles," *The Journal of Physical Chemistry,* pp. 3122-3133, 10 January 2013.

[5]   Q. C. F. H. M. Lidong Li, "Controllable metal-enhanced fluorescence in organized films and colloidal system," *Advances in Colloid and Interface Science,* pp. 164-177, 2014.

[6]   S. P. M. H. M. J. a. P. F. N. Xiaoying Liu, "Hybrid nanostructures of well-organized arrays of colloidal quantum dots and a self-assembled monolayer of gold nanoparticles for enhanced fluorescence," *Nanotechnology,* pp. 285-301, 2016.

[7]   C. H. W. C. M. W. a. Y. F. C. C. W. Chen, "Tunable emission based on the composite of Au nanoparticles and CdSe quantum dots deposited on elastomeric film," *Applied Physics Letters,* vol. 94, no. 7, 2009.

[8]   J. K. B. M.Haridas, "Controlled photoluminescence from self-assembled semiconductor-metal quantum dot hybrid array films," *Nanotechnology,* vol. 21, p. 415202, 2010.

[9]   J. K. B. ,. D. J. G. a. G. P. W. M. Haridas, "Photoluminescence spectroscopy and lifetime measurements from self-assembled semiconductor-metal nanoparticle hybrid arrays," *Applied Physics Letters,* p. 083307, 2010.

[10]   Z. A. P. a. X. Peng, "Formation of High-Quality CdTe, CdSe, and CdS Nanocrystals Using CdO as Precursor," *J. Am. Chem. Soc.,* pp. 183-184, 2001.

[11]   N. S. C. M. S. S. G. J. M. L. B. L. A. R. a. R. B. L. Muriel K. Corbierre, "Polymer-Stabilized Gold Nanoparticles and Their Incorporation into Polymer Matrices," *J. Am. Chem. Soc.,* pp. 10411-10412, 2001.

[12]   t. f. e. Wikipedia, "Ultraviolet–visible spectroscopy," Wikipedia, [Online]. Available: https://en.wikipedia.org/wiki/Ultraviolet%E2%80%93visible_spectroscopy. [Accessed 23 09 2017].

[13]   E. I. Ltd., "Operating Instructions - F900 Fluorescence Spectrometer Software," [Online]. Available: https://www.tcd.ie/Physics/research/groups/1d-nanostructures/resources/equipment/NIR%20PL.pdf. [Accessed 25 09 2017].

[14]   G.Frens, "Controlled Nucleation for the Regulation of the Particle Size in Monodisperse Gold Suspensions," *Nature Physical Science,* vol. 241, pp. 20-22, 1973.

[15]   t. f. m. r. Wikimedia Commons, "Rotary Evaporator.svg," 30 10 2009. [Online]. Available: https://commons.wikimedia.org/wiki/File:Rotary_Evaporator.svg#filelinks. [Accessed 28 09 2017].

[16]   t. f. e. Wikipedia, "Transmission electron microscopy," [Online]. Available: https://en.wikipedia.org/wiki/Transmission_electron_microscopy. [Accessed 29 09 2017].

[17]   R. T. B. &. B. N. Bahadur K.C., "Gold nanoparticle-based gene delivery: promises and challenges," *Nanotechnology Reviews,* pp. 269-280, 2013.

[18]   M. V. M. M. a. M. A. H. Christophe Sinturel, "Solvent Vapor Annealing of Block Polymer Thin Films," *Macromolecules,* pp. 5399-5415, 2013.

[19]   R.J Young and P.A .Lovell, Introduction to polymers, Second ed., Hong Kong: Chapman and Hall, 1991.

[20]   P. C. H. a. T. P.Lodge, Polymer Chemistry, Second ed., Boca Raton FL: Taylor & Francis Group, 2007.

[21]   H. C.-Y. Pan Cai-Yuan, Developments in Block Copolymer Science and Technology - Chapter 3 : Synthesis and Characterizations of Block Copolymers Prepared via Controlled Radical polymerization Methods, I.W.Hamley, Ed., Leeds: John Wiley & Sons, Ltd, 2004.

[22]   E. R. S. H. T. Graeme Moad, "Living Free-Radical Polymerization by Reversible Addition-Fragmentation Chain Transfer: The Raft Process," *Macromolecules,* vol. 31, pp. 5559-5562, 10 June 1998.

[23]   S. G. Gaynor, "Controlled Radical Polymerization by Degenerative Transfer: Effect of the Structure of the Transfer Agent," *Macromolecules,* pp. 8051-8056, November 1995.

[24]   Y. L. B. L. a. S. Z. Xiaoguang Wang, "Ab initio Batch Emulsion RAFT Polymerization of Styrene Mediated by Poly(acrylic acid-b-styrene) Trithiocarbonate," *Macromolecules,* pp. 6414-6421, 31 July 2009.

[25]   Y. M. Adi Eisenberg, "Self-assembly of block copolymers," *Chem Soc Rev,* pp. 5969-5985, 2 April 2012.

[26]   P. C. H. a. R. Rajagopalan, Principles of Colloid and Surface Chemistry, Third edition, Revised and expanded ed., New York: Marcel Dekker Inc., 1997.

[27]   B. Valeur, Molecular Fluorescence: Principles and Applications, Paris: Wiley-VCH, 2001.

[28]   A. O. AI Ekimov, "Quantum size effect in three-dimensional microscopic semiconductor crystals," *JETP Lett,* pp. 345-349, 29 July 1981.

[29]   M. A. Kasfner, "Artificial Atoms," *Physics Today,* pp. 24-31, January 1993.

[30]   S. M. R. a. M. Manninen, "Electronic structure of quantum dots," *Rev. Mod. Phys.,* pp. 1283-1342, 26 November 2002.

[31]   M. L. S. a. L. E. B. M G Bawendi, "The Quantum Mechanics of Larger Semiconductor Clusters ("Quantum Dots")," *Annual Review of Physical Chemistry,* pp. 477-496, October 1990.

[32]   P. Reiss, "Synthesis of semiconductor nanocrystals in organic solvents," in *Semiconductor Nanocrystal Quantum Dots - Synthesis, Assembly, Spectroscopy and Applications*, Munich, SpringerWienNewYork - Andrey L. Rogach, 2008, pp. 35-72.

[33]   D. Wang, "Semiconductor nanocrystal-polymer composites: using polymers for nanocrystal processing," in *Semiconductor Nanocrystal Quantum Dots - Synthesis, Assembly, Spectroscopy and Applications*, Munich, SpringerWienNewYork - Andrey L. Rogach, 2008, pp. 171-196.

[34]   W. C. A.-H. L. G. L. G. Z. J.-H. Z. a. B. Y. Jia-Yu Wang, "Controlled Fabrication of Cross-Linked Nanoparticles/Polymer Composite," *JACS Communications,* pp. 13358-13359, 2002.

[35]   P. S. D. J. N. V. N. A. H. B. A. L. Benoit Dubertret, "In Vivo Imaging of Quantum Dots Encapsulated in Phospholipid Micelles," *Science,* pp. 1759-1762, 2002.

[36]   H. S. a. T. Emrick, "Reversible Addition Fragmentation ChainTransfer (RAFT) Polymerization fromUnprotected Cadmium Selenide Nanoparticles," *Angewandte Chemie,* pp. 5383-5386, 2004.

[37]   X. P. a. A. P. A. N. C. Greenham, "Charge separation and transport in conjugated-polymer/semiconductor-nanocrystal composites studied by photoluminescence quenching and photoconductivity," *APS Physics - Physical Reviews B,* pp. 17628 - 17637, 1996.

[38]   B. J. T. S. S. M. K. L. K. T. T. a. A. V. Yasuhiro Tachibana, "Origin of surface trap states in CdS quantum dots:relationship between size dependent photoluminescence and sulfur vacancy trap states," *Physical Chemistry Chemical Physics,* pp. 2850-2858, 2015.

[39]   Y. Q. H. L. K. Z. F. L. Shao Pu Liu, "A study on the sizes and concentrations of gold nanoparticles by spectra of absorption, resonance Rayleigh scattering and resonance non-linear scattering," *Spectrochimica Acta Part A,* pp. 2861-2866, 2004.

[40]   t. f. e. Wikipedia, "Colloidal gold," Wikipedia, [Online]. Available: https://en.wikipedia.org/wiki/Colloidal_gold. [Accessed 16 09 2017].

[41]   V. B. Y. K. H. K. W. T. M. Z. P. A. H. R. W. H. T. M. C. W. M. B. L. R. D. Monic Shah, "Gold nanoparticles: various methods of synthesis and antibacterial applications," *Frontiers in Bioscience,* pp. 1320-1344, 2014.

[42]   S.-A. Co., "Gold Nanoparticles: Properties and Applications," Sigma-Aldrich, [Online]. Available: http://www.sigmaaldrich.com/technical-documents/articles/materials-science/nanomaterials/gold-nanoparticles.html. [Accessed 14 09 2017].

[43]   A. Maijerink, "Exciton dynamics and energy transfer processes in semiconductor nanocrystals," in *Semiconductor Nanocrystal Quantum Dots - Synthesis, Assembly, Spectroscopy and Applications*, Munich, SpringerWienNewYork - Andrey L. Rogach , 2008, pp. 277-310.

[44]   J. C. J. Z. J. P. W. L. a. Z. Z. Qianqian Huang, "Enhanced Photoluminescence Property for Quantum Dot-Gold Nanoparticle Hybrid," *Nanoscale Research Letters,* 2015.

[45]   J. M. I. G. Z. G. J. R. L. Badri P. Maliwal, "Fluorescence Properties of Labeled Proteins Near Silver Colloid Surfaces," *Biopolymers (Biospectroscopy),* pp. 585-594, 2003.

[46]   Sigma-Aldrich,   "Quantum   Dots,"   [Online].   Available: http://www.sigmaaldrich.com/technical-documents/articles/materials-science/nanomaterials/quantum-dots.html. [Accessed 5 08 2017].